SURFACE MODIFYING AMPHIPHILIC ADDITIVES FOR THE IMPROVEMENT OF FOULING-RELEASE PROPERTIES OF SILOXANE-POLYURETHANE COATINGS

A Dissertation
Submitted to the Graduate Faculty
of the
North Dakota State University
of Agriculture and Applied Science

By

Jackson Robert Benda

In Partial Fulfillment of the Requirements
for the Degree of
DOCTOR OF PHILOSOPHY

Major Department:
Coatings and Polymeric Materials

April 2022

Fargo, North Dakota

North Dakota State University
Graduate School

Title

Surface modifying amphiphilic additives for the improvement of fouling-release properties in siloxane-polyurethane coatings

By

Jackson Robert Benda

The Supervisory Committee certifies that this ***disquisition*** complies with North Dakota State University's regulations and meets the accepted standards for the degree of

DOCTOR OF PHILOSOPHY

SUPERVISORY COMMITTEE:

Dr. Dean C. Webster
Chair

Dr. Mohiuddin Quadir

Dr. Dante Battocchi

Dr. Glenn Dorsam

Approved:

04/28/2022
Date

Dr. Dean C. Webster
Department Chair

ABSTRACT

Since mankind has navigated the world's oceans, marine biofouling has been a persistent problem with several negative economic and environmental consequences. In modern times, the buildup of biofouling causes a significant reduction in vessel speed, leading to increased power consumption, higher costs of operation, and an increase in greenhouse gas emissions. Two of the most widely used protection strategies to combat this highly complex and dynamic phenomenon include the application of biocide containing anti-fouling (AF), or more environmentally friendly non-toxic fouling-release (FR) coatings. Traditional FR coatings utilize low surface energy components such as polydimethylsiloxane (PDMS), but often suffer mechanical failure and poor adhesion to the substrate.

Recently, the development of a self-stratifying siloxane-polyurethane (SiPU) FR coating combined the desirable FR properties of PDMS containing materials, with the mechanically durable and tough attributes of a polyurethane. Several methods to improve on the FR properties of these coating systems involved the incorporation of hydrophilic moieties like polyethylene glycol (PEG), zwitterionic polymers, or carboxylic acid containing groups into the SiPU network, producing a heterogenous, amphiphilic surface. These types of amphiphilic surfaces have great potential to become a major component of the next generation of highly performing FR coatings.

In this work, the use of non-reactive surface modifying amphiphilic additives (SMAAs) consisting of PDMS and PEG was explored as a viable method for further improvement of FR properties of SiPU coatings, while also maintaining coating integrity in marine environments. Additives with varying amounts of PDMS and PEG content were incorporated at several concentrations in both hydrophobic, and inherently amphiphilic SiPU FR coating systems. It was shown that these additives significantly alter the surface properties and morphology, producing surfaces that improve AF/FR performance against several model marine fouling organisms. The methodologies used for these types of coatings were also applied to a non-FR, polyurethane coating. This allowed for a more fundamental investigation into how these SMAAs are distributed throughout a coating system, and how FR properties arise. Lastly, commonly used FR coatings, including SiPUs, were applied to oil boom fabrics to observe their effect on FR properties and cleanability.

ACKNOWLEDGMENTS

As my time as a doctoral candidate is ending, I've been reflecting on all the wonderful experiences I've had at the Department of Coatings and Polymeric Materials here at North Dakota State University. I want to personally thank everyone that has been a part of this department over the years of my education. The close-knit relationship that students have between themselves, along with the friendliness of professors and associated staff have been a blessing. This department is truly unique and provides a nurturing environment for those who wish to pursue the grand complexities of coatings and polymeric materials.

I would like to extend a special thanks to my advisor Dr. Dean C. Webster. Your continual support of my academic endeavors, as well as your mentoring and guidance throughout my research work is greatly appreciated. I'll never forget the first time we first discussed the field of polymers and coatings. I was looking to perform research in the CPM department as an undergraduate researcher and from that moment, I was hooked. My experiences in your research group for the last 6 years have been life-changing, and your approach to research, and this field in general, has shaped me into the scientist I am today. It has been a privilege and an honor to be your student and I wish you all the best in your future endeavors.

To my supervisory committee members, Dr. Mohiuddin Quadir, Dr. Dante Battocchi, and Dr. Glenn Dorsam; thank you for your contributions to my continual growth and education as a doctoral student throughout my time at the CPM department. Dr. Quadir, it was a pleasure having your office close to my workstation. I was always grateful for the discussion about research, science in general, and career paths in the field of coatings and polymers. Dr. Battocchi, thank you for your advice on presenting research more clearly throughout several of my seminars. It will be very helpful moving forward with my career. Dr. Dorsam, your insight and comments during the original research proposal process helped me understand how to communicate a research idea to a broader audience.

To my parents and my family, I would like to thank you for never stopping the overwhelming support you have for me. Dad, you helped shape me into the man I am today, and for that I am eternally grateful. I would say that 90% of my sense of humor comes directly from you and that is something that can never be taken away. You helped teach me integrity, humility, and honesty, which I try to incorporate

into everything I do. Mom, your ceaseless love, and kindness throughout my life is something I can never repay. I save every one of your ‘special cards’, and will, for as long as I am able. To my siblings, thank you for all your support during my journey at NDSU. It is always a fun time when we all get together to visit mom and dad. To my sister Mary, I cannot thank you enough for enabling me to pursue my education, while living a comfortable life in the apartment we share. Thank you for helping me both physically and mentally through the most difficult part of my life. I’m not sure what I would’ve done if you weren’t there.

To my mentors, Dr. Teluka Galhenage and Dr. Madhura Pade, I would like to thank you for helping me explore the world of coatings and polymers. You helped me understand much of the science behind this field and were never hesitant on answering my constant barrage of questions. I couldn’t have asked for better mentors to usher me into the vast and complex nature of working in the Office of Naval Research program. I would also like to express my gratitude to several other former Webster group members; Dr. Eric Krall, Dr. Arvin Yu, and Dr. Alison Rohly. Each of you helped my transition to become a full-fledged graduate student and I am very grateful. To the undergraduate and foreign scholars that have worked with me; Ryan Burgett, Jonas Sahouani, and Hayato Narikiyo, I would like to thank you for your help in finishing studies that would eventually be published. Lastly, I would like to thank both Dr. Alireza Rahimi and Raul Setien for being supportive of my graduate career in the Webster group in the CPM department. Many long days (often weeks at a time), were put in, and it was always a pleasure to be able to discuss anything with you to help unwind. I will cherish our friendship always.

I would also like to thank all the friends I have gained during my time here; Dr. Alison Rohly, Dr. Eric Krall, Dr. Teluka Galhenage, Dr. Arvin Yu, Dr. Madhura Pade, Dr. Alireza Rahimi, Raul Setien, Zachary B., Joseph D., Michael O., Marta V., Kristen P., David B., Jason S., Alex D., and many others. All of you have made the past 6 years an incredible experience.

To Jim Bahr, Shane Stafslien, Lyndsi Vanderwal, Greg Strommen, and Chunju Gu; thank you for all you support with running a multitude of characterization methods, biological assay testing, and the use of labs and equipment. I would also like to extend my gratitude to our UK collaborators John A. Finlay, Anthony S. Clare, and Nicholas Aldred for accepting and evaluating samples for several biological assay experiments. To our collaborators at the Florida Institute of Technology; Geoffrey Swain, Kelli Hunsucker,

and associated students, thank you for performing field testing measurements on oil boom samples and others I sent your way. To Janice, Ben, and Sarah, thank you for all your help with administrative duties, ordering of chemicals, group photos, and organizing the short course and several other events in the CPM department. My time here as a graduate student would've been filled with even more headaches had you not been so helpful.

Finally, I am very grateful towards the Office of Naval Research for providing the financial assistance for this research under grant numbers N00014-16-1-3064, N00014-16-1-2988, N00014-16-1-3125, N00014-20-1-2151, N00014-20-1-2248, and N00014-17-1-2153. In addition, I am thankful towards the NDSU College of Science and Mathematics for awarding me 3rd place in the annual three-minute thesis (3MT) competition, as well as PPG, BASF, Eastmann Chemical Company, and the American Coatings Association for their financial support *via* awards and scholarships.

DEDICATION

I would like to dedicate this dissertation to my parents, Stanley, and Ann Benda, for their unwavering support of my education here at NDSU. They enabled me to perform my best every day, listening to me and helping me grow as a person. I love you both and I'm eternally grateful for everything that you do. I wish you all the best.

TABLE OF CONTENTS

LIST OF TABLES

LIST OF FIGURES

LIST OF APPENDIX TABLES

LIST OF APPENDIX FIGURES

CHAPTER 1. GENERAL INTRODUCTION

Marine Biofouling – Economic and Environmental Impact

The phenomenon of marine biofouling is often defined as the undesirable accumulation of marine organisms on structures submerged in a marine environment.[1] Marine biofouling is a serious global concern for ocean-going vessels involved with the transportation of people and goods, as well for the defense of international waterways.[2] The accumulation of biofouling brings with it a multitude of negative consequences that affect many aspects of shipping operation. In most cases (depending on ship size) the contribution of frictional drag to the overall drag of a vessel with a smooth hull is upwards of 90%.[3, 4] As organisms build up on ships hulls, this produces a significant increase in roughness, which in turn, increases frictional drag, reduces maneuverability, and ultimately leads to a large increase in fuel consumption.[5, 6] This increased fuel usage also leads to elevated levels of greenhouse gas emissions, which is a major concern given the current environmental climate of the world. In addition, the organisms that adhere to ships hulls are live organisms, often causing widespread damage to the applied paint through metabolic processes. This rapid deterioration of a ships protective coating often leads to changes in ionic concentrations and dissolved oxygen concentrations near the surface of the ships hulls, resulting in aggressive corrosion.[7] Because of this, ships with extensive layers of biofouling build-up are frequently placed in dry-dock for cleaning, and resurfacing, further increasing the overall cost of operation.[8, 9] It is estimated that the United States Navy spends upwards of 56 million dollars for its midsized vessels (Arleigh Burke DDG-51 Destroyers), totaling close to 1 billion dollars over a period of 15 years.[4] Lastly, many of the ocean-going vessels travel to several different parts of the world. This can lead to transfer of non-native invasive species that could result in dire consequences for not just local marine ecosystems but could have effects on human health as well.[8, 10] To begin to address the problems caused by this phenomenon, a closer look at the process, with the interactions between substrate and organism, must be performed.

Mechanism of Biofouling

The complex and dynamic nature of marine biofouling makes it a difficult problem to address for several reasons. It has been estimated that there are over 4000 different fouling species which can take part in this process.[1] General classifications of these organisms include micro-foulants such as marine

bacterium, diatom, and algae spores, with common macrofoulants including barnacles, mussels, tubeworms, bryozoans, and algae.[8, 11] These organisms all have varying methods of adhesion to submerged surfaces, that can be affected by several environmental factors such as the local water temperature, availability of nutrients, salinity, amount of sunlight, changes in current flow, and the presence of other fouling species.[11, 12] Developing solutions to this problem means addressing these factors, making an economically feasible, environmentally friendly, long-lasting approach a monumental task.

The biofouling process typically begins as soon as surfaces are submerged in seawater. A 'conditioning film' is first formed on the surface and is largely composed of an array of biomolecules such as polysaccharides, proteins, and glycoproteins.[2] This film forms the basis for the succession of other biological processes that promote the settlement and adhesion of a wide variety of different fouling species. Figure 1.1 details a simplified, time-dependent model of this process.

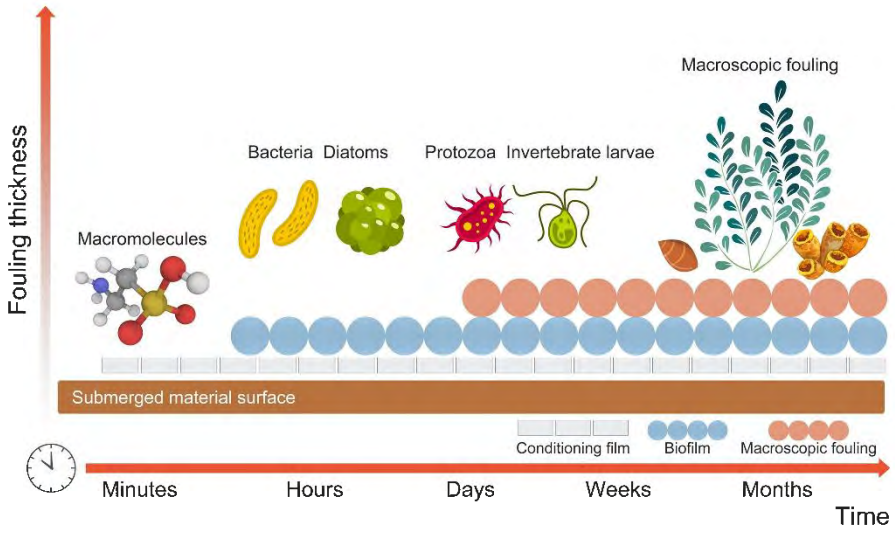

Figure 1.1. Timeline of biofouling settlement and adhesion on a substrate submerged in seawater. Reproduced from reference 13.[13]

Within seconds, microfouling organisms such as marine bacteria and diatoms are often the first to settle on the surface, forming colonies, and contributing to the growth of a biofilm.[2, 8, 14] The growth of these biofilms is further complimented by a biochemical signaling phenomenon referred to as Quorum Sensing (QS).[15] This mechanism is a way for microbiological communities to communicate between individuals, and the colony as a whole, to respond to environmental stresses, and also assist in the adhesion to surfaces for better chances of survival.[15] In the following minutes to hours of immersion, there

is continued biofilm growth, with an increasing number of soft fouling algae spores, sponges, tunicates, and eventually hard macrofoulers such as barnacles, mussels, tubeworms, and bryozoans attaching to the surface.[1, 12, 16] Although this chain of events is often seen as linear, these different settlement and attachment processes can occur parallel with each other, as well as some process like macrofouling seaweed, barnacle, and bryozoans attachment occurring earlier in the process, with some even before biofilm formation.[17-20] Therefore, this biofouling process should be seen as a complex, dynamic interaction between the many thousands of fouling organisms and substrates immersed in marine environments.

Another consideration for the mechanism of action for marine biofouling, is the varying composition of adhesives secreted by these organisms, as well as their surface preferences. Several marine bacteria, including the gram negative *Cellulophaga lytica* adhere to surfaces *via* extracellular polymeric substances largely composed of polysaccharide fibrils.[16, 21] The resulting biofilm growth due to intense EPS secretions enable these colonies of bacteria to adhere to a wide range of surfaces depending on the surface energy of the substrate, and several factors such as water temperature, salinity, pH, etc.[22-24] Other microfoulants such as marine diatoms, including *Navicula incerta*, also utilize secretions of EPS to adhere to surfaces. However, they often exhibit a primary adhesive action by secreting small amounts of EPS, and along with van der Waals and electrostatic interactions, form a temporary adhesion to the substrate. Then, a reorientation process takes place to enable the irreversible, secondary adhesion by excess secretion of EPS.[25, 26] These types of microalgae tend to prefer settlement and adhesion on surfaces with lower surface energies, particularly those with large concentrations of silicon containing compounds.[25, 27] Macrofouling algae like *Ulva linza* have yet another method for settlement and adhesion to substrates submerged in seawater. Zoospores of *U. linza* remain static in the nearby water column until a surface suitable for settlement is found. Through turbulent forces, these zoospores secrete adhesive molecular substances that provide initial attachment to the surface. Then, metamorphosis into sporelings occurs which further strengthens their adhesion to the substrate. These organisms have been shown to prefer more hydrophobic surfaces for initial zoospore attachment, but subsequent sporelings display a stronger adhesion to higher surface energy, hydrophilic surfaces.[28, 29] Lastly, adult marine barnacles *Amphibalanus amphitrite* and marine mussel *Geukensia demissa* secrete special adhesive blends consisting of several different combinations of barnacle cement proteins and

dopamine based mussel foot proteins respectively.[30, 31] In addition, it was shown that these organisms tend to prefer hydrophilic, or higher surface energy, substrates.[32, 33] It is clear to see that there is a multitude of environmental, substrate, and species related factors involved in the settlement and adhesion of marine biofoulants, making it very difficult to engineer surfaces that offer broad spectrum performance for the prevention of this undesirable accumulation.

Methods of Fouling Protection: Anti-Fouling Coatings

The term 'Anti-fouling' often carries several different meanings. In this context, it is best described as the prevention of marine biofouling buildup by reducing the number of organisms able to adhere to the substrate. This has been accomplished through a variety of methods since humanity began to navigate the world's oceans. The hulls of wooden ships were typically lined with protective alloys of copper or lead, while other methods utilized coatings of tar, wax, or asphalt admixtures that produced an inhospitable environment for marine organisms.[34, 35] As changes in ship-building technology shifted towards the use of iron and steel for the construction of ship hulls, the use of alloy sheaths of differing composition results in galvanic corrosion, damaging hulls, and making the use of these methods a non-viable option.[35] Therefore, some of the earliest anti-fouling (AF) paints consisted of the dispersion of toxins, later referred to as biocides, into natural resin binders such as linseed oil, tar, and rosin. At the start of the 1950s, advances in polymer resin technologies resulted in the development of binders that could control the release of dispersed biocides, resulting in a more effective method of AF protection.[34, 35] A representation of these types of paint systems is shown in Figure 1.2.

These biocide-containing, controlled release AF paints were used extensively, with organotin compounds such as tributyl-tin (TBT) being the most effective.[1, 9] As fouling organisms would attempt to settle onto surfaces coated with these TBT-containing paints, they would die rapidly, therefore preventing the initial attachment of these foulants. However, concerns over the highly toxic nature of TBT towards non-target organisms in the marine environments, as well as dangers posed to humans, led to restrictions on their usage in 2003, with an outright ban on TBT-based AF paints in 2008 by the International Maritime Organization (IMO).[8, 36-38] Because of this, research has been focused on developing alternatives to the use of these highly toxic AF paints.

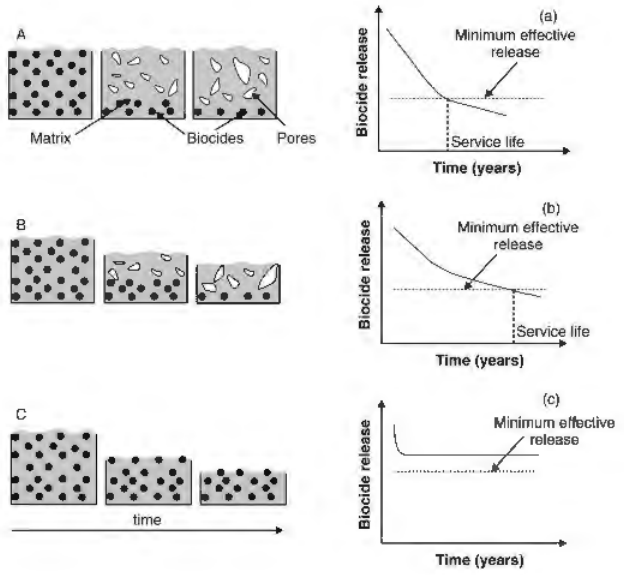

Figure 1.2. Detailed graphic showing the kinetic properties of three common controlled release AF paints. (a) Contact leaching coatings; (b) Controlled depletion coatings; Self-polishing coatings. Reproduced from reference 39.[39]

As an early replacement for TBT-containing AF paints, copper and zinc containing compounds such as copper oxide, zinc oxide, or zinc pyrithione were blended into paint formulations and used to great effect.[8, 40] In addition, there are several organic biocide 'boosters', or 'co-biocides', that are commonly used in these types of AF paints to help deter copper resistant organisms, and consist of Dichlofluanid, Tolylfluanid, Sea-Nine 211, Zineb, Irgarol 1051, and Selektope.[8] Although AF paints incorporating these biocides performed well, there is still much concern over their leaching into local marine environments, continuing to cause widespread damage to marine life outside of target fouling organisms.[41-43] Therefore, development of more eco-friendly biocides, along with the investigation of several different approaches to provide surfaces with AF behavior have been explored.

An attractive source for novel, eco-friendly AF compounds is found in several marine organisms such as coral, algae, and wide variety of microorganisms.[44, 45] Several compounds extracted from these organisms such as steroids, terpenoids, phenolics, alkaloids, and peptides have shown anti-fouling activity in laboratory studies, with a majority being derived from sponges and coral.[46-49] In one study, 36 different species of Indian sponge were evaluated for anti-fouling activity against common fouling bacteria, as well as cyprid larvae of the marine barnacle *Balanus amphitrite*. It was observed that several species showed high inhibitory activity towards biofilm growth, and resisted settlement of cyprid larvae.[50] Work has also been performed investigating the extracellular polymeric substances (EPS) of 9 different

bacterial strains for their AF properties against the growth of other bacterial biofilms. The bacterial extracts of the strain associated with *Pseudomonas taiwanensis* showed high levels of toxicity towards competing biofilms and offers a promising mixtures of compounds for use as biocides.[51] Despite the potential for a wide range of bio-derived, eco-friendly biocides, there are still issues such as feasibility in the extraction of these components, whether they can be synthesized for scale up operations, as well as strict regulations enforced on the introduction of new biocides into paint formulations.[8, 52]

Another approach towards generating an AF surface involves the manipulation of the topographical features of the substrate and coating itself, without the use of biocides. Inspiration for this method of AF protection is largely attributed to strategies utilized by several marine organisms, often referred to as bio-inspired, or bio-mimicked surfaces.[53] These organisms typically employ combinations of chemical, physical, mechanical, and behavioral methods that produce AF surfaces. Figure 1.3 details some of the representative surface topographies from various marine organisms.

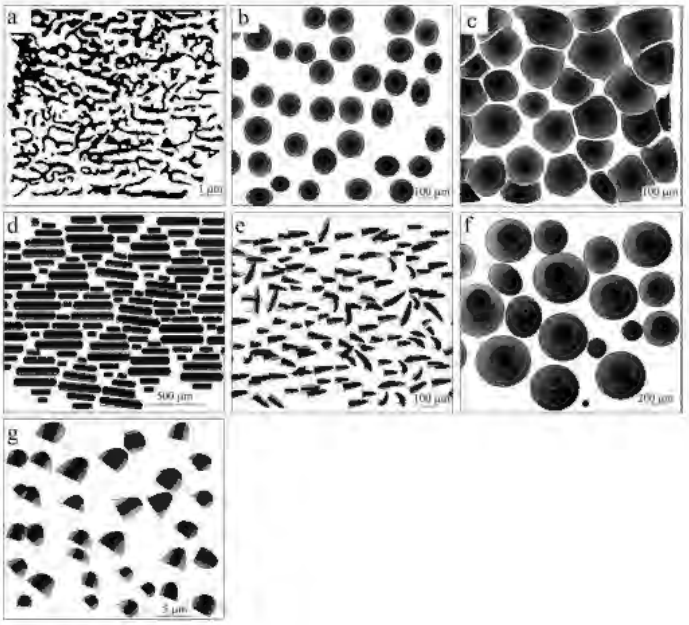

Figure 1.3. Illustrations of surface topographies from varying marine organisms. (a) Pilot whale *Globicephala melas*, (b) and (c) sea stars *Cryptasterina pentagona* and *Archaster typicus*, (d) Galapagos shark *Carcharhinus galapagensis*, (e) yellowfin leatherjacket *Triacanthus blochii*, (f) and (g) crab carapace *Cancer pagurus*. Reproduced from reference 53.[53]

One of the most studied of these topographies has been related to sharkskin mimicking surfaces. Sharkskin was initially investigated for it promising drag-reducing properties in the late 1990s to early 2000s.[54, 55] Surfaces from PDMS elastomers were explored, with the typical patterns resembling the

riblets of shark placoids, albeit at much smaller size scales, with ridges of riblets being 4 µm high, 2 µm wide, and spaced 2 µm apart.[56] These Sharklet AF™ surfaces were shown to reduce the settlement of *Ulva* spores by as much as 86% compared to smooth PDMS. When compared to surfaces which had channels, triangles, pits, and ridges of varying height and spacing, it was observed that not only did Sharklet AF™ patterned surfaces have lower overall settlement, even minor changes in spacing or type of pattern, increased settlement of spores by over 150% compared to a smooth PDMS surface.[57, 58] Other studies have been performed to investigate AF properties towards other species of marine foulants such as cyprids of *Balanus amphitrite*. Here, it was shown that the typical pattern based off sharkskin was not well optimized for these cyprid larvae, with the optimal height of ridges being as high as 40 µm.[59] This highlights one of the potential drawbacks for utilizing bio-inspired surfaces. Nature is incredibly proficient at reproducing extraordinarily complex topographies that suit the needs of the organism. In practice, it is difficult to replicate these systems and leads to a lack of broad-spectrum AF performance. In a more recent study, the patterning of a PDMS substrate was approached utilizing a different method. Sharkskin tissue samples were obtained from four separate locations on the body of shortfin mako shark specimens. After preparation of these tissues, a mold of the surface was made from PDMS, and further used to prepare polymethylmethacrylate (PMMA) replicas.[60] A graphical representation of this process is shown in Figure 1.4.

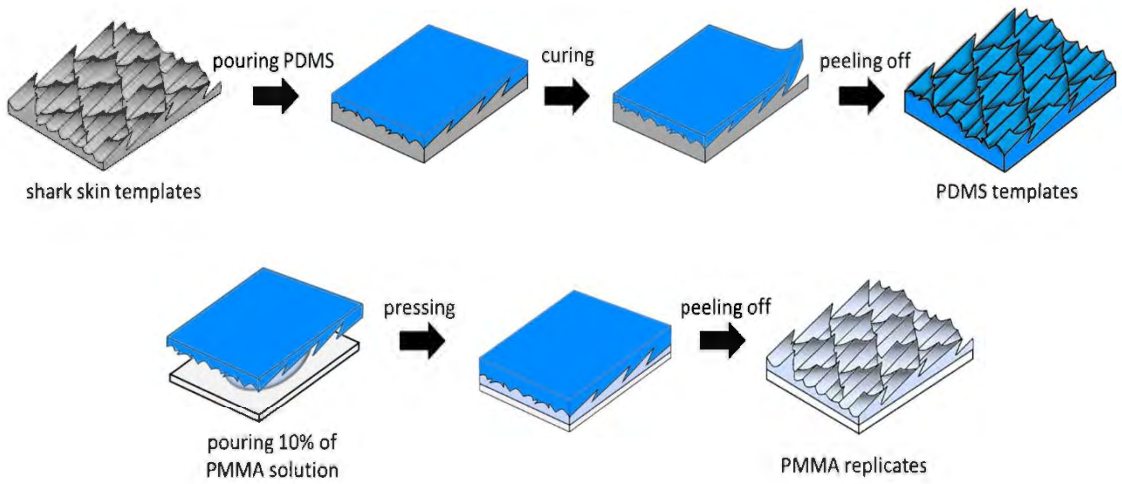

Figure 1.4. The process of creating sharkskin patterned replica using PMMA. Reproduced from reference 60.[60]

It was observed that the process of making these replicas was very efficient, with only minor defects due to material preparation. The settlement of bacteria was promoted at the earliest stages, especially with smoother sections of replicated sharkskin surfaces. However, as roughness increased, so too did hydrophobicity of the patterned surface, leading to a significant inhibition of biofilm growth.[60] Although it has been shown that surface topography significantly affects settlement of several marine organisms, there are still questions on the feasibility and practical nature of producing these types of surfaces for large-scale AF operations.

Other sources of bio-inspiration stem from the plant kingdom. Investigations into the microstructures present on the lotus leaf have uncovered their potential for producing AF capable surfaces.[61-64] Surfaces modified with these types of structures are often superhydrophobic (water contact angles >150°), which results from air that is trapped in between these microstructures due to the differences in roughness of surface features. This is phenomenon is described by the Cassie-Baxter and Wenzel equations and can be seen in Figure 1.5.[65, 66]

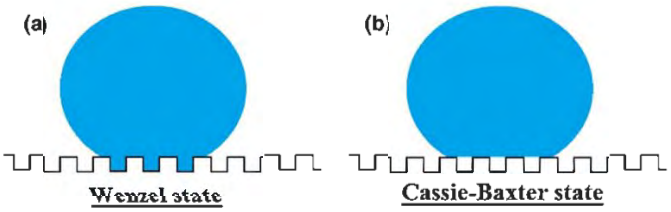

Figure 1.5. A water droplet shown in the (a) Wenzel state, and the (b) Cassie-Baxter state. Reproduced from reference 67.[67]

Much of the work involved in replicating these types of surfaces for practical use are concerned with preserving the Cassie-Baxter state, which is not stable when submerged, retaining superhydrophobic properties that contribute to AF performance.[14] Another plant-inspired avenue of AF research is that of the *Nepenthes* pitcher plant. It was shown that as insects would move closer the rim of its peristome, the surface would become extremely slippery, and they would fall into the plant's digestive juices.[68] This is due to a combination of micro/nanostructures, surface roughness, and the slippery liquid that infuses the surface. A representation of these types of surfaces is shown in Figure 1.6. Work to engineer these slippery liquid infused porous surfaces (SLIPS) with these characteristics involves the generation of a micro/nanoporous surface through a variety of chemical and physical means. Then, suitable liquids such as silicone or fluoropolymer oils are used to infuse these materials.[69] These surfaces have shown

significant reductions in biofilm growth, as well as reduction in settlement of macrofoulers such as marine barnacles and mussels.[70, 71] Some practical challenges to using SLIPS are overcoming the difficulty in adhering these materials to substrates used in marine environments, as well limiting the depletion of the infused liquid, which results in a loss of AF performance.[13]

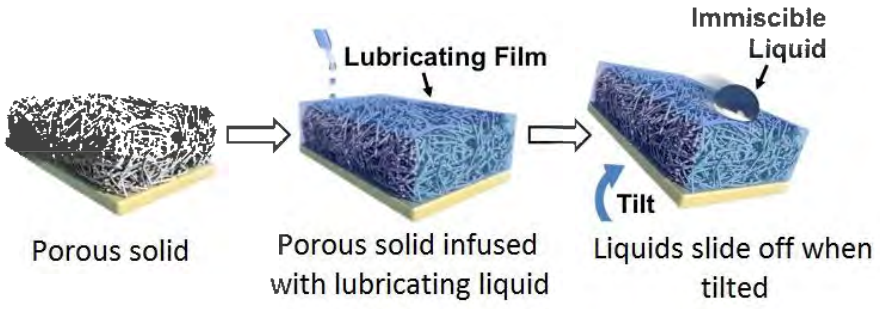

Figure 1.6. Representation of SLIPS. Reproduced from reference 69.[69]

Lastly, much work has been devoted to understanding the AF capabilities of hydrophilic/charged surfaces made up of self-assembled monolayers[72-76], hydrogels[77-79], or polymer brushes[80-82].[13, 83] Two of the most researched polymeric materials in this work are polyethylene glycol (PEG) and zwitterionic species such as sulfobetaine, carboxybetaine, and phosphorylcholine.[83] These materials are highly protein resistant, which is an integral component in the adhesives of marine organisms.[2, 16] There are a couple common reasonings behind the AF effectiveness of these materials. One reason is that there is a physical/energetic barrier that results from these moieties on the surface of these substrates. This is largely due to the formation of a hydration layer that makes the disruption of water molecules, necessary for spreading of many organisms' adhesive substances, thermodynamically unfavorable (Figure 1.7).[13, 84] While PEG composed surfaces provide a sufficient hydration layer to confer protein resistance, zwitterionic polymers bind more water molecules, and bind them more tightly, to produce a more effective AF surface character. Another reason is due to the steric repulsion these surfaces present, which serves to prevent large, globular proteins from properly rearranging onto surfaces. Despite the promising attributes that these hydrophilic/charged surfaces have towards fouling-resistance and overall AF properties, there are still several concerns with their mechanical durability, long-term AF effectiveness, and practical application on ships hulls in harsh marine environments.

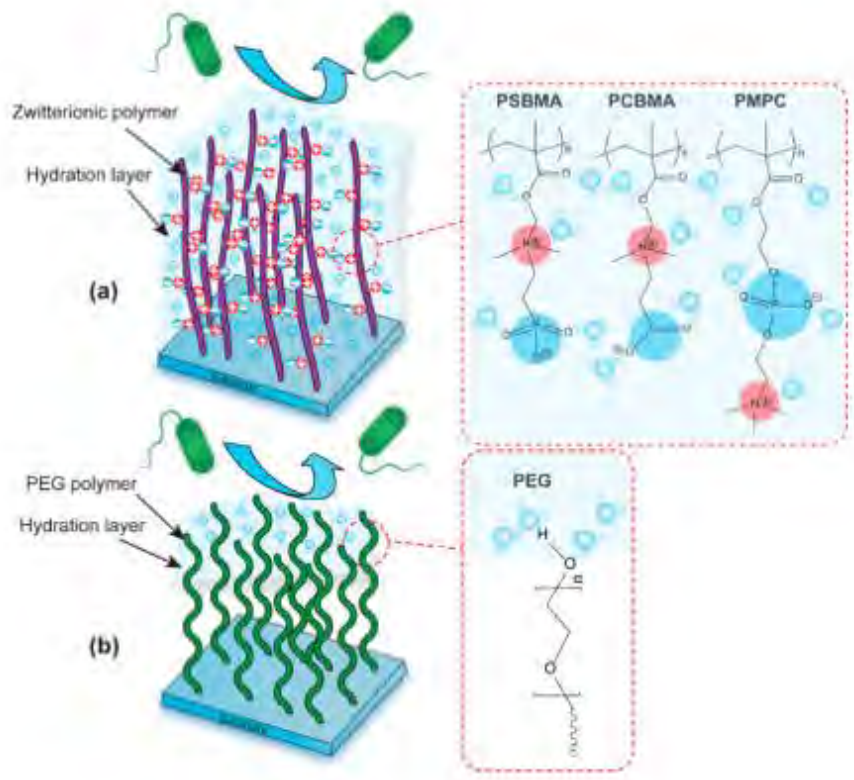

Figure 1.7. Diagram detailing the hydration layer formation for PEG and zwitterionic based materials. Reproduced from reference 85.[85]

Methods of Fouling Protection: Fouling-Release Coatings

Other efforts to reduce the use of toxic, biocide-containing AF coatings, are focused on developing fouling-release (FR) coatings. Traditional coatings of this type were primarily focused on providing surfaces that do not necessarily prevent the attachment of marine organisms, but instead, aim to weaken the adhesion of a broad range of fouling organisms, facilitating their removal by hydrodynamic forces (i.e. movement of ships or cleaning with directed water pressures).[2, 8, 83] However, as will be discussed later on, much of the recent advances in this area of research have been able to provide surfaces that display some AF properties, becoming 'fouling-resistant'. Some of the advantages to using FR coatings over biocide-containing AF coatings include their potential for long service times (5-10 years), unaffected by biocide legislation, speeding up the implementation process, added fuel efficiency and savings due to ultrasmooth surfaces reducing drag forces, and also requiring only one layer of top-coat as opposed to several for traditional AF paints.[8]

It has been well established that a range of parameters involving the surface energetics of a system significantly affects the strength of bioadhesion from marine organisms. A combination of

chemical group composition, presence of moieties that prevent electrostatic and physical adsorption interaction from bioadhesives, manufacturing methods that generate surfaces which make mechanical spread of adhesive difficult, and materials that resist the diffusion of adhesive through the surface all play an important part in developing an effective FR coating system.[8] Perhaps one of the most influential factors in determining the effectiveness of a surface to be fouling-release, is the critical surface tension (γ_C). Investigations into this critical surface tension and its effects on bioadhesion were performed by Robert E. Baier. It was determined that there was a minimum in relative bioadhesion between 22-24 mN/m, with polymers that have critical surface tension values falling between 20-30 mN/m achieving desirable FR properties (Baier curve, Figure 1.8).[86]

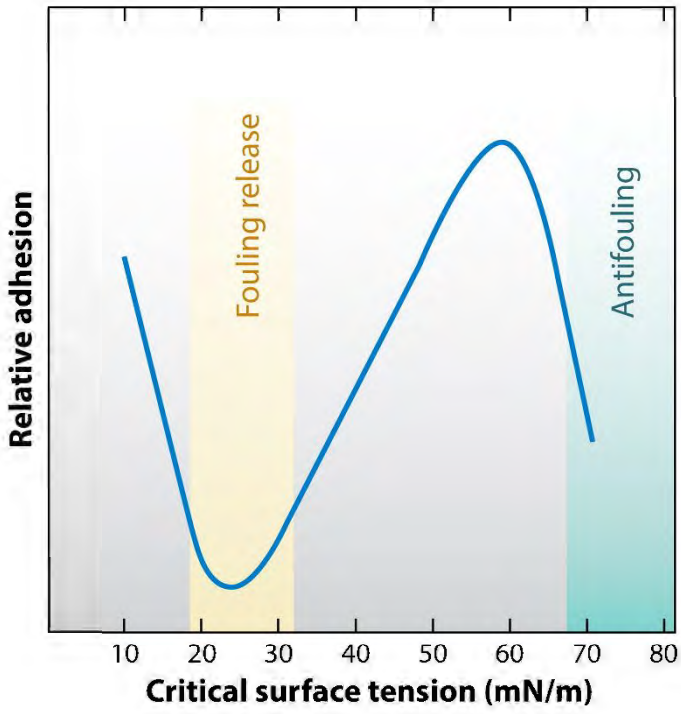

Figure 1.8. Representation of the Baier curve, showing the range of critical surface tension of surfaces with desirable FR properties. Reproduced from reference 83.[83]

While this empirical relationship had been determined, there are several classes of materials that fall outside of this range such as superhydrophilic surfaces, self-assembled monolayers via hyperbranched structures, or amphiphilic surfaces that will be discussed later in this chapter. Other factors such as thickness and modulus of coatings systems also play a key role in their ability as effective FR systems. In general a lower elastic modulus of the surface results in a decreased critical force of removal for adhered marine organisms.[8] Coatings that have lower modulus values are typically made up

of polymer chains that more flexible and mobile, able to rearrange at the surface in response to external stresses, resisting the mechanical and diffusion mechanisms seen during the spreading of bioadhesives.[87, 88] For thicker coatings, it was observed that there was an overall lower removal force, resulting from weaker adhesion to the coating surface, for several marine organisms.[29, 88, 89] However, in practice, it is a combination of thickness, low modulus, and low critical surface tension on the surface of FR coatings that provides optimal broad spectrum protection. Two main groups of materials that can achieve these properties are silicone and fluorine-containing polymers.

Silicone-Based Fouling-Release Coatings

Polydimethylsiloxane (PDMS) has many advantages compared to other materials when used in a FR coating system. These types of coatings are typically formed through room-temperature condensation, or platinum-catalyzed hydrosilylation reactions to form PDMS elastomers which have relatively low crosslink densities (Figure 1.9).[8, 34]

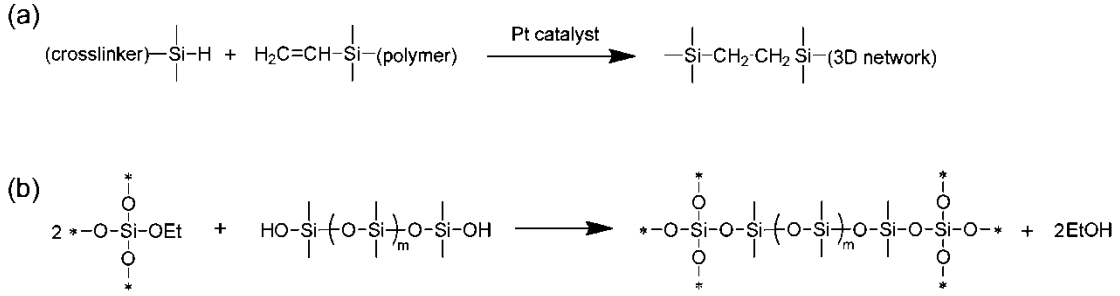

Figure 1.9. (a) Hydrosilylation curing mechanism of silicone elastomers. (b) Condensation curing mechanism of silicone elastomers. Reproduced from reference 90.[90]

The resultant coatings have surface tensions of ~22 mN/m, low elastic modulus values of ~0.5-5 MPa, are resistant to heat and UV degradation, and highly flexible, being very processable and applicable to a wide range of surfaces.[8, 34, 90] Due to these highly desirable mechanical and FR properties, several commercially available PDMS elastomers such as Silastic®T2, Sylgard®184 and RTV11, have been utilized as standards for comparison of newly developed FR coatings. In addition, commercial FR coatings based on silicone elastomers have been developed by companies such as Hempel, Akzo Nobel International Paint, PPG, and Sherwin-Williams, and have seen global use on a variety of vessels and vessel sizes.[8]

Fluorine-Based Fouling-Release Coatings

Fluoropolymers are another attractive material for use in FR coatings due to similar characteristics as silicone-containing polymers, but have significantly lower critical surface tension values of ~10-20 mN/m, a lower coefficient of friction (useful in reducing drag forces), as well as excellent chemical, UV, and heat stability.[8] One of the first patented fluoropolymer systems was the use of polytetrafluoroethylene (PTFE) to cover ships hulls.[91] Other methods included the use of highly fluorinated epoxy and polyurethane coatings, which displayed excellent FR properties and cleanability over a period of 13 years.[8] More recent work has been focused on the use of perfluoroalkyl containing copolymers, perfluoropolyether polymers, and polyethylene glycol-fluoropolymers.

Siloxane-Polyurethane (SiPU) Fouling-Release Coatings

Although FR coatings comprised of either silicone, fluoropolymers, or a combination of both have shown exceptional performance towards the removal of marine organisms, there are several disadvantages that make it difficult to compete with other, more established biocide-containing AF paints. These FR coatings, due to their rubbery nature, are often easily damaged from several means. Mechanical durability is especially important in a marine environment, where a loss of coating leads to an aggressive build-up of marine organisms. They also exhibit poor adhesion to many substrates, often require a 'tie-coat', which is applied before the FR top-coat to promote adhesion to the subsequent layers. A loss of adhesion would again lead to loss of performance, necessitating the need for increased dry-dock time, and increasing the cost of operation. The relatively high cost of using these materials, as well as their potential for leaching unreacted species into local marine environments (fluoropolymers being very detrimental to human and marine life) restricts their use in many cases. In addition to these physical aspects of using FR coatings based on these materials, it has been observed that several marine organisms show a preference to settling on hydrophobic surfaces, as well as seeing a significant build-up of fouling species in static conditions, highly the poor AF properties of these systems.[27, 92, 93] A novel coating system involving the self-stratification of a siloxane component to the surface of a polyurethane bulk matrix was thus developed at NDSU to address some of these concerns (Figure 1.10).

The main components of these siloxane-polyurethane (SiPU) FR coatings include a polyisocyanate, acrylic polyol crosslinker, amine-terminated PDMS, catalyst, and a pot-life extender.

Several studies were performed to develop an optimized formulation, investigating the effect of mixing time, stoichiometric ratios of isocyanate, crosslinker, and PDMS, overall content of PDMS, etc.[94-99] These coatings displayed desirable mechanical properties, with an increase in adhesion to primed panels, without the need of a tie-coat, as well as a higher overall durability and mechanical strength compared to commercial FR formulations. In addition, the AF/FR properties were evaluated utilizing a suite of biological assays developed at NDSU, along with investigations into their performance in field immersion sites. It was observed that these coatings performed comparable, and in some cases better, than commercial FR standards towards a variety of micro- and macrofouling organisms.[100-102] Much work to further improve the AF/FR properties of these SiPUs has been continued at NDSU and is discussed further in this chapter.

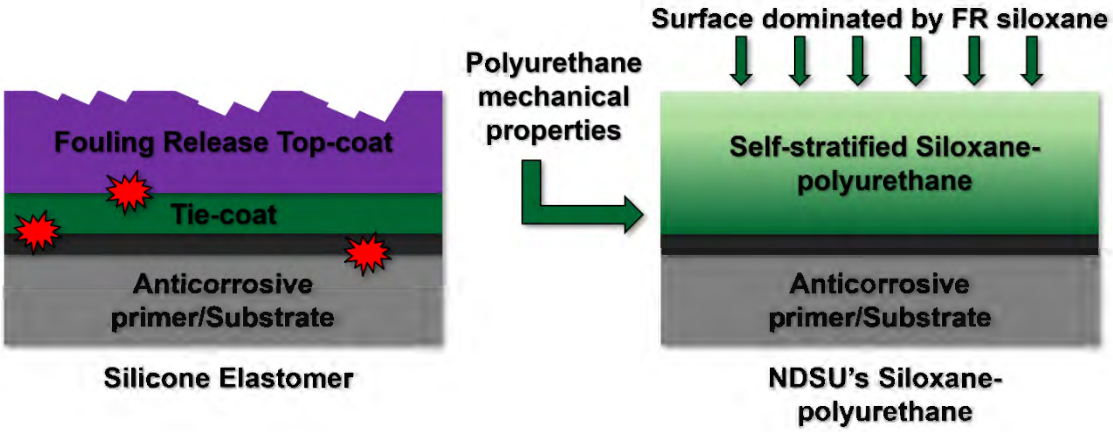

Figure 1.10. A typical FR elastomer is shown on the left, displaying signs of damage to the topcoat, with the red bubbles placed at interfaces where adhesive failure could occur. On the right is shown NDSU's SiPU FR coating, with the polyurethane bulk having good mechanical properties and adhesion, with desirable FR properties on the surface due to the presence of PDMS.

Hybrid Coatings for Fouling Protection: Generation of Amphiphilic Surfaces

AF/FR properties of surfaces submerged in marine environments are significantly affected by several factors such as surface energy and wettability, roughness, micro/nanoscale patterns, presence of several chemical moieties, mechanical and physical properties including modulus and thickness, as well as the environment surrounding these surfaces.[2] Additionally, the methods of which marine organisms foul submerged structures, as well as the chemical makeup of their bioadhesives, are highly complex, making for a very dynamic process. Developing a fouling protection system that can perform in a variety

of environments, on several different substrates, and provide broad-spectrum AF/FR performance to a wide range of organisms is the ‘holy grail’ of this area of research.

Biocide-containing AF paints were first introduced to tackle this challenge, and proved to be very effective with a number of different controlled release coatings, along with several effective biocide compositions.[1] Concerns over their highly toxic nature has motivated researchers to pursue other avenues of AF coatings that involve more eco-friendly naturally derived biocides, and surfaces which are composed of (super) hydrophilic groups that offer excellent protein/fouling resistant properties. But, the prohibitive cost, and long timeline for new biocide development, coupled with lack of removal performance if organisms end up adhering to these substrates has drawn concerns for viability of these newer generation of AF coatings. Fouling-release coatings are another form of fouling protection which utilizes non-toxic, surface modifying strategies to weaken the adhesion of fouling organisms, making it easier to remove them under light hydrodynamic pressures. However, it was observed that these types of coatings perform poorly under static conditions, quickly building up a layer of biofilm ‘slime’ that is more difficult to remove, reducing performance.[8] Also, these coatings are typically hydrophobic, which some organisms prefer to settle on, making it a challenge to attain broad-spectrum fouling protection performance.[11, 34] This preference for surface is seen across many other marine fouling organisms, due in large part to the heterogenous, amphiphilic makeup of bioadhesives.[8, 90, 103] Therefore, a significant research effort is now focused on developing heterogenous, amphiphilic surfaces, which combine the protein and adhesion resistance of hydrophilic moieties, with the superior fouling removal properties of hydrophobic moieties (Figure 1.11).

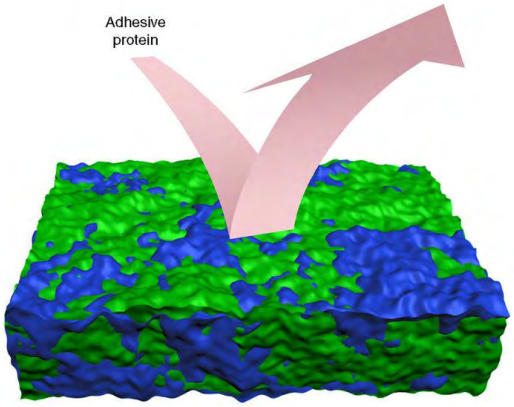

Figure 1.11. Representation of a ‘mosaic-like’ heterogenous amphiphilic surface. Reproduced from reference 2.[2]

Polymeric materials are often utilized to significant effect during the development of these amphiphilic surfaces. The choice of polymeric material used to generate a heterogenous, amphiphilic surface is of utmost importance. The hydrophobicity/hydrophilicity, polar or non-polar attributes, the molecular characteristics such as flexibility, chain mobility, resistance to environmental degradation, as well their charged character are just some of the characteristics investigated.[14, 103] Some of the ideal candidates include using PDMS and fluoropolymers for the hydrophobic component, while PEG and zwitterionic polymers are used as the hydrophilic component.[103] As a result of the early work dedicated towards these amphiphilic surfaces, several commercially available paint formulations such as Intersleek® 900 and the improved slime-release formula, Intersleek® 1100SR are offered by International Paint. Hempel has also developed its own line of amphiphilic coatings with the introduction of Hempasil X3+, a silicone-based hydrogel. A brief outline of the historical development of these heterogenous, amphiphilic coating systems, along with some of the more recent research approaches, is discussed.

Three common methods are typically used to produce an amphiphilic surface: 1) The use of amphiphilic copolymers as the base material or reacted within a coating matrix to form a composite; 2) Incorporation of amphiphilic, surface active copolymers as additives in coating systems; 3) Grafting of amphiphilic moieties directly to surfaces. One of the initial investigations into the AF/FR properties of amphiphilic surfaces involved a system of hyperbranched fluoropolymer (HBFP) and linear polyethylene glycol (PEG) composite coatings.[104] The amount of PEG incorporated into the hyperbranched structure was varied, with the highest concentration being ~55 wt.% in the network. These copolymer compositions were grafted onto the surface of glass slides functionalized with (3-aminopropyl)triethoxysilane (3-APS), and the surface and AF/FR properties were evaluated (Figure 1.12).[104] It was observed that the surface tension of these coatings increased with an increase in the PEG concentration in the copolymer. In addition, the adsorption of several biomacromolecules such as bovine serum albumin (BSA), and lipopolysaccharides was evaluated and determined that as the surface character became more heterogenous (~45% PEG in the copolymer had optimal properties), resistance to these molecules increased.[104] During AF/FR evaluation using spores of *Ulva linza*, increasing amount of hydrophilic PEG in the copolymer composition also decreased spore settlement, with the HBFP-PEG-45 formulation retaining desirable removal properties.[104] The efficacy of these copolymer films with respect to AF/FR

properties is thought to arise from the dynamic nature of the amphiphilic surface. The phase incompatibility between the fluoropolymer and PEG portion results in heterogenous separation, providing a surface which undergoes local rearrangements in response to changes in environment.

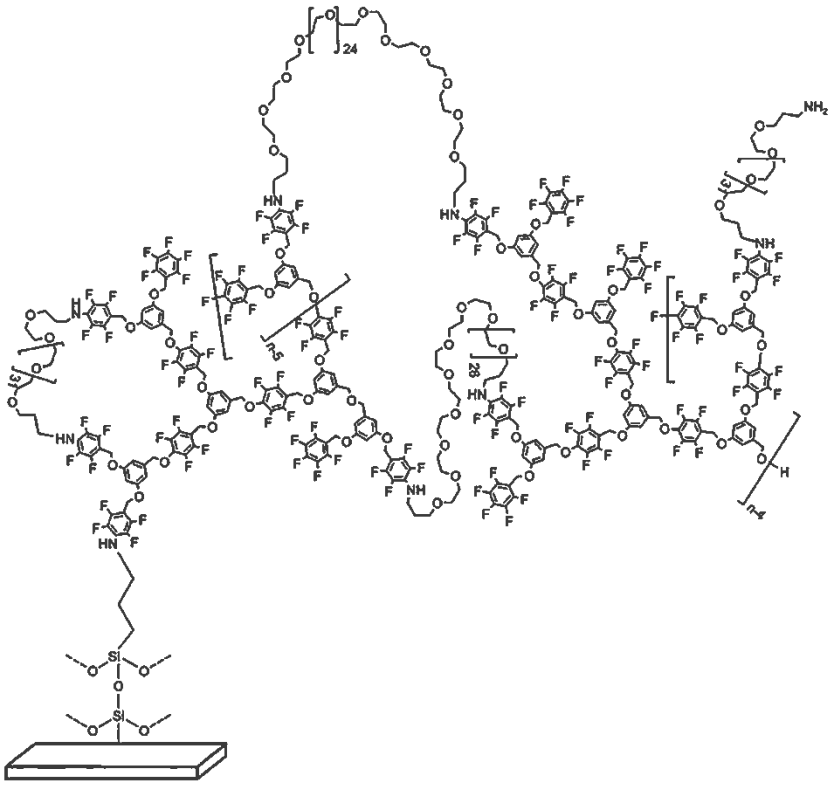

Figure 1.12. Diagram of a hyperbranched fluoropolymer-PEG copolymer. Reproduced from reference 103.[103]

Several studies were performed following this work and were mainly concerned with increasing the mechanical durability of these grafted copolymer films, evaluating their AF/FR performance against other organisms such as marine barnacle cyprids and microalgae diatoms.[105-108]

Synthesis of surface-active block copolymers (SABC), and their subsequent use with poly(styrene-block-ethylene-random-butylene)-block-poly(styrene) (SEBS) thermoplastic elastomers is another method that was initially investigated for the generation of amphiphilic surfaces.[103] In one study, amphiphilic side chains containing fluoroalkyl and PEG segments and were copolymerized with styrene to form an surface-active block copolymer.[109] Polymer films were prepared, with a SEBS-based bottom layer, and the SABC as the top layer. Advancing and receding contact angles, as well as captive bubble contact angles were measured, and it was observed that the surfaces with SABC as a top layer had a

large contact angle hysteresis (~60°), with captive bubble contact angles decreasing from 55°, to 31° after two weeks of immersion.[109] Near-edge X-ray absorption fine structure spectroscopy (NEXAFS), along with angle-resolved X-ray photoelectron spectroscopy (XPS), were used to demonstrate how the surface composition changed upon addition of the SABC, as well as providing the basis for a mathematical model that helped to explain the self-segregation and surface rearrangement of the fluoroalkyl component of the SABC (Figure 1.13). AF/FR properties of these films were evaluated with two different species of algae, each preferring either a hydrophilic or a hydrophobic surface. Results from these assays showed that there was significantly greater percent removal for the generated amphiphilic surface compared to a glass substrate, and PDMS, demonstrating their effectiveness in fouling protection.[109]

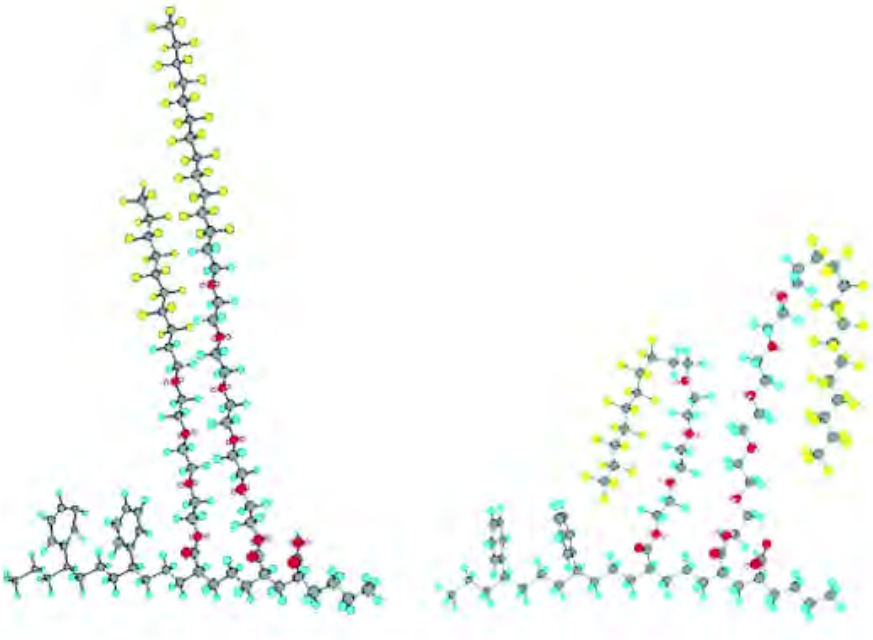

Figure 1.13. The proposed structures that result from surface rearrangement of the fluoroalkyl segment of the SABC. The structure on the left indicates the polymer/air interface, while the structure on the right is between the polymer and water. Reproduced from reference 109.[109]

Another study, using SEBS copolymer as the base layer, involved the synthesis of a SABC with PDMS and PEG chains copolymerized with styrene.[110] A suite of surface characterization techniques were utilized to determine the surface composition and behavior and include advancing and receding contact angle measurements, NEXAFS, XPS, and atomic force microscopy (AFM). It was observed that the surfaces of amphiphilic polymer layers were dominated by SABC, with no presence of styrene at the surface confirmed via NEXAFS and XPS.[110] In addition, receding contact angles decreased upon greater incorporation of PEG, leading to an increase in water contact angle hysteresis, producing a more

heterogeneous surface. Resistance towards bovine serum albumin (BSA) was significantly increased upon incorporation of PEG in the copolymer, both in the dry and hydrated states.[110] In addition, the AF/FR properties towards the marine algae *U. linza* and *N. incerta* were evaluated, where polymer films which contained more amphiphilic content had significantly lower attachment, and greater removal of both species. Much of the earlier work utilizing the SABC concept was concerned with fluoropolymer containing amphiphilic surfaces. However, this work demonstrated the ability of PDMS, and PEG based systems to provide a sufficiently heterogenous surface necessary for desirable AF and FR properties of amphiphilic coating systems. Several other studies have been performed over the last decade which continue to explore these copolymer systems.[111-114]

As opposed to using surface grafting techniques, or by incorporating SABCs into solution cast SEBS based copolymer films, another method of producing heterogeneous, amphiphilic surfaces involves the incorporation of hydrophilic and hydrophobic moieties through condensation reactions, or crosslinking, into polymer matrices. This approach is highly tunable, robust, and offers a wide range of different reactive chemistries that can be tailored to a variety of different systems. One early study involving this concept utilized disilanol-terminated PDMS with several triethoxy-silane PDMS-PEG tethers to produce a crosslinked, amphiphilic network through sol-gel processing conditions.[115]

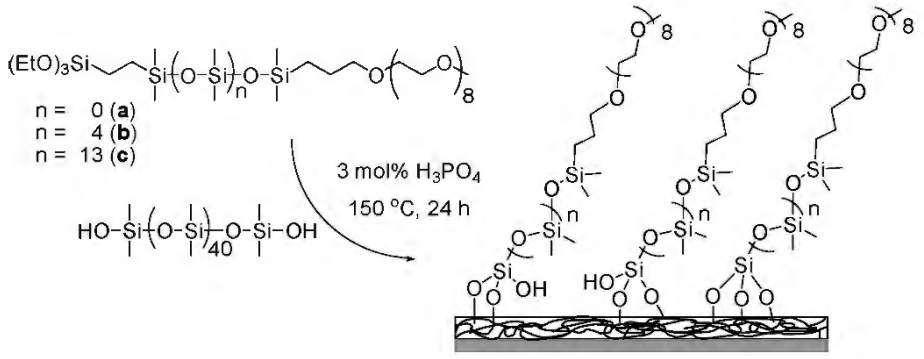

Figure 1.14. Sol-gel reaction between PDMS-PEG copolymers and a disilanol-terminated PDMS to form an amphiphilic coating. Reproduced from reference 115.[115]

Several surface characterization techniques showed that the length of siloxane tether was critical in facilitating the mobilization of PEG to the surface, increasing heterogeneity. In addition, adsorption of bovine serum albumin (BSA) was significantly reduced with these amphiphilic surfaces when compared to PDMS and polyethylene oxide (PEO) control surfaces.[115] This study provided a 'backbone' for further

studies concerned with increasing the AF/FR properties towards other fouling organisms and gave further insight into how to generate amphiphilic coatings systems via condensation/crosslinking reactions.[116-118]

Work performed by Wang *et al.* involved a UV-curable coating system composed of dimethacryloxy-functionalized perfluoropolyether (PFPE-DMA) and hydrophilic monomethacryloxy functionalized poly(ethylene glycol) macromonomers (PEG-MA).[119] Photo-cured samples were prepared, changing the ratio of PFPE-DMA and PEG-MA in the formulation, as well as changing the molecular weight of PEG on the PEG macromonomers from 300, 475, and 1100 g mol^{-1}. Surface and thermomechanical characterizations were performed, and it was observed that the length of PEG had a significant effect on surface energy, morphology, and overall flexibility of the cured samples.[119] Furthermore, amphiphilic surfaces generated through this crosslinking mechanism displayed excellent AF/FR properties towards *U. linza*, marine diatoms *N. incerta*, and barnacle cyprids of *B. amphitrite*. Again, as PEG chain length increased, reductions in settlement and adhesion were seen for these organisms, with PEG1100 having the highest overall performance.[119]

A series of hydrophobic, siloxane-polyurethane (SiPU) FR coatings were developed at NDSU during the mid-to-late 2000s (discussed previously). These coatings were to be smooth, mechanically durable, and showed excellent FR properties against a wide range of fouling organisms. However, some foulants such as the marine diatom *N. incerta* showed a high preference for settlement on these coatings, which could reduce their performance in real-world applications. To improve the AF/FR character of these SiPU coatings, the amine-terminated PDMS was functionalized with pendant carboxylic acid groups.[120] Surface characterization such as water contact angle, confocal Raman spectroscopy (CRM), and ATR-FTIR were utilized to determine presence of acid groups on the surface. In addition, AF/FR biological assays were performed using a range of micro- and macrofouling organisms. It was shown that these amphiphilic surfaces, utilizing carboxylic functional groups, were able to significantly reduce the settlement and adhesion of the marine diatom *N. incerta*. However, settlement and adhesion performance were decreased for the macroalgae *U. linza* and marine barnacle *A. amphitrite*.[120]

To improve upon this '1st-gen' amphiphilic SiPU, Galhenage *et al.* focused on the synthesis of amphiphilic pre-polymers composed of PDMS and PEG, for incorporation into a SiPU network.[121] Different concentrations of pre-polymer were incorporated into the coating matrix, with three different

PDMS molecular weights of 1000, 5000, and 10,000 g mol^{-1}, along with two different molecular weights of PEG at 550 and 750 g mol^{-1}. Surface characterization such as ATR-FTIR and XPS showed that both PDMS and PEG were seen at the surface of these coatings, with PDMS chain length having the most significant effect in surface composition.[121] Atomic force microscopy (AFM) was utilized to image surface morphology of these coatings, and it was observed that changes in the molecular weights of PDMS and PEG affected the various phase separated microdomains at the surface. Lastly, AF/FR performance was evaluated against several common marine fouling organisms. Several formulations were identified that had broad-spectrum AF/FR performance, with some even performing comparable to commercial standards Intersleek® 1100SR. The optimal formulations contained higher concentrations of prepolymer, with PDMS and PEG molecular weights of 10,000 and 750 g mol^{-1} respectively.[121] This work has been continued in the Webster group at NDSU and is discussed throughout this dissertation.

This brief look at some of the early investigations into amphiphilic coatings shows that one must consider several aspects such as the surface activity, surface functionality, surface structure, and surface reconstruction of these coatings to produce a system with practical application in mind.[103] To this end, there are several directions this body of research is currently pursuing to improve upon these amphiphilic systems. Surfaces modified with charged moieties such as zwitterionic compounds, acid functional compounds, and others, are being investigated by utilizing the formation of polymer brushes[122-124], hydrogels[125-127], surface active copolymers[128-131], and formation of crosslinked networks.[83, 130, 132-136] An example of one of these newer generation amphiphilic coatings systems is outlined by Xie *et al.*[137] In this work, a degradable amphiphilic surface was developed by UV-induced radical polymerization of a methacrylate-functional tertiary carboxybetaine ester, with 2-methylene-1,3-dioxepane (MDO), and 7-methacryloyloxy-4-methylcoumarin (MAMC) (Figure 1.15). After casting of this mixture of monomers, films were cured, and characterization of hydrolytic behavior was performed. It was observed that as samples were immersed for up to 30 days in artificial seawater, hydrolysis occurred and resulted in zwitterionic surfaces. During protein resistance and marine bacterium AF assays, surfaces showed increasing resistance as pre-immersion time in ASW was increased.[137] This is a promising route for the preparation of amphiphilic surfaces, where tuning the degree of zwitterionic character is important. However, more

work needs to be performed to investigate mechanical properties of these coatings, as well as life-time assessments.

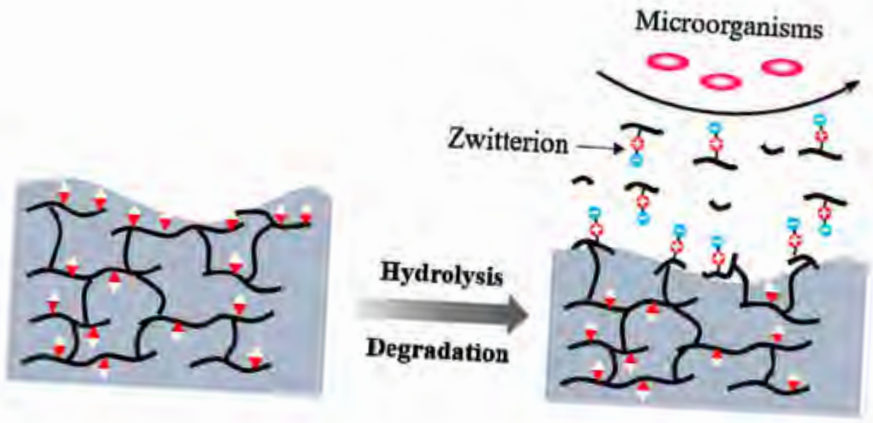

Figure 1.15. Graphical representation of the formation of a charged, zwitterionic surface after hydrolysis in artificial seawater (ASW). Reproduced from reference 137.[137]

Other amphiphilic surfaces currently being investigated include peptide-mimic (peptoid) based surfaces[138-142], amphiphilic polysaccharide containing coatings[126, 143, 144], highly durable, amphiphilic coatings[145-149], and lastly, surfaces modified *via* amphiphilic additives, especially those utilizing non-reactive copolymers.[150-153]

Surface Modifying Amphiphilic Additives

Early investigations into improving the performance of FR coatings systems involved the use of several types of non-reactive additives, commonly referred to as 'silicone oils'.[34] These additives were blended into a range of silicone elastomers, segregating to the surface/air interface upon curing, providing a 'lubrication layer' that greatly decreased the attachment strength of a wide range of marine organisms.[8, 154-156] While these types of coatings were used to great effect, preferences of several marine organisms like the slime-forming diatom *N. incerta* for these hydrophobic systems caused long-term concerns when statically immersed in marine environments.[8, 157]

To address the inadequacy of AF protection for these oil-incorporating FR coatings, as well as potentially improving the release of several marine organisms, amphiphilic, surface-active additives are currently being investigated.[8, 90] Some of the major objectives of this method are to conserve the mechanical properties of the coating system, provide AF protection in static environments, and to improve the FR properties for long-term performance. PDMS and PEG are typically used in the synthesis of these additives, but several hydrophobic and hydrophilic moieties can be utilized such as zwitterionic

compounds and fluoroalkyl containing polymers. Grunlan *et al.* first investigated the use of PEO-based surface modifying additives (SMAs), with varying chain length of PDMS. Two different additive architectures, diblock and triblock copolymers, were compared to a reactive PEO-silane amphiphile that was studied in previous work (Figure 1.16).[118, 158]

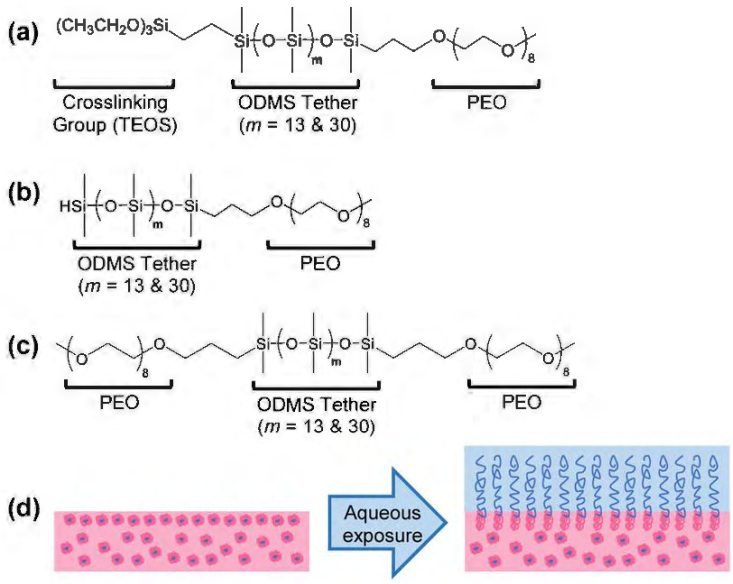

Figure 1.16. Structure of the various SMAs synthesized and incorporated into a silicone elastomer. (a) Crosslink-able diblock amphiphile with varying PDMS tether, (b) diblock amphiphile with varying PDMS tether, (c) triblock amphiphile with varying PDMS tether, and (d) amphiphilic-modified silicone showing PEG chain swelling upon aqueous exposure. Reproduced from reference 158.[158]

It was observed that the surfaces of all coatings had significant decreases in water contact angle values over a period of five min, with the largest decreases seen with SMAs containing shorter PDMS tethers, with diblock amphiphile architecture. In addition, water uptake over two weeks was evaluated, with the crosslink-able, diblock amphiphiles having the least amount of water uptake. However, when the PDMS tether length was increased, diblock and triblock SMAs were observed to have comparable performance. Lastly, protein resistance towards human fibrinogen (HF) was evaluated for these coatings. Regardless of architecture, reactivity, or PDMS tether length (apart from triblock SMAs with higher tether length), all surfaces were observed to have excellent resistance towards this protein, making these SMAs as a potential candidate for AF/FR coatings.[158]

Another example of these amphiphilic AF/FR coatings produced by incorporating non-reactive surface modifying amphiphilic additives is outline by Guo *et al.* In this work, a surface modifying amphiphile was synthesized *via* controlled free radical polymerization, composed of polyvinylpyrrolidone

(PVP) as the hydrophilic group, and PDMS as the hydrophobic group.[159] Additives with increasing amounts of PVP were incorporated into a PDMS silicone elastomer coating a different concentrations and evaluated for surface free energy, psuedobarnacle attachment strength, laboratory attachment and removal of the diatom *N. parva*, as well as field testing for ~120 days. It was observed that surface free energies were significantly increased for higher concentrations of PVP in the additive, as well as higher concentrations of additive in the elastomer. Very low attachment of *N. parva* was seen on all surfaces, with almost all diatoms being removed, with higher concentrations of PVP and additive having the highest overall removal.[159] A similar trend was seen for psuedobarnacle adhesion was seen. Field testing of these coatings showed a significant reduction in accumulation of biomass, showcasing their potential as AF/FR coatings.

Yet another system developed by Rahimi *et al.* involves the synthesis of di- and triblock surface modifying additives consisting of poly(sulfobetainemethacrylate) (PSBMA) and PDMS. The molecular weight of both poly(SBMA) and PDMS were varied, as well as the concentration of additives incorporated into a hydrophobic self-stratifying siloxane-polyurethane (SiPU) FR coating. Results from a suite of AF/FR biological assays demonstrated the effectiveness of the various additives in providing an amphiphilic surface to improve upon the AF/FR properties of SiPU coatings. It was noted that the molecular weight of the PDMS in the additives, as well as the overall concentration in the coating were the most influential factors.[150]

These examples of surface modifying amphiphilic additives highlight the potential for this approach to improve upon existing marine coatings systems, as well as intriguing avenues for novel AF/FR marine coatings. Some of the main considerations one should have when developing these systems are the hydrophobic and hydrophilic moieties used, the coating matrix into which additives are incorporated, and the concentrations of which they are added. A careful balance must be made between these three criteria to preserve the mechanical properties of the coating system, and to optimize AF/FR properties. In addition, future work in this area of research should be focused on more fundamental aspects of incorporating these SMAs into a wide range of coatings to better understand diffusion processes through the bulk. In many crosslinked coatings, organic solvents are often used as vehicles for binder, pigments, etc. Due to the amphiphilic nature of these additives, it is hypothesized that different

combinations of solvent may alter the arrangement and dispersion of the SMAs throughout the coating, potentially affecting surface properties. Other work should be focused on determining the rates of diffusion of SMAs through the bulk of various coatings. This goes hand in hand with investigating the leaching rates of these 'unbound' SMAs, as this is a crucial parameter in determining the long-term efficacy of these systems. Lastly, work should be performed to identify other hydrophobic and hydrophilic components of these additives that not only better resist environmental degradation but could also be used to modify the mechanical properties of the bulk coating to the desired effect of more durable, toughened coatings systems.

Research Scope and Purpose

The purpose of the research reported in this dissertation was to design and synthesize an array of surface modifying amphiphilic additives (SMAAs) consisting of PDMS and PEG, for use in established SiPU coatings to further improve AF/FR properties towards a broad range of marine organisms. In addition, investigation into using SiPU FR coatings for applications other than ships hulls was performed. Three SiPU coatings systems were considered for this work. Chapter two focused on building the groundwork of novel additive synthesis, with structures of amphiphiles consisting of comb-like copolymers between PDMS and PEG, partial comb-like copolymers with varying degrees of PEG chain grafting, as well as additives that were based on a cyclosiloxane small molecule to form a star-like copolymer. The molecular weight of the grafted PEG chains was also varied, with molecular weight ranges of the siloxane backbones between 900-2400 g/mol. These additives were incorporated into hydrophobic SiPU A4-20 to evaluate changes in surface character, as well as AF/FR performance. Chapter three involved the incorporation of a previously synthesized additive, with a partial comb-like structure, into an amphiphilic SiPU based on isocyanate prepolymers containing PDMS and PEG. Additionally, the concentration of PDMS and PEG were varied in the prepolymer composition. The main objectives of this study were to determine if properties could be further improved with incorporated additive due to an increased compatibility with the bulk, as well as observe any changes due to changes in prepolymer composition. A suite of surface characterizations was performed such as WCA/MICA/SE measurements, ATR-FTIR, AFM, as well as several biological AF/FR assays to determine fouling protection performance. Chapter four focused on selecting a range of SMAAs based on the work done in chapter two and incorporating

them into a traditionally non-fouling release polyurethane coating. The resultant coatings had increasing amounts of additive and were evaluated utilizing previously established surface characterization techniques and biological assays. The work performed in chapter five took a departure from the studies performed in chapters two through four. In this chapter, three different coatings, A4-20, Intersleek® tie-coat, and Hempasil® tie-coat, were applied to several different oil boom fabrics and their adhesion properties were evaluated utilizing a novel water-jet adhesion characterization protocol. Samples were prepared having been treated with different surface treatments such as sandblasting, corona treatment, and by application of five different adhesion promoting chlorinated polyolefins to determine if these could improve coating adhesion to the fabrics. Promising candidates were then selected for large scale field testing to assess durability and cleanability. Chapter six involves an introductory investigation into novel hydrophilic additives for use in various FR coatings systems. A hyperbranched polyglycerol (HBPG) was synthesized *via* ring-opening multi branching polymerization (ROMBP). The free hydroxyls on this HBPG were then functionalized with acetoacetate groups, which would not undergo reaction with isocyanates commonly used in SiPU FR coatings.

References

1. Yebra, D. M.; Kiil, S. K.; Dam-Johansen, K., Antifouling Technology—Past, Present and Future Steps Towards Efficient and Environmentally Friendly Antifouling Coatings. *Prog. Org. Coat.* **2004,** *50* (2), 75.

2. Callow, J. A.; Callow, M. E., Trends in the development of environmentally friendly fouling-resistant marine coatings. *Nature Communications* **2011,** *2*, 244.

3. Kempf, G., On the effect of roughness on the resistance of ships. *Trans INA* **1937,** *79*, 109-119.

4. Schultz, M. P.; Bendick, J. A.; Holm, E. R.; Hertel, W. M., Economic Impact of Biofouling on a Naval Surface Ship. *Biofouling* **2011,** *27* (1), 87.

5. Lindholdt, A.; Dam-Johansen, K.; Olsen, S.; Yebra, D. M.; Kiil, S., Effects of biofouling development on drag forces of hull coatings for ocean-going ships: a review. *Journal of Coatings Technology and Research* **2015,** *12* (3), 415-444.

6. Schultz, M. P., Effects of coating roughness and biofouling on ship resistance and powering. *Biofouling* **2007,** *23* (5), 331-341.

7. Dexter, S. C., Role of microfouling organisms in marine corrosion. *Biofouling* **1993,** *7* (2), 97-127.

8. Lejars, M.; Margaillan, A.; Bressy, C., Fouling release coatings: a nontoxic alternative to biocidal antifouling coatings. *Chemical reviews* **2012,** *112* (8), 4347-4390.

9. Kiil, S.; Weinell, C. E.; Yebra, D. M.; Dam-Johansen, K., Marine biofouling protection: design of controlled release antifouling paints, in Chemical Product Design: toward a perspective through case stories. In *Computer aided chemical engineering*, Elsevier: 2006; pp 181-239.

10. Piola, R. F.; Dafforn, K. A.; Johnston, E. L., The influence of antifouling practices on marine invasions. *Biofouling* **2009,** *25* (7), 633-644.

11. Magin, C. M.; Cooper, S. P.; Brennan, A. B., Non-Toxic Antifouling Strategies. *Mater. Today* **2010,** *13* (4), 36.

12. Callow, M. E.; Callow, J. A., Marine Biofouling: A Sticky Problem. *Biologist* **2002,** *49* (1), 10.

13. Jin, H.; Tian, L.; Bing, W.; Zhao, J.; Ren, L., Bioinspired marine antifouling coatings: Status, prospects, and future. *Progress in Materials Science* **2022,** *124*, 100889.

14. Qiu, H.; Feng, K.; Gapeeva, A.; Meurisch, K.; Kaps, S.; Li, X.; Yu, L.; Mishra, Y. K.; Adelung, R.; Baum, M., Functional Polymer Materials for Modern Marine Biofouling Control. *Progress in Polymer Science* **2022**, 101516.

15. Dobretsov, S.; Teplitski, M.; Paul, V., Mini-review: quorum sensing in the marine environment and its relationship to biofouling. *Biofouling* **2009,** *25* (5), 413-427.

16. Pradhan, S.; Kumar, S.; Mohanty, S.; Nayak, S. K., Environmentally benign fouling-resistant marine coatings: A review. *Polymer-Plastics Technology and Materials* **2019,** *58* (5), 498-518.

17. Callow, M. E.; Callow, J. A.; Pickett-Heaps, J. D.; Wetherbee, R., Primary adhesion of enteromorpha (chlorophyta, ulvales) propagules: quantitative settlement studies and video microscopy 1. *Journal of Phycology* **1997,** *33* (6), 938-947.

18. Roberts, D.; Rittschof, D.; Holm, E.; Schmidt, A., Factors influencing initial larval settlement: temporal, spatial and surface molecular components. *Journal of Experimental Marine Biology and Ecology* **1991,** *150* (2), 203-221.

19. Petrone, L.; Di Fino, A.; Aldred, N.; Sukkaew, P.; Ederth, T.; Clare, A. S.; Liedberg, B., Effects of Surface Charge and Gibbs Surface Energy on the Settlement Behaviour of Barnacle Cyprids (Balanus Amphitrite). *Biofouling* **2011,** *27* (9), 1043.

20. Aldred, N.; Gatley-Montross, C. M.; Lang, M.; Detty, M. R.; Clare, A. S., Correlative assays of barnacle cyprid behaviour for the laboratory evaluation of antifouling coatings: a study of surface energy components. *Biofouling* **2019,** *35* (2), 159-172.

21. Flemming, H.-C.; Griebe, T.; Schaule, G., Antifouling strategies in technical systems—a short review. *Water Science and Technology* **1996,** *34* (5-6), 517-524.

22. Liu, Y.; Zhao, Q., Influence of surface energy of modified surfaces on bacterial adhesion. *Biophysical chemistry* **2005,** *117* (1), 39-45.

23. Dexter, S.; Sullivan Jr, J.; Williams III, J.; Watson, S., Influence of substrate wettability on the attachment of marine bacteria to various surfaces. *Applied microbiology* **1975,** *30* (2), 298-308.

24. Ista, L. K.; Callow, M. E.; Finlay, J. A.; Coleman, S. E.; Nolasco, A. C.; Simons, R. H.; Callow, J. A.; Lopez, G. P., Effect of substratum surface chemistry and surface energy on attachment of marine bacteria and algal spores. *Applied and environmental microbiology* **2004,** *70* (7), 4151-4157.

25. Finlay, J. A.; Callow, M. E.; Ista, L. K.; Lopez, G. P.; Callow, J. A., The influence of surface wettability on the adhesion strength of settled spores of the green alga Enteromorpha and the diatom Amphora. *Integrative and comparative biology* **2002,** *42* (6), 1116-1122.

26. Robert Stone, J.; Fritz, S. C., Three-dimensional modeling of lacustrine diatom habitat areas: Improving paleolimnological interpretation of planktic: benthic ratios. *Limnology and Oceanography* **2004,** *49* (5), 1540-1548.

27. Molino, P. J.; Campbell, E.; Wetherbee, R., Development of the initial diatom microfouling layer on antifouling and fouling-release surfaces in temperate and tropical Australia. *Biofouling* **2009,** *25* (8), 685-694.

28. Callow, M. E.; Callow, J.; Ista, L. K.; Coleman, S. E.; Nolasco, A. C.; López, G. P., Use of self-assembled monolayers of different wettabilities to study surface selection and primary adhesion processes of green algal (Enteromorpha) zoospores. *Applied and Environmental Microbiology* **2000,** *66* (8), 3249-3254.

29. Callow, J. A.; Callow, M. E.; Ista, L. K.; Lopez, G.; Chaudhury, M. K., The influence of surface energy on the wetting behaviour of the spore adhesive of the marine alga Ulva linza (synonym Enteromorpha linza). *Journal of the Royal Society Interface* **2005,** *2* (4), 319-325.

30. Liang, C.; Strickland, J.; Ye, Z.; Wu, W.; Hu, B.; Rittschof, D., Biochemistry of barnacle adhesion: an updated review. *Frontiers in Marine Science* **2019**, 565.

31. Bandara, N.; Zeng, H.; Wu, J., Marine mussel adhesion: biochemistry, mechanisms, and biomimetics. *Journal of adhesion science and technology* **2013,** *27* (18-19), 2139-2162.

32. Rittschof, D.; Costlow, J. D., Bryozoan and barnacle settlement in relation to initial surface wettability: A comparison of laboratory and field studies. *Sci. Mar.* **1989,** *53* (2), 411-416.

33. Crisp, D.; Walker, G.; Young, G.; Yule, A., Adhesion and substrate choice in mussels and barnacles. *Journal of Colloid and Interface Science* **1985,** *104* (1), 40-50.

34. Hellio, C.; Yebra, D. M., *Advances in Marine Antifouling Coatings and Technologies*. 2009.

35. Jones, G., The battle against marine biofouling: a historical review. *Advances in marine antifouling coatings and technologies* **2009**, 19-45.

36. Maguire, R. J., Environmental aspects of tributyltin. *Applied Organometallic Chemistry* **1987,** *1* (6), 475-498.

37. Alzieu, C., Tributyltin: case study of a chronic contaminant in the coastal environment. *Ocean & coastal management* **1998,** *40* (1), 23-36.

38. Antizar-Ladislao, B., Environmental levels, toxicity and human exposure to tributyltin (TBT)-contaminated marine environment. A review. *Environment international* **2008,** *34* (2), 292-308.

39. Bressy, C.; Margaillan, A.; Faÿ, F.; Linossier, I.; Réhel, K., 18 - Tin-free self-polishing marine antifouling coatings. In *Advances in Marine Antifouling Coatings and Technologies*, Hellio, C.; Yebra, D., Eds. Woodhead Publishing: 2009; pp 445-491.

40. Konstantinou, I. K.; Albanis, T. A., Worldwide Occurrence and Effects of Antifouling Paint Booster Biocides in the Aquatic Environment: A Review. *Environ. Int.* **2004,** *30* (2), 235.

41. Omae, I., General aspects of tin-free antifouling paints. *Chemical reviews* **2003,** *103* (9), 3431-3448.

42. Arai, T.; Harino, H.; Ohji, M.; Langston, W. J., *Ecotoxicology of antifouling biocides*. Springer: 2009.

43. Thomas, K. V.; Brooks, S., The environmental fate and effects of antifouling paint biocides. *Biofouling* **2010,** *26* (1), 73-88.

44. Hellio, C.; Maréchal, J.-P.; Da Gama, B.; Pereira, R.; Clare, A., Natural marine products with antifouling activities. In *Advances in marine antifouling coatings and technologies*, Elsevier: 2009; pp 572-622.

45. Satheesh, S.; Ba-akdah, M. A.; Al-Sofyani, A. A., Natural antifouling compound production by microbes associated with marine macroorganisms—A review. *Electronic Journal of Biotechnology* **2016,** *21*, 26-35.

46. Feng, D.; Ke, C.; Li, S.; Lu, C.; Guo, F., Pyrethroids as promising marine antifoulants: laboratory and field studies. *Marine Biotechnology* **2009,** *11* (2), 153-160.

47. Yang, L.; Lee, O. O.; Jin, T.; Li, X.; Qian, P., Antifouling properties of 10β-formamidokalihinol-A and kalihinol A isolated from the marine sponge Acanthella cavernosa. *Biofouling* **2006,** *22* (1), 23-32.

48. Sera, Y.; Adachi, K.; Nishida, F.; Shizuri, Y., A new sesquiterpene as an antifouling substance from a Palauan marine sponge, Dysidea herbacea. *Journal of natural products* **1999,** *62* (2), 395-396.

49. Dobretsov, S.; Al-Wahaibi, A. S.; Lai, D.; Al-Sabahi, J.; Claereboudt, M.; Proksch, P.; Soussi, B., Inhibition of bacterial fouling by soft coral natural products. *International Biodeterioration & Biodegradation* **2015,** *98*, 53-58.

50. Mol, V. L.; Raveendran, T.; Abhilash, K.; Parameswaran, P., Inhibitory effect of Indian sponge extracts on bacterial strains and larval settlement of the barnacle, Balanus amphitrite. *International Biodeterioration & Biodegradation* **2010,** *64* (6), 506-510.

51. Viju, N.; Anitha, A.; Vini, S. S.; Shankar, C.; Satheesh, S.; Punitha, S., Antibiofilm activities of extracellular polymeric substances produced by bacterial symbionts of seaweeds. **2014**.

52. Maréchal, J.-P.; Hellio, C., Challenges for the development of new non-toxic antifouling solutions. *International Journal of Molecular Sciences* **2009,** *10* (11), 4623-4637.

53. Scardino, A. J.; de Nys, R., Mini review: biomimetic models and bioinspired surfaces for fouling control. *Biofouling* **2011,** *27* (1), 73-86.

54. Ball, P., Engineering shark skin and other solutions. *Nature* **1999,** *400* (6744), 507-509.

55. Bechert, D.; Bruse, M.; Hage, W., Experiments with three-dimensional riblets as an idealized model of shark skin. *Experiments in fluids* **2000,** *28* (5), 403-412.

56. Wilson, L. H.; Schumacher, J. F.; Finlay, J.; Perry, R.; Callow, M.; Callow, J.; Brennan, A. B. In *Towards minimally fouling substrates: surface grafting and topography*, ACS, 2005.

57. Carman, M. L.; Estes, T. G.; Feinberg, A. W.; Schumacher, J. F.; Wilkerson, W.; Wilson, L. H.; Callow, M. E.; Callow, J. A.; Brennan, A. B., Engineered antifouling microtopographies–correlating wettability with cell attachment. *Biofouling* **2006,** *22* (1), 11-21.

58. Schumacher, J. F.; Carman, M. L.; Estes, T. G.; Feinberg, A. W.; Wilson, L. H.; Callow, M. E.; Callow, J. A.; Finlay, J. A.; Brennan, A. B., Engineered antifouling microtopographies–effect of feature size, geometry, and roughness on settlement of zoospores of the green alga Ulva. *Biofouling* **2007,** *23* (1), 55-62.

59. Schumacher, J. F.; Aldred, N.; Callow, M. E.; Finlay, J. A.; Callow, J. A.; Clare, A. S.; Brennan, A. B., Species-specific engineered antifouling topographies: correlations between the settlement of algal zoospores and barnacle cyprids. *Biofouling* **2007,** *23* (5), 307-317.

60. Chien, H.-W.; Chen, X.-Y.; Tsai, W.-P.; Lee, M., Inhibition of biofilm formation by rough shark skin-patterned surfaces. *Colloids and Surfaces B: Biointerfaces* **2020,** *186*, 110738.

61. Li, J.; Wang, G.; Meng, Q.; Ding, C.; Jiang, H.; Fang, Y., A biomimetic nano hybrid coating based on the lotus effect and its anti-biofouling behaviors. *Applied surface science* **2014,** *315*, 407-414.

62. Atthi, N.; Sripumkhai, W.; Pattamang, P.; Thongsook, O.; Srihapat, A.; Meananeatra, R.; Supadech, J.; Klunngien, N.; Jeamsaksiri, W., Fabrication of robust PDMS micro-structure with hydrophobic and antifouling properties. *Microelectronic Engineering* **2020,** *224*, 111255.

63. Neinhuis, C.; Barthlott, W., Characterization and distribution of water-repellent, self-cleaning plant surfaces. *Annals of botany* **1997,** *79* (6), 667-677.

64. Li, Z.; Guo, Z., Bioinspired surfaces with wettability for antifouling application. *Nanoscale* **2019,** *11* (47), 22636-22663.

65. Wenzel, R. N., Resistance of solid surfaces to wetting by water. *Industrial & Engineering Chemistry* **1936,** *28* (8), 988-994.

66. Cassie, A.; Baxter, S., Wettability of porous surfaces. *Transactions of the Faraday society* **1944,** *40*, 546-551.

67. Darmanin, T.; Guittard, F., Superhydrophobic and superoleophobic properties in nature. *Materials today* **2015,** *18* (5), 273-285.

68. Bohn, H. F.; Federle, W., Insect aquaplaning: Nepenthes pitcher plants capture prey with the peristome, a fully wettable water-lubricated anisotropic surface. *Proceedings of the National Academy of Sciences* **2004,** *101* (39), 14138-14143.

69. Wong, T.-S.; Kang, S. H.; Tang, S. K.; Smythe, E. J.; Hatton, B. D.; Grinthal, A.; Aizenberg, J., Bioinspired self-repairing slippery surfaces with pressure-stable omniphobicity. *Nature* **2011,** *477* (7365), 443-447.

70. Epstein, A. K.; Wong, T.-S.; Belisle, R. A.; Boggs, E. M.; Aizenberg, J., Liquid-infused structured surfaces with exceptional anti-biofouling performance. *Proceedings of the National Academy of Sciences* **2012,** *109* (33), 13182-13187.

71. Zhang, H.; Liang, Y.; Wang, P.; Zhang, D., Design of slippery organogel layer with room-temperature self-healing property for marine anti-fouling application. *Progress in Organic Coatings* **2019,** *132*, 132-138.

72. Thome, I.; Bauer, S.; Vater, S.; Zargiel, K.; Finlay, J. A.; Arpa-Sancet, M. P.; Alles, M.; Callow, J. A.; Callow, M. E.; Swain, G., Conditioning of self-assembled monolayers at two static immersion test sites along the east coast of Florida and its effect on early fouling development. *Biofouling* **2014,** *30* (8), 1011-1021.

73. Schilp, S.; Rosenhahn, A.; Pettitt, M. E.; Bowen, J.; Callow, M. E.; Callow, J. A.; Grunze, M., Physicochemical properties of (ethylene glycol)-containing self-assembled monolayers relevant for protein and algal cell resistance. *Langmuir* **2009,** *25* (17), 10077-10082.

74. Ederth, T.; Ekblad, T.; Pettitt, M. E.; Conlan, S. L.; Du, C.-X.; Callow, M. E.; Callow, J. A.; Mutton, R.; Clare, A. S.; D'Souza, F., Resistance of galactoside-terminated alkanethiol self-assembled monolayers to marine fouling organisms. *ACS applied materials & interfaces* **2011,** *3* (10), 3890-3901.

75. Mertgen, A.-S.; Guex, A. G.; Tosatti, S.; Fortunato, G.; Rossi, R. M.; Rottmar, M.; Maniura-Weber, K.; Zürcher, S., A low-fouling, self-assembled, graft co-polymer and covalent surface coating for controlled immobilization of biologically active moieties. *Applied Surface Science* **2022**, 152525.

76. Bauer, S.; Finlay, J.; Thomé, I.; Nolte, K.; Franco, S. C.; Ralston, E.; Swain, G.; Clare, A.; Rosenhahn, A., Attachment of algal cells to zwitterionic self-assembled monolayers comprised of different anionic compounds. *Langmuir* **2016,** *32* (22), 5663-5671.

77. Kim, S.; Gim, T.; Jeong, Y.; Ryu, J. H.; Kang, S. M., Facile construction of robust multilayered PEG films on polydopamine-coated solid substrates for marine antifouling applications. *ACS applied materials & interfaces* **2017,** *10* (9), 7626-7631.

78. Zhu, H.-W.; Zhang, J.-N.; Su, P.; Liu, T.; He, C.; Feng, D.; Wang, H., Strong adhesion of poly (vinyl alcohol)–glycerol hydrogels onto metal substrates for marine antifouling applications. *Soft Matter* **2020,** *16* (3), 709-717.

79. Ekblad, T.; Bergström, G.; Ederth, T.; Conlan, S. L.; Mutton, R.; Clare, A. S.; Wang, S.; Liu, Y.; Zhao, Q.; D'Souza, F., Poly (ethylene glycol)-containing hydrogel surfaces for antifouling applications in marine and freshwater environments. *Biomacromolecules* **2008,** *9* (10), 2775-2783.

80. Higaki, Y.; Nishida, J.; Takenaka, A.; Yoshimatsu, R.; Kobayashi, M.; Takahara, A., Versatile inhibition of marine organism settlement by zwitterionic polymer brushes. *Polymer Journal* **2015,** *47* (12), 811-818.

81. Yang, W. J.; Neoh, K.-G.; Kang, E.-T.; Teo, S. L.-M.; Rittschof, D., Polymer brush coatings for combating marine biofouling. *Progress in Polymer Science* **2014,** *39* (5), 1017-1042.

82. Wang, J.; Wei, J., Hydrogel brushes grafted from stainless steel via surface-initiated atom transfer radical polymerization for marine antifouling. *Applied Surface Science* **2016,** *382*, 202-216.

83. Leonardi, A. K.; Ober, C. K., Polymer-based marine antifouling and fouling release surfaces: strategies for synthesis and modification. *Annual review of chemical and biomolecular engineering* **2019,** *10*, 241-264.

84. Chen, S.; Li, L.; Zhao, C.; Zheng, J., Surface hydration: Principles and applications toward low-fouling/nonfouling biomaterials. *Polymer* **2010,** *51* (23), 5283-5293.

85. Ghasemlou, M.; Daver, F.; Ivanova, E. P.; Rhim, J.-W.; Adhikari, B., Switchable dual-function and bioresponsive materials to control bacterial infections. *ACS applied materials & interfaces* **2019,** *11* (26), 22897-22914.

86. Baier, R. E., Surface behaviour of biomaterials: the theta surface for biocompatibility. *Journal of Materials Science: Materials in Medicine* **2006,** *17* (11), 1057-1062.

87. Brady Jr, R. F., A fracture mechanical analysis of fouling release from nontoxic antifouling coatings. *Progress in organic coatings* **2001,** *43* (1-3), 188-192.

88. Brady Jr, R. F.; Singer, I. L., Mechanical factors favoring release from fouling release coatings. *Biofouling* **2000,** *15* (1-3), 73-81.

89. Wendt, D.; Kowalke, G.; Kim, J.; Singer, I., Factors that influence elastomeric coating performance: the effect of coating thickness on basal plate morphology, growth and critical removal stress of the barnacle Balanus amphitrite. *Biofouling* **2006,** *22* (1), 1-9.

90. Hu, P.; Xie, Q.; Ma, C.; Zhang, G., Silicone-based fouling-release coatings for marine antifouling. *Langmuir* **2020,** *36* (9), 2170-2183.

91. Berque, T., Coating for undersea protection. *FR2157074* **1973**.

92. Casse, F.; Swain, G. W., The development of microfouling on four commercial antifouling coatings under static and dynamic immersion. *International biodeterioration & biodegradation* **2006,** *57* (3), 179-185.

93. Holland, R.; Dugdale, T.; Wetherbee, R.; Brennan, A.; Finlay, J.; Callow, J.; Callow, M. E., Adhesion and motility of fouling diatoms on a silicone elastomer. *Biofouling* **2004,** *20* (6), 323-329.

94. Majumdar, P.; Ekin, A.; Webster, D. C., Thermoset Siloxane—Urethane Fouling Release Coatings. ACS Publications: 2007.

95. Webster, D. C.; Pieper, R. J.; Ekin, A., Thermoset siloxane-urethane fouling release coatings. Google Patents: 2011.

96. Ekin, A.; Webster, D. C., Combinatorial and High-Throughput Screening of the Effect of Siloxane Composition on the Surface Properties of Crosslinked Siloxane–Polyurethane Coatings. *J. Comb. Chem.* **2007,** *9* (1), 178.

97. Bodkhe, R. B.; Thompson, S. E. M.; Yehle, C.; Cilz, N.; Daniels, J.; Stafslien, S. J.; Callow, M. E.; Callow, J. A.; Webster, D. C., The Effect of Formulation Variables on Fouling-Release Performance of Stratified Siloxane-Polyurethane Coatings. *Journal of Coatings Technology Research* **2012,** *9* (3), 235.

98. Ekin, A.; Webster, D. C., Library synthesis and characterization of 3-aminopropyl-terminated poly (dimethylsiloxane) s and poly (ϵ-caprolactone)-b-poly (dimethylsiloxane) s. *Journal of Polymer Science Part A: Polymer Chemistry* **2006,** *44* (16), 4880-4894.

99. Pieper, R. J.; Ekin, A.; Webster, D. C.; Casse, F.; Callow, J. A.; Callow, M. E., A Combinatorial Approach to Study the Effect of Acrylic Polyol Composition on the Properties of Crosslinked Siloxane-Polyurethane Fouling-Release Coatings. *Journal of Coatings Technology Research* **2007,** *4* (4), 453.

100. Stafslien, S. J.; Bahr, J. A.; Daniels, J. W.; Wal, L. V.; Nevins, J.; Smith, J.; Schiele, K.; Chisholm, B., Combinatorial Materials Research Applied to the Development of New Surface Coatings Vi: An Automated Spinning Water Jet Apparatus for the High-Throughput Characterization of Fouling-Release Marine Coatings. *Rev. Sci. Instrum.* **2007,** *78* (7), 072204.

101. Stafslien, S. J.; Sommer, S.; Webster, D. C.; Bodkhe, R.; Pieper, R.; Daniels, J.; Vander Wal, L.; Callow, M. C.; Callow, J. A.; Ralston, E., Comparison of laboratory and field testing performance evaluations of siloxane-polyurethane fouling-release marine coatings. *Biofouling* **2016,** *32* (8), 949-968.

102. Sommer, S.; Ekin, A.; Webster, D. C.; Stafslien, S. J.; Daniels, J.; VanderWal, L. J.; Thompson, S. E. M.; Callow, M. E.; Callow, J. A., A Preliminary Study on the Properties and Fouling-Release Performance of Siloxane-Polyurethane Coatings Prepared from Pdms Macromers. *Biofouling* **2010,** *26* (8), 961.

103. Galli, G.; Martinelli, E., Amphiphilic polymer platforms: surface engineering of films for marine antibiofouling. *Macromolecular rapid communications* **2017,** *38* (8), 1600704.

104. Gudipati, C. S.; Finlay, J. A.; Callow, J. A.; Callow, M. E.; Wooley, K. L., The antifouling and fouling-release perfomance of hyperbranched fluoropolymer (HBFP)− poly (ethylene glycol)(PEG) composite coatings evaluated by adsorption of biomacromolecules and the green fouling alga Ulva. *Langmuir* **2005,** *21* (7), 3044-3053.

105. Powell, K. T.; Cheng, C.; Wooley, K. L., Complex amphiphilic hyperbranched fluoropolymers by atom transfer radical self-condensing vinyl (co) polymerization. *Macromolecules* **2007,** *40* (13), 4509-4515.

106. Cheng, C.; Wooley, K. L.; Khoshdel, E., Hyperbranched fluorocopolymers by atom transfer radical self-condensing vinyl copolymerization. *Journal of Polymer Science Part A: Polymer Chemistry* **2005,** *43* (20), 4754-4770.

107. Imbesi, P. M.; Finlay, J. A.; Aldred, N.; Eller, M. J.; Felder, S. E.; Pollack, K. A.; Lonnecker, A. T.; Raymond, J. E.; Mackay, M. E.; Schweikert, E. A., Targeted surface nanocomplexity: two-dimensional control over the composition, physical properties and anti-biofouling performance of hyperbranched fluoropolymer–poly (ethylene glycol) amphiphilic crosslinked networks. *Polymer Chemistry* **2012,** *3* (11), 3121-3131.

108. Pollack, K. A.; Imbesi, P. M.; Raymond, J. E.; Wooley, K. L., Hyperbranched fluoropolymer-polydimethylsiloxane-poly (ethylene glycol) cross-linked terpolymer networks designed for marine and biomedical applications: heterogeneous nontoxic antibiofouling surfaces. *ACS Applied Materials & Interfaces* **2014,** *6* (21), 19265-19274.

109. Krishnan, S.; Ayothi, R.; Hexemer, A.; Finlay, J. A.; Sohn, K. E.; Perry, R.; Ober, C. K.; Kramer, E. J.; Callow, M. E.; Callow, J. A., Anti-biofouling properties of comblike block copolymers with amphiphilic side chains. *Langmuir* **2006,** *22* (11), 5075-5086.

110. Sundaram, H. S.; Cho, Y.; Dimitriou, M. D.; Weinman, C. J.; Finlay, J. A.; Cone, G.; Callow, M. E.; Callow, J. A.; Kramer, E. J.; Ober, C. K., Fluorine-free mixed amphiphilic polymers based on PDMS and PEG side chains for fouling release applications. *Biofouling* **2011,** *27* (6), 589-602.

111. Martinelli, E.; Menghetti, S.; Galli, G.; Glisenti, A.; Krishnan, S.; Paik, M. Y.; Ober, C. K.; Smilgies, D. M.; Fischer, D. A., Surface engineering of styrene/PEGylated-fluoroalkyl styrene block copolymer thin films. *Journal of Polymer Science Part A: Polymer Chemistry* **2009,** *47* (1), 267-284.

112. Zhou, Z.; Calabrese, D. R.; Taylor, W.; Finlay, J. A.; Callow, M. E.; Callow, J. A.; Fischer, D.; Kramer, E. J.; Ober, C. K., Amphiphilic triblock copolymers with PEGylated hydrocarbon structures as environmentally friendly marine antifouling and fouling-release coatings. *Biofouling* **2014,** *30* (5), 589-604.

113. Krishnan, S.; Paik, M. Y.; Ober, C. K.; Martinelli, E.; Galli, G.; Sohn, K. E.; Kramer, E. J.; Fischer, D. A., NEXAFS depth profiling of surface segregation in block copolymer thin films. *Macromolecules* **2010,** *43* (10), 4733-4743.

114. Weinman, C. J.; Finlay, J. A.; Park, D.; Paik, M. Y.; Krishnan, S.; Sundaram, H. S.; Dimitriou, M.; Sohn, K. E.; Callow, M. E.; Callow, J. A., ABC triblock surface active block copolymer with grafted ethoxylated fluoroalkyl amphiphilic side chains for marine antifouling/fouling-release applications. *Langmuir* **2009,** *25* (20), 12266-12274.

115. Murthy, R.; Cox, C. D.; Hahn, M. S.; Grunlan, M. A., Protein-resistant silicones: incorporation of poly (ethylene oxide) via siloxane tethers. *Biomacromolecules* **2007,** *8* (10), 3244-3252.

116. Murthy, R.; Bailey, B. M.; Valentin-Rodriguez, C.; Ivanisevic, A.; Grunlan, M. A., Amphiphilic silicones prepared from branched PEO-silanes with siloxane tethers. *Journal of Polymer Science Part A: Polymer Chemistry* **2010,** *48* (18), 4108-4119.

117. Hawkins, M. L.; Rufin, M. A.; Raymond, J. E.; Grunlan, M. A., Direct observation of the nanocomplex surface reorganization of antifouling silicones containing a highly mobile PEO-silane amphiphile. *Journal of Materials Chemistry B* **2014,** *2* (34), 5689-5697.

118. Hawkins, M. L.; Faÿ, F.; Réhel, K.; Linossier, I.; Grunlan, M. A., Bacteria and diatom resistance of silicones modified with PEO-silane amphiphiles. *Biofouling* **2014,** *30* (2), 247-258.

119. Wang, Y.; Pitet, L. M.; Finlay, J. A.; Brewer, L. H.; Cone, G.; Betts, D. E.; Callow, M. E.; Callow, J. A.; Wendt, D. E.; Hillmyer, M. A., Investigation of the role of hydrophilic chain length in amphiphilic perfluoropolyether/poly (ethylene glycol) networks: towards high-performance antifouling coatings. *Biofouling* **2011,** *27* (10), 1139-1150.

120. Bodkhe, R. B.; Stafslien, S. J.; Cilz, N.; Daniels, J.; Thompson, S. E.; Callow, M. E.; Callow, J. A.; Webster, D. C., Polyurethanes with amphiphilic surfaces made using telechelic functional PDMS having orthogonal acid functional groups. *Progress in Organic Coatings* **2012,** *75* (1-2), 38-48.

121. Galhenage, T. P.; Webster, D. C.; Moreira, A. M. S.; Burgett, R. J.; Stafslien, S. J.; Vanderwal, L.; Finlay, J. A.; Franco, S. C.; Clare, A. S., Poly (ethylene) glycol-modified, amphiphilic, siloxane–polyurethane coatings and their performance as fouling-release surfaces. *Journal of Coatings Technology and Research* **2017,** *14* (2), 307-322.

122. Xu, G.; Liu, P.; Pranantyo, D.; Xu, L.; Neoh, K.-G.; Kang, E.-T., Antifouling and antimicrobial coatings from zwitterionic and cationic binary polymer brushes assembled via “click” reactions. *Industrial & Engineering Chemistry Research* **2017,** *56* (49), 14479-14488.

123. Zhang, Y.; Hu, H.; Pei, X.; Liu, Y.; Ye, Q.; Zhou, F., Polymer brushes on structural surfaces: a novel synergistic strategy for perfectly resisting algae settlement. *Biomaterials science* **2017,** *5* (12), 2493-2500.

124. Huang, H.; Zhang, C.; Crisci, R.; Lu, T.; Hung, H.-C.; Sajib, M. S. J.; Sarker, P.; Ma, J.; Wei, T.; Jiang, S., Strong Surface Hydration and Salt Resistant Mechanism of a New Nonfouling Zwitterionic Polymer Based on Protein Stabilizer TMAO. *Journal of the American Chemical Society* **2021,** *143* (40), 16786-16795.

125. Koc, J.; Schönemann, E.; Amuthalingam, A.; Clarke, J.; Finlay, J. A.; Clare, A. S.; Laschewsky, A.; Rosenhahn, A., Low-fouling thin hydrogel coatings made of photo-cross-linked polyzwitterions. *Langmuir* **2018,** *35* (5), 1552-1562.

126. Yu, W.; Wanka, R.; Finlay, J. A.; Clarke, J. L.; Clare, A. S.; Rosenhahn, A., Degradable hyaluronic acid/chitosan polyelectrolyte multilayers with marine fouling-release properties. *Biofouling* **2020,** *36* (9), 1049-1064.

127. Schardt, L.; Martínez Guajardo, A.; Koc, J.; Clarke, J. L.; Finlay, J. A.; Clare, A. S.; Gardner, H.; Swain, G. W.; Hunsucker, K.; Laschewsky, A., Low fouling polysulfobetaines with variable hydrophobic content. *Macromolecular Rapid Communications* **2021**, 2100589.

128. Koschitzki, F.; Wanka, R.; Sobota, L.; Gardner, H.; Hunsucker, K. Z.; Swain, G. W.; Rosenhahn, A., Amphiphilic Zwitterionic Acrylate/Methacrylate Copolymers for Marine Fouling-Release Coatings. *Langmuir* **2021,** *37* (18), 5591-5600.

129. Koschitzki, F.; Wanka, R.; Sobota, L.; Koc, J.; Gardner, H.; Hunsucker, K. Z.; Swain, G. W.; Rosenhahn, A., Amphiphilic dicyclopentenyl/carboxybetaine-containing copolymers for marine fouling-release applications. *ACS Applied Materials & Interfaces* **2020,** *12* (30), 34148-34160.

130. Ruiz-Sanchez, A. J.; Guerin, A. J.; El-Zubir, O.; Dura, G.; Ventura, C.; Dixon, L. I.; Houlton, A.; Horrocks, B. R.; Jakubovics, N. S.; Guarda, P.-A., Preparation and evaluation of fouling-release properties of amphiphilic perfluoropolyether-zwitterion cross-linked polymer films. *Progress in Organic Coatings* **2020,** *140*, 105524.

131. Leonardi, A.; Zhang, A. C.; Duzen, N.; Aldred, N.; Finlay, J. A.; Clarke, J. L.; Clare, A. S.; Segalman, R. A.; Ober, C. K., Amphiphilic Nitroxide-Bearing Siloxane-Based Block Copolymer Coatings for Enhanced Marine Fouling Release. *ACS Applied Materials & Interfaces* **2021,** *13* (24), 28790-28801.

132. Ventura, C.; Guerin, A. J.; El-Zubir, O.; Ruiz-Sanchez, A. J.; Dixon, L. I.; Reynolds, K. J.; Dale, M. L.; Ferguson, J.; Houlton, A.; Horrocks, B. R., Marine antifouling performance of polymer coatings incorporating zwitterions. *Biofouling* **2017,** *33* (10), 892-903.

133. Wang, H.; Zhang, C.; Wang, J.; Feng, X.; He, C., Dual-mode antifouling ability of thiol–ene amphiphilic conetworks: minimally adhesive coatings via the surface zwitterionization. *ACS Sustainable Chemistry & Engineering* **2016,** *4* (7), 3803-3811.

134. Koc, J.; Schönemann, E.; Wanka, R.; Aldred, N.; Clare, A. S.; Gardner, H.; Swain, G. W.; Hunsucker, K.; Laschewsky, A.; Rosenhahn, A., Effects of crosslink density in zwitterionic hydrogel coatings on their antifouling performance and susceptibility to silt uptake. *Biofouling* **2020,** *36* (6), 646-659.

135. Wang, D.; Xu, J.; Tan, J.; Yang, J.; Zhou, S., In situ generation of amphiphilic coatings based on a self-catalytic zwitterionic precursor and their antifouling performance. *Chemical Engineering Journal* **2021,** *422*, 130115.

136. Hu, P.; Zeng, H.; Zhou, H.; Zhang, C.; Xie, Q.; Ma, C.; Zhang, G., Silicone Elastomer with Self-Generating Zwitterions for Antifouling Coatings. *Langmuir* **2021,** *37* (27), 8253-8260.

137. Xie, Q.; Xie, Q.; Pan, J.; Ma, C.; Zhang, G., Biodegradable polymer with hydrolysis-induced zwitterions for antibiofouling. *ACS applied materials & interfaces* **2018,** *10* (13), 11213-11220.

138. Calabrese, D. R.; Wenning, B.; Finlay, J. A.; Callow, M. E.; Callow, J. A.; Fischer, D.; Ober, C. K., Amphiphilic oligopeptides grafted to PDMS-based diblock copolymers for use in antifouling and fouling release coatings. *Polymers for Advanced Technologies* **2015,** *26* (7), 829-836.

139. Patterson, A. L.; Wenning, B.; Rizis, G.; Calabrese, D. R.; Finlay, J. A.; Franco, S. C.; Zuckermann, R. N.; Clare, A. S.; Kramer, E. J.; Ober, C. K., Role of backbone chemistry and monomer sequence in amphiphilic oligopeptide-and oligopeptoid-functionalized PDMS-and PEO-based block copolymers for marine antifouling and fouling release coatings. *Macromolecules* **2017,** *50* (7), 2656-2667.

140. Calabrese, D. R.; Wenning, B. M.; Buss, H.; Finlay, J. A.; Fischer, D.; Clare, A. S.; Segalman, R. A.; Ober, C. K., Oligopeptide-modified hydrophobic and hydrophilic polymers as antifouling coatings. *Green Materials* **2017,** *5* (1), 31-43.

141. Leng, C.; Buss, H. G.; Segalman, R. A.; Chen, Z., Surface structure and hydration of sequence-specific amphiphilic polypeptoids for antifouling/fouling release applications. *Langmuir* **2015,** *31* (34), 9306-9311.

142. Barry, M. E.; Davidson, E. C.; Zhang, C.; Patterson, A. L.; Yu, B.; Leonardi, A. K.; Duzen, N.; Malaviya, K.; Clarke, J. L.; Finlay, J. A., The role of hydrogen bonding in peptoid-based marine antifouling coatings. *Macromolecules* **2019,** *52* (3), 1287-1295.

143. Jakobi, V.; Schwarze, J.; Finlay, J. A.; Nolte, K. A.; Spöllmann, S.; Becker, H.-W.; Clare, A. S.; Rosenhahn, A., Amphiphilic alginates for marine antifouling applications. *Biomacromolecules* **2018,** *19* (2), 402-408.

144. Jung, S.; Song, R.; Kim, J.; Ko, J. H.; Lee, J., Controlling the release of amphiphilic liposomes from alginate hydrogel particles for antifouling paint. *Langmuir* **2020,** *36* (6), 1515-1522.

145. Wang, P.; He, B.; Wang, B.; Wang, L.; Yu, H.; Liu, S.; Ye, Q.; Zhou, F., Durable self-polishing antifouling coating based on fluorine-containing pyrrolidone amphiphilic copolymer-functionalized nanosilica. *Progress in Organic Coatings* **2022,** *165*, 106706.

146. Rahimi, A.; Murphy, M.; Faiyaz, K.; Stafslien, S. J.; Vanderwal, L.; Pade, M.; Finlay, J. A.; Clare, A. S.; Webster, D. C., Amphiphilic marine coating systems of self-stratified PDMS-PEG surfaces with an epoxy-polyurethane matrix. *Journal of Coatings Technology and Research* **2022**, 1-18.

147. Zhang, Z.; Guo, L.; Hao, J., Emulsion-Based Organohydrogels with Switchable Wettability and Underwater Adhesion toward Durable and Ecofriendly Marine Antifouling Coatings. *ACS Applied Polymer Materials* **2021,** *3* (6), 3060-3070.

148. Lin, X.; Xie, Q.; Ma, C.; Zhang, G., Self-healing, highly elastic and amphiphilic silicone-based polyurethane for antifouling coatings. *Journal of Materials Chemistry B* **2021,** *9* (5), 1384-1394.

149. Lu, G.; Tian, S.; Li, J.; Xu, Y.; Liu, S.; Pu, J., Fabrication of bio-based amphiphilic hydrogel coating with excellent antifouling and mechanical properties. *Chemical Engineering Journal* **2021,** *409*, 128134.

150. Rahimi, A.; Stafslien, S. J.; Vanderwal, L.; Finlay, J. A.; Clare, A. S.; Webster, D. C., Amphiphilic zwitterionic-PDMS-based surface-modifying additives to tune fouling-release of siloxane-polyurethane marine coatings. *Progress in Organic Coatings* **2020,** *149*, 105931.

151. Benda, J.; Stafslien, S.; Vanderwal, L.; Finlay, J. A.; Clare, A. S.; Webster, D. C., Surface modifying amphiphilic additives and their effect on the fouling-release performance of siloxane-polyurethane coatings. *Biofouling* **2021**, 1-18.

152. Guazzelli, E.; Lusiani, N.; Monni, G.; Oliva, M.; Pelosi, C.; Wurm, F. R.; Pretti, C.; Martinelli, E., Amphiphilic Polyphosphonate Copolymers as New Additives for PDMS-Based Antifouling Coatings. *Polymers* **2021,** *13* (19), 3414.

153. He, B.; Du, Y.; Wang, B.; Zhao, X.; Liu, S.; Ye, Q.; Zhou, F., Self-healing polydimethylsiloxane antifouling coatings based on zwitterionic polyethylenimine-functionalized gallium nanodroplets. *Chemical Engineering Journal* **2022,** *427*, 131019.

154. Hoipkemeier-Wilson, L.; Schumacher, J. F.; Carman, M. L.; Gibson, A. L.; Feinberg, A. W.; Callow, M. E.; Finlay, J. A.; Callow, J. A.; Brennan, A. B., Antifouling Potential of Lubricious, Micro-Engineered, Pdms Elastomers against Zoospores of the Green Fouling Alga Ulva (Enteromorpha). *Biofouling* **2004,** *20* (1), 53.

155. Kavanagh, C. J.; Swain, G. W.; Kovach, B. S.; Stein, J.; Darkangelo-Wood, C.; Truby, K.; Holm, E.; Montemarano, J.; Meyer, A.; Wiebe, D., The effects of silicone fluid additives and silicone elastomer matrices on barnacle adhesion strength. *Biofouling* **2003,** *19* (6), 381-390.

156. Stein, J.; Truby, K.; Wood, C. D.; Gardner, M.; Swain, G.; Kavanagh, C.; Kovach, B.; Schultz, M.; Wiebe, D.; Holm, E.; Montemarano, J.; Wendt, D.; Smith, C.; Meyer, A., Silicone Foul Release Coatings: Effect of the Interaction of Oil and Coating Functionalities on the Magnitude of Macrofouling Attachment Strengths. *Biofouling* **2003,** *19*, 71.

157. Galhenage, T. P.; Hoffman, D.; Silbert, S. D.; Stafslien, S. J.; Daniels, J.; Miljkovic, T.; Finlay, J. A.; Franco, S. C.; Clare, A. S.; Nedved, B. T.; Hadfield, M. G.; Wendt, D. E.; Waltz, G.; Brewer, L.; Teo, S. L. M.; Lim, C.-S.; Webster, D. C., Fouling-Release Performance of Silicone Oil-Modified Siloxane-Polyurethane Coatings. *ACS Applied Materials & Interfaces* **2016,** *8* (42), 29025-29036.

158. Rufin, M. A.; Ngo, B. K. D.; Barry, M. E.; Page, V. M.; Hawkins, M. L.; Stafslien, S. J.; Grunlan, M. A., Antifouling silicones based on surface-modifying additive amphiphiles. *Green Materials* **2017,** *5* (1), 4-13.

159. Guo, H.; Chen, P.; Tian, S.; Ma, Y.; Li, Q.; Wen, C.; Yang, J.; Zhang, L., Amphiphilic Marine Antifouling Coatings Based on a Hydrophilic Polyvinylpyrrolidone and Hydrophobic Fluorine–Silicon-Containing Block Copolymer. *Langmuir* **2020,** *36* (48), 14573-14581.

CHAPTER 2. SURFACE MODIFYING AMPHIPHILIC ADDITIVES AND THEIR EFFECT ON FOULING-RELEASE PERFORMANCE IN SILOXANE-POLYURETHANE COATINGS

Introduction

The undesirable accumulation of marine organisms on structures submerged in seawater is referred to as marine biofouling.[1] The process of marine biofouling involves over 4000 different marine organisms, not including prokaryotes, having varying sizes and modes of adhesion, which makes dealing with this phenomenon very difficult.[1-3] When structures are submersed in seawater, proteins, nutrients, and other small molecules attach to the surface and form a conditioning film.[3] From this point, a highly complex and dynamic process of marine organism settlement is observed. Marine bacteria, diatoms and other unicellular organisms are typically the first of many to adhere via reversible mechanisms.[4] Larger organisms, such as the spores of macroalgae then settle and introduce more diversity to the biofilm. Larvae of invertebrates, such as barnacles, mussels, and tubeworms may preferentially settle on substrates composed of these micro-foulant-rich biofilms.[4] Marine biofouling is often viewed as a linear chain of events, with biofilm and micro-foulant settlement occurring within seconds to days, and macro-foulant accumulation anywhere from days-months.[3] However, some organisms such as the barnacle *A. amphitrite* and green algae *U. linza* are known to settle and adhere to clean or newly submersed substrates, making the process of marine biofouling harder to predict, and consequently, to protect against.[3]

Aside from the negative aesthetic effects of marine biofouling, the major problem that needs to be addressed is the effect on overall performance of marine vessels. The accumulation of marine organisms on ships' hulls causes large decreases in ship maneuverability and speed.[5, 6] This leads to an increase in fuel consumption, and in turn, an increase in the production of harmful greenhouse gases. Additionally, protecting against marine biofouling has enormous financial costs. For example, the accrued cost due to this phenomenon on US Naval destroyers alone, a medium sized ship, is estimated to be around $56 million per year.[6] Historically a variety of toxic coatings have been used to combat biofouling. At the advent of the 20th century, petroleum-based resin systems were being developed, and between 1960-

1970s, triorganotin biocides, such as tributyltin oxide (TBTO), were incorporated into self-polishing copolymer coating systems leading to greatly improved antifouling performance.[1, 2] The inadvertent effects of these TBT-containing coatings proved harmful to marine environments, resulting in restrictions on use and eventually a complete ban of these tin-containing coatings by the International Maritime Organization (IMO) in 2008.[1] Although the use of inorganic and organic biocides in coatings systems is still the standard method to combat biofouling, development of non-toxic, non-biocide containing antifouling (AF)/fouling-release (FR) coatings has been a major area of research and development for the past 20 years. As a result, several commercially available FR coatings such as Sigmaglide® 1290 (PPG), Intersleek® 970 and 1100SR (International), and Hempasil® X3+ (Hempel) are available for use on ocean-going vessels.

Traditional FR coating systems are mainly based on elastomers consisting of poly(dimethylsiloxane) (PDMS), or other silicones, as well as fluoropolymer-based systems, which result in low surface energy coatings.[3] These coating systems prevent many marine organisms from adhering strongly to their surfaces and under hydrodynamic shear the organisms can be removed with little effort.[3] However, due to issues with mechanical durability and the difficulties in producing tie-coats that achieve proper adhesion to the substrate, there is a need to develop new and effective FR coating systems.[1, 3] One potential approach is to use siloxane-polyurethane coatings (SiPU). These SiPU coatings incorporate PDMS and polyurethane segments and exhibit self-stratifying behavior during curing. PDMS predominates at the surface due to its low surface energy and offers FR performance comparable to commercially available FR coatings.[7-9] The other part of the coating composition consists of the polyurethane, which resides in the bulk of the coating, offering good adhesion to the substrate and improved mechanical properties compared to traditional elastomeric coating systems.[10-12]

Much progress has been made developing FR coatings primarily based upon hydrophobic, low surface energy moieties with promising results. However, many marine organisms are still able to settle on and adhere to these coatings, leading to detrimental effects. Since a common method of adhesion for marine organisms consists of the secretion of a proteinaceous substance(s) that can later crosslink/solidify, methods in which to impart protein resistance to FR coatings systems are being investigated.[4, 13, 14] Amphiphilic FR coatings contain hydrophobic and hydrophilic moieties that interfere

with protein adhesion and are generally hydrophilic in nature. In this respect, poly(ethylene) glycol (PEG) is one of the most studied and has a low interfacial energy with water (<5 mN/m). A 'hydration layer' of water molecules forms at the interface making it thermodynamically unfavorable for biomolecules, like proteins, to disrupt this layer, and adsorb to the surface.[15] Other examples of these hydrophilic moieties include zwitterionic poly(sulfobetaine) methacrylate (pSBMA), polysaccharides, and peptide-mimic polymers.[16] A major method of incorporating these moieties is through crosslinking with the copolymer networks, forming regions of heterogeneity. These systems typically include a hydrophobic backbone providing mechanical strength, with side chains of the desired hydrophilic group. These chains are often copolymers between fluoroalkyl or silicone containing groups.[4, 13, 14, 16] Although these amphiphilic coatings systems offer positive FR performance, it is difficult to balance the amount of hydrophilic/hydrophobic content without compromising the coatings' mechanical properties. To work around this problem, surface amphiphilicity can also be achieved through incorporation of non-reactive, surface modifying amphiphilic additives.[16]

The Grunlan research group has successfully synthesized surface modifying additives (SMAs) consisting of poly(ethylene) oxide (PEO) and oligomeric poly(dimethylsiloxane) (ODMS). The non-reactive SMAs varied in ODMS length, length of the PEO chain, and whether the SMAs were di- or triblock copolymers.[17] Small amounts of the additives were blended with an RTV silicone elastomer. It was hypothesized that the SMAs would migrate to the air/solution interface with the hydrophilic PEO groups extending and presenting a protein resistant surface.[17] Water contact angle measurements showed rapid surface restructuring due to a reduction in contact angle within 5 minutes to values <40°, pointing to a highly hydrophilic surface. Additionally, human fibrinogen (HF) adsorption assays showed very little adsorption in comparison to an unmodified silicone elastomer, suggesting that a highly protein-resistant surface was achieved through amphiphilic non-reactive SMAs.[17] Several other approaches to incorporating PDMS- and PEG-based copolymer additives for biofouling applications have been reported.[18-21] In addition, several commercial fouling-release coatings systems are reported to incorporate surface-modifying additives.[22-25]

The purpose of this study was to investigate the effect of incorporating non-reactive surface-modifying amphiphilic additives (SMAAs) into an SiPU formulation, known as A4-20, and to determine

their effects on fouling-release performance. The A4-20 system is a dynamic fouling-release coating with a unique self-stratifying behavior. Non-reactive amphiphilic additives have yet to be studied in this system. The SMAAs used in this study were synthesized via hydrosilylation between several polymethylhydrosiloxanes (PMHS) and allyl-terminated polyethylene glycol monomethyl ethers (APEG) of varying molecular weight. A total of 24 different additives were synthesized and incorporated into A4-20 formulations. It was expected that the hydrophobic segment of the SMAA (PDMS) would facilitate the diffusion of the amphiphilic additive towards the coating/air interface due to its low surface energy and incompatibility with other components of the coatings composition.[11, 12] Once these SMAAs reached the surface, the PEG chains would swell in the aqueous marine environment, providing a layer of hydration which could potentially offer resistance to marine organism settlement. A range of biological assays, on several different marine fouling organisms, was performed to assess fouling-release performance of these modified coatings.

Experimental

Materials

Solvents used in the experiments included tetrahydrofuran (THF), toluene, chloroform, acetone, and methyl amyl ketone (MAK). These were purchased from Sigma Aldrich (MO, USA) with the drying of these solvents facilitated by 4Å molecular sieves, also purchased from Sigma Aldrich (MO, USA). PEG-750, a 750 $\bar{M}_n$ hydroxyl-terminated polyethylene glycol monomethyl ether, allyl bromide, a 60% w/w dispersion of sodium hydride (NaH) in mineral oil, and anhydrous magnesium sulfate ($MgSO_4$) were purchased from Sigma Aldrich (MO, USA). Three allyl-terminated polyethylene glycol monomethyl ethers (Polyglykol® 250 AM, Polyglykol® 350 AM, and Polyglykol® 1000 AM) were provided by Clariant (KY, USA), with the product numbers corresponding to their molecular weight. Karstedt's Catalyst (Pt ~2% in xylenes), acetylacetone, d-chloroform 1% (v/v) in tetramethylsilane (TMS), and dibutyltin diacetate (DBTDAc) were also purchased from Sigma Aldrich (MO, USA). Potassium bromide crystal optic disks were used for FT-IR experiments and were purchased from Alfa Aesar (MA, USA). Three different 100 mol% Si-H trimethylsiloxyl-terminated polymethylhydrosiloxanes (PMHS) with molecular weight ranges, HMS-991:1400-1800, HMS-992:1800-2100, and HMS-993: 2100-2400 g/mol, were purchased from Gelest Inc (PA, USA). Additionally, two different methylhydrosiloxane-dimethylsiloxane copolymers with

different molecular weights and mol% of Si-H functionality, HMS-301: 25-35 mol% Si-H, 1900-2000 g/mol, and HMS-501: 45-55 mol% Si-H, 900-1200 g/mol, along with Si-H functional 1,3,5,7-tetramethylcyclotetrasiloxane (D'4) were purchased from Gelest Inc (PA, USA). Activated carbon, Darco® G-60 (100 mesh) was also purchased from Sigma Aldrich (MO, USA). Polyisocyanate Desmodur Z 4470 BA was provided by Covestro LLC (PA, USA). An 80% butyl acrylate and 20% 2-hydroxyethyl acylate acrylic polyol (AP), 50% by wt. in toluene, was synthesized via free-radical polymerization. Aminopropyl-terminated polydimethyl siloxane (APT-PDMS) of 20,000 $\bar{M}_n$ was synthesized via a ring-opening equilibration reaction. More in-depth descriptions of acrylic polyol and APT-PDMS syntheses can be found in a previous work.[12]

Intersleek® 700 (IS700), Intersleek® 900 (IS900), Intersleek® 1100SR (IS1100SR), and Intergard 264 were provided by AkzoNobel, International Paint LLC (TN, USA). Silastic® T2 silicone elastomer (T2) was provided by Dow Corning (MI, USA). Aluminum panels (4" x 8", 0.6-mm thick, A 3003 H14) purchased from Q-Lab (OH, USA) were sandblasted and primed with Intergard 264 marine primer via air-assisted spray before coating application. Falcon sterile, bacterial grade polystyrene 24-multiwell plates were purchased from VWR International (PA, USA) and modified with 1-in. diameter circular disks cut from coated primed aluminum panels.[26]

Experimental Approach

A main objective of this study was to determine if there was a combination of surface modifying amphiphilic additive (SMAA), at 1, 5, or 10 wt. % in relation to non-volatile components, in a hydrophobic, self-stratifying siloxane-polyurethane (A4-20) that could improve its antifouling and fouling-release performance. To accomplish this, a series of 24 different SMAAs, shown in Table 2.1, were synthesized with varying molecular weight and functionality of polymethylhydrosiloxane (PMHS) backbone, with four different molecular weights of allyl-terminated polyethylene glycol monomethyl ether (APEG).

Table 2.1. Compositions of the synthesized surface modifying amphiphilic additives (SMAAs)

Siloxanes	M.W. (g/mol)	Functionality	Allyl-terminated PEG
HMS-991	1400-1800	100 mol% Si-H	4 different M.W.: 250, 350, 750, and 1100
HMS-992	1800-2100	100 mol% Si-H	
HMS-993	2100-2400	100 mol% Si-H	
HMS-301	1900-2000	25-35 mol% Si-H	
HMS-501	900-1200	45-55 mol% Si-H	
D'4	240.51	Cyclosiloxane, Si-H functionality = 4	

The naming of the additives shown in Table 2.1 is as follows: the type of siloxane backbone is described first (i.e. HMS-991, 992, etc.), followed by the graft notation g, and ending with the molecular weight of grafted PEG chains (i.e. 250, 350, 750, or 1100). For example, if HMS-991 was used as siloxane backbone, with 250 $\bar{M}_n$ PEG chains, the notation would be 991-g-250. After confirming the successful synthesis of these SMAAs, a total of 72 coatings were formulated (Table A1). Again, the variables of interest here were the functionality and structure of the siloxane backbone (i.e. how many available sites for PEG chain grafting), molecular weight of grafted PEG chains, and wt.% of incorporated SMAA in the coating. An example of a sample ID of siloxane backbone HMS-991, with 250 $\bar{M}_n$ PEG chains, at 1 wt.% in A4-20 coating is 991-g-250-1%. Sample ID numbers assigned to these 72 coatings is found in Table A1. These ID numbers will be used for formulation identification in subsequent data analysis. From these 72 formulations, 8 experimental formulations were chosen to perform further biofouling assays of macrofoulants and surface analysis experiments. Macrofoulants included in this study were Ulva linza, Amphibalanus amphitrite, and Geukensia demissa. Formulations that performed the best during initial biofouling assays using C. lytica biofilm growth and adhesion (Figures A7-A10) and N. incerta growth and release (Figure A11-A14) were selected and shown in Table 2.2. Due to coating delamination after water ageing in several formulations, sample ID numbers were reassigned for evaluating biological assay data of C. lytica and N. incerta shown in Table A2.

Table 2.2. Formulations chosen from initial *C. lytica* and *N. incerta* biological assays

Formulation ID #	Formulation ID	Mol % Si-H	PEG M.W.	Wt. % SMAA	SMAA % Hydrophilic Content
3	991_250_10%	100	250	10	81
15	501_250_10%	45-55	250	10	68
33	501_350_10%	45-55	350	10	75
36	D'4_350_10%	f[a] = 4	350	10	85
44	993_750_5%	100	750	5	93
47	301_750_5%	25-35	750	5	79
50	501_750_5%	45-55	750	5	87
54	D'4_750_10%	f[a] = 4	750	10	93

[a] Mol % Si-H of the siloxane backbone is based on the functionality (f) of D4 cyclotetrasiloxane

Synthesis of APEG-750 and SMAAs

Allyl-terminated polyethylene glycol monomethyl ethers (APEG) of molecular weights 250, 350, and 1100 $\bar{M}_n$ were provided by Clariant (KY, USA). To synthesize all the SMAAs outlined in Table 2.1, APEG with a $\bar{M}_n$ of 750 was synthesized according to previous literature.[27] A detailed procedure for this synthesis can be found in Appendix A. After synthesis of APEG-750, the SMAAs in Table 2.1 were synthesized according to previous literature.[17] Each additive was synthesized the same way and a detailed procedure can also be found in Appendix A.

Coating Formulation

After synthesis of the surface modifying amphiphilic additives shown in Table 2.1, they were incorporated into a hydrophobic, self-stratifying siloxane-polyurethane fouling-release coating (A4-20) at 1, 5, and 10 wt.% relative to overall non-volatile content. It was hypothesized that the addition of both a hydrophilic component and more hydrophobic components to this coating would improve its AF/FR performance. An example formulation for sample ID 991-*g*-350-1% is as follows. APT-PDMS (1.1298 g), acetylacetone (0.5297 g), and acrylic polyol (5.5377 g) were added to a 20 mL glass vial, vortexed for 3-5 minutes, and then stirred for 24 hours at room temperature. The next day, polyisocyanate Desmodur Z 4470 BA (1.8428 g), and a solution of DBTDAc 1% in MAK (0.2670 g) were added to the vial, vortexed, and then stirred for 30 minutes, after which 991-g-350 (0.0859 g) was added, vortexed again and stirred for an additional 30 minutes. After mixing, the formulations were then cast on 4” x 8” aluminum panels,

primed with Intergard 264 via air-assisted spray application, using a Gardco wire wound drawdown bar with 80 µm wet-film thickness. These coatings were cured for 24 hours at ambient conditions and then placed in an oven at 80℃ for 45 min.

Control and Commercial Standard Coatings

Several coatings were selected for comparison during surface analysis and biological assay experiments. A4-20, mentioned previously, served as an internal siloxane-polyurethane (SiPU) control, and was prepared according to a previous study.[12] Several other control, and standard coatings used during biological assay testing are detailed in Table 2.3. All coatings were prepared according to their manufacturer's specifications and cast on 4" x 8" aluminum panels primed with Intergard 264.

Table 2.3. Details of control and reference coatings used in this work

Coating Name	Coating ID	Composition
A4-20	A4	Internal SiPU FR control
PU	PU	NDSU prepared polyurethane standard
Poly	Poly	Polystyrene negative control
Dow Corning® T2	T2	Silicone elastomer commercial FR standard coating
Intersleek® 700	IS700	Intersleek commercial FR standard coating
Intersleek® 900	IS900	Intersleek commercial FR standard coating
Intersleek® 1100SR	IS1100SR	Intersleek commercial FR standard coating with a "slime release" component

^{1}H-NMR

A Jeol-ECA 400 MHz FT-NMR instrument was used to collect and record all ^{1}H-NMR spectra for both the synthesized APEG 750 and SMAAs. ACD/Labs NMR processing software was utilized to analyze peaks. All samples were dissolved in deuterated chloroform ($CDCl_3$) with 1% (v/v) TMS.

Fourier Transform – Infrared Spectroscopy

Fourier-Transform Infrared Spectroscopy was also used to determine whether synthesis of APEG 750 or SMAAs was successful. A Thermo Scientific Nicolet 8700 FT-IR instrument was used to gather all spectra. Transmission Infrared Spectroscopy was the mode used to perform these measurements. To prepare samples, 1-2 drops of liquid sample was placed directly onto an optical disk of potassium bromide (KBr). The sample was carefully smeared across the disk to form a uniform layer, and then placed into a sample holder to record the spectra.

Surface Characterization

Techniques used during surface characterization were performed before coated panels were subjected to water ageing. To measure the water contact angle (WCA) and methylene iodide contact angle (MICA), a Krüss DSA100 drop shape analyzer with Advance™ processing software was used. Coatings were placed on the sample platform and a 3 µL drop of water and methylene iodide was dosed using a dual-pressure dosing unit. A delay of 5 s was set before measurements were recorded. Three measurements were performed on each sample to assess static contact angle and surface energy changes in the experimental formulations. The Owens-Wendt method was used to calculate surface energy (SE) for these measurements.[28]

To observe potential changes to surface morphology of the selected formulations, atomic force microscopy (AFM) was utilized in both a dry and hydrated state. A Dimension 3100 microscope with Nanoscope controller was used to scan the surface of experimental formulations. In a dry state (ambient conditions in air), an image with a sample area of 100 x 100 µm was generated in tapping mode. A silicon probe (mikromasch, HQ: CSC37/Al BS) with a spring constant of 0.3-2.0 N/m and 30-55 kHz resonance frequency was used. In a hydrated state (sample area immersed in a small amount of deionized water), an image with a sample area of 100 x 100 µm was again generated in tapping mode. A specialty silicon probe (Bruker, DNP-S10) with a spring constant of 0.6-0.12 N/m and 18-24 kHz resonance frequency was used. Images were analyzed using NanoScope Analysis software.

Water Ageing

After surface characterization of experimental formulations was completed, coated panels were immersed in tanks filled with circulating tap water at ambient temperature. These tanks automatically filled every 4 hours for 28 days of pre-leaching. It is important to pre-leach these coatings as there could be some DBTDAc or other toxic ingredients left over from processing that could leach out and be harmful to the marine organisms used in biological assays. Hence, all AF/FR assessments were performed after this leaching period. This leaching and water aging step also provided a preliminary assessment of coatings stability and adhesion to substrate.

Biological Laboratory Assays

Selection of Marine Fouling Organisms

As previously mentioned, there are over 4000 known fouling species that contribute to marine biofouling. Previous work by our team has been focused on developing an array of testing methods that is based on 5 common marine organisms that contribute to the fouling of ocean-going vessels. Two microfouling organisms, *Cellulophaga lytica* and *Navicula incerta*, and three macrofouling organisms, *Ulva linza*, *Amphibalanus amphitrite*, and *Geukensia demissa* were used in these assays. It was determined that these organisms have provided good correlation between laboratory scale assays and the resulting AF/FR properties of submerged samples during field testing.[29] Thus, these biological assays are useful as screening methods to select promising candidates for further study in real-world environments.

Macroalga 7-day Growth and Release (Ulva linza)

A more detailed description of the procedure for this biological assay can be found in other work.[30] Before the start of the experiment, all multi-well plates were equilibrated in 0.22 µm filtered artificial seawater (ASW) (Tropic Marin) at Newcastle for 2 h. To assess growth and release of *U. linza* sporelings, 1 mL of *U. linza* suspension was adjusted to 3.3 x 10^5 spores mL^{-1} (0.05 OD at absorbance 660 nm) in single-strength enriched seawater medium and added to each well.[31] The spores that settled on the plates were grown for 7 days inside an illuminated incubator at 18℃ with 16:8 light to dark cycle at a photon flux density of 45 µmol/m^2/s, renewing nutrients every 72 hours. After 7 days of sporeling growth, the biomass that was generated was assessed from a single row of wells (6) from each plate. The remaining rows were subjected to a waterjet produced by a spinjet apparatus at surface impact pressures of 18, 67, or 110 kPa.[32] Chlorophyll was extracted by adding 1 mL of DMSO to each well and the fluorescence measured at 360 nm excitation and 670 nm emission wavelengths. The removal of sporelings at each pressure was compared to unsprayed wells with fluorescence being directly proportional to biomass present on each coated surface.

Microalga 2 h Cell Attachment and Release (Navicula incerta)

Detailed methods to assess the growth and release of microalgal (*N. incerta*) diatom cells can be found elsewhere.[30, 33] Briefly, a 1 mL suspension of *N. incerta* cells with 4 x 10^5 cells mL^{-1} (adjusted to

0.03 OD at absorbance 660 nm) in Guillard's F/2 medium was deposited into each coated well. To stimulate cell attachment, plates were subjected to static incubation for 2 h under ambient conditions in the dark. The suspension was then removed, and wells were subjected to water-jet treatments using a spinjet apparatus.[30] Assessment of cell attachment was performed on the first column of wells (3 wells), which was not subject to water-jet pressures. The second and third columns (3 wells each) were subjected to 69 kPa and 138 kPa water pressures, emerging from water-jets, respectively for 10 s. To quantify the biomass of the wells, chlorophyll was extracted with 0.5 mL DMSO and fluorescence was measured at an excitation wavelength of 360 nm and emission wavelength of 670 nm. The relative fluorescence units (RFU) were directly proportional to the biomass remaining on coatings surfaces after water-jet treatments. The percent removal of diatom cells was determined by comparing the RFUs of non-jetted and water-jetted wells.

Bacterial Biofilm 24 h Growth and Adhesion (Cellulophaga lytica)

The assessment of marine bacterium (*C. lytica*) biofilm growth and adhesion has been described in detail in previous works.[34] To coated multi-well plates, a 1 mL suspension of marine bacterium *C. lytica*, at 10^7 cells/mL in ASW with 0.5 g/L peptone and 0.1 g/L of yeast extract, was added. These plates were then incubated for 24 h at 28℃ and then gently rinsed 3 times with deionized water to remove any loose bacteria. Again, the first column (3 wells) did not receive water-jet treatments whilst the other two columns (3 wells each) were subjected to 69 kPa and 138 kPa water pressure for 5 s. To determine biomass remaining on the wells that underwent water-jetting, wells were stained with a crystal violet solution (0.3 wt.% in deionized water) for 15 min and then rinsed 3 times with deionized water. Multi-well plates were then dried at ambient conditions for 1 h before extracting the crystal violet dye with 0.5 mL 33% acetic acid solution for 15 min. Resulting eluates (0.15 mL/ well) were measured for absorbance at 600 nm wavelength. The obtained absorbance measurements were directly proportional to the biomass on the coatings surface before and after water-jet treatments.

Adult Barnacle 2-Week Reattachment and Adhesion (Amphibalanus amphitrite)

To assess marine barnacle (*A. amphitrite)* attachment and adhesion, a procedure outlined by Stafslien et al. was performed.[35, 36] Primed 4" x 8" aluminum panels coated with the experimental formulations were used throughout this experiment. After 28 days pre-leaching in circulating water tanks,

adult barnacles (~5 mm in diameter and provided by Duke University Marine Laboratory, Beaufort, North Carolina, USA) attached to silicone substrates (n = 6) were removed and immobilized onto the surface of the experimental coatings. Barnacles could reattach and grow for 2 weeks while immersed in ASW tank systems with daily feeding of brine shrimp. Temperature of circulating ASW was kept at 25 ℃. After 2 weeks, barnacles were pushed off with shear force using a handheld force gauge mounted on a semi-automated device. The peak force of removal for each barnacle was recorded, along with using Sigma Scan Pro 5.0 image analysis software used to quantify the base plate area of each dislodged barnacle. The adhesion strength (MPa) of each barnacle was calculated by taking the ratio of the force for removal to basal plate area and the average adhesion strength for each coating was reported as the total number of barnacles removed with a measurable force.

Marine Mussel 3-Day Attachment and Adhesion (Geukensia demissa)

To perform marine mussel (*G. demissa)* attachment and adhesion measurements, mussels were obtained from Duke University Marine Laboratory in Beaufort, North Carolina, USA. These mussels then had a 4-cm-long acetal plastic rod (product # 98873A105, McMaster-Carr) attached via 3M® acrylic adhesive (product # 7467A135, McMaster-Carr) perpendicular to the ventral edge. The modified mussels were then immobilized onto each experimental coating surface followed by placing custom PVC sheets against the plastic rods to keep the mussels in contact with the surface. These coatings were then placed in ASW circulating tanks and fed DT's Premium Reef Blend Phytoplankton daily. Temperature of circulating ASW was kept at 25 ℃. After 3 days, the coatings were removed and the total number of mussels with byssus threads attached to each experimental coating was recorded. Next, the plastic rod from each mussel was attached to an individual load cell of 5 N that was part of a custom-built force gauge where the mussels were then pulled off at a rate of 1 mm/s. The force required (N) for detachment of the byssus thread was averaged and the pull-off value for each coating was recorded. Any non-attached mussels were recorded as well.

Statistical Analysis

To gain insight on the statistical significance of AF/FR data, one-way ANOVA was performed using Minitab statistical software. Biological assays that were analyzed include growth and settlement assays for *C. lytica* and *N. incerta*, release assays for *U. linza*, *C. lytica*, and *N. incerta*, as well as

barnacle reattachment assays involving *A. amphitrite*. The highest water/impact pressures in these assessments (i.e. 138 kPa for *C. lytica* and *N. incerta* or 110 kPa for *U. linza*) were used for analysis. The results from these assays were treated as part of a completely randomized design, with one factor level (formulation type). The significance level (α) was set at α = 0.05, with statistically significant results having *P*-values < 0.05.Tukey method was used to make comparisons between the difference of means from each treatment group. Means that do not share a letter in Tables A3-A8 in Appendix A are significantly different.

Results and Discussion

In the ongoing research and development of non-toxic, antifouling/fouling-release (AF/FR) coatings to combat marine biofouling, amphiphilic coatings systems present a unique surface through which settlement and adhesion of a broad array of fouling organisms may be reduced. Two main approaches to achieving an amphiphilic surface are commonly explored: introducing hydrophobic and hydrophilic moieties into the coating formulation via crosslinking, or incorporation of non-reactive, unbound amphiphilic additives. This study focused on investigating the effect that surface modifying amphiphilic additives (SMAAs) would have on the surface characteristics and AF/FR properties of a hydrophobic, self-stratifying siloxane-polyurethane (SiPU) FR coating, denoted as A4-20.[12] These SMAAs were synthesized via hydrosilylation using several different polymethylhydrosiloxanes (PMHS) with four different molecular weights (250, 350, 750, and 1100 $\bar{M}_n$) of allyl-terminated polyethylene glycol (APEG). SMAAs were then incorporated into coatings formulations at 1, 5, and 10 wt.% relative to non-volatile content.

To prepare the SMAAs listed in Table 2.1, APEG with a molecular weight of 750 $\bar{M}_n$ had to be synthesized from hydroxy-terminated polyethylene glycol monomethyl ether and allyl bromide described in Figure A1. After the final product was obtained, FT-IR and ^{1}HNMR was used to characterize successful synthesis. In the FT-IR spectra of APEG 750, shown in Figure A3, the appearance of signals for sp^2 C-H stretching (3080 cm^{-1}), C=C stretching (1640 cm^{-1}), and C-O stretching (1100 cm^{-1}) confirm the successful synthesis of APEG 750. In addition, there is no appreciable O-H stretching (~3550-3200 cm^{-1}), again pointing to successful synthesis. Proton peaks in ^{1}HNMR spectra, shown in Figure A4, also help to confirm a successful synthesis of APEG 750. The characteristic protons about a C=C appear at locations

a (5.83 ppm) and b (5.15 ppm), with other protons indicative of polyethylene oxide (PEO) units appearing at locations c (3.94 ppm), d (3.56 ppm), and e (3.29 ppm).

Synthesis of SMAAs involved the grafting of APEG to PMHS via hydrosilylation assisted by Karstedt's catalyst, detailed in Figure A2. Each SMAA in Table 2.1 was synthesized using the same procedure, as well as being characterized using FT-IR and ^{1}HNMR to determine disappearance of the allyl and silane functional groups. The FT-IR spectra for SMAA 991-*g*-350, Polyglykol® 350 AM, and HMS-991 are shown in Figure A5. The absence of peaks from C=C (1640 cm^{-1}) and Si-H (2156 cm^{-1}) stretching, as well as the appearance of overlapping C-O (1106 cm^{-1}) and Si-O (1029 cm^{-1}) peaks point to a successful synthesis of SMAA. The ^{1}HNMR spectrum for 991-*g*-350, shown in Figure A6, also helps confirm successful synthesis of the additive. The characteristic signal for PMHS Si-H proton (~4.7 ppm) is not seen, as well as an absence of allyl group protons (5.83 and 5.15 ppm). Additionally, peaks pertaining to protons being influenced by silicon are seen at positions a and b (0.45 ppm, 1.56 ppm), with methyl protons along the siloxane backbone from position f (0.04 ppm), and PEO protons at positions c, e, and d (3.35 ppm, 3.60 ppm).

After synthesis of SMAAs, coatings formulations were made utilizing the A4-20 SiPU with an incorporation of SMAAs at 1, 5, and 10 wt.%, shown in Table A1. After 28 days water immersion 65 formulations, shown in Table A2, underwent biological assay testing with *C. lytica* and *N. incerta*. Formulations that had lower overall growth and adhesion for *C. lytica*, as well as lower overall cell attachment and adhesion of *N. incerta*, were selected for further AF/FR assessments using the macrofouling organisms *U. linza*, *G.demissa*, and *A. amphitrite*. Eight total formulations were chosen using these criteria and are shown in Table 2.2.

Water contact angle (WCA) and methylene iodide contact angle (MICA) measurements were used to monitor the change in surface properties when the SMAAs were incorporated into the A4 20 siloxane-polyurethane coating system. Surface energy (SE) calculations were performed using the Owens-Wendt method.[28] Changes in the surface properties both due to the structure of the additive, as well as the molecular weight of the grafted PEG chains were examined. Water contact angles (WCA) of the experimental formulations are given in Figure 2.1A. Most formulations showed changes in WCA as compared to A4-20, which contained no SMAA. Formulations 3, 15, and 54 showed the most variation in

contact angle values. The siloxane backbone of formulation 3 had 100 mol% Si-H functionality, with grafted PEG chains of 250 MW forming a dense ‘comb-like’ structure. Despite having lower molecular weight PEG groups, the structure of this additive may impede its diffusion to the surface, resulting in a significantly higher WCA than the other formulations. In contrast, formulation 15 has a siloxane backbone that contains about half as much grafted PEG chains of 250 molecular weight. The WCA value for this formulation is much lower than that of 3, most likely due to the less dense structure of the SMAA allowing faster diffusion to the surface of the coating, decreasing the WCA values through swelling of PEG chains upon exposure to water. Lastly, formulation 54 has a cyclosiloxane backbone which only accommodates four grafted PEG chains of 750 molecular weight. The WCA for this surface was again significantly higher than A4-20, similar to formulation 3. One explanation for this is the small size of SMAA 54. When dispersed in the coating formulation, this SMAA may be able to form more tightly packed aggregates, which could slowly diffuse through the coating system, resulting in a higher WCA. Values for methylene iodide contact angles (MICA), shown in Figure 2.1A, also follow a similar pattern. In these measurements, the more hydrophobic the surface is, the higher the value for MICA. Formulations 3 and 54 both show significantly higher MICAs than A4-20, largely due to PEG not being readily available at the surface. This is supported by the fact that formulation 15 has a lower MICA, due to its ability to diffuse easily through the coating system and allow the PEG chains to swell. Surface energy values, shown in Figure 2.1B, were calculated using WCA and MICA values and again display the same general trend. Lower surface energies are seen in formulations 3 and 54, while the highest surface energy value comes from formulation 15. Overall, incorporation of these SMAAs modified the surface of the hydrophobic SiPU A4-20 coating. The largest change in values of WCA, MICA, and SE was seen in formulations whose structures varied from dense, or less dense ‘comb-like’, to more of a small molecule structure seen when cyclosiloxane was grafted with PEG chains.

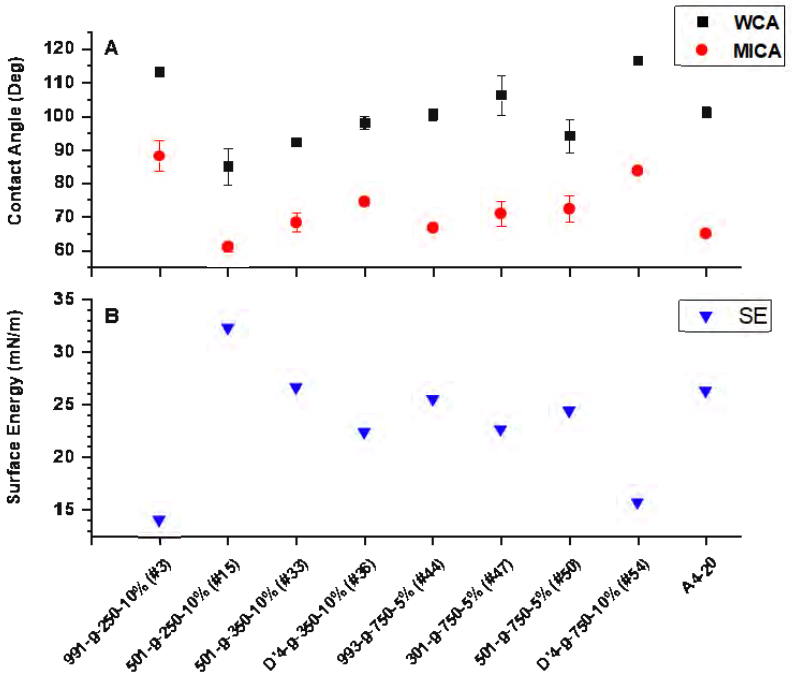

Figure 2.1. Contact angle values for A4-20 coating systems containing SMAA . (A) Static water contact angles (WCA) and methylene iodide contact angles (MICA). (B) Surface energy values calculated via Owens-Wendt method using WCA and MICA values. The X-axis corresponds to the formulation number in Table 2.2.

To better observe changes in the surface morphology of these SMAA A4-20 formulations, atomic force microscopy (AFM) in the dry state (ambient conditions in air) was performed. Formulations 33, 44, 47, and 50 showed the most dramatic change in surface morphology in the dry state compared to A4-20 (no additive). The phase surface plots of these surfaces can be seen in Figure 2.2. In the dry state, the softer PDMS domains in these coatings are typically lighter in color, with a higher phase angle. On the other hand, darker, lower phase angles tend to represent other domains, such as PEG moieties, or the polyurethane background. In Figure 2.2, the experimental formulations all had SMAAs with grafted PEG chains of 750 molecular weight except for 33, which was grafted with PEG chain of 350 molecular weight. These surfaces had more widespread change in phase, pointing to a highly heterogenous surface due to the presence of SMAAs. In terms of additive structure, larger, more dynamic domains were seen with a less dense “comb-like” structure such as in formulation 50. For comparison, there was relatively little change of phase in the surface morphology of A4-20; a siloxane-polyurethane formulation with no additive. AFM imaging in the hydrated state, shown in Figure 2.2, was also performed on these formulations to investigate how the surface morphology changed when exposed to deionized water. As

was observed for the surface of A4-20 in the dry state, there was relatively no change of phase in the surface morphology of A4-20 in the hydrated state. However, there was a significant change in surface morphology in each of the experimental coating formulations, albeit, less pronounced for formulation 33. The changes are most likely due to the grafted PEG chains on the SMAAs, which became swollen while under the droplet of water. The larger the molecular weight of grafted PEG chains, the more swelling occurred, producing the change in domains. Root mean square (R_q) and arithmetic average (R_a) roughness values in the dry state and hydrated state were also determined using NanoScope Analysis software, which can be found in Table A9. In general, R_q values in the dry and hydrated state fell between a narrow range of 43.0-132.0 nm. There was no discernible trend to be seen except that the addition of additive lowered the surface roughness as compared to A4-20 with no additive. These additives could be providing a smoother, more fluid-like layer at the surface due to their non-reactive diffusive action through the bulk of the coating. Additionally, formulations 47 and 50 showed an almost 2-fold increase in surface roughness going from a dry, to a hydrated state. This increase could be explained by the presence of PEG 750 chains, which experience greater swelling in a hydrated state, as opposed to lower molecular PEG chains, providing a rougher surface.

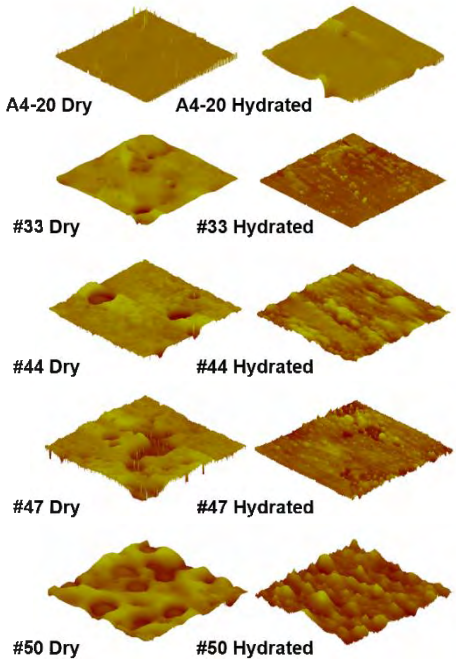

Figure 2.2. AFM phase surface plots for A4-SMAA coatings in a dry and hydrated state. All scans were 100 x 100 µm in area, with a height range of 0 to 50 degrees with respect to change in phase angle. Labels are formulation number followed by the state of the surface.

Before laboratory biological assays were performed, all experimental formulations were pre-leached in circulating water for 28 days. After which, leachate toxicity assessments for organisms *C. lytica*, *N. incerta*, and *U. linza* were performed on all selected coatings according to previously described methods.[37, 38] Results from these assessments are shown in Figures A15-A17. Each organism showed nominal growth, relative to a positive growth control, in overnight extracts from the experimental coatings (artificial seawater and nutrients). Thus, these experimental coatings were considered non-toxic, with AF/FR properties not being influenced by any residual materials left over from the production processes.

A major marine fouling organism studied in these experiments was *U. linza*.[39] Multi-well plates with experimental formulations were exposed to *U. linza* spores and the growth and removal of sporelings (young plants) was evaluated. As with many other marine fouling organisms, the settlement, growth, and overall adhesion of *U. linza* is greatly affected by the wettability and surface characteristics of the substrate.[40-42] In general, the settlement of spores of *U. linza* is lower on surfaces with hydrophilic character. But, once settlement occurs, the adhesion strength of these spores is higher, making them difficult to remove. On the other hand, the spores settle more readily and tend to form more clumps on hydrophobic surfaces, but with weaker adhesion strength, making them easier to remove. In the current study, there are a wide range of surfaces, as seen from CA and AFM experiments. It was expected that there would be variation in assay data due to several factors such as structure/functionality of siloxane backbone and molecular weight of the grafted PEG chains. There were only small differences in sporeling biomass production between the experimental and control/standard formulations, shown in Figure A18. This suggests that the settlement of these spores was not affected by this set of experimental formulations with incorporated SMAAs. However, the release properties were significantly affected, producing removal both higher and lower than the control coatings and A4-20 shown in Figure 2.3.

Those coatings that contained SMAAs with grafted PEG chains of 250 and 350 molecular weight (3, 15, and 33) had lower removal than the A4-20 control (Table A3**)**. These SMAAs all had varying degree of mol% Si-H in the siloxane backbone, leading to varying densities of grafted PEG chains. It was shown that the less densely grafted the SMAA, the more mobile it was. This might explain the lower removal as the additives are more readily available at the surface, providing hydrophilic character. However, formulation 36 contained an additive with 350 molecular weight grafted PEG chains but had

significantly higher removal than other similar SMAAs. The additive in formulation 36 has four PEG 350 chains grafted to a low molecular weight cyclosiloxane as a backbone. Due to these features this SMAA may be able to experience greater entanglement between PEG chains, forming larger aggregates that would make diffusion to the surface more difficult. This would leave the surface with a more hydrophobic character, ideal for removal of sporelings. More investigation is needed to better understand this result. Formulations 44 and 50, which have SMAAs with 750 molecular weight grafted PEG chains, had greater removal relative to the A4-20 formulation (Table A3). It appears that the higher molecular weight PEG dominates diffusion of SMAA to the surface regardless of the overall chain density. These additives are most likely not as readily available compared to lower molecular weight counterparts. However, AFM images showed that most of the formulations containing this type of SMAA still produced a heterogenous surface, which reduced the adhesion of *U. linza* to coatings' surfaces. Overall, several coatings had greater removal performance than polyurethane standard, polystyrene negative control, and A4-20 internal control, but commercial standards Dow Corning Silastic® T2 and Intersleek® 1100SR had the highest sporeling removal at near 100%.

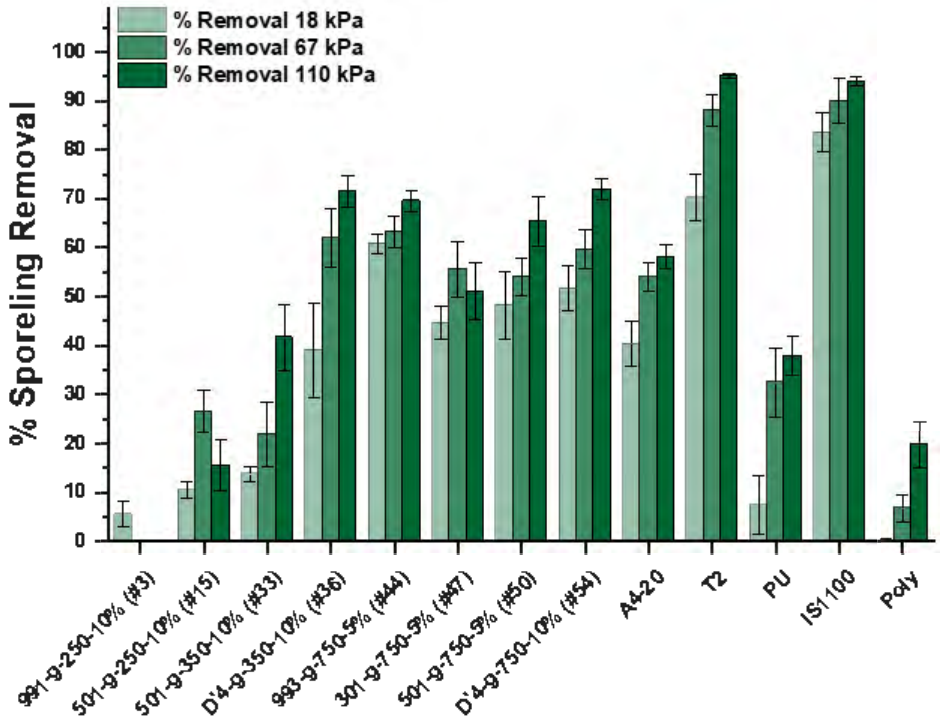

Figure 2.3. Sporeling removal of U. linza at water-jet treatments of 18, 67, and 110 kPa. The bars represent the average removal of six measurements with standard deviation. The X-axis is labeled to indicate formulation number in Table 2.2, along with commercial standards and controls.

Another alga studied was the microalgal diatom *Navicula incerta*. This slime-forming alga typically has significantly increased attachment and adhesion to hydrophobic surfaces.[41, 43] Surfaces on several of the experimental formulations were able to offer some form of resistance to cell attachment due to the presence of the SMAA. The *N. incerta* cell attachment and biomass remaining results are shown in Figure 2.4. Coating formulations 44, 47, and 50 had the lowest overall cell attachment in comparison to A4-20 control formulation (Table A4). These coatings had varying densities of grafted 750 molecular weight PEG chains going from ~100% grafted chains, to ~25%, and finally ~45 %. Even though these SMAAs were present at lower densities at the surface of the coatings, they still presented a heterogenous surface. This heterogeneity is largely caused by the larger PEG chains generating many more phase separated domains. It is suspected that the size and dispersion of these domains affects the settlement of microfoulants such as *N. incerta*. In contrast, formulations 15, 33, and 36 all had SMAAs with smaller molecular weights but with a similar backbone structure to 44, 47, and 50. These formulations had a higher removal of attached diatoms compared to A4-20 control formulation (Table A5**)**. This is likely due to increased mobility of the SMAA through the coating, increasing the chance of it populating the surface. The more SMAA present at the surface, the greater the number of these smaller molecular weight PEG chains, which could further disrupt adhesion of *N. incerta*. In summary, several experimental formulations had lower cell attachment and greater removal than A4-20, Dow Corning® T2, and Intersleek® 700, with formulation 33 being comparable to Intersleek® 900. Structure and mobility of SMAA, as well as molecular weight of grafted PEG chains again seem to be the most influential factors.

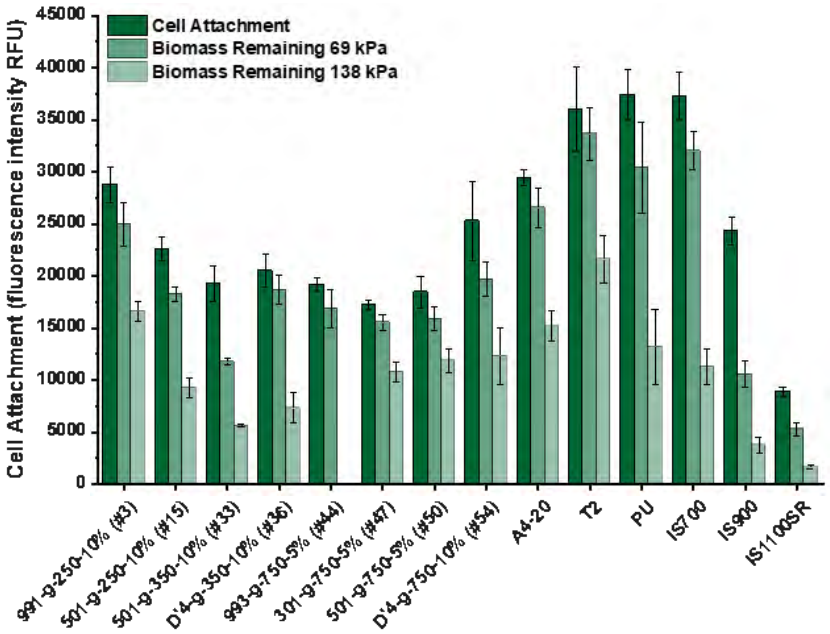

Figure 2.4. Cell attachment and biomass remaining of N. incerta after water-jet treatment at 69 and 138 kPa water column pressure. The dark green bars represent diatom cell attachment, whilst light green bars represent biomass remaining after water-jet treatment at 69 kPa, and the lightest green bars represent biomass remaining after water-jet treatment at 138 kPa for three replicate measurements and standard deviations. The X-axis is labeled to indicate formulation number in Table 2.2, along with commercial standards and controls. *** represents coating being damaged during analysis. No data for this formulation could be recovered.

In addition to performing biological assays with marine algae, biofilm growth and retention for the bacterium *Cellulophaga lytica* was performed on the coatings. This marine bacterium settles on both hydrophilic and hydrophobic surfaces.[3] Results from these assays can be seen in Figure 2.5. Experimental coatings that had significantly lower biofilm growth, compared to A4-20 control formulation, included formulations 3 and 15 (Table A6). In terms of biofilm removal, formulations 3, 15, 33, and 36 had significantly less biomass remaining as compared to A4-20 control formulation and all commercial standards (Table A7). The SMAAs in these coatings have lower molecular weight PEG chains and may simply present many more smaller-sized domains at the surface than their counterpart formulations 44, 47, 50, and 54. These organisms prefer a wide range of surfaces and so it is not perhaps simply a matter of whether the coating's surface is largely hydrophilic or hydrophobic which influences bacterial biofilm growth and adhesion, but how that surface presents itself. One explanation is that due to the incorporation of SMAA, the surface becomes much more heterogenous. Even the slightest increase in this heterogeneity may disrupt the formation of a biofilm, reducing growth and the ability for bacteria to

remain on the coated surfaces. Overall, introducing SMAAs into A4-20 significantly improved AF/FR properties towards marine bacterium *C. lytica*. Formulations 15 and 33 saw the largest benefit and both significantly outperform commercial standard Intersleek® 1100SR, with virtually zero biomass remaining after water-jet treatment.

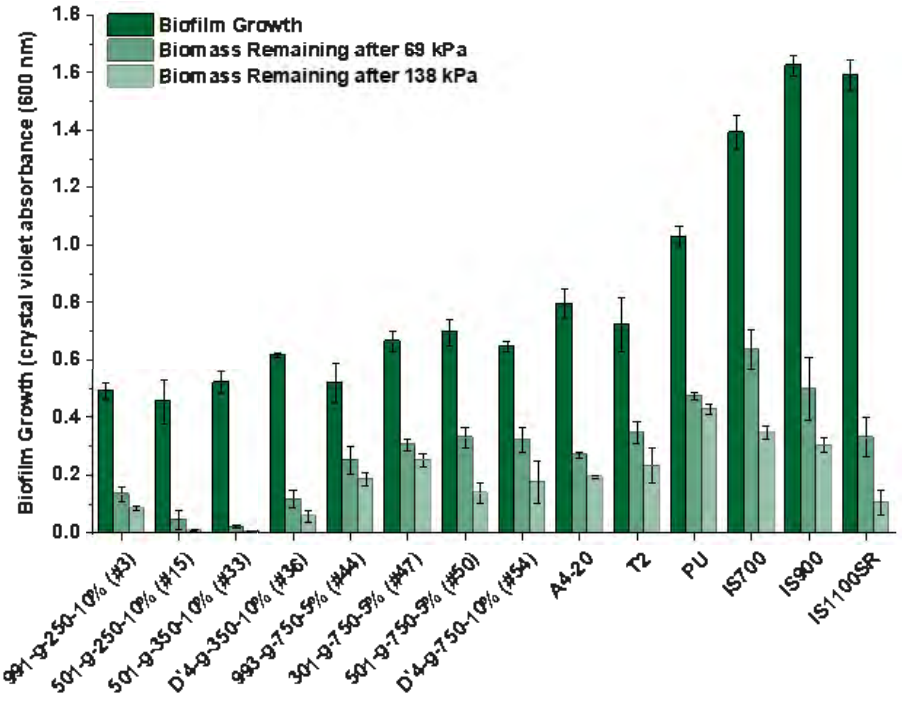

Figure 2.5. Bacterial biofilm growth and retention of C. lytica after water-jet treatment at 69 and 138 kPa water column pressure. The dark green bars represent biofilm growth, whilst the light green bars represent biomass remaining after water-jet treatment at 69 kPa, and the lightest green bars represent biomass remaining after water-jet treatment at 138 kPa for 3 replicate measurements with standard deviations. The X-axis is labeled to indicate formulation number in Table 2.2, along with commercial standards and controls.

In addition to evaluating AF/FR performance of coatings against algae and bacteria, it was important to study the efficacy against major macrofouling invertebrates such as adult barnacles of *Amphibalanus amphitrite.*[35] This species of barnacle is a major fouling organism that accounts for significant reductions in performance of marine vessels.[1, 44, 45] Hydrophilic surfaces are generally preferred for optimal spreading of adhesive, but this species can adhere to hydrophobic surfaces as well.[35, 46, 47] A push-off test was performed to measure reattached barnacle adhesion for coatings and is shown in Figure 2.6. In addition, the number of barnacles that attached, compared to the total number of available barnacles, is shown in Figure 2.6. While results from this assay show lower adhesion values

from formulations 44, 50, and 54 compared to A4-20 control formulation, statistical analysis using one-way ANOVA with Tukey method for multiple comparisons showed statistical insignificance in adhesion values (Table A8). However, there was also an insignificant increase in barnacle adhesion values from the other experimental formulations, except formulation 47 (suspected coating damage before testing, leading to attachment of barnacles to a poor epoxy surface). When performing barnacle reattachment and removal assays, there was much variation in mean adhesion values for many of the coating formulations evaluated, as seen from the error bars of the mean values in Figure 2.6. This is not uncommon when evaluating silicone-based fouling-release coatings as there are several factors affecting barnacle reattachment and adhesion such as basal plate diameter, health of reared barnacles, and environment of holding tanks.[36, 48] The main takeaway from this assay is that there was no significant increase or decrease in barnacle reattachment and adhesion between experimental coatings and A4-20 control formulation and commercial standards. These findings, combined with results from other biological assays in this work, point to the potential for several experimental formulations as having broad spectrum FR performance.

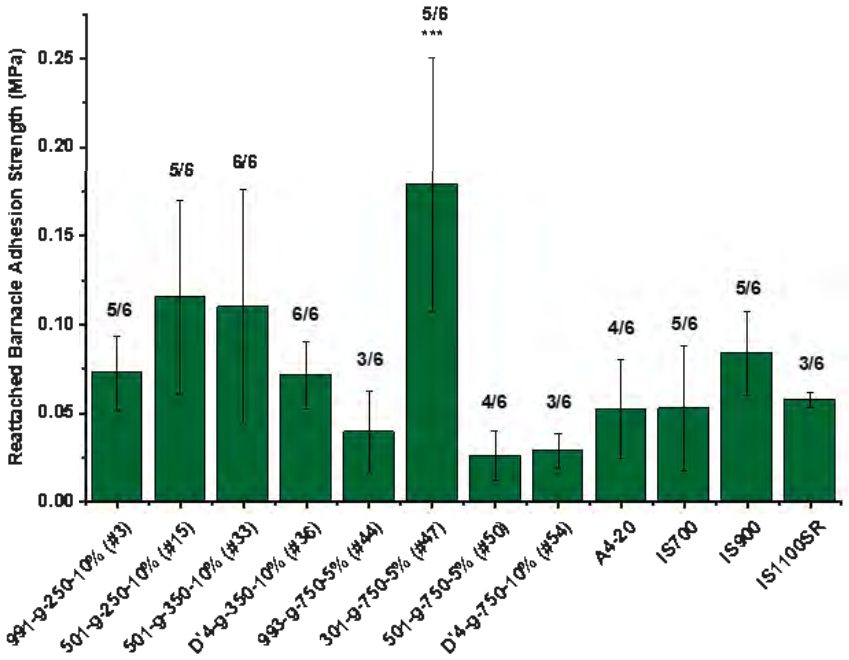

Figure 2.6. Reattached barnacle adhesion strength of A. amphitrite. Each bar represents the average adhesion strength of successfully pushed off barnacles. The ratio corresponds to the number of attached barnacles over the number of total available barnacles. *** denotes the breakage of an attached barnacle upon removal. The X-axis is labeled to indicate formulation number in Table 2.2, along with commercial standards and controls.

The last organism that was studied was the macrofoulant marine mussel *Geukensia demissa*. Species of mussel, like *G.* demissa, perform a complex search period to determine if a surface is suitable for attachment. If a surface is unsuitable, the mussels will typically not adhere, and search for another substrate.[49] The mussel removal force, as well as overall number of attached byssal threads was evaluated using a pull-off method and is shown in Figure 2.7. No mussels attached to the A4 20 or to formulations 36, 44, 50, and 54, making it difficult to assess if incorporation of SMAAs in these formulations had any effect. Most of the mussels evaluated did, however, attach to formulations 3, 15, 33, and 47, exhibiting relatively high mussel removal force. As mentioned previously, formulation 47 was suspected to have sustained coating damage (delamination/defects) throughout several assays and did not provide reliable data. The higher mussel removal values for the other formulations could be attributed to a markedly reduced surface heterogeneity due to SMAAs with lower molecular weight grafted PEG chains. Surface heterogeneity is being increasingly investigated as it is thought to play an important role in the deterrence of several marine foulants.[50-53] Formulations with these additives likely have a more homogenous hydrophilic surface, which some mussel foot proteins adhere to more strongly.[4, 54] On the other hand, formulations 44, 50, and 54 were shown to be more heterogenous in aqueous environments, potentially affecting the probing and eventual attachment of marine mussels to the surface. Overall, some formulations had performances comparable to the A4-20 internal control and Intersleek® commercial standards.

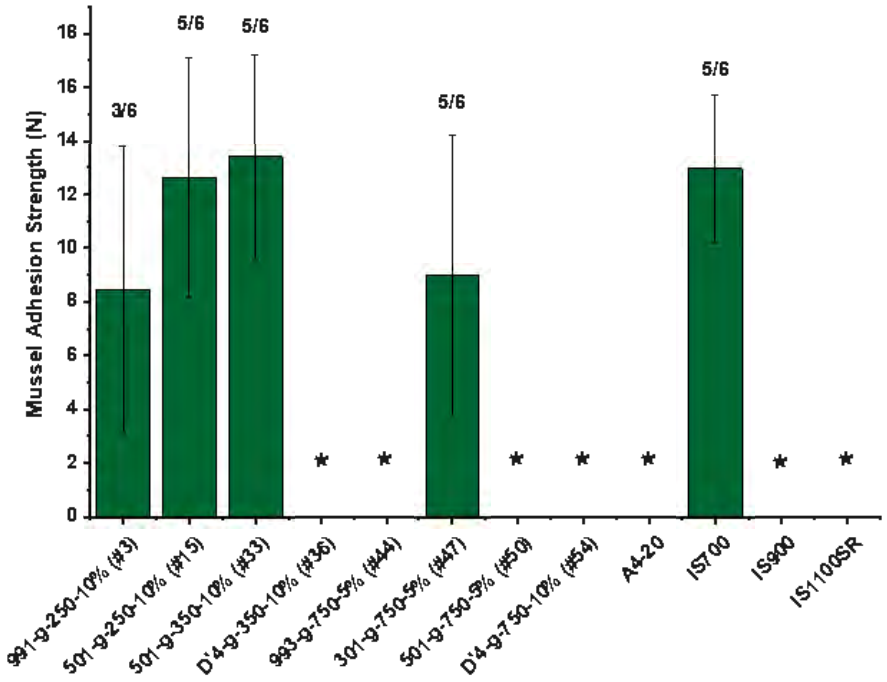

Figure 2.7. Mussel removal force of G. demissa. Six attempted attachments were performed for each coating. The removal force value represents the average force for removal of successfully attached mussels. The ratio corresponds to the number of attached mussels over the number of total available mussels. * denotes there were no mussels attached to coatings. The X-axis is labeled to indicate formulation number in Table 2.2, along with commercial standards and controls.

Conclusions

In this study, an array of surface-modifying amphiphilic additives (SMAAs) was successfully synthesized via hydrosilylation of various polymethylhydrosiloxanes (PMHS) and allyl-terminated polyethylene glycol monomethyl ethers (APEG). The SMAAs were then incorporated into the fouling-release coating A4-20; a self-stratifying siloxane-polyurethane (SiPU). Coatings contained either 1, 5, or 10 wt.% of SMAA relative to non-volatile content, and the objective was to obtain an amphiphilic, heterogenous surface with domains of both PDMS and PEG. Formulations were subjected to a set of AF/FR screening experiments using *C. lytica* and *N. incerta* to select candidates that had potential for good performance in further biological assays. Measurements from contact angle experiments from these selected formulations showed that several SMAAs had the ability to modify the surface of A4-20. The most significant change in contact angles was seen in formulations containing SMAAs with lower molecular weight grafted PEG chains. Images of the coated surfaces using AFM in the dry state (substrate exposed to air) showed changes to surface morphology brought about by incorporation of

SMAAs. When these surfaces were imaged in the hydrated state (substrate exposed to deionized water), significant increases in domain size were seen due to swelling of PEG chains at the surface. Formulations that exhibited the highest amount of surface change were those containing SMAAs with higher molecular weight PEG chains. Evaluation of AF/FR properties was carried out using a range of test organisms comprising a bacteria, micro- and macro-algae, and barnacles and mussels. It was shown that several formulations with varying SMAA significantly affected the AF/FR performance of A4-20 against these organisms. However, broad-spectrum performance was best for formulations 44, 50, and 54. These coatings contained SMAAs with 750 molecular weight grafted PEG chains with varying chain density along the siloxane backbone. As seen through surface characterizations, as well as biological assays, the two most influential factors in performance were the ability for the SMAA to produce a heterogenous surface via diffusion through the coating, and the molecular weight of the grafted PEG chains. Moving forward, further work will be carried out to provide more evidence of these relationships in a variety of AF/FR coatings systems.

References

1. Yebra, D. M.; Kiil, S. K.; Dam-Johansen, K., Antifouling Technology—Past, Present and Future Steps Towards Efficient and Environmentally Friendly Antifouling Coatings. *Prog. Org. Coat.* **2004,** *50* (2), 75.

2. Hellio, C.; Yebra, D. M., *Advances in Marine Antifouling Coatings and Technologies*. 2009.

3. Lejars, M.; Margaillan, A.; Bressy, C., Fouling release coatings: a nontoxic alternative to biocidal antifouling coatings. *Chemical reviews* **2012,** *112* (8), 4347-4390.

4. Callow, J. A.; Callow, M. E., Trends in the development of environmentally friendly fouling-resistant marine coatings. *Nature Communications* **2011,** *2*, 244.

5. Callow, M. E.; Callow, J. A., Marine Biofouling: A Sticky Problem. *Biologist* **2002,** *49* (1), 10.

6. Schultz, M. P.; Bendick, J. A.; Holm, E. R.; Hertel, W. M., Economic Impact of Biofouling on a Naval Surface Ship. *Biofouling* **2011,** *27* (1), 87.

7. Majumdar, P.; Ekin, A.; Webster, D. C., Thermoset Siloxane—Urethane Fouling Release Coatings. ACS Publications: 2007.

8. Webster, D. C.; Ekin, A., Functionalized polysiloxane polymers. Google Patents: 2010.

9. Webster, D. C.; Pieper, R. J.; Ekin, A., Thermoset siloxane-urethane fouling release coatings. Google Patents: 2011.

10. Ekin, A.; Webster, D. C., Combinatorial and High-Throughput Screening of the Effect of Siloxane Composition on the Surface Properties of Crosslinked Siloxane–Polyurethane Coatings. *J. Comb. Chem.* **2007,** *9* (1), 178.

11. Sommer, S.; Ekin, A.; Webster, D. C.; Stafslien, S. J.; Daniels, J.; VanderWal, L. J.; Thompson, S. E. M.; Callow, M. E.; Callow, J. A., A Preliminary Study on the Properties and Fouling-Release Performance of Siloxane-Polyurethane Coatings Prepared from Pdms Macromers. *Biofouling* **2010,** *26* (8), 961.

12. Bodkhe, R. B.; Thompson, S. E. M.; Yehle, C.; Cilz, N.; Daniels, J.; Stafslien, S. J.; Callow, M. E.; Callow, J. A.; Webster, D. C., The Effect of Formulation Variables on Fouling-Release Performance of Stratified Siloxane-Polyurethane Coatings. *Journal of Coatings Technology Research* **2012,** *9* (3), 235.

13. Krishnan, S.; Wang, N.; Ober, C. K.; Finlay, J. A.; Callow, M. E.; Callow, J. A.; Hexemer, A.; Sohn, K. E.; Kramer, E. J.; Fischer, D. A., Comparison of the fouling release properties of hydrophobic fluorinated and hydrophilic PEGylated block copolymer surfaces: attachment strength of the diatom Navicula and the green alga Ulva. *Biomacromolecules* **2006,** *7* (5), 1449-1462.

14. Martinelli, E.; Hill, S. D.; Finlay, J. A.; Callow, M. E.; Callow, J. A.; Glisenti, A.; Galli, G., Amphiphilic modified-styrene copolymer films: Antifouling/fouling release properties against the green alga Ulva linza. *Progress in Organic Coatings* **2016,** *90*, 235-242.

15. Andrade, J. D.; King, R. N.; Gregonis, D. E.; Coleman, D. L. In *Surface characterization of poly (hydroxyethyl methacrylate) and related polymers. I. Contact angle methods in water*, 1979; Wiley Online Library: pp 313-336.

16. Galli, G.; Martinelli, E., Amphiphilic polymer platforms: surface engineering of films for marine antibiofouling. *Macromolecular rapid communications* **2017,** *38* (8), 1600704.

17. Rufin, M. A.; Ngo, B. K. D.; Barry, M. E.; Page, V. M.; Hawkins, M. L.; Stafslien, S. J.; Grunlan, M. A., Antifouling silicones based on surface-modifying additive amphiphiles. *Green Materials* **2017,** *5* (1), 4-13.

18. Sundaram, H. S.; Cho, Y.; Dimitriou, M. D.; Weinman, C. J.; Finlay, J. A.; Cone, G.; Callow, M. E.; Callow, J. A.; Kramer, E. J.; Ober, C. K., Fluorine-free mixed amphiphilic polymers based on PDMS and PEG side chains for fouling release applications. *Biofouling* **2011,** *27* (6), 589-602.

19. Noguer, A. C.; Olsen, S.; Hvilsted, S.; Kiil, S., Diffusion of surface-active amphiphiles in silicone-based fouling-release coatings. *Progress in Organic Coatings* **2017,** *106*, 77-86.

20. Patterson, A. L.; Wenning, B.; Rizis, G.; Calabrese, D. R.; Finlay, J. A.; Franco, S. C.; Zuckermann, R. N.; Clare, A. S.; Kramer, E. J.; Ober, C. K., Role of backbone chemistry and monomer sequence in amphiphilic oligopeptide-and oligopeptoid-functionalized PDMS-and PEO-based block copolymers for marine antifouling and fouling release coatings. *Macromolecules* **2017,** *50* (7), 2656-2667.

21. Tanoue, H.; Inutsuka, M.; Yamada, N. L.; Ito, K.; Yokoyama, H., Kinetics of dynamic polymer brush formation. *Macromolecules* **2017,** *50* (14), 5549-5555.

22. International Intersleek 1100SR Product Page. https://www.international-marine.com/product/intersleek-1100sr (accessed June 6th).

23. Olsen, S.; Yebra, D. Polysiloxane-based fouling release coats including enzymes. EP2726559B1, April, 5th, 2017.

24. Olsen, S.; Yebra, D. Novel polysiloxane-based fouling release coatings including biocide(s). EP2899240B1, January 8th, 2020.

25. Thorlaksen, P.; Blom, A.; Bork, U. Fouling control coating compositions. US9534121B2, January 3rd, 2017.

26. Galhenage, T. P.; Webster, D. C.; Moreira, A. M. S.; Burgett, R. J.; Stafslien, S. J.; Vanderwal, L.; Finlay, J. A.; Franco, S. C.; Clare, A. S., Poly (ethylene) glycol-modified, amphiphilic, siloxane–polyurethane coatings and their performance as fouling-release surfaces. *Journal of Coatings Technology and Research* **2017,** *14* (2), 307-322.

27. Hooper, R.; Lyons, L. J.; Mapes, M. K.; Schumacher, D.; Moline, D. A.; West, R., Highly Conductive Siloxane Polymers. *Macromolecules* **2001,** *34* (4), 931-936.

28. Owens, D. K.; Wendt, R. C., Estimation of the Surface Free Energy of Polymers. *J. Appl. Polym. Sci.* **1969,** *13* (8), 1741.

29. Stafslien, S. J.; Christianson, D.; Daniels, J.; VanderWal, L.; Chernykh, A.; Chisholm, B. J., Combinatorial materials research applied to the development of new surface coatings XVI: fouling-release properties of amphiphilic polysiloxane coatings. *Biofouling* **2015,** *31* (2), 135-149.

30. Casse, F.; Stafslien, S. J.; Bahr, J. A.; Daniels, J.; Finlay, J. A.; Callow, J. A.; Callow, M. E., Combinatorial materials research applied to the development of new surface coatings V. Application of a spinning water-jet for the semi-high throughput assessment of the attachment strength of marine fouling algae. *Biofouling* **2007,** *23* (2), 121-130.

31. Starr, R. C.; Zeikus, J. A., UTEX: the culture collection of algae at the University of Texas at Austin. *Journal of phycology* **1987,** *23*.

32. Stafslien, S. J.; Bahr, J. A.; Daniels, J. W.; Wal, L. V.; Nevins, J.; Smith, J.; Schiele, K.; Chisholm, B., Combinatorial materials research applied to the development of new surface coatings VI: An automated spinning water jet apparatus for the high-throughput characterization of fouling-release marine coatings. *Review of Scientific Instruments* **2007,** *78* (7), 072204.

33. Callow, M. E.; Callow, J. A.; Conlan, S.; Clare, A. S.; Stafslien, S., Efficacy testing of nonbiocidal and fouling-release coatings. *Biofouling methods* **2014**, 291-316.

34. Stafslien, S.; Daniels, J.; Mayo, B.; Christianson, D.; Chisholm, B.; Ekin, A.; Webster, D.; Swain, G., Combinatorial Materials Research Applied to the Development of New Surface Coatings. Iv: A High-Throughput Bacterial Retention and Retraction Assay for Screening Fouling-Release Performance of Coatings. *Biofouling* **2007,** *23* (1), 45.

35. Rittschof, D.; Orihuela, B.; Stafslien, S.; Daniels, J.; Christianson, D.; Chisholm, B.; Holm, E., Barnacle Reattachment: A Tool for Studying Barnacle Adhesion. *Biofouling* **2008,** *24* (1), 1.

36. Stafslien, S.; Daniels, J.; Bahr, J.; Chisholm, B.; Ekin, A.; Webster, D.; Orihuela, B.; Rittschof, D., An Improved Laboratory Reattachment Method for the Rapid Assessment of Adult Barnacle Adhesion Strength to Fouling-Release Marine Coatings. *Journal of Coatings Technology and Research* **2012,** *9* (6), 651.

37. Casse, F.; Ribeiro, E.; Ekin, A.; Webster, D. C.; Callow, J. A.; Callow, M. E., Laboratory Screening of Coating Libraries for Algal Adhesion. *Biofouling* **2007,** *23* (4), 267.

38. Majumdar, P.; Lee, E.; Patel, N.; Ward, K.; Stafslien, S. J.; Daniels, J.; Chisholm, B. J.; Boudjouk, P.; Callow, M. E.; Callow, J. A., Combinatorial materials research applied to the development of new surface coatings IX: an investigation of novel antifouling/fouling-release coatings containing quaternary ammonium salt groups. *Biofouling* **2008,** *24* (3), 185-200.

39. Hoipkemeier-Wilson, L.; Schumacher, J. F.; Carman, M. L.; Gibson, A. L.; Feinberg, A. W.; Callow, M. E.; Finlay, J. A.; Callow, J. A.; Brennan, A. B., Antifouling Potential of Lubricious, Micro-Engineered, Pdms Elastomers against Zoospores of the Green Fouling Alga Ulva (Enteromorpha). *Biofouling* **2004,** *20* (1), 53.

40. Callow, M. E.; Callow, J.; Ista, L. K.; Coleman, S. E.; Nolasco, A. C.; López, G. P., Use of self-assembled monolayers of different wettabilities to study surface selection and primary adhesion processes of green algal (Enteromorpha) zoospores. *Applied and Environmental Microbiology* **2000,** *66* (8), 3249-3254.

41. Finlay, J. A.; Callow, M. E.; Ista, L. K.; Lopez, G. P.; Callow, J. A., The influence of surface wettability on the adhesion strength of settled spores of the green alga Enteromorpha and the diatom Amphora. *Integrative and comparative biology* **2002,** *42* (6), 1116-1122.

42. Callow, J.; Callow, M.; Ista, L.; Lopez, G.; Chaudhury, M., The influence of surface energy on the wetting behaviour of the spore adhesive of the marine alga Ulva linza (synonym Enteromorpha linza). *Journal of the Royal Society Interface* **2005,** *2* (4), 319-325.

43. Holland, R.; Dugdale, T.; Wetherbee, R.; Brennan, A.; Finlay, J.; Callow, J.; Callow, M. E., Adhesion and motility of fouling diatoms on a silicone elastomer. *Biofouling* **2004,** *20* (6), 323-329.

44. Aldred, N.; Clare, A. S., The adhesive strategies of cyprids and development of barnacle-resistant marine coatings. *Biofouling* **2008,** *24* (5), 351-363.

45. Gittens, J. E.; Smith, T. J.; Suleiman, R.; Akid, R., Current and emerging environmentally-friendly systems for fouling control in the marine environment. *Biotechnology advances* **2013,** *31* (8), 1738-1753.

46. Rittschof, D.; Costlow, J., Bryozoan and barnacle settlement in relation to initial surface wettability: a comparison of laboratory and field studies. *Scientia Marina (Barcelona)* **1989,** (2-3).

47. Di Fino, A.; Petrone, L.; Aldred, N.; Ederth, T.; Liedberg, B.; Clare, A. S., Correlation between surface chemistry and settlement behaviour in barnacle cyprids (Balanus improvisus). *Biofouling* **2014,** *30* (2), 143-152.

48. Kim, J.; Nyren-Erickson, E.; Stafslien, S.; Daniels, J.; Bahr, J.; Chisholm, B. J., Release characteristics of reattached barnacles to non-toxic silicone coatings. *Biofouling* **2008,** *24* (4), 313-319.

49. Prendergast, G. S., Settlement and Behaviour of Marine Fouling Organisms. *Biofouling* **2009**, 30.

50. Finlay, J. A.; Krishnan, S.; Callow, M. E.; Callow, J. A.; Dong, R.; Asgill, N.; Wong, K.; Kramer, E. J.; Ober, C. K., Settlement of Ulva zoospores on patterned fluorinated and PEGylated monolayer surfaces. *Langmuir* **2008,** *24* (2), 503-510.

51. Martinelli, E.; Sarvothaman, M. K.; Galli, G.; Pettitt, M. E.; Callow, M. E.; Callow, J. A.; Conlan, S. L.; Clare, A. S.; Sugiharto, A. B.; Davies, C., Poly (dimethyl siloxane)(PDMS) network blends of amphiphilic acrylic copolymers with poly (ethylene glycol)-fluoroalkyl side chains for

fouling-release coatings. II. Laboratory assays and field immersion trials. *Biofouling* **2012,** *28* (6), 571-582.

52. Kirillova, A.; Marschelke, C.; Friedrichs, J.; Werner, C.; Synytska, A., Hybrid hairy Janus particles as building blocks for antibiofouling surfaces. *ACS applied materials & interfaces* **2016,** *8* (47), 32591-32603.

53. Dudchenko, A. V.; Bengani-Lutz, P.; Asatekin, A.; Mauter, M. S., Foulant Adsorption to Heterogeneous Surfaces with Zwitterionic Nanoscale Domains. *ACS Applied Polymer Materials* **2020**.

54. Ohkawa, K.; Nishida, A.; Honma, R.; Matsui, Y.; Nagaya, K.; Yuasa, A.; Yamamoto, H., Studies on fouling by the freshwater mussel Limnoperna fortunei and the antifouling effects of low energy surfaces. *Biofouling* 1999, *13* (4), 337-350.

CHAPTER 3. STUDYING THE EFFECT OF PRE-POLYMER COMPOSITION AND INCORPORATION OF SURFACE MODIFYING AMPHIPHILIC ADDITIVES ON THE FOULING-RELEASE PERFORMANCE OF AMPHIPHILIC SILOXANE-POLYURETHANE COATINGS

Introduction

A common problem that faces structures submerged in seawater is that of marine biofouling. This phenomenon involves the settlement and growth of over 4000 different micro- and macrofoulants on these structures, which leads to a variety of negative impacts, especially on the hulls of seafaring vessels.[1, 2] Accumulation of these foulants on ships' hulls causes increased drag and fuel consumption, overall higher economic cost of operation, and greater greenhouse gas emissions, while also promoting highly detrimental invasive species transfer.[3-6] It is estimated that the United States Navy spends nearly 56 million dollars per year for their midsized vessels such as destroyers, with projections of over 1 billion dollars after a period of 15 years to contend with biofouling.[3] A major reason for such a high cost of maintenance of these marine vessels, is the highly complex and dynamic nature of the phenomenon of biofouling along with the numerous number of foulants each having various sizes and modes of adhesion.[7] Several different stages are involved in this process, which usually begins with a 'conditioning' layer made up largely of proteins, nutrients, and other small molecules. Other stages that follow include bacterial or microalgae biofilms, which often lead to settlement of macrofouling organisms such as macroalgae, barnacles, mussels, and tunicates. However, being dynamic in nature, the amount, and subsequent timing, of each fouling stage varies greatly, making protection against marine biofouling a difficult task for any single approach.[2, 7]

Methods of preventing marine biofouling have undergone numerous changes ever since navigation of the world's oceans began.[2] Layers of copper alloy, lead sheaths, and mixtures of tar and hot pitch were widely used on wooden ships as antifouling (AF) countermeasures.[8] However, as steel built ships became more prevalent, along with the advances in materials science at the advent of the 20th

century, methods including the use of resins or biodegradable polymer matrices containing biocides became widely accepted.[9] Arguably the most successful biocides utilized in these coatings were alkyl tin-containing paints notably those with tributyltin (TBT). These antifouling (AF) paints were widely used until a world-wide ban was ratified by the International Maritime Organization (IMO) in 2003 due to concerns of their high toxicity towards nontargeted organisms and overall impact on local aquatic ecosystems.[10] Currently, antifouling paint formulations mostly contain biocidal pigments based on copper and zinc oxides which, while effective, are still seen to accumulate in local aquatic environments, leading to increased scrutiny regarding toxicity concerns.[11, 12] Due to the constant concerns for use of biocides as a fouling deterrent, non-toxic solutions involving fouling-release (FR) coatings have been widely studied. These FR coatings function by preventing strong adhesion of marine foulants to surfaces, so that under hydrodynamic forces, the organisms will be easier to remove.[2, 7] Several traditional FR systems have been utilized that are comprised of low surface energy materials such as polydimethylsiloxane (PDMS) or polyfluoroalkyl (PFA) polymers. However, these coatings often suffer from poor durability, poor mechanical properties, and difficult adhesion to substrates, often needing tie-coats to get the desired protection.[1, 2, 7] To remedy these issues, self-stratifying siloxane-polyurethane (SiPU) FR coatings were developed and showed a significant increase in mechanical properties, adhesion and durability, while maintaining excellent FR properties.[13, 14] However, these coatings were largely hydrophobic to which some organisms prefer to settle, limiting their performance compared to more fouling-resistant surfaces.[15-17]

To address some of the issues with using hydrophobic FR coating systems, amphiphilic FR coatings have been developed which incorporate a hydrophilic component to offer fouling resistance, while also maintaining the good release properties of hydrophobic surfaces.[18-20] There are typically two methods to achieve such a heterogenous, amphiphilic surface. One method is to alter the composition of a coating system using reactive hydrophilic and hydrophobic moieties. The most widely used hydrophilic component is typically polyethylene glycol (PEG), while the hydrophobic component is often PDMS or PFA polymers.[18, 21-23] Galhenage et al. developed coatings based upon previously research SiPU technologies that included synthesizing amphiphilic isocyanate prepolymers containing PEG and PDMS chains of varying molecular weight and amount, and then reacting them further to form an amphiphilic

SiPU network.[24] These coatings provided broad-spectrum FR performance for several different micro- and macrofoulants that were comparable to commercial standard coatings such as Intersleek® 1100SR and Hempasil® X3. Other amphiphilic coating systems being investigated include zwitterionic moieties,[25-30] polyelectrolyte systems,[31, 32] and those containing peptide mimicking 'peptoid' molecules.[33, 34]

Another method of imparting amphiphilic character to a coating's surface is by using surface-active additives that have both hydrophilic and hydrophobic components. Again, PEG and PDMS are the most widely used hydrophilic and hydrophobic moieties being used in several different coatings systems.[35-39] Zwitterionic-based co-polymers,[40-42] poly(vinylpyrrolidone) containing additives,[43] and poly(oxazoline)-based amphiphilic additives have also been used to improve AF/FR properties of coating systems.[44] Recently, Benda et al. prepared a series of surface-modifying amphiphilic additives (SMAAs) that varied in molecular weight of grafted PEG chains, as well as the degree of grafting onto a polysiloxane backbone. These SMAAs were incorporated into a hydrophobic SiPU coating at varying amounts. It was shown that the molecular weight of grafted PEG chains had the largest effect on FR performance, followed by the degree of grafting of PEG chains.[38] However, this SMAA system, along with the vast majority of coatings that incorporate amphiphilic additives, does so in hydrophobic coating matrices. Incorporating these amphiphilic additives into inherently amphiphilic coating matrices could further increase AF/FR performance.

In this study, further investigation of previously prepared amphiphilic isocyanate prepolymers, and their subsequent amphiphilic coatings, was performed. Prepolymers were prepared using isophorone diisocyanate polyisocyanate reacted with monocarbinol terminated 10,000 g/mol PDMS, and hydroxy terminated 750 g/mol PEG. The equivalents of isocyanate/hydroxyl groups were kept at 3:2, but the amount of PDMS or PEG in the prepolymer was varied. FTIR, isocyanate titrations, and GPC were utilized to determine the remaining isocyanate content, variation in PDMS and PEG content, as well as the general distribution of prepolymer species. These prepolymers were then mixed with additional polyisocyanate, an acrylic polyol, and varying amounts of an SMAA to generate amphiphilic SiPU FR coatings. Water contact angle (WCA) and methylene iodide contact angle (MICA) were measured and surface energy was determined for each experimental formulation before and after 28 days of immersion in circulating tap water. ATR-FTIR and AFM were utilized to determine the presence of PDMS and PEG

at the surface, as well as changes in surface morphology when the amount of PDMS and PEG was changed in the prepolymer and the amount of incorporated SMAA was increased. Lastly, the FR properties of these coatings were evaluated using biological assays involving the marine bacterium *Cellulophaga lytica*, the diatom *Navicula incerta*, the green macroalga *Ulva linza*, the barnacle *Amphibalanus amphitrite*, and the mussel *Geukensia demissa*.

Experimental

Materials

The solvents toluene, HPLC grade tetrahydrofuran (THF), methyl amyl ketone (MAK), isopropanol, ethyl-3-ethoxyproprionate (EEP), and acetone were purchased from Sigma Aldrich. PEG-750, a 750 $\bar{M}_n$ hydroxyl-terminated polyethylene glycol monomethyl ether, platinum(0)-1,3-divinyl-1,1,3,3-tetramethyldisiloxane complex solution with ~2 % Pt in xylenes (Karstedt's catalyst), dibutyltin diacetate (DBTDAc), acetylacetone, dibutylamine, and anhydrous benzyl alcohol were also purchased from Sigma Aldrich. Monocarbinol-terminated polydimethylsiloxane (PDMS) with a molecular weight of 10,000 g/mol (MCR-C22) was purchased from Gelest Inc. Monoallyl-terminated polyethylene glycol monomethyl ether with molecular weight of 350 g/mol (Polyglykol® 350 AM) was provided by Clariant. Polyisocyanate Desmodur Z 4470 BA was provided by Covestro LLC. Hydrochloric acid with 0.1 N, and potassium bromide optical discs used for Fourier Transform Infrared Spectroscopy (FTIR) experiments were purchased from Alfa Aesar. For use in coatings formulations, an acrylic polyol consisting of 80% butyl acrylate and 20% 2-hydroxyethyl acrylate was synthesized via conventional free radical polymerization and diluted to 50% by weight in toluene. A more detailed description of the synthesis can be found elsewhere.[14] A surface-modifying amphiphilic additive (SMAA) with a polysiloxane backbone of molecular weight between 900-1200 g/mol, and approximately 45-55% of the backbone consisting of chains of PEG-350, was synthesized according to previous work,[38] and used in coatings formulations. Coatings were cast on both 76 x 152 mm and 102 x 203 mm aluminum panels (0.6 mm thick, type A, alloy 3003 H14) purchased from Q-lab. These panels were first sandblasted and primed with Intergard 264 marine primer, provided by AkzoNobel International Paint. Intersleek® 700 (IS700), 900 (IS900), and 1100SR (IS1100SR) were used as commercial FR coatings and provided by AkzoNobel International Paint. Dow

Corning® T2, a silicone elastomer, was used as a standard coating and was provided by Dow Corning. Falcon sterile polystyrene 24-multiwell plates were purchased from VWR International.

Experimental Approach

Previously, an amphiphilic siloxane-polyurethane (AMP-SiPU) FR coating had been reported by Galhenage et al.[24] This coating system had both polyethylene glycol (PEG) and polydimethylsiloxane (PDMS) chains as the hydrophilic and hydrophobic components on a polyisocyanate pre-polymer backbone. Once the prepolymers had been synthesized, they were mixed with an acrylic polyol and additional polyisocyanate and cured to form a self-stratifying SiPU FR coating. In that work, the amount of amphiphilic pre-polymer in the total formulation was varied, as well as the molecular weights of both the PDMS and PEG chains on the pre-polymer. The surfaces of the coatings were largely influenced by the molecular weights of both PDMS and PEG, with more significant heterogeneity resulting from higher molecular weights of PDMS. In addition, increasing the amount of amphiphilic modified pre-polymer in the formulation produced larger surface domains, also increasing surface heterogeneity. FR performance followed a similar trend, with higher removal occurring with higher molecular weights of PDMS and increased pre-polymer content in the formulation. Interestingly, similar trends were also observed for ice adhesion to the surfaces of these coatings.[45]

To further investigate the surfaces and the FR properties of these coatings, two main objectives were established. The first was to vary the ratio of hydrophobic (PDMS) and hydrophilic (PEG) content in the pre-polymer composition and observe the changes in the surfaces of these coatings, along with their effect on FR properties. The initial AMP-SiPU chosen consisted of a 10 wt.% PDMS and 10 wt.% PEG isocyanate pre-polymer, resulting in a total of 20 wt.% amphiphilic pre-polymer in the final formulation weight. The molecular weight of the PEG was 750 $\bar{M}_n$, with the molecular weight of PDMS at 10,000 g/mol. This formulation was selected as it had one of the highest overall removal values for each marine fouling organism studied by Galhenage et al.[24] Changes in the PDMS:PEG ratio consisted of 5 wt.% intervals about the base pre-polymer composition of 10 wt.% of both PDMS and PEG. This resulted in formulations with a 20:0, 15:5, 10:10, 5:15, and 0:20 ratio of PDMS to PEG wt.% in the pre-polymer.

The second objective of this study was to investigate the effects of incorporating a surface modifying amphiphilic additive (SMAA) at a range of concentrations relative to the overall formulation of

solids, into these AMP-SiPU FR coatings. It was expected that the amphiphilic nature of the SMAA would be more compatible with an amphiphilic coating matrix, potentially causing a variety of changes to surface morphology, as well as in increase in FR performance. The chosen SMAA for this study (Figure 3.1) consisted of a polysiloxane backbone of ~900-1200 g/mol, with ~45-55% of the backbone being grafted with chains of PEG with a molecular weight of 350 g/mol. The details on formulations prepared to investigate these methods of producing an amphiphilic coating system can be found in Table 3.1.

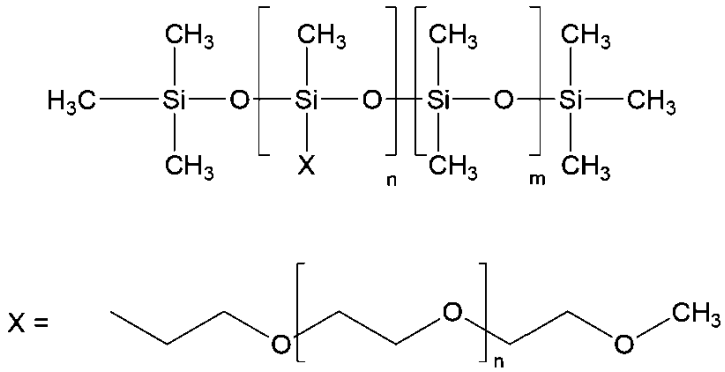

Figure 3.1. Structure of the SMAA used in AMP-SiPU FR coatings, where “X” is equivalent to a grafted PEG-350 chain on a polysiloxane backbone of ~900-1200 g/mol.

Table 3.1. Experimental formulations used in this work including the ratios of PDMS to PEG (wt.%) in the prepolymers, wt.% of added SMAA, and total hydrophobic and hydrophilic content from PDMS and PEG (wt.%)

Formulation	PDMS:PEG Wt.%	SMAA wt.%	Wt. % PDMS (hydrophobic content)	Wt. % PEG (hydrophilic content)
F1	20 : 0	0	20.00	0.00
F2		5	21.25	3.75
F3		10	22.50	7.50
F4	15 : 5	0	15.00	5.00
F5		5	16.25	8.75
F6		10	17.50	12.50
F7	10 : 10	0	10.00	10.00
F8		5	11.25	13.75
F9		10	12.50	17.50
F10	5 : 15	0	5.00	15.00
F11		5	6.25	18.75
F12		10	7.50	22.50
F13	0 : 20	0	0.00	20.00
F14		5	1.25	23.75
F15		10	2.50	27.50

To determine the theoretical amphiphilic content of these formulations, the hydrophilic content of the additive had to be determined. This was accomplished by dividing the molecular weight (g/mol) of the grafted PEG chains by the total theoretical molecular weight (g/mol) of the SMAA. The content was found to be 75% PEG and 25% PDMS. These values were used, in conjunction with the PDMS and PEG wt. % in the pre-polymer compositions, to determine the theoretical hydrophobic and hydrophilic content based on total formulation solids of 15 g (Table 3.1).

Amphiphilic Isocyanate-Functional Pre-Polymer Synthesis

For use in coatings formulations, an isophorone diisocyanate (IPDI) trimer (Desmodur Z4470 BA) was modified with monofunctional PDMS (10,000 g/mol) and hydroxy-terminated PEG (750 g/mol), resulting in amphiphilic prepolymers. Several different pre-polymer compositions were synthesized as shown in Table 3.1. Detailed procedures for the synthesis of these prepolymers can be found elsewhere.[24] However, a general procedure for the synthesis of the pre-polymer used in F9 (10 wt. % PDMS and 10 wt.% PEG based off total formulation solids) from Table 3.1 is as follows. To prepare 30 g of total formulation weight, PEG-750 (1.5000 g) was added to a 100 mL plastic cup, along with ethyl-3-ethoxyproprionate (EEP, 1.5000 g) and a Teflon coated magnetic stir bar. This mixture was stirred until PEG-750 was dissolved, and then PDMS (1.5000 g) was added and mixed vigorously with a vortex mixer for 3-5 minutes. Lastly, IPDI trimer (1.6491 g) and catalyst solution (DBTDAc 1 wt.% in MAK, 0.2079 g) was added to the mixture and again mixed vigorously with a vortex mixer for 3-5 minutes. Afterwards, the mixture was stirred overnight for 24 h. The isocyanate to total hydroxyl equivalents ratio was kept at 3:2 for all pre-polymer syntheses. A representative structure of these prepolymers is shown in Figure 3.2.

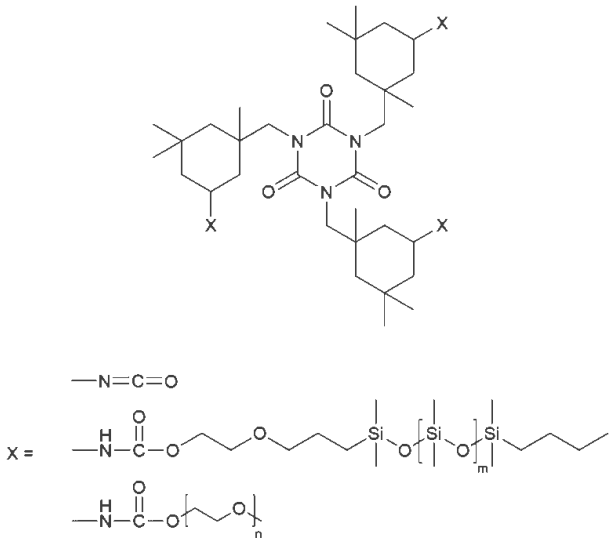

Figure 3.2. General structure of IPDI prepolymers where “X” can be either isocyanate groups, chains of PDMS (10,000 g/mol), or chains of PEG (750 g/mol).

Pre-Polymer Isocyanate Titrations

To characterize the isocyanate groups after pre-polymer synthesis, isocyanate titrations were performed. These were performed after pre-polymer solutions had been stirred for 24 hours and a general procedure, modified from ASTM D2572-19, is as follows. To a 250 mL Erlenmeyer flask, a 0.3-0.5 g sample of pre-polymer was added and diluted with 100 mL of isopropanol. Then, 25 mL of 0.1 N dibutyl amine solution in toluene was added, followed by an additional 25 mL of isopropanol. This solution was mixed for 15 minutes and then a few drops of bromophenol blue indicator solution was added. Using 0.1 N hydrochloric acid, the solution was titrated until an endpoint transition of blue to pale yellow. The amount of hydrochloric acid dispensed was recorded and a blank sample was also performed, omitting the addition of pre-polymer samples. Isocyanate content (%NCO) was then calculated using the equation provided in ASTM D2572-19.

Fourier-Transform Infrared Spectroscopy

To further assess the presence of remaining isocyanate in the pre-polymer samples, FT-IR was performed using a Thermo Scientific Nicolet 8700 FT-IR spectrometer. Liquid pre-polymer samples were spread over a potassium bromide optical disk and placed in the instrument after obtaining a background spectrum.

DryAdd Simulations: Estimating Reactions Between Primary Isocyanate and Hydroxyl Groups

To help determine the molecular distribution of the different pre-polymer structures, DryAdd Pro+, a Monte Carlo simulation package developed for polymer chain growth and network formation by Oxford Materials, was used. Generating predicted data from this type of software typically involves defining the materials present, defining the reactions that occur, and defining some general parameters of the reactions between the materials used. In this study, the materials used were a primary aliphatic polyisocyanate (IPDI trimer), carbinol-terminated PDMS, and hydroxy-terminated PEG. The IPDI trimer has three total isocyanate groups, with PDMS and PEG containing one hydroxyl group each. The two reactions of interest were defined as the reaction between carbinol-terminated PDMS and IPDI trimer, and between the hydroxy-terminated PEG and IPDI trimer. The amounts, in grams and mols, of these materials were also entered into the software. Lastly, the number of molecules simulated (population size) was set at 1 million, stopping at 100% conversion. Simulations of the formulations were performed and data about the distribution of different pre-polymer structures was obtained.

Gel-Permeation Chromatography

A Tosoh Bioscience EcoSEC HLC-8320 GPC system was utilized to provide experimental evidence of a distribution of pre-polymer structures for data gathered from DryAdd simulations. To prepare samples for GPC analysis, leftover isocyanate was reacted with benzyl alcohol. Excess amounts of benzyl alcohol were added to the prepolymers, solutions were heated to 60℃, and stirred for an additional hour. Samples were then prepared by diluting with HPLC grade THF and added to 1.5 mL sample vials. After thermal equilibrium, samples were passed through a TSKgel SuperH3000 column at a flow rate of 0.35 mL/min, with both column and pump temperature at 40°C and pressure at 3.5 MPa. Chromatograms were recorded utilizing a refractive index detector.

Coating Formulation

Following pre-polymer synthesis, coating formulations were prepared as outlined by Galhenage et al.[24] A representative procedure for formulation F9 is as follows. After 24 hours of stirring the pre-polymer solution, additional IPDI (5.5635 g), a 50% by wt. in toluene, 80:20 BA:HEA acrylic polyol (14.4879 g), and pot-life extender acetylacetone (0.3000 g) was added to the mixture. The surface modifying amphiphilic additive (1.6919 g), described in Figure 3.1, was added and the solution was mixed

vigorously with a vortex mixer for 3-5 minutes, and then stirred for an additional hour on a stir plate. The isocyanate to total hydroxyl equivalents was kept at 1.1:1.0. After 1 hour, the formulations were cast on both 76 x 152 mm and 102 x 203 mm primed aluminum panels using a Gardco #80 wire wound drawdown bar, as well as on 75 x 25 mm glass microscope slides. The coated panels and glass slides were left to cure at ambient temperatures for 24 hours and then placed in an oven at 80℃ for 45 minutes. The remaining formulations were prepared in the same way, but with changes in wt. % SMAA incorporation and composition of pre-polymer, as described in Table 3.1.

Control and Commercial Standard Coatings

As a comparison to the prepared experimental formulations, standard and control coatings were prepared for use in biological assays. These coatings (Table 3.2) were prepared according to manufacturer's specifications on 102 x 203 mm aluminum panels primed with Intergard 264 and deposited in multi-well plates on primed aluminum disks.

Table 3.2. Control and commercial standard coatings used in this work

Control Name	Control ID	Composition
Polyurethane	PU	NDSU prepared polyurethane standard
Dow Corning® T2	T2	Silicone elastomer commercial FR standard coating
Polystyrene	Poly	Polystyrene negative control
Intersleek® 700	IS700	Intersleek commercial FR standard coating
Intersleek® 900	IS900	Intersleek commercial FR standard coating
Intersleek® 1100SR	IS1100SR	Intersleek commercial FR standard coating with a "slime release" component

Surface Characterization

A Thermo Scientific Nicolet 8700 FT-IR spectrometer, with a Smart iTR diamond plate ATR sampling accessory, was used to gather Attenuated Total Reflectance Fourier-Transform Infrared Spectroscopy (ATR-FT-IR) spectra.

Water contact angle (WCA) and methylene iodide contact angle (MICA) measurements were gathered for all formulations using a First Ten Angstroms FTA100 series dynamic contact angle analyzer. Three measurements for each experimental formulation were taken at 2-minute intervals for 10 minutes. A primed aluminum panel, coated with the experimental formulations, was placed on the sample platform and a 10 µl drop of distilled water was carefully placed on the top, middle, and bottom portions of the

panel. Measurements were started after a delay of 10 s. The values at each time interval were averaged and their standard deviation calculated. The Owens-Wendt method was utilized to calculate surface energy at each time interval over the course of 10 minutes and represented as mN/m.46

Analysis of WCA, MICA, and surface energy calculations was also performed on experimental formulations after water ageing. Coated primed aluminum panels were placed in circulating water tanks using tap water and left for 28 days at ambient temperatures. After drying the surfaces of coated samples, WCA, MICA, and surface energy values were determined using the same procedure described previously.

Atomic Force Microscopy (AFM) measurements were made following a general procedure. Sample panels were placed on the sample holder of an Oxford Asylum Jupiter XR microscope and controller. A silicon cantilever (AC240TS-R3) with resonant frequency of 50-90 kHz and a spring constant of 0.6-3.5 N/m from Oxford Instruments was affixed to the instrument and calibrated. An area of 100 x 100 µm was scanned in air and height and phase images were gathered. Images were analyzed using Igor Analysis software.

Water Ageing

Before submitting samples for biological assays, all formulations were placed in circulating water tanks for at least 28 days of preleaching at ambient temperature. This is an important step before performing biological assays. Residual toxic components of the coating system, such as dibutyltin diacetate, could potentially remain in the coating, resulting in errors during AF/FR evaluations due to leaching of these compounds. After preleaching for 28 days, panels were removed from water immersion, rinsed with deionized water, and dried overnight. Small disks were punched out from coated panels to be used in *C. lytica*, *N. incerta*, and *U. linza* biological assays. Larger, 102 x 203 mm primed aluminum panels coated with formulations were used as is for *G. demissa* and *A. amphitrite* macrofouling assays.

Biological Assays

Macroalgae 7-Day Growth and Release (Ulva linza)

Samples for this assay included multi-well plates with coated disks glued into the wells and were evaluated after 28 days pre-leaching in circulating tap water. A more detailed description of the procedure for this biological assay can be found elsewhere.[47] Before the start of the experiment, all multi-well plates

were equilibrated in 0.22 µm filtered artificial seawater (FSW) (Tropic Marin) at Newcastle for 2 h. To assess growth and release of *U. linza* sporelings, 1 mL of *U. linza* suspension was adjusted to 3.3 x 10^5 spores mL^{-1} (0.05 OD at absorbance 660 nm) in single strength enriched seawater medium and added to each well.[48] The spores that settled on the plates were grown for 7 days inside an illuminated incubator at 18℃ with 16:8 light to dark cycle at a photon flux density of 45 µmol/m/s, renewing nutrients every 72 hours. After 7 days of sporeling growth, the biomass that was generated was assessed from a single row of wells (6) from each plate. The remaining rows were subjected to water spraying from a spinjet apparatus at pressures of 18, 67, or 110 kPa.[49] Chlorophyll was extracted by adding 1 mL of DMSO to each well and determination of fluorescence at excitation at 360 nm and emission at 670 nm wavelengths. The removal of sporelings at each pressure was compared to unsprayed wells with fluorescence being directly proportional to biomass present on each coated surface.

Microalgae 2 h Cell Attachment and Release (Navicula incerta)

Detailed methods to assess the growth and release of microalgae (*N. incerta*) diatom cells can be found elsewhere.[47, 50] A brief description is as follows. A 1 mL suspension of *N. incerta* cells with 4 x 10^5 cells mL^{-1} (adjusted to 0.03 OD at absorbance 660 nm) in Guillard's F/2 medium was deposited into each coated well. To stimulate cell attachment, plates were subjected to static incubation for 2 h under ambient conditions in the dark. The suspension was then removed and wells were subjected to water-jet treatments using a spinjet apparatus.[49] Assessment of cell attachment was performed on the first column of wells (3 wells), which was not subject to water-jet pressures. The second and third columns (3 wells each) were subjected to 69 kPa and 138 kPa psi water pressures respectively for 10 s. To quantify the biomass of the wells, chlorophyll was extracted with 0.5 mL DMSO and fluorescence was measured at an excitation wavelength of 360 nm and emission wavelength of 670 nm. The relative fluorescence units (RFU) was directly proportional to the biomass remaining on coatings surfaces after water-jet treatments. The percent removal of diatom cells was determined by comparing the RFUs of non-jetted and water-jetted wells.

Bacterial Biofilm 24 h Growth and Adhesion (Cellulophaga lytica)

The assessment of marine bacterium (*C. lytica*) biofilm growth and adhesion has been described in detail in previous works.[49-51] To coated multi-well plates, a 1 mL suspension of marine bacterium *C.*

lytica, at 10^7 cells/mL in ASW with 0.5 g/L peptone and 0.1 g/L of yeast extract, was added. These plates were then incubated for 24 h at 28℃ and then gently rinsed 3 times with deionized water to remove any loose bacteria. Again, the first column (3 wells) did not receive water-jet treatments whilst the other two columns (3 wells each) were subjected to 69 kPa and 138 kPa water pressure for 5 s. To determine biomass remaining on the wells that underwent water-jetting, wells were stained with a crystal violet solution (0.3 wt.% in deionized water) for 15 min and then rinsed 3 times with deionized water. Multi-well plates were then dried at ambient conditions for 1 h before extracting the crystal violet dye with 0.5 mL 33% acetic acid solution for 15 min. Resulting eluates (0.15 mL/ well) were measured for absorbance at 600 nm wavelength. The obtained absorbance measurements were directly proportional to the biomass on the coatings surface before and after water-jet treatments.

Adult Barnacle 2-Week Reattachment and Adhesion (Amphibalanus amphitrite)

To assess marine barnacle (*A. amphitrite)* attachment and adhesion, a custom procedure developed at NDSU was performed.[52, 53] Primed 102 x 203 mm aluminum panels coated with the experimental formulations were used throughout this experiment. After 28 days pre-leaching in circulating water tanks, adult barnacles (~5 mm in diameter and provided by Duke University Marine Laboratory, Beaufort, North Carolina, USA) attached to silicone substrates (n = 6) were removed and immobilized onto the surface of the experimental coatings. Barnacles could reattach and grow for 2 weeks while immersed in ASW tank systems with daily feeding of brine shrimp. After 2 weeks, barnacles were pushed off the surface with shear force generated by a handheld force gauge mounted on a semi-automated stage. The peak force of removal for each barnacle was recorded along with the base plate area of each dislodged barnacle, which was measured using Sigma Scan Pro 5.0 image analysis software. The adhesion strength (MPa) of each barnacle was calculated by taking the ratio of the force for removal to basal plate area and the average adhesion strength for each coating was reported as the total number of barnacles removed with a measurable force.

Marine Mussel 3-Day Attachment and Adhesion (Geukensia demissa)

To perform marine mussel (*G. demissa)* attachment and adhesion measurements, mussels were obtained from Duke University Marine Laboratory in Beaufort, North Carolina, USA. The mussels had a 4-cm-long acetal plastic rod (product # 98873A105, McMaster-Carr) attached via 3M® acrylic adhesive

(product # 7467A135, McMaster-Carr) perpendicular to the ventral edge. The modified mussels were then immobilized onto each experimental coating surface followed by placing custom PVC sheets against the plastic rods to keep the mussels in contact with the surface. These coatings were then placed in ASW circulating tanks and fed DT's Premium Reef Blend Phytoplankton daily. After 3 days, the coatings were removed and the total number of mussels with byssus threads attached to each experimental coating was recorded. Next, the plastic rod from each mussel was attached to an individual load cell of 5 N that was part of a custom-built force gauge where the mussels were then pulled off at a rate of 1 mm/s. The force required (N) for detachment of the byssus thread was averaged and the pull-off value for each coating was recorded. Any non-attached mussels were recorded as well.

Further Analysis of U. linza Spore Settlement, and 7-Day Growth and Removal on Selected Formulations

Previous biological assays were carried out using the green algae *Ulva linza*, which measured sporeling growth and removal at water-jet pressures of 18, 67, and 110 kPa. To study the AF/FR properties of several selected formulations when subjected to much weaker hydrodynamic forces, a separate assay utilizing a turbulent flow cell was employed and a general description of the procedure is as follows.[54] Selected formulations included two different ratios of PDMS:PEG wt.% in the pre-polymer, along with formulations containing SMAAs at 5 wt.%. Coatings prepared on standard 75 x 25 mm glass microscope slides were first equilibrated in 0.22 µm filtered artificial seawater for 48 hrs prior to testing. To measure spore settlement (i.e. spore density), a suspension of zoospores (10 mL; $1x10^6$ spores mL^{-1}) was added to individual compartments of quadriPERM dishes containing the samples. Sample dishes were kept in the dark for 45 minutes at 20℃, and then slides were washed by moving back and forth 10 times through a beaker of seawater to remove unsettled spores. Next, on one slide of each treatment group, attached spores were fixed using 2.5% glutaraldehyde in seawater. The density of zoospores attached to the surface was counted using an image analysis system attached to a fluorescence microscope. Spores were visualized by autofluorescence of chlorophyll and counts were made for 30 fields of view (each 0.15 mm^2) on each slide.

To measure sporeling growth, spores were settled on selected coatings via the same procedure used to measure spore density. After settlement, the spores were cultured using supplemented seawater medium for 7 days to produce sporelings (young plants) on 4 replicate slides for each selected coating

sample. Sporeling growth medium was refreshed every 48 hrs. Sporeling biomass was determined *in situ* by measuring the fluorescence of chlorophyll contained within the sporelings in a Tecan fluorescence plate reader. The biomass was quantified in terms of relative fluorescence units (RFU). The RFU value for each slide is the mean of 70-point fluorescence readings taken from the central portion. Assessing sporeling removal was accomplished by placing these samples in a turbulent flow cell and subjecting them to 42 Pa of shear stress. Biomass remaining was determined using the same method used to determine sporeling growth. The percentage removal was calculated from readings taken before and after exposure to the shear stress.

Barnacle Cypris Larvae 48-h Settlement (Balanus improvisus)

To perform settlement assays, cypris larvae of *Balanus improvisus* (=*Amphibalanus improvisus*) were obtained from broodstock which are maintained in a semicontinuous culture at Newcastle University, UK. The original population of barnacles from which the broodstock has been cultured was from Sven Lovén Center for Marine Sciences, Tjärnö, Sweden. Adult barnacles were maintained in a recirculating aquarium kept at 19℃, with brackish conditions, 25 ppt artificial seawater (ASW; Tropic Marin) and fed daily with *Artemia* sp. and *ad libitum* with the chlorophyte *Tetraselmis suecica*. Larvae were collected by removing adult barnacles overnight, and then immersing them, resulting in the release of nauplius larvae into the water column. These larvae were collected by attraction to a point light source. Nauplii (~10,000) were then transferred to 10 L buckets containing aerated ASW at a salinity of 25 ppt. Nauplii were fed with a mixture of 50:50 *T. suecica* and *Thalassiosira pseudonana* with the proportion of the latter being reduced to zero by the third day of culture. The metamorphosis into cypris took approximately 4-5 days, when they were collected by filtration and stored in the dark at 6℃ for 3 days.

To analyze settlement of three-day-old *B. improvisus* cyprids on selected coating samples, a general procedure is as follows.[54] Six replicate coated slides were placed in quadriPERM dishes, and 1 mL of ASW was initially added to each surface as a droplet. The cypris larvae were added 20 per drop, which had sufficient height for free movement of the larvae. The plates were then closed and covered in a moist tissue paper to minimize evaporation. Plates were incubated in the dark at 28℃ for 48 hrs. The number of larvae that settled on the samples was expressed as a proportion of the total, averaged per surface, and then compared between surfaces.

Statistical Analysis

One-way ANOVA was performed using Minitab statistical software on data gathered from the biological assays. These included growth and settlement assays for *U. linza*, *C. lytica*, and *N. incerta*, release assays for *C. lytica* and *N. incerta*, as well as reattachment assays involving *A. amphitrite*. The highest water/impact pressures, 138 kPa for *C. lytica* and *N. incerta*, were used for analysis. The results from these assays were treated as part of a completely randomized design, with two factors (pre-polymer composition and SMAA wt.%) having five levels and three levels respectively for each factor, resulting in a total of fifteen treatment groups. The significance level (α) was set at $\alpha = 0.05$, with statistically significant results having P-values < 0.05. Tukey method was used to make comparisons between the difference of means from each treatment group. Means that do not share a letter in Tables B5-B22 are significantly different.

Results and Discussion

The formulation of antifouling/fouling-release (AF/FR) coatings that offer protection from a wide variety of marine fouling organisms is a challenging prospect, largely due to the opposing surface preferences of these organisms. Recently, it has been shown that several coatings systems presenting an amphiphilic surface consisting of both hydrophobic and hydrophilic domains perform better than traditional FR coatings systems. Two major methods of achieving this surface, as shown by Galhenage et al.[24] and Benda et al.,[38] involve formulating coatings with hydrophobic and hydrophilic domains within the coating's matrix itself, and by incorporating non-covalently bound amphiphilic additives into a hydrophobic siloxane-polyurethane coating. Both methods reported an improvement in FR properties compared to coatings which did not have amphiphilic character and performed better than several commercial standard FR coatings. This study aimed to combine both methods of preparing an amphiphilic coating surface to investigate the effect on surface characteristics and AF/FR properties using biological assay testing with several well-known marine foulants. Several isophorone diisocyanate (IPDI) based prepolymers, modified with PDMS and PEG, were synthesized according to a previous study.[24] Five unique prepolymers with different compositions were prepared by varying the relative amounts of PDMS and PEG, as shown in Table 3.1. Prepolymers with PDMS and PEG molecular weights of 10,000 and 750 g/mol were chosen for this study because they showed superior FR performance compared to other

compositions as reported by Galhenage et al.[24] These prepolymers were combined with additional IPDI trimer (Desmodur Z 4470 BA) and an acrylic polyol with an 80:20 ratio of butyl acrylate to hydroxyethyl acrylate to generate amphiphilic siloxane-polyurethane FR coatings (AMP-SiPU). In addition, a surface modifying amphiphilic additive (SMAA), shown in Figure 3.1, was synthesized according to previous work, and incorporated into these AMP-SiPU formulations at 5 and 10 wt.%. The selected additive performed well, compared to other SiPU coatings with several other SMAAs with different structures, in biological FR assays reported by Benda et al.[38]

To prepare isocyanate prepolymers with varying PDMS and PEG compositions, an isophorone diisocyanate trimer (Desmodur Z 4470 BA) was reacted with 10k g/mol carbinol-terminated polydimethylsiloxane (PDMS) and 750 g/mol hydroxy-terminated polyethylene glycol monomethyl ether (PEG) in the presence of dibutyltin diacetate solution in methyl amyl ketone. The ratio of isocyanate to total hydroxyl equivalents was kept constant at 3:2 to ensure leftover isocyanate necessary for subsequent coatings formulation. A modified isocyanate titration method based on ASTM D2572-19, along with FT-IR was used to determine successful synthesis of prepolymers.

Table 3.3 shows the theoretical and actual % solids and % NCO values of the prepolymers with varying PDMS and PEG wt. %. In each pre-polymer, a remaining amount of NCO sufficient for further crosslinking is evident. This suggests successful synthesis of the desired prepolymers. Deviations from the theoretical % NCO content could be explained by reaction of isocyanate with moisture, incomplete reaction with dibutyl amine solution used during titrations, as well as a reduction in actual % solids, which will cause a decrease in actual % NCO content.

Table 3.3. Theoretical and actual average isocyanate (% NCO) and non-volatile content (% solids) for synthesized prepolymers with varying PDMS and PEG wt.% according to Table 3.1

Formulation (PDMS:PEG)	Theoretical		Actual	
	% Solids	% NCO	% Solids ± SD	% NCO ± SD
F1 (20:0)	49.70	0.24	49.23 ± 0.18	0.09 ± 0.05
F4 (15:5)	51.38	0.75	49.75 ± 0.70	0.45 ± 0.05
F7 (10:10)	54.00	1.18	50.90 ± 0.27	0.83 ± 0.05
F10 (5:15)	54.80	1.50	52.11 ± 0.02	0.98 ± 0.05
F13 (0:20)	55.71	1.74	52.76 ± 0.18	1.15 ± 0.01

Figure 3.3 shows the FT-IR spectra for the synthesized prepolymers. All spectra (3.3A-E) show a peak around 2300 cm^{-1}, belonging to remaining isocyanate, necessary for further crosslinking reactions. In spectra 3.3A, belonging to F1 in Table 3.3 which only had 20 wt.% PDMS in the pre-polymer, characteristic peaks around 3000, 1100-1000, and 800 cm^{-1} showed the presence of methyl groups along the PDMS backbone, Si-O-Si stretching, and Si-C vibrations, respectively. Conversely, spectra 3.3E, belonging to F13 in Table 3.3, which only had 20 wt.% PEG in the pre-polymer, showed peaks around 2900 and 1100 cm^{-1} belonging to methylene groups along the PEG chain as well as C-O-C ether stretching, respectively. Although the signature peaks for Si-O-Si and C-O-C overlap to some extent, the remaining spectra of 3.3B-D show gradual changes in composition based on the region of 1100-1000 cm^{-1}. Spectra 3.3B showed a more PDMS dominant region, while spectra 3.3D showed a more PEG dominant region. This is due to the change in PDMS:PEG ratio going from F4 at 15:5, to F10 at 5:15 shown in Table 3.3. Overall, more evidence of successful synthesis of these prepolymers with varying PDMS and PEG wt.% was obtained through FT-IR.

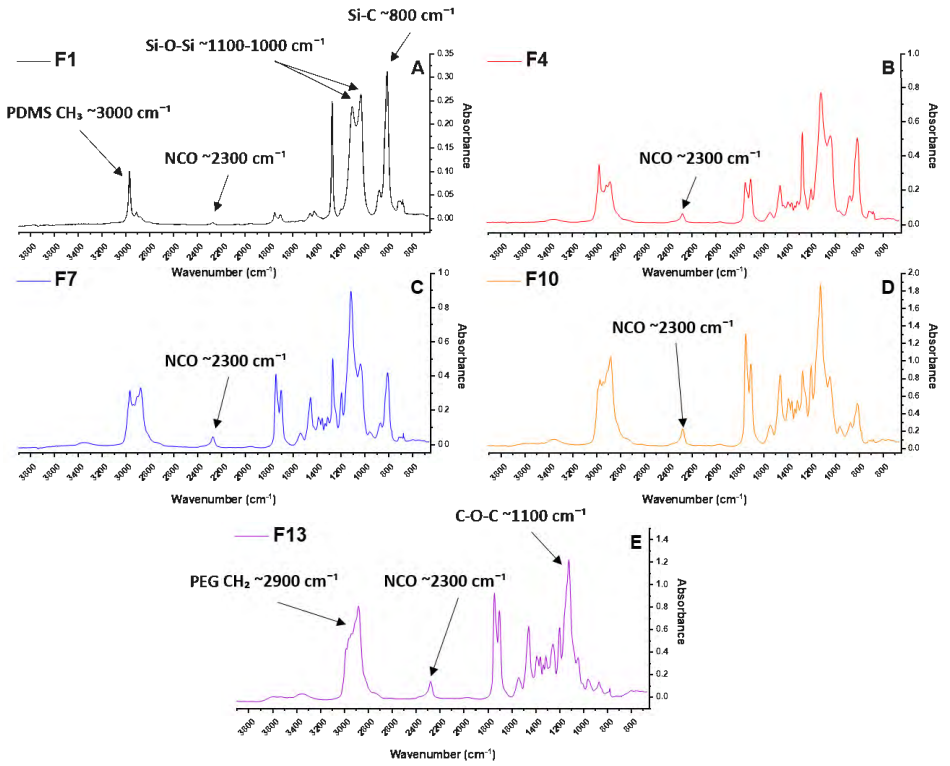

Figure 3.3. FTIR spectra showing characteristic PDMS, PEG, and isocyanate peaks for prepolymers shown in Table 3.3.

In addition to confirming the successful synthesis of amphiphilic isocyanate prepolymers using FTIR and NCO titrations, we sought to understand the general structures in the prepolymers. Due to the presence of three isocyanate functional groups on the IPDI trimer with the similar reactivity of the hydroxyl groups of the PDMS and PEG, a distribution of products is likely to form due to the statistical nature of the isocyanate-hydroxyl reactions. While an “ideal” pre-polymer structure could be one that has one chain of PDMS, one chain of PEG, and one unreacted isocyanate group, there may be other structures such as an IPDI trimer fully reacted with PDMS, PEG, or combinations of both. To explore this hypothesis, we utilized DryAdd Pro+, a Monte Carlo simulation software package that can predict composition of molecular species during polymerizations or reactions between defined functional groups such as hydroxyl and isocyanate groups. After performing these simulations on the prepolymers formed in Table 3.3, gel permeation chromatography (GPC) was carried out to determine if there was a correlation between computational and experimental findings.

Data gathered from DryAdd simulations, as well as GPC plots, can be found in Table B2 and Figure B1 of appendix B. Overall, it was determined from DryAdd that for all the prepolymers, the number of reacted isocyanate groups of the IPDI trimer had a similar distribution, with ~9 mol% unreacted NCO trimer, ~33 mol% having one reacted NCO group, ~41 mol% having two reacted NCO groups, and finally ~17 mol% of a completely reacted NCO trimer. This range of pre-polymer species was not entirely unexpected as this was a simple reaction between an NCO and a primary alcohol. However, the data we gathered suggested that our generalized structure in Figure 3.2 is only slightly more dominant than the other species. What is more intriguing is the predicted abundance of fully reacted pre-polymer species, which would now be a non-covalently bound amphiphilic polymeric species that does not undergo reaction into the coating matrix. In Figure B1, GPC plots of the different prepolymers with varying PDMS and PEG weight % show several peaks pertaining to pre-polymer species, which contain varying amounts of PDMS and PEG chains reacted onto the isocyanate trimer. It is clear to see that there is a shift in molecular weights for species containing an increased amount of PEG as opposed to PDMS chains on the pre-polymer. However, quantitative analysis was not performed using this technique and future work will be concerned with utilizing methods such as MALDI-TOF mass spectrometry to explore the % fraction of these pre-polymer species to corroborate findings in DryAdd simulations.

After the prepolymers were synthesized, coatings formulations were prepared as shown in Table 3.1. Surface characterization using ATR-FTIR, WCA/MICA and surface energy calculations, as well as AFM were performed to investigate the effect of varying PDMS and PEG wt.% in the pre-polymer as well as incorporation of varying levels of SMAA wt.%. We hypothesized that as changes in the wt.% of PDMS and PEG, and in the amount of SMAA incorporated in the coating, there would be a change in surface composition that could be detected via ATR-FTIR. Figure 3.4 shows the ATR-FTIR spectra for coatings F1, F4, F7, F10, and F13 described in Table 3.1. These coatings contained no SMAA and only had changes in PDMS and PEG wt.% in the pre-polymer. The region for an isocyanate peak seen around 2250 cm-1, shown by the solid black circle, is virtually absent in all formulations, signaling a fully crosslinked coating. The other region of interest, shown by the dashed circle, is between 1000-1100 cm-1. This region contains an overlap between Si-O-Si stretching and C-O-C ether stretching indicative of PDMS and PEG, respectively. In F1, there was a calculated amount of PDMS at 20 wt.% in the pre-polymer, with 0 wt.% PEG. The characteristic 'double' peak of Si-O-Si can be seen here, with no evidence of C-O-C from PEG. Contrary to this formulation, F13 contained 0 wt.% PDMS and 20 wt.% PEG. In this formulation, the surface shows the characteristic C-O-C ether stretching from PEG. For the rest of the formulations (F4, F7, and F10), various intensities of both Si-O-Si and C-O-C stretching peaks can be seen, with more PEG observed at the surface of F10 and more PDMS at the surface of F4

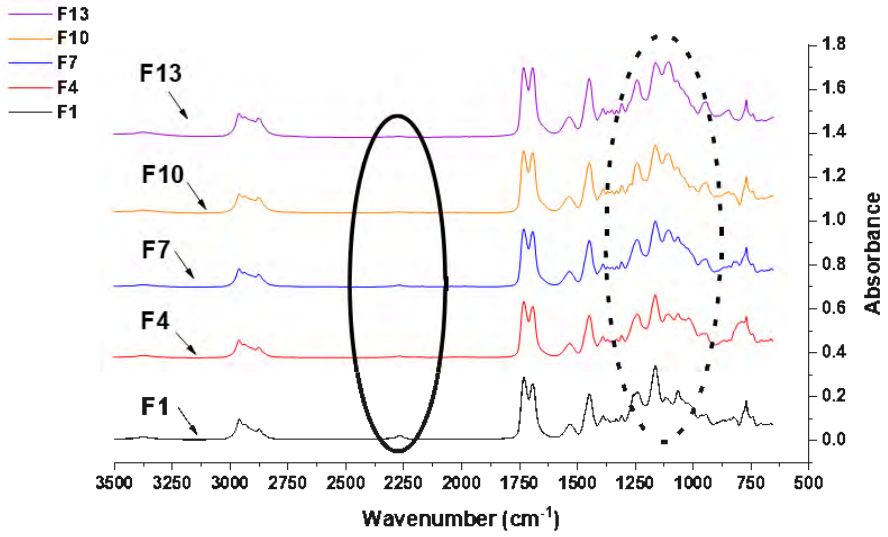

Figure 3.4. ATR-FTIR spectra for formulations shown in Table 3.1 with no incorporated SMAA. The solid black circle indicates the NCO region ~2250 cm-1, while the dashed circle indicates the region containing Si-O-Si and C-O-C stretching ~1000-1100 cm-1.

Figure 3.5 shows the ATR-FTIR spectra obtained for formulations in Table 3.1 that had 10 wt.% SMAA incorporated into the coating (F3, F6, F9, F12, and F15). These spectra look like the ones shown in Figure 3.4, with the main difference being characteristic Si-O-Si and C-O-C peaks can be seen in all formulations regardless of pre-polymer composition. Overall, ATR-FTIR was able to observe the variation in PDMS and PEG content, from both changes in pre-polymer compositions and SMAA incorporation, at the surface of these coatings.

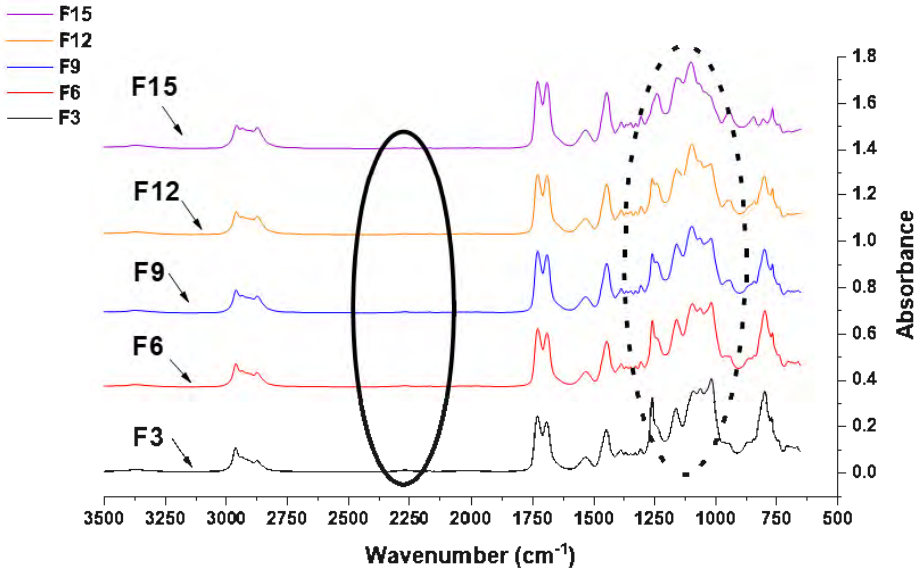

Figure 3.5. ATR-FTIR spectra for formulations shown in Table 3.1 with 10 wt.% incorporated SMAA. The solid black circle indicates the NCO region ~2250 cm^{-1}, while the dashed circle indicates the region containing Si-O-Si and C-O-C stretching ~1000-1100 cm^{-1}.

Measuring the water and methylene iodide contact angles (WCA/MICA) and then calculating surface energy (SE) can provide valuable information on the amphiphilic character of the surface, as well as surface activity due to SMAA incorporation for these formulations. Figure 3.6 shows the WCA, MICA, and SE values for formulations in Table 3.1, before water ageing (Figure 3.6A, 3.6C, and 3.6E) and after water ageing (Figure 3.6B, 3.6D, and 3.6F). In each series, an increase in formulation number going from 1 to 15, was associated with an overall increase of PEG content. The WCA values showed a slight downward trend when the amount of PEG in the pre-polymer composition was increased. These values all stayed above 90°, indicating that the surface of these coatings was still hydrophobic. However, as PDMS content was reduced in the pre-polymer composition, such as in F13, the WCA value dropped to ~80°, becoming more hydrophilic. The same trend was seen in MICA and SE values, where pre-polymer

composition had only a minor effect on surface character except for the fully hydrophilic pre-polymer compositions. Additionally, WCA, MICA, and SE values were not significantly changed (apart from evaporation of the water droplet) after 10 min of analysis.

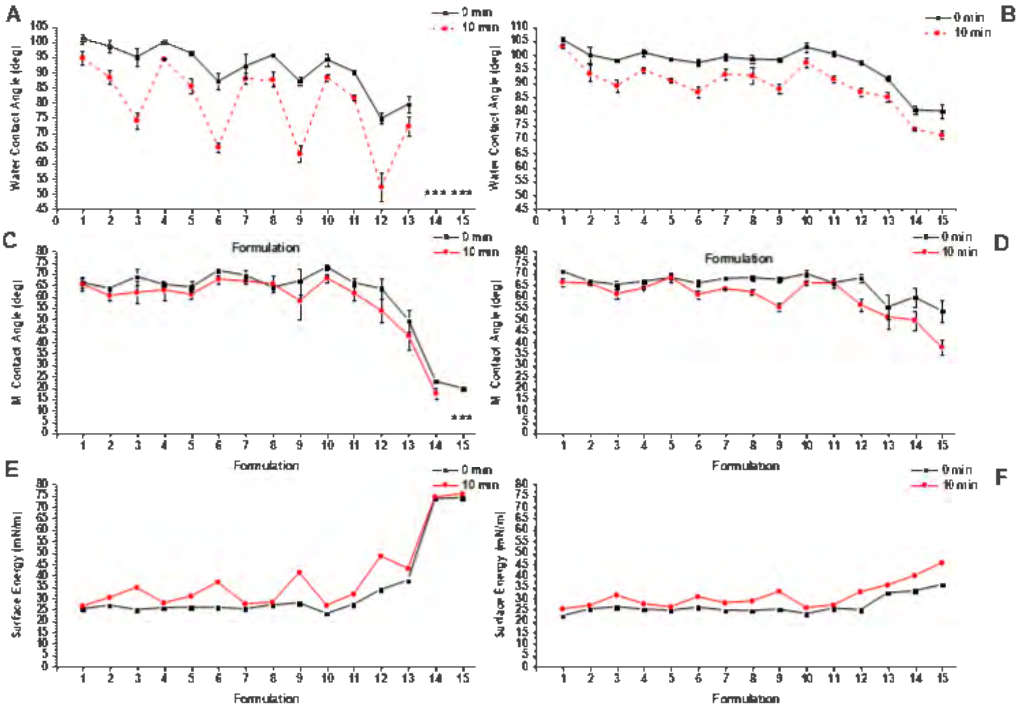

Figure 3.6. Water contact angles (WCA) plots A and B, methylene iodide contact angles (MICA) plots C and D, and surface energy calculations (SE) plots E and F on formulations shown in Table 3.1. A, C, and E were measurements performed before 28 days of water ageing, with B, D, and F having been performed after water ageing. The '***' in 3.6A and 3.6C denote a completely wetted surface where no value could be obtained (effectively 0°).

On the other hand, incorporation of SMAA did have a significant effect on WCA values for coatings of all pre-polymer compositions. There was some decrease in WCA across formulations at the 0 min point of the measurements, with an insignificant effect on MICA and SE measurements. However, after 10 min of analysis, large decreases in WCA occurred for all formulations, with formulations containing 10 wt.% SMAA having the most effect. Also, formulations F14 and F15, which had 5 wt.% and 10 wt.% SMAA respectively, were considered completely wetted and no contact angle could be measured at either 0 or 10 min of analysis. This large decrease in contact angle over 10 min is not seen in MICA measurements. But SE calculations showed an increase in value after 10 min for formulations containing 5 wt.% and 10 wt.% SMAA, with 10 wt.% having the largest effect. These observations suggest that the

presence of SMAA at the surface of these coatings has a more significant effect on surface hydrophilicity/hydrophobicity than changes in pre-polymer composition alone. The PEG chains grafted onto the additive modify the surface making it more hydrophilic under hydrated conditions, which causes a decrease in WCA and an increase in SE. The plots in 6B, 6D, and 6F show the same WCA, MICA, and SE values, but they were performed after 28 days water ageing. Overall, the changes in WCA and SE follow a similar trend to that recorded before immersion, but with a much-reduced effect. This is likely due to surface rearrangement of these coatings after immersion in circulating tap water. Studying the potential 'leaching' of SMAA in formulations will be carried out in future work.

In addition to performing ATR-FTIR and WCA, MICA, and SE measurements, AFM was utilized to observe the surface morphology of formulations. Figure 3.7 shows AFM phase images of formulations F1, F4, F7, F10, and F13 which did not have any incorporated SMAA. Typically, in phase images, a surface with little difference in color would signal a largely homogenous surface, with differences in color signaling a more heterogenous surface. In the case of the surfaces presented in this work, more heterogenous is defined as having both domains of PDMS and PEG on the surface of a polyurethane (PU) coating. A homogenous coating can be seen as either consisting of PDMS on the PU surface, or just PEG alongside PU moieties. In F1, which has 20 wt.% PDMS and no PEG in the prepolymer, there are many irregular domains of PDMS that can be seen on the surface of the coating. Due to the low surface energy and hydrophobicity of PDMS, this was expected, as PDMS would prefer to not associate with a PU bulk. As the amount of PEG was increased throughout the formulations with differing prepolymer composition, these domains begin to form more regular shapes, showing distinct difference in phase between PEG and PU moieties. Formulation F4 shows very large circular domains of PDMS with just a small increase in PEG content. In formulation F7, the concentration of PDMS and PEG are set to be equal at 10 wt.% each. This results in surface morphology with smaller PDMS domains, spread more regularly throughout the coatings surface as there is not as significant a difference in amounts of the different materials present. Formulation F10 again shows quite distinct PDMS domains amongst a PEG and PU surface, but these are much smaller and less dense due to only containing 5 wt.% PDMS in the prepolymer. Lastly, formulation F13 has a prepolymer composition that has 20 wt.% PEG and no PDMS, showing a phase image that is largely unchanged (homogenous), consisting of PEG and PU moieties. From these phase

images, increases and decreases in PDMS and PEG content in the pre-polymer composition have a significant effect on surface morphology.

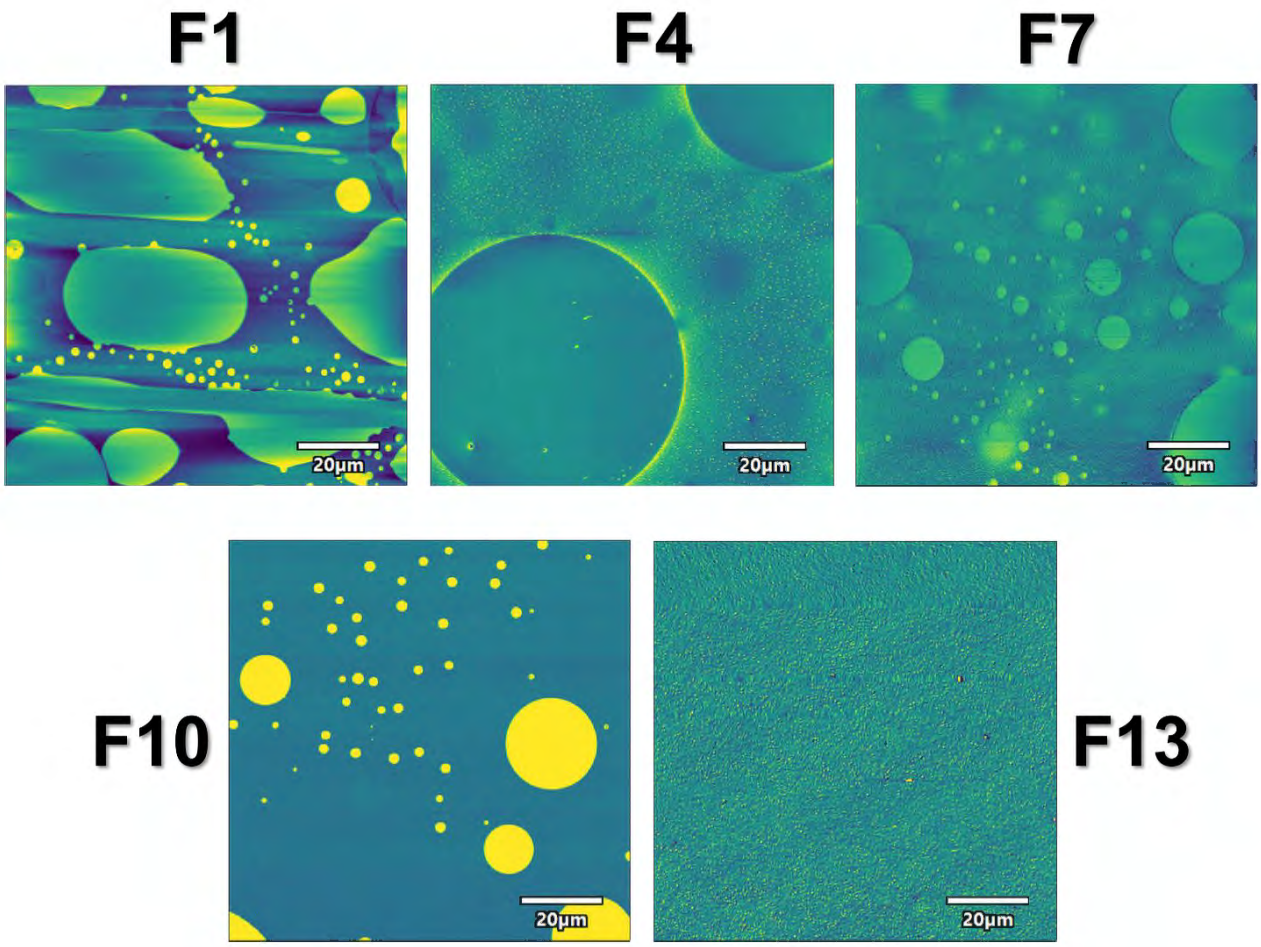

Figure 3.7. Phase images for AFM performed in air for formulations F1, F4, F7, F10, and F13. Each image is a 100 x 100 µm scan of the coatings surface.

In Figure 3.8, formulation F1 and F13 represent pre-polymer compositions of 20 wt.% PDMS, 0 wt.% PEG and 0 wt.% PDMS and 20 wt.% PEG respectively, with no added SMAA. F3 and F15 represent those same pre-polymer compositions, but with 10 wt.% incorporated SMAA. Comparing images of F1 and F3, as the SMAA was incorporated, the surface still showed large, irregular domains of PDMS on a PU surface. However, smaller, more regular domains are also seen, which are thought to be droplets of additive that have spread throughout the surface. This could be due to the addition of PEG via the SMAA making the surface even more heterogenous. This effect is also seen between F13 and F15, where there is no PDMS in the pre-polymer of F13. But this time, introduction of PDMS via the SMAA results in large, circular domains of PDMS aggregating on a largely PEG and PU surface. These phase images show that

not only does the pre-polymer composition affect the surface morphology of these coatings, but that incorporation of SMAA does as well.

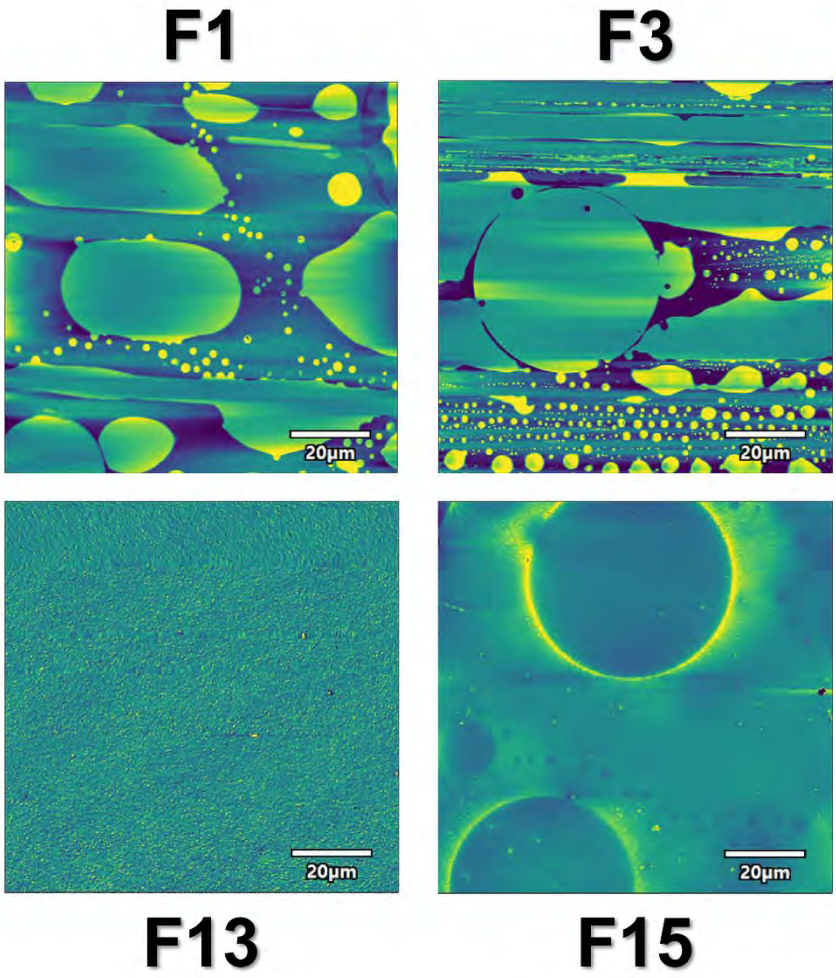

Figure 3.8. Phase images for AFM performed in air for formulations F1, F3, F13, and F15. F3 and F15 contain 10 wt.% SMAA and have the same pre-polymer composition as F1 and F13 respectively. Each image is a 100 x 100 µm scan of the coatings surface.

Before laboratory assays were performed, panels coated with experimental formulations, as well as the control and commercial standard coatings in Table 3.2, were pre-leached in circulating water tanks for 28 days. After this time, leachate toxicity assessments for *C. lytica*, *N. incerta*, and *U. linza* were performed according to previously described methods.[47, 55] Procedures for these assays can be found in appendix B, along with Figures B2-B4 detailing the results from these assessments. Compared to a positive growth control, each organism tested showed nominal growth in overnight extracts (ASW and nutrients) from the experimental coatings. This indicates that the experimental formulations were non-

toxic after the pre-leaching step and that the results from the laboratory assays were due to surface effects and not compromised by toxic materials leaving the coatings.

Green macroalgae such as *Ulva linza* are recognized as widely distributed fouling organisms.[56] The settlement, growth, and adhesion of many marine fouling species, including *U. linza*, is significantly affected by the wetting and surface characteristics of the substrate.[57-59] *U. linza* reproduces through the production of motile spores (ca 5 µm in length), which travel through the seawater to locate a surface suitable for settlement. Once attached, the spores germinate and develop into sporelings (young plants). Spore settlement densities are typically lower on hydrophilic than hydrophobic surfaces but there attachment is stronger.[60] For surfaces with hydrophobic character, the opposite is true. Multi-well plates containing experimental formulations were exposed to spores of *U. linza* which grew into sporelings of approx. 100 µm in length before adhesion was evaluated.

Sporeling growth after 7 days, shown in Figure B5**,** did not show any significant trends with regards to pre-polymer composition. Coatings with pre-polymer compositions that contained both PDMS and PEG showed the lowest amounts of growth when SMAA was incorporated, with some performing as well as, or better than the commercial standard IS1100SR (Table B5**)**. The adhesion of sporelings to the coatings was assessed by measuring the removal at three different water-jet impact pressures of 18, 67, and 110 kPa (Figure 3.9**)**. Formulations with varying PDMS and PEG concentrations in the pre-polymer all showed less than or equal to 60% removal at the highest water pressure. The formulations which contained more PEG in the pre-polymer had higher levels of removal than those with only PDMS, or low concentrations of PDMS, in the pre-polymer. This seems to deviate from the expected behavior of hydrophilic surfaces having lower removal. But, as seen through CA and AFM measurements, even the surfaces of coatings, which only contained PEG in the pre-polymer, showed a non-uniform surface with dynamic surface activity. In this case, the addition of a hydrophilic moiety, such as PEG, to these coatings systems may improve release properties towards *U. linza*. Another significant and surprising observation was that for nearly every coating that contained the addition of SMAA to the formulations, even at 5 wt.%, the sporelings spontaneously released from the surface upon disturbance of the dishes. The detached rafts of sporelings are shown in Figure 3.10.

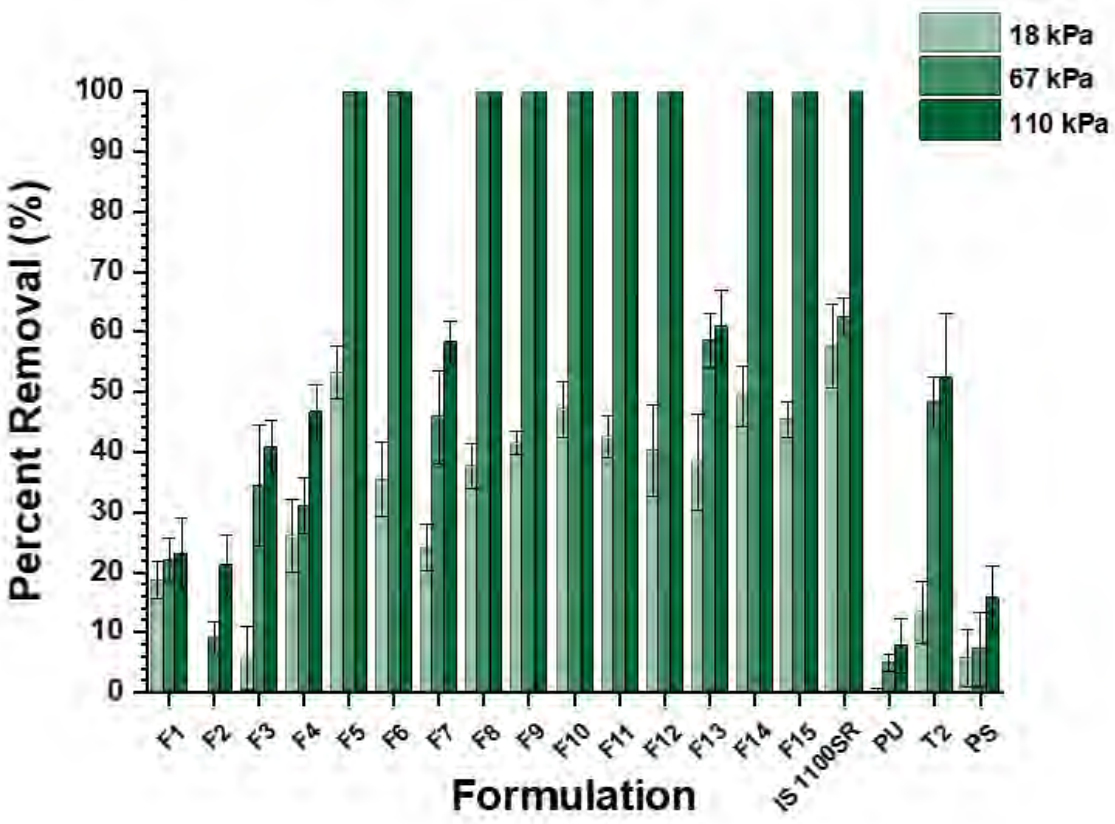

Figure 3.9. Removal of *U. linza* sporelings at water-jet treatments of 18, 67, and 110 kPa. Bars represent the average removal from six replicates with standard deviation. The X-axis is labeled to indicate formulation number as described in Table 3.2, along with commercial standards and controls.

The addition of SMAA also corresponds to an overall increase in PEG content within the coating, while also producing excellent removal in nearly every formulation. Again, this suggests that the notion of hydrophilic surfaces performing poorly in removal assays does not necessarily apply to these types of coatings. Overall, it was shown that changing the composition of the pre-polymer, by increasing the PEG content, improved removal performance, and that the inclusion of SMAAs had a significantly greater effect in increasing fouling-release performance towards the green alga *U. linza.*

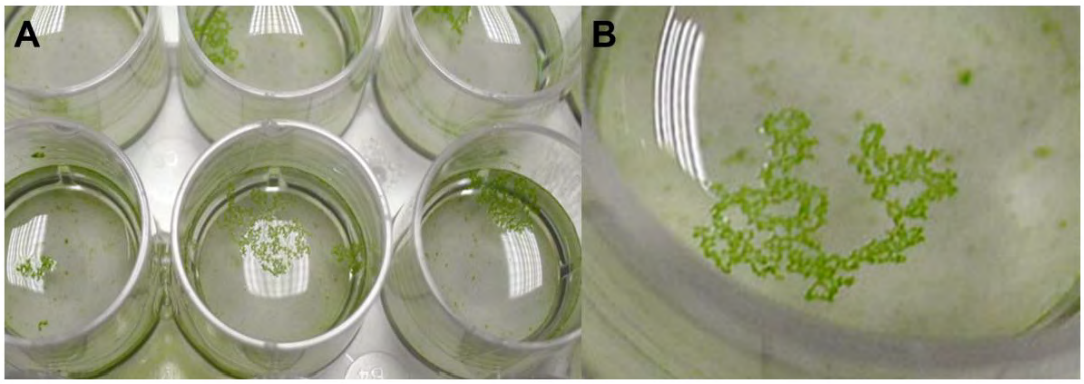

Figure 3.10. A) Image of floating *U. linza* sporelings that have spontaneously released from coated surfaces in plastic 24-well plates. B) Close-up of released sporelings.

Experimental coatings were also subjected to the growth and adhesion of another marine alga, the slime-forming diatom *Navicula incerta*, and FR properties were evaluated. Typically, *N. incerta* prefer hydrophobic surfaces, especially those consisting of PDMS, to attach to and form a slime film.[59, 61] Previous work carried out by Benda et al. showed that as the surface of a PDMS-rich surface became more heterogenous via introduction of hydrophilic domains, cell attachment and adhesion decreased.[38] The types of surfaces explored in this work follow a similar trend. Figure 3.11 details the cell attachment and removal of *N. incerta* on experimental coatings, as well as controls and commercial standards. The highest cell attachment densities were on the F1 coating, which contained 20 wt.% PDMS and 0 wt.% PEG in the pre-polymer with no added SMAA. As the amount of PEG in the pre-polymer increased, only coating F7 containing 10 wt.% of both PDMS and PEG, showed significantly lower cell attachment comparable to the commercial standard IS900 (Table B13). The most significant effect for coatings incorporating SMAA was seen for formulations F1-F3, containing 20 wt.% PDMS in the pre-polymer. As more SMAA was added, significantly lower cell attachment occurred, with results comparable to the amphiphilic slime release commercial standard IS1100SR (Table B15). Overall, only a slight decrease in cell attachment was seen when PDMS and PEG content were varied in the pre-polymer. However, more significant decreases in cell attachment were seen when the SMAA was incorporated, suggesting that a more heterogenous, amphiphilic surface can reduce diatom attachment, even in highly hydrophobic, PDMS-rich surfaces.

After water-jet treatment at 138 kPa, significantly lower biomass levels remained on all experimental formulations than on the T2 silicone elastomer standard. However, there was no significant

difference between removal with changes in PDMS and PEG content in the pre-polymer (Table B16). In contrast, incorporation of SMAA resulted in a significant decrease in biomass remaining for each pre-polymer composition. It was shown that inclusion of 10 wt.% of SMAA resulted in the lowest amounts of biomass remaining, with higher removal performance occurring as the total PEG content in the coatings increased (Table B18). Coating formulation F15, with 20 wt.% PEG in the pre-polymer, along with 10 wt.% SMAA performed comparably to the commercial standard IS1100SR. Again, incorporation of SMAA seemed to provide a more significant decrease in biomass remaining. This provides more evidence that the presence of this dynamic, amphiphilic surface layer helps to disrupt attachment and adhesion of *N. incerta*, facilitating its removal.

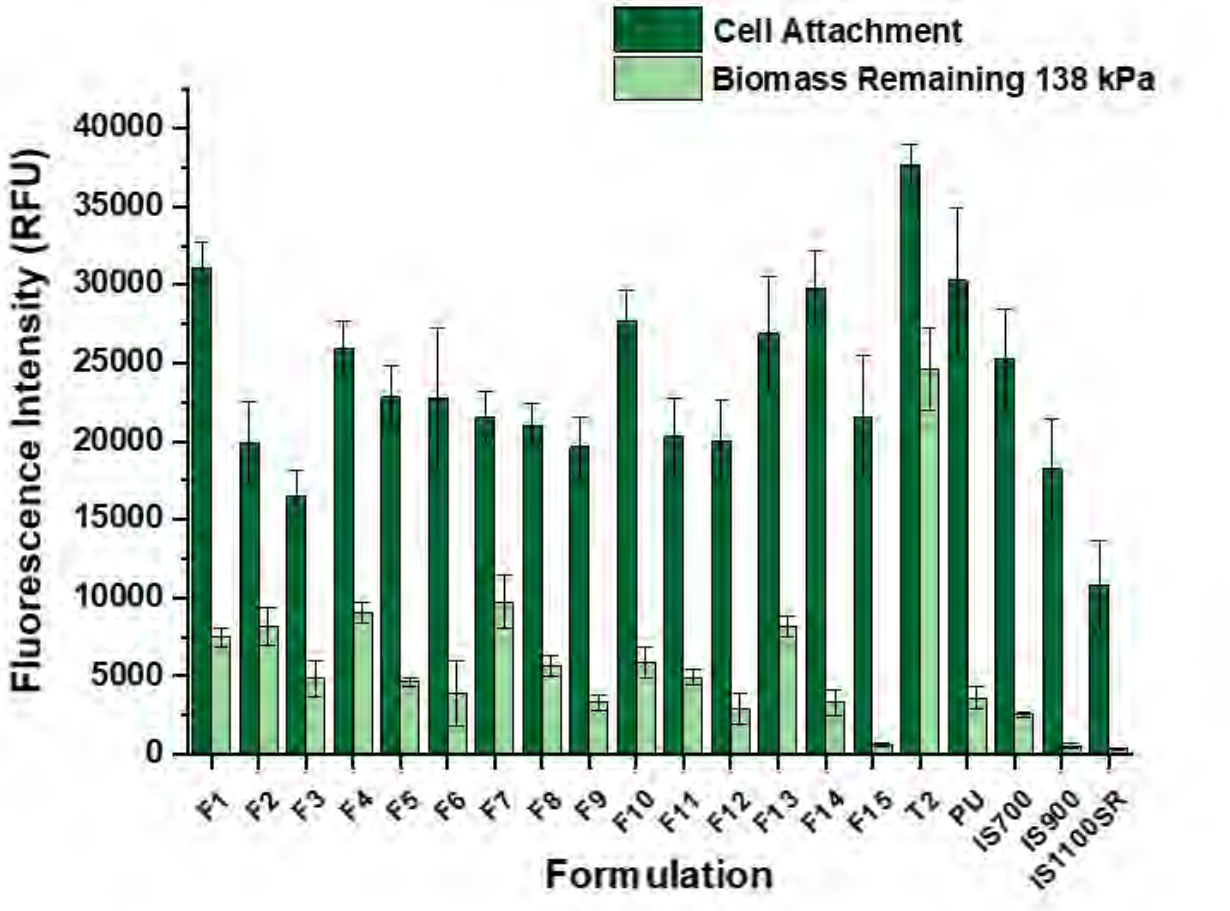

Figure 3.11. Cell attachment and biomass of *N. incerta* remaining after water-jet treatment at 138 kPa water column pressure. The dark green bars represent diatom cell attachment, whilst light green bars represent biomass remaining after water-jet treatment at 138 kPa for three replicate measurements and standard deviations. The X-axis is labeled to indicate formulation number in Table 3.2, along with commercial standards and controls.

Another marine organism that can be a major contributor to marine biofouling, is the bacterium *Cellulophaga lytica*. Both hydrophobic and hydrophilic surfaces offer suitable surfaces for this marine bacterium to settle on, which can make it challenging to combat.[7] Biofilm growth and retention assays were performed on experimental coatings, along with controls and commercial standards, and the results can been seen in Figure 3.12. Virtually all experimental coatings showed lower growth of the bacteria compared to all the controls and commercial standards. Some formulations, especially those with both PDMS and PEG in the prepolymers, performed significantly better (Table B8). Comparing the formulations in which the PDMS and PEG content varied in the pre-polymer, there was no significant difference in both growth and removal of bacterial biofilms (Table B7, Table B10). As SMAA was added to these formulations, only formulations F2 and F3 resulted in significantly decreased biofilm growth (Table B9). However, removal of these biofilms was significantly greater when SMAA was incorporated into each formulation except for the purely PEG-containing pre-polymer formulations F13-F15 (Table B12). Again, there is evidence that the coatings containing SMAAs had significantly lower growth and higher removal of *C. lytica*, despite its affinity for both hydrophobic and hydrophilic surfaces.

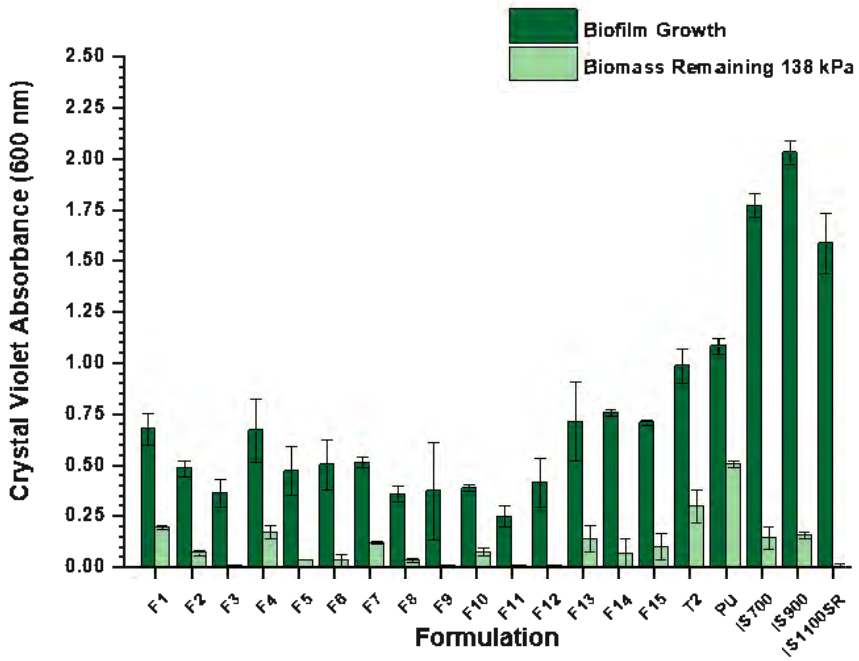

Figure 3.12. Bacterial biofilm growth and retention of C. lytica after water-jet treatment at 138 kPa water column pressure. The dark green bars represent biofilm growth, whilst the light green bars represent biomass remaining after water-jet treatment at 138 kPa for 3 replicate measurements with standard deviations. The X-axis is labeled to indicate formulation number in Table 3.2, along with commercial standards and controls.

The biological assays with algae and bacteria were supplemented with macrofouling assays using the marine barnacle *Amphibalanus amphitrite* and marine mussel *Geukensia demissa*. Fouling of ships' hulls with the macrofoulant *A. amphitrite* accounts for significant reductions in performance of marine vessels.[9, 62, 63] Barnacles in general secrete specialized adhesives to adhere to surfaces. The adhesive of this particular species tends to spread more readily on hydrophilic surfaces, but still offers relatively high adhesion strengths on hydrophobic dominant surfaces.[16, 52, 64] The force needed to push barnacles off surfaces is summarized in Figure 3.13 for all experimental coatings, including controls and commercial standards. Overall, there was a trend of increasing adhesion strength with increasing PEG in the pre-polymer(Table B19). It is also seen that formulations F4, F7, and F10, containing a mixture of PDMS and PEG in their prepolymers, did not show any significant difference in barnacle adhesion strength. When analyzing the formulations which had varying amounts of SMAA added to the formulations, again there was no significant difference between formulations with or without additive (Table B21). The main finding of this assay was that formulations with high hydrophilic content tended to release the reattached barnacles less well than the more hydrophobic coatings. In some cases, the adhesive bond to the surface was so strong that the basal plates cracked. However, the performance of several formulations with more hydrophobic content was comparable to the commercial standard IS1100SR. The addition of SMAA did not significantly decrease FR performance and was shown to improve the performance of highly hydrophilic coatings surfaces, through the introduction of higher wt.% PDMS in the formulation, as seen in F14 and F15.

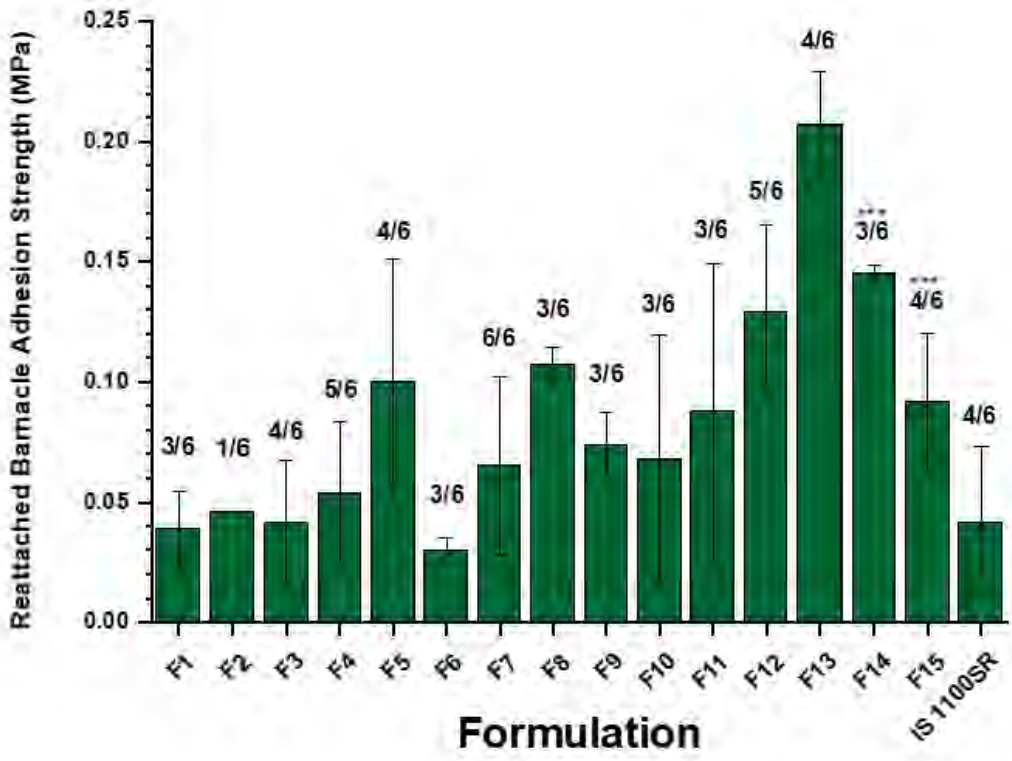

Figure 3.13. Reattached barnacle adhesion strength of *A. amphitrite*. Each bar represents the average adhesion strength of successfully pushed off barnacles. The ratio corresponds to the number of attached barnacles over the number of total available barnacles. *** denotes the breakage of an attached barnacle upon removal. The X-axis is labeled to indicate formulation number in Table 3.2, along with commercial standards and controls.

The marine mussel *G. demissa* is another macrofouling organism that secretes several adhesive proteins called mussel foot-proteins. These mussels typically perform a 'search' action to find a suitable substrate on which to deposit their adhesives, favoring hydrophilic surfaces over hydrophobic surfaces.[65, 66] Figure B6 shows the mussel removal force, as well as overall number of attached byssal threads during pull-off adhesion measurements. Remarkably, no mussels attached to surfaces of formulations F1-F12, possibly due to sufficient heterogeneity of the surfaces caused by incorporation of SMAAs, as well as a mixture of PDMS and PEG in the pre-polymer. However, the mussels were able to attach to coatings that contained more hydrophilic content in the pre-polymer even with incorporated SMAA. It is likely that in these cases sufficient hydrophilic groups were presenting at the surface to make it favorable for the mussels to attach. Regardless of this, these coatings were shown to be highly effective in preventing mussel attachment and adhesion, which could prove useful in environments with higher populations of these marine foulants.

To gain a better understanding of those formulations that exhibited spontaneous release of *U. linza* sporelings, growth and removal assays utilizing a turbulent flow cell with significantly weaker shear forces was employed. Formulations F7, F8, F10, and F11 were selected to determine if there is an effect between different PDMS:PEG amounts in the pre-polymer (F7, F10), and how adding SMAA to the coatings may affect growth and removal (F8, F11**)**. These coatings were cast on standard microscope slides (75 x 25 mm) along with a glass control, and a PDMS elastomer standard (Bluesil™). Results from these assays can be seen in Figure B7. The PDMS reference, and glass control surfaces displayed very similar growth, being less than that of the experimental formulations. There was no significant difference in growth between F7 and F10, which contained differing amounts of PDMS and PEG in the pre-polymer composition. However, incorporation of SMAA in both pre-polymer compositions produced a significantly higher amount of growth on coated slides. In removal assays, at 42 Pa hydrodynamic shear force, there was virtually no removal from the glass control and PDMS standard surfaces. Formulations F7 and F10 show significantly greater amounts of biomass removal than the controls, with F7 performing better than F10. Again, when SMAA was incorporated (F8, F11), a significant increase in biomass removal was seen, with F8 showing removal of almost all sporelings that grew on the coated slide. Overall, despite formulations containing SMAA having considerably more sporeling growth, they still far outperformed all other formulations in removal of sporelings at relatively weak hydrodynamic forces, making them attractive candidates for FR coatings.

Lastly, settlement assays of *Balanus improvisus* cyprid larvae were carried out on the selected formulations (F7, F8, F10, F11), as well as glass and trimethoxy(octadecyl)silane coated substrates. As opposed to biological assays involving the reattachment of adult barnacles on the surfaces of experimental formulations, this cyprid settlement assay provides insight into how barnacles in earlier stages of their life cycle (cypris larvae) settle and ultimately undergo metamorphosis to adhere to the surface. The settlement of cypris larvae of barnacle species such as *B. improvisus* has been shown to be affected by surface chemistries, surface morphology, and overall surface wettability (hydrophilic vs. hydrophobic), with higher settlement typically seen on smooth, hydrophobic surfaces.[64, 67] Results from these settlement assays can be seen in Figure B8. The main observation was that virtually all the available cyprids were unable to settle on these surfaces compared to ~95% settlement on a smooth

hydrophobic surface, and ~25% settlement on a clean glass microscope slide (75 x 25 mm). As larvae were performing their search actions for a suitable surface, an adsorptive effect was observed where cyprids were immobilized, but could not settle properly, and subsequently released from the surface. This effect was seen in all formulations, but was most prominent in F8 and F11, which contained 5 wt.% SMAA. It is thought that these surfaces were sufficiently heterogenous in nature to deter larvae from attaching after contact with the initial 'oil' layer brought about by the additives. Because of this effect, removal experiments could not be performed, but current efforts are underway to replicate this experiment and obtain useful removal values.

Overall, these biological assays provided valuable insight into the AF/FR performance of these amphiphilic siloxane-polyurethanes with varying PDMS and PEG content in the pre-polymer, as well as formulations containing surface-modifying amphiphilic additive. Growth and settlement of the marine foulants analyzed showed only slightly lower values than most of the commercial standards and controls, with only some of the formulations being comparable to IS1100SR. Growth tended to be lower on surfaces which had ratios of PDMS and PEG of 10:10 and 5:15 percent. However, inclusion of SMAA had a significantly larger effect on this growth than changing pre-polymer PDMS and PEG compositions in the experimental formulations. In each biological assay, formulations which contained SMAA, and had a mixture of PDMS and PEG in the pre-polymer composition, had lower growth values than other experimental formulations and control coatings, with some formulations performing comparable to IS1100SR. The FR properties of these coatings share a similar trend. Changes in pre-polymer composition only showed a slight increase in performance, with formulations containing pre-polymer with a PDMS:PEG ratio of 10:10 and 5:15 again showing the best performance. When SMAA was incorporated, there was a significant increase in FR performance across all experimental formulations. Several formulations that contained SMAA at 10 wt.% showed higher removal properties than even the commercial standard IS1100SR, with formulations having 5 wt.% SMAA still performing comparably, if not slightly worse than commercial standards.

Conclusions

Synthesis of five different isocyanate prepolymers with varying PDMS and PEG wt.% was performed via established procedures. As the amount of PDMS was decreased, and PEG increased,

FTIR showed a decrease and increase in peaks associated with these moieties as well as the presence of isocyanate leftover from the reaction to form a crosslinked network. DryAdd simulations were performed to determine the distribution of pre-polymer species and showed that there was a wide range of pre-polymer species formed during synthesis. The highest fraction of pre-polymer species had two out of three available isocyanate groups reacted with either PDMS or PEG polymer chains. However, also present was a significant amount of completely unreacted isocyanate, as well as fully reacted isocyanate groups, which could possibly affect surface and AF/FR properties. GPC was performed to try and confirm these findings. Results from these experiments agreed with DryAdd simulations that there was indeed a broad range of pre-polymer species formed, but quantification was not possible and is currently being explored.

Formulations including these prepolymers, with additional isocyanate, a synthesized acrylic polyol, acetylacetone, and catalyst solution were prepared and cast on primed aluminum panels. Additionally, a previously synthesized unreactive surface-modifying amphiphilic additive (SMAA) was incorporated into these pre-polymer formulations at 5 and 10 wt.% solids. Coated samples were subjected to an array of surface characterization techniques to determine surface properties, as well as biological assays to assess AF/FR performance. ATR-FTIR was performed on all experimental formulations and showed an insignificant amount of isocyanate remaining, signaling cured coatings. In addition, formulations that did not contain SMAA again showed decreases and increases in peaks associated with PDMS and PEG moieties, displaying amphiphilic surfaces with varying hydrophobic and hydrophilic components. Peaks associated with PDMS and PEG were seen in all formulations which contained SMAAS, regardless of pre-polymer concentration, pointing to the SMAAs concentrating at the surface of these coatings. WCA/MICA measurements showed that there was only a slight drop in contact angles over 10 min as PEG content in the pre-polymer was increased. However, formulations which contained SMAA, especially at 10 wt.% solids, showed significant drops in water contact angle after 10 min, suggesting SMAAs present at the surface had a major effect on wettability of the coatings surface. The highest decreases in WCA were seen in formulations with higher concentrations of PEG in the pre-polymer containing 10 wt.% SMAA. AFM was also performed and collected phase images showed that formulations with only PDMS in the pre-polymer had a largely homogenous surface morphology, with

similar results seen in formulations with only PEG in the pre-polymer. As these ratios were varied, large changes in surface morphology were observed, making the surfaces more heterogeneous via inclusion of both PDMS and PEG at the surface. Additionally, images were taken of surfaces which contained only PDMS or PEG in the pre-polymer, but also with 10 wt.% incorporated SMAA. When SMAA was added, the surfaces also displayed large changes in morphology, again becoming more heterogenous.

Several biological assays were performed to assess the AF/FR performance of these experimental formulations and compare them to controls and commercial standards. Settlement and growth of microfoulants such as *C. lytica* and *N. incerta* were not significantly affected across all experimental formulations. However, FR properties were greatly enhanced compared to controls and commercial standards. Overall, it was shown that experimental formulations that contained SMAA, even at 5 wt.% incorporation, exhibited a significant decrease in biomass remaining after water-jet procedures. Some experimental formulations, notably those with higher PEG content in the pre-polymer composition, while also incorporating SMAA, showed comparable, or better performance relative to commercial standards and controls in settlement and growth assays for the marine macroalgae *Ulva linza*. During removal assays for this alga, virtually every experimental formulation with SMAA displayed spontaneous release of settled sporelings upon shaking of test well-plates. To investigate this effect further, several formulations were selected with and without SMAA incorporation, for use in growth and release assays of *U. linza* involving a turbulent flow cell with low hydrodynamic forces ~42 Pa. Although spontaneous release was not observed during this experiment, the incorporation of SMAA at only 5 wt.% caused a significant increase in removal of sporelings at low hydrodynamic forces. Barnacle reattachment and adhesion assays utilizing *Amphibalanus amphitrite* were also performed on experimental formulations and compared to commercial standard IS100SR. Overall, formulations with lower concentrations of PEG, either through pre-polymer composition or SMAA incorporation, showed lower amounts of barnacle reattachment, and lower removal strength comparable to IS1100SR. As PEG content was increased, stronger adhesion was observed. Additionally, cyprids of *Balanus improvisus* were used to evaluate settlement and adhesion of selected formulations both with and without SMAA incorporation. These surfaces were shown to be excellent at resisting larval settlement, with each formulation having virtually no larvae settle on their surfaces, precluding removal experiments. Lastly, marine mussel *Geukensia*

demissa attachment and removal assays were performed and it was shown that no mussels could adhere to any of the experimental formulations except those with the highest amounts of PEG content. Overall, these coatings displayed broad spectrum AF/FR performance in comparison to commercial standards and controls. Addition of SMAA had a more significant effect to both surface properties and FR properties than a change in PDMS and PEG wt.% in the pre-polymer composition. Further work studying the interaction between these additives and various other coatings systems is currently underway.

References

1. Callow, J. A.; Callow, M. E., Trends in the development of environmentally friendly fouling-resistant marine coatings. *Nature Communications* **2011,** *2*, 244.

2. Hellio, C.; Yebra, D. M., *Advances in Marine Antifouling Coatings and Technologies*. 2009.

3. Schultz, M. P.; Bendick, J. A.; Holm, E. R.; Hertel, W. M., Economic Impact of Biofouling on a Naval Surface Ship. *Biofouling* **2011,** *27* (1), 87.

4. Callow, M. E.; Callow, J. A., Marine Biofouling: A Sticky Problem. *Biologist* **2002,** *49* (1), 10.

5. Magin, C. M.; Cooper, S. P.; Brennan, A. B., Non-Toxic Antifouling Strategies. *Mater. Today* **2010,** *13* (4), 36.

6. Drake, J. M.; Lodge, D. M., Hull fouling is a risk factor for intercontinental species exchange in aquatic ecosystems. *Aquatic Invasions* **2007,** *2* (2), 121-131.

7. Lejars, M. n.; Margaillan, A.; Bressy, C., Fouling release coatings: a nontoxic alternative to biocidal antifouling coatings. *Chemical reviews* **2012,** *112* (8), 4347-4390.

8. Jones, G., The battle against marine biofouling: a historical review. *Advances in marine antifouling coatings and technologies* **2009**, 19-45.

9. Yebra, D. M.; Kiil, S. K.; Dam-Johansen, K., Antifouling Technology—Past, Present and Future Steps Towards Efficient and Environmentally Friendly Antifouling Coatings. *Prog. Org. Coat.* **2004,** *50* (2), 75.

10. Konstantinou, I. K.; Albanis, T. A., Worldwide Occurrence and Effects of Antifouling Paint Booster Biocides in the Aquatic Environment: A Review. *Environ. Int.* **2004,** *30* (2), 235.

11. Ytreberg, E.; Karlsson, J.; Eklund, B., Comparison of toxicity and release rates of Cu and Zn from anti-fouling paints leached in natural and artificial brackish seawater. *Science of the Total Environment* **2010,** *408* (12), 2459-2466.

12. Matthiessen, P.; Reed, J.; Johnson, M., Sources and potential effects of copper and zinc concentrations in the estuarine waters of Essex and Suffolk, United Kingdom. *Marine Pollution Bulletin* **1999,** *38* (10), 908-920.

13. Sommer, S.; Ekin, A.; Webster, D. C.; Stafslien, S. J.; Daniels, J.; VanderWal, L. J.; Thompson, S. E. M.; Callow, M. E.; Callow, J. A., A Preliminary Study on the Properties and Fouling-Release Performance of Siloxane-Polyurethane Coatings Prepared from Pdms Macromers. *Biofouling* **2010,** *26* (8), 961.

14. Bodkhe, R. B.; Thompson, S. E. M.; Yehle, C.; Cilz, N.; Daniels, J.; Stafslien, S. J.; Callow, M. E.; Callow, J. A.; Webster, D. C., The Effect of Formulation Variables on Fouling-Release Performance of Stratified Siloxane-Polyurethane Coatings. *Journal of Coatings Technology Research* **2012,** *9* (3), 235.

15. Holland, R.; Dugdale, T.; Wetherbee, R.; Brennan, A.; Finlay, J.; Callow, J.; Callow, M. E., Adhesion and motility of fouling diatoms on a silicone elastomer. *Biofouling* **2004,** *20* (6), 323-329.

16. Rittschof, D.; Costlow, J. D., Bryozoan and barnacle settlement in relation to initial surface wettability: A comparison of laboratory and field studies. *Sci. Mar.* **1989,** *53* (2), 411-416.

17. Callow, M. E.; Callow, J.; Ista, L. K.; Coleman, S. E.; Nolasco, A. C.; López, G. P., Use of self-assembled monolayers of different wettabilities to study surface selection and primary adhesion processes of green algal (Enteromorpha) zoospores. *Applied and Environmental Microbiology* **2000,** *66* (8), 3249-3254.

18. Galli, G.; Martinelli, E., Amphiphilic polymer platforms: surface engineering of films for marine antibiofouling. *Macromolecular rapid communications* **2017,** *38* (8), 1600704.

19. Leonardi, A. K.; Ober, C. K., Polymer-based marine antifouling and fouling release surfaces: strategies for synthesis and modification. *Annual review of chemical and biomolecular engineering* **2019,** *10*, 241-264.

20. Pade, M.; Webster, D. C., Self-stratified siloxane-polyurethane fouling-release marine coating strategies: A review. Central West Publishing: Australia: 2019; pp 1-36.

21. Lin, X.; Xie, Q.; Ma, C.; Zhang, G., Self-healing, highly elastic and amphiphilic silicone-based polyurethane for antifouling coatings. *Journal of Materials Chemistry B* **2021,** *9* (5), 1384-1394.

22. Stafslien, S. J.; Christianson, D.; Daniels, J.; VanderWal, L.; Chernykh, A.; Chisholm, B. J., Combinatorial materials research applied to the development of new surface coatings XVI: fouling-release properties of amphiphilic polysiloxane coatings. *Biofouling* **2015,** *31* (2), 135-149.

23. Yi, L.; Xu, K.; Xia, G.; Li, J.; Li, W.; Cai, Y., New protein-resistant surfaces of amphiphilic graft copolymers containing hydrophilic poly (ethylene glycol) and low surface energy fluorosiloxane side-chains. *Applied Surface Science* **2019,** *480*, 923-933.

24. Galhenage, T. P.; Webster, D. C.; Moreira, A. M. S.; Burgett, R. J.; Stafslien, S. J.; Vanderwal, L.; Finlay, J. A.; Franco, S. C.; Clare, A. S., Poly (ethylene) glycol-modified, amphiphilic, siloxane–polyurethane coatings and their performance as fouling-release surfaces. *Journal of Coatings Technology and Research* **2017,** *14* (2), 307-322.

25. Ruiz-Sanchez, A. J.; Guerin, A. J.; El-Zubir, O.; Dura, G.; Ventura, C.; Dixon, L. I.; Houlton, A.; Horrocks, B. R.; Jakubovics, N. S.; Guarda, P.-A., Preparation and evaluation of fouling-release properties of amphiphilic perfluoropolyether-zwitterion cross-linked polymer films. *Progress in Organic Coatings* **2020,** *140*, 105524.

26. Koschitzki, F.; Wanka, R.; Sobota, L.; Koc, J.; Gardner, H.; Hunsucker, K. Z.; Swain, G. W.; Rosenhahn, A., Amphiphilic dicyclopentenyl/carboxybetaine-containing copolymers for marine fouling-release applications. *ACS Applied Materials & Interfaces* **2020,** *12* (30), 34148-34160.

27. Koschitzki, F.; Wanka, R.; Sobota, L.; Gardner, H.; Hunsucker, K. Z.; Swain, G. W.; Rosenhahn, A., Amphiphilic Zwitterionic Acrylate/Methacrylate Copolymers for Marine Fouling-Release Coatings. *Langmuir* **2021,** *37* (18), 5591-5600.

28. Bodkhe, R. B.; Stafslien, S. J.; Daniels, J.; Cilz, N.; Muelhberg, A. J.; Thompson, S. E.; Callow, M. E.; Callow, J. A.; Webster, D. C., Zwitterionic siloxane-polyurethane fouling-release coatings. *Progress in Organic Coatings* **2015,** *78*, 369-380.

29. Wang, H.; Zhang, C.; Wang, J.; Feng, X.; He, C., Dual-mode antifouling ability of thiol–ene amphiphilic conetworks: minimally adhesive coatings via the surface zwitterionization. *ACS Sustainable Chemistry & Engineering* **2016,** *4* (7), 3803-3811.

30. Wang, D.; Xu, J.; Tan, J.; Yang, J.; Zhou, S., In situ generation of amphiphilic coatings based on a self-catalytic zwitterionic precursor and their antifouling performance. *Chemical Engineering Journal* **2021,** *422*, 130115.

31. Zhu, X.; Guo, S.; Jańczewski, D.; Parra Velandia, F. J.; Teo, S. L.-M.; Vancso, G. J., Multilayers of fluorinated amphiphilic polyions for marine fouling prevention. *Langmuir* **2014,** *30* (1), 288-296.

32. Yu, W.; Wanka, R.; Finlay, J. A.; Clarke, J. L.; Clare, A. S.; Rosenhahn, A., Degradable hyaluronic acid/chitosan polyelectrolyte multilayers with marine fouling-release properties. *Biofouling* **2020,** *36* (9), 1049-1064.

33. Patterson, A. L.; Wenning, B.; Rizis, G.; Calabrese, D. R.; Finlay, J. A.; Franco, S. C.; Zuckermann, R. N.; Clare, A. S.; Kramer, E. J.; Ober, C. K., Role of backbone chemistry and monomer sequence in amphiphilic oligopeptide-and oligopeptoid-functionalized PDMS-and PEO-based block copolymers for marine antifouling and fouling release coatings. *Macromolecules* **2017,** *50* (7), 2656-2667.

34. van Zoelen, W.; Buss, H. G.; Ellebracht, N. C.; Lynd, N. A.; Fischer, D. A.; Finlay, J.; Hill, S.; Callow, M. E.; Callow, J. A.; Kramer, E. J., Sequence of hydrophobic and hydrophilic residues in amphiphilic polymer coatings affects surface structure and marine antifouling/fouling release properties. *ACS Macro Letters* **2014,** *3* (4), 364-368.

35. Guazzelli, E.; Martinelli, E.; Pelloquet, L.; Briand, J.-F.; Margaillan, A.; Bunet, R.; Galli, G.; Bressy, C., Amphiphilic hydrolyzable polydimethylsiloxane-b-poly (ethyleneglycol methacrylate-co-trialkylsilyl methacrylate) block copolymers for marine coatings. II. Antifouling laboratory tests and field trials. *Biofouling* **2020,** *36* (4), 378-388.

36. Rahimi, A.; Stafslien, S. J.; Vanderwal, L.; Bahr, J.; Safaripour, M.; Finlay, J. A.; Clare, A. S.; Webster, D. C., Critical Amphiphilic Concentration: Effect of the Extent of Amphiphilicity on Marine Fouling-Release Performance. *Langmuir* **2021,** *37* (8), 2728-2739.

37. Rufin, M. A.; Ngo, B. K. D.; Barry, M. E.; Page, V. M.; Hawkins, M. L.; Stafslien, S. J.; Grunlan, M. A., Antifouling silicones based on surface-modifying additive amphiphiles. *Green Materials* **2017,** *5* (1), 4-13.

38. Benda, J.; Stafslien, S.; Vanderwal, L.; Finlay, J. A.; Clare, A. S.; Webster, D. C., Surface modifying amphiphilic additives and their effect on the fouling-release performance of siloxane-polyurethane coatings. *Biofouling* **2021**, 1-18.

39. Wenning, B. M.; Martinelli, E.; Mieszkin, S.; Finlay, J. A.; Fischer, D.; Callow, J. A.; Callow, M. E.; Leonardi, A. K.; Ober, C. K.; Galli, G., Model amphiphilic block copolymers with tailored molecular weight and composition in PDMS-based films to limit soft biofouling. *ACS applied materials & interfaces* **2017,** *9* (19), 16505-16516.

40. Rahimi, A.; Stafslien, S. J.; Vanderwal, L.; Finlay, J. A.; Clare, A. S.; Webster, D. C., Amphiphilic zwitterionic-PDMS-based surface-modifying additives to tune fouling-release of siloxane-polyurethane marine coatings. *Progress in Organic Coatings* **2020,** *149*, 105931.

41. Seetho, K.; Zhang, S.; Pollack, K. A.; Zou, J.; Raymond, J. E.; Martinez, E.; Wooley, K. L., Facile synthesis of a phosphorylcholine-based zwitterionic amphiphilic copolymer for anti-biofouling coatings. *ACS Macro Letters* **2015,** *4* (5), 505-510.

42. Wang, S.-Y.; Fang, L.-F.; Cheng, L.; Jeon, S.; Kato, N.; Matsuyama, H., Improved antifouling properties of membranes by simple introduction of zwitterionic copolymers via electrostatic adsorption. *Journal of Membrane Science* **2018,** *564*, 672-681.

43. Guo, H.; Chen, P.; Tian, S.; Ma, Y.; Li, Q.; Wen, C.; Yang, J.; Zhang, L., Amphiphilic Marine Antifouling Coatings Based on a Hydrophilic Polyvinylpyrrolidone and Hydrophobic Fluorine–Silicon-Containing Block Copolymer. *Langmuir* **2020,** *36* (48), 14573-14581.

44. Portier, E.; Azemar, F.; Benkhaled, B. T.; Bardeau, J.-F.; Fay, F.; Réhel, K.; Lapinte, V.; Linossier, I., Poly (oxazoline) for the design of amphiphilic silicone coatings. *Progress in Organic Coatings* **2021,** *153*, 106116.

45. Upadhyay, V.; Galhenage, T.; Battocchi, D.; Webster, D., Amphiphilic icephobic coatings. *Progress in Organic Coatings* **2017,** *112*, 191-199.

46. Owens, D. K.; Wendt, R. C., Estimation of the Surface Free Energy of Polymers. *J. Appl. Polym. Sci.* **1969,** *13* (8), 1741.

47. Casse, F.; Stafslien, S. J.; Bahr, J. A.; Daniels, J.; Finlay, J. A.; Callow, J. A.; Callow, M. E., Combinatorial materials research applied to the development of new surface coatings V. Application of a spinning water-jet for the semi-high throughput assessment of the attachment strength of marine fouling algae. *Biofouling* **2007,** *23* (2), 121-130.

48. Starr, R. C.; Zeikus, J. A., UTEX: the culture collection of algae at the University of Texas at Austin. *Journal of phycology* **1987,** *23*.

49. Stafslien, S. J.; Bahr, J. A.; Daniels, J. W.; Wal, L. V.; Nevins, J.; Smith, J.; Schiele, K.; Chisholm, B., Combinatorial materials research applied to the development of new surface coatings VI: An automated spinning water jet apparatus for the high-throughput characterization of fouling-release marine coatings. *Review of Scientific Instruments* **2007,** *78* (7), 072204.

50. Callow, M. E.; Callow, J. A.; Conlan, S.; Clare, A. S.; Stafslien, S., Efficacy testing of nonbiocidal and fouling-release coatings. *Biofouling methods* **2014**, 291-316.

51. Stafslien, S.; Daniels, J.; Mayo, B.; Christianson, D.; Chisholm, B.; Ekin, A.; Webster, D.; Swain, G., Combinatorial Materials Research Applied to the Development of New Surface Coatings. Iv: A High-Throughput Bacterial Retention and Retraction Assay for Screening Fouling-Release Performance of Coatings. *Biofouling* **2007,** *23* (1), 45.

52. Rittschof, D.; Orihuela, B.; Stafslien, S.; Daniels, J.; Christianson, D.; Chisholm, B.; Holm, E., Barnacle Reattachment: A Tool for Studying Barnacle Adhesion. *Biofouling* **2008,** *24* (1), 1.

53. Stafslien, S.; Daniels, J.; Bahr, J.; Chisholm, B.; Ekin, A.; Webster, D.; Orihuela, B.; Rittschof, D., An Improved Laboratory Reattachment Method for the Rapid Assessment of Adult Barnacle Adhesion Strength to Fouling-Release Marine Coatings. *Journal of Coatings Technology and Research* **2012,** *9* (6), 651.

54. Leonardi, A.; Zhang, A. C.; Düzen, N.; Aldred, N.; Finlay, J. A.; Clarke, J. L.; Clare, A. S.; Segalman, R. A.; Ober, C. K., Amphiphilic Nitroxide-Bearing Siloxane-Based Block Copolymer Coatings for Enhanced Marine Fouling Release. *ACS Applied Materials & Interfaces* **2021**.

55. Majumdar, P.; Lee, E.; Patel, N.; Ward, K.; Stafslien, S. J.; Daniels, J.; Chisholm, B. J.; Boudjouk, P.; Callow, M. E.; Callow, J. A., Combinatorial materials research applied to the development of new surface coatings IX: an investigation of novel antifouling/fouling-release coatings containing quaternary ammonium salt groups. *Biofouling* **2008,** *24* (3), 185-200.

56. Hoipkemeier-Wilson, L.; Schumacher, J. F.; Carman, M. L.; Gibson, A. L.; Feinberg, A. W.; Callow, M. E.; Finlay, J. A.; Callow, J. A.; Brennan, A. B., Antifouling Potential of Lubricious, Micro-Engineered, Pdms Elastomers against Zoospores of the Green Fouling Alga Ulva (Enteromorpha). *Biofouling* **2004,** *20* (1), 53.

57. Callow, M. E.; Callow, J. A.; Ista, L. K.; Coleman, S. E.; Nolasco, A. C.; Lopez, G. P., Use of Self Assembled Monolayers of Different Wettabilities to Study Surface Selection and Primary Adhesion Processes of Green Algae (Enteromorpha) Zoosporesuse of Self Assembled Monolayers of Different Wettabilities to Study Surface Selection and Primary Adhesion Processes of Green Algae (Enteromorpha) Zoospores. *Applied and Enviornmental Microbiology* **2000,** *66* (8), 3249.

58. Callow, J. A.; Callow, M. E.; Ista, L. K.; Lopez, G.; Chaudhury, M. K., The Influence of Surface Energy on the Wetting Behavior of the Spore Adhesive of Marine Alga. *J. R. Soc., Interface* **2005,** *2*, 319.

59. Finlay, J. A.; Callow, M. E.; Ista, L. K.; Lopez, G. P.; Callow, J. A., The Influence of Surface Wettability on the Adhesion Strength of Settled Spores of the Green Alga Enteromorpha and the Diatom Amphora. *Integr. Comp. Biol.* **2002,** *42* (6), 1116.

60. Statz, A.; Finlay, J.; Dalsin, J.; Callow, M.; Callow, J. A.; Messersmith, P. B., Algal antifouling and fouling-release properties of metal surfaces coated with a polymer inspired by marine mussels. *Biofouling* **2006,** *22* (6), 391-399.

61. Holland, R.; Dugdale, T. M.; Wetherbee, R.; Brennan, A. B.; Finlay, J. A.; Callow, J. A.; Callow, M. E., Adhesion and Motility of Fouling Diatoms on a Silicone Elastomer. *Biofouling* **2004,** *20* (6), 323.

62. Aldred, N.; Clare, A. S., The adhesive strategies of cyprids and development of barnacle-resistant marine coatings. *Biofouling* **2008,** *24* (5), 351-363.

63. Gittens, J. E.; Smith, T. J.; Suleiman, R.; Akid, R., Current and emerging environmentally-friendly systems for fouling control in the marine environment. *Biotechnology advances* **2013,** *31* (8), 1738-1753.

64. Di Fino, A.; Petrone, L.; Aldred, N.; Ederth, T.; Liedberg, B.; Clare, A. S., Correlation between surface chemistry and settlement behaviour in barnacle cyprids (Balanus improvisus). *Biofouling* **2014,** *30* (2), 143-152.

65. Prendergast, G. S., Settlement and Behaviour of Marine Fouling Organisms. *Biofouling* **2009**, 30.

66. Waite, J. H., The formation of mussel byssus: anatomy of a natural manufacturing process. *Structure, cellular synthesis and assembly of biopolymers* **1992**, 27-54.

67. Dahlström, M.; Jonsson, H.; Jonsson, P. R.; Elwing, H., Surface wettability as a determinant in the settlement of the barnacle Balanus Improvisus (DARWIN). *Journal of Experimental Marine Biology and Ecology* **2004,** *305* (2), 223-232.

CHAPTER 4. INVESTIGATING THE BEHAVIOR OF A SURFACE MODIFYING AMPHIPHILIC ADDITIVE IN A POLYURETHANE COATING SYSTEM FOR THE REMOVAL OF MARINE BIOFOULING

Introduction

Much of the world still relies heavily on ocean going vessels for the transportation of people and goods, as well as for defense purposes. As such, these vessels are in a constant struggle against marine biofouling. Marine biofouling is referred to as the undesirable accumulation of marine organisms on structures submerged in seawater.[1] This phenomenon is a highly complex and dynamic process with over 4000 known fouling species. Accumulation of biofoulants typically occurs within minutes to hours with the growth of bacterial and algal biofilms on submerged substrates, and larger organisms such as mussels, barnacles, and tunicates settling over the following days, weeks, and months.[2-4] The varying sizes of micro- and macrofouling organisms, along with their various methods for settlement, growth, and adhesion to these surfaces, makes marine biofouling a difficult challenge.[5, 6] There are several negative impacts of marine biofouling which include a higher economic cost of operation, increased drag and fuel consumption when underway, greater release of greenhouse gas emissions, esthetically unpleasant areas of hull, as well as the potential for introduction of non-native species which have the potential of devastating local ecosystems.[3, 7-9] In terms of economics, it has been reported that the cost of marine biofouling (through maintenance, increased fuel use, etc.) for US Navy mid-sized destroyers equates to 56 million dollars per year, with estimations of over 1 billion dollars per year extended to other ships in the fleet.[7]

Due to the detrimental effects of marine biofouling, coupled with nature's adaptability and persistence, many different methods of prevention have been used to combat this phenomenon throughout history. Wooden ships often were covered in mixtures of tar and hot pitch, which forms a highly hydrophobic, toxic coating to deter settlement. Other methods of prevention included covering areas of these ships in copper alloy, or lead sheaths.[10, 11] As ships made primarily of iron/steel became commonplace, methods shifted towards newer technologies involving synthetic resins that could be modified to contain biocides. These anti-fouling (AF) coatings became widely used, especially with the

incorporation of tributyltin (TBT), a highly toxic, and very efficient, biocide. But, after investigations into TBT lingering in local ecosystems, devastating populations of several marine organisms, a world-wide ban was imposed on the use of TBT and TBT related biocides by the International Maritime Organization (IMO) in 2008.[5, 12] Because of this, efforts have been shifted to developing more environmentally friendly AF coatings, with much interest being placed in improving the performance of non-toxic fouling-release (FR) coating systems.

Many of the currently available anti-fouling paints contain metal-oxide biocides such as copper or zinc oxides. While effective in the prevention of biofouling accumulation, these biocidal pigments are still shown to concentrate locally in marine environments, again causing harm to the local ecosystems.[13-15] In addition to these metal-oxide based systems, use of organic biocides such as zinc pyrithione, Sea-Nine 211 (DCOIT), and other organic 'booster' biocides have seen widespread use in several marine environments.[16] However, problems with accumulation and indirect toxicity are still an issue, as well as the approval of more environmentally friendly solutions taking large amounts of time and resources to be granted approval for use. Therefore, non-toxic fouling-release (FR) paints have been seeing increased usage in recent years.

These FR paints typically rely on low surface-energy components such as polysiloxanes or fluoroalkyl containing polymers incorporated into a coating matrix. Marine organisms show a weak adhesion to these types of paints, and under hydrodynamic forces, are more easily removed from the substrates.[2, 5] Several commercially available formulations have been marketed including Intersleek® from AkzoNobel International Paint, SigmaGlide® from PPG Industries, and Hempasil® from Hempel.[5, 17, 18] Even though these types of FR paints have shown great promise in the mitigation of marine fouling, an issue still remains. Traditionally, these paints are applied on top of a tie-coat (a layer of paint that helps the FR top layer adhere to the substrate), which is more resource intensive than traditional AF paints. In addition, due to the soft, elastomeric nature of these coatings, they are easily damaged and not very durable. This may lead to the loss of the coating, resulting in severely decreased performance.[5, 6] Therefore, several research groups have performed work to develop durable, tough, FR coatings without the need for a tie-coat.[19-22] More specifically, the Webster group has developed self-stratifying siloxane-polyurethane (SiPU) FR coatings that combines the desired surface properties of PDMS containing

materials, with the mechanical properties, toughness, durability, and enhanced adhesion to the substrate offered by the PU bulk.[23-25] But, even with the recent advances made towards these FR coatings systems, broad spectrum fouling performance still falls short of many of the traditional AF paints. To further improve these FR coatings, surface modifying additives have been used to great effect.

Non-reactive silicone oils (hydrophobic surface modifying additives) have been studied the most with respect to the improvement of AF/FR properties of FR coatings.[5, 26-29] There are many variations of these 'silicone oils', with structures that contain some ratio of phenylmethyl/dimethyl silicone moieties typically showing superior performance than other compositions.[28] These oils usually offer this enhanced protection through the generation of a lubricated layer on the surface of the coatings, which can further weaken the bonds between the organisms and the substrate.[30, 31] But, some organisms that prefer to settle on, and subsequently adhere to highly hydrophobic surfaces, make the use of these hydrophobic additives as broad spectrum FR coatings difficult. Hydrophilic modified surfaces have been shown to disrupt settlement and attachment of marine organisms to these substrates through what is generally referred to as a 'hydration layer'.[32] Water molecules align themselves strongly to these hydrophilic surfaces, making them thermodynamically unfavorable to displace, reducing attachment of proteins and marine microorganisms. One of the most studied polymers used to generate these types of surfaces is polyethylene glycol (PEG).[32, 33] However, concerns over the stability of PEG in aqueous environments, as well as the fragile nature of largely hydrophilic coatings, have led to increased interest and use of amphiphilic modified surfaces. These surfaces can be achieved through incorporation of both hydrophobic and hydrophilic moieties into the coating matrix through chemical linkage, as well as the blending of non-reactive amphiphilic co-polymer additives. Co-polymers based on PEG and PDMS are by far the most widely studied and have displayed increased AF/FR properties in several FR coatings systems.[34-37] Other systems, utilizing various hydrophilic and hydrophobic moieties, are also being investigated including zwitterionic-based co-polymers[38-40], fluoroalkyl containing co-polymers[35, 41], and poly(vinylpyrrolidone) containing copolymers.[42]

Although much work has been established concerning the enhancement of AF/FR performance by utilizing these surface modifying additives, these have largely been incorporated into hydrophobic, inherently FR coating systems. This can lead to a sort of 'masking' of the true surface properties afforded

by these additives. Studying the fundamental interactions of these additives in model coating systems may provide a better insight into their AF/FR properties, which can be applied to several widely used coatings systems such as polyurethanes or epoxies.

The purpose of this work was to investigate how the addition of a surface modifying amphiphilic additive (SMAA), composed of PDMS and PEG, would affect the surface and bulk properties of a pure polyurethane coating composition. Additionally, the AF/FR performance of these systems was evaluated to determine if the inclusion of SMAA could convert a non-FR coating into one that has properties typically seen in FR coatings. The SMAA selected for this work has been previously studied and shown to be effective in changing the surface morphology of various FR coating systems, as well as improving their AF/FR properties.[36] This additive was incorporated into a PU coating, consisting of isophorone diisocyanate trimer and synthesized acrylic polyol, at several different loading levels based upon the concentration of PDMS and PEG in the coating formulation. Surface characterization techniques such as ATR-FT-IR, water/methylene iodide contact angle measurements, advancing and receding contact angle measurements, AFM, XPS, and TEM were utilized to assess the change in surface properties due to additive incorporation. To determine the bulk properties of these coatings' formulations, several ASTM derived methods to measure coating flexibility, hardness, solvent resistance, and adhesion were performed. Lastly, biological assays were performed to assess the FR performance of these coatings utilizing a range of micro- and macrofouling marine organisms.

Experimental

Materials

Solvents used throughout this work such as toluene, methyl amyl ketone (MAK), tetrahydrofuran (THF), chloroform, and acetone were purchased from Sigma Aldrich (MO, USA). Molecular sieves, of 4 Å size, utilized in the drying of these solvents were also purchased from Sigma Aldrich (MO, USA). Sherwin-Williams reducer No. 15 (mixture of ethylbenzene, xylene, and methyl isobutyl ketone) was purchased from Sherwin-Williams Paint Store (ND, USA). A 750 $\bar{M}_n$ hydroxyl-terminated polyethylene glycol monomethyl ether, along with a 60% w/w dispersion of sodium hydride (NaH) in mineral oil, anhydrous magnesium sulfate ($MgSO_4$) and diatomaceous earth (Celite®), used as a filter aid, were also purchased from Sigma Aldrich (MO, USA). Dibutyltin diacetate (DBTDAc), d-chloroform 1% (v/v) in

tetramethylsilane (TMS), Karstedt's catalyst (~2 wt.% Pt in xylenes), acetylacetone, and activated carbon (Darco®) G-60 (100 mesh) were also purchased from Sigma Aldrich (MO, USA). A methylhydrosiloxane-dimethylsiloxane copolymer (HMS-151) with a molecular weight of 1900-2000 g mol^{-1}, with 15-18 mol% Si-H available as grafting sites was purchased from Gelest Inc (PA, USA). Potassium bromide crystal optic disks were used for FT-IR experiments and were purchased from Alfa Aesar (MA, USA). A 20,000 $\bar{M}_n$ aminopropyl-terminated polydimethyl siloxane (APT-PDMS) was synthesized in-house *via* a ring-opening equilibration polymerization. Additionally, an 80 wt.% butyl acrylate, 20 wt.% hydroxyethyl acrylate acrylic polyol (AP) was synthesized in-house *via* free-radical polymerization, and further diluted to 50 wt.% in toluene. Detailed descriptions of these syntheses have been provided by Bodkhe et al. 2012.[24] Aluminum panels (3" x 6" and 4" x 8", 0.6-mm thick, A 3003 H14), and steel panels (3" x 6", 0.6-mm thick, QD-36) were purchased from Q-lab (OH, USA) and were used as substrates for the various characterization methods. Aluminum panels were also subjected to sandblasting and were primed with Intergard 264 marine primer *via* air-assisted spray in preparation for biological assays. Intergard 264, Intersleek® 700 (IS700), Intersleek® 900 (IS900), and Intersleek® 1100SR (IS1100SR) were provided by AkzoNobel, International Paint LLC (TN, USA). A silicone elastomer (Silastic® T2) was provided by Dow Corning (MI, USA). Falcon sterile, bacterial grade polystyrene 24-multiwell plates were purchased from VWR International (PA, USA) and modified with 1-in. diameter circular disks that had been punched from primed aluminum panels.

Experimental Approach

An overarching objective for this study was to further investigate the usage of surface modifying amphiphilic additives (SMAAs), containing both polyethylene glycol (PEG) and polydimethylsiloxane (PDMS), in coatings systems used in the protection of the hulls of marine vessels from marine biofouling. Recently, there have been several studies concerned with the anti-fouling (AF)/fouling-release (FR) properties of traditionally AF/FR coatings which have incorporated hydrophobic, hydrophilic, and amphiphilic surface modifying additives.[36, 43-45] But these coatings were designed to have inherent AF/FR properties (i.e., containing low-surface energy siloxanes to offer desired surface properties) before addition of SMAAs, with little investigation being performed in coatings systems with polyurethane or epoxy binders, having no significant AF/FR properties.

Therefore, a polyurethane based on cycloaliphatic isophorone diisocyanate (IPDI) polyisocyanate and an acrylic polyol synthesized from butyl acrylate and 2-hydroxyethyl acrylate was selected as the base polyurethane. This composition was chosen because this polyurethane forms the bulk coating matrix of several of the fouling-release coatings systems developed in previous work.[23, 24, 46] Due to no inherent PDMS or PEG chains crosslinked into the network, we hypothesize that any change in surface properties and morphology, as well as AF/FR properties from biological assays, will likely be due to the incorporation of SMAAs. The additive, a partially grafted copolymer, to be studied in these coatings consisted of a polysiloxane backbone grafted with PEG chains, with ~66 molecular wt. % of the additive consisting of PEG, and ~34 molecular wt. % being PDMS. A detailed structure of this additive can be found in appendix C (Figure C1). This partially grafted copolymer structure, and wt. % of PEG, has shown favorable performance as an additive in several other FR coatings systems and our goal was to determine if this AF/FR performance could be translated to a pure polyurethane coating as described previously.

Coating formulations were designed to include six unique combinations of PU and SMAA, shown in Table 4.1. The amount of additive (wt.% based off total formulation solids) varied between 3.8 – 22%. This is typically the range that additives (whether they are hydrophobic, hydrophilic, or amphiphilic) are used in commercial AF/FR coatings such as in Intersleek® 1100SR or Hempasil® X3+.[47] Also, formulations F1-F3 gradually increased the overall concentration of PEG within the coating from 2.5, 5, and finally to 7.5 wt.%, whereas F4-F6 varied the overall concentration of PDMS within the coating from 2.5, 5, and 7.5 wt.%. Characterization methods were focused on how the overall amount of SMAA affects the surface and bulk coatings properties, as well as the AF/FR performance. Lastly, these formulations were compared to the polyurethane control, F7, with no incorporated SMAA.

Table 4.1**.** Details of the varying PDMS, PEG, and overall wt.% of SMAA in the experimental formulations used in this work

Formulation ID	PDMS wt.%	PEG wt.%	Total additive wt.%
F1	1.30	2.50	3.80
F2	2.60	5.00	7.60
F3	3.90	7.50	11.40
F4	2.50	4.81	7.31
F5	5.00	9.63	14.63
F6	7.50	14.44	21.94
F7-PU	0.00	0.00	0.00

Synthesis of a Surface Modifying Amphiphilic Additive

To synthesize the chosen SMAA for this study, allyl-terminated polyethylene glycol monomethyl ether with an $\bar{M}_n$ of 750 g/mol was prepared. This synthesis, along with the methods used to synthesize the SMAA consisting of PDMS and PEG are found in previous work.[36] Detailed procedures are shown in appendix C.

Instrumentation

Fourier Transform-Infrared Spectroscopy (FT-IR)

A Thermo Scientific Nicolet 8700 FT-IR instrument (MA, USA) was used to gather spectra of APEG 750 and SMAA. A drop of liquid sample was placed onto a KBr optical disk, and then placed into a sample holder where transmission infrared spectroscopy was used to gather spectra.

Proton Nuclear Magnetic Resonance Spectroscopy (^{1}H-NMR)

To obtain ^{1}H-NMR spectra of APEG 750 and the chosen SMAA, a JOEL-ECA 400 MHz FT-NMR instrument (MA, USA) was used. TopSpin NMR processing software, provided by Bruker, was used to analyze spectra to determine success of synthesis. Samples were dissolved in deuterated chloroform ($CDCl_3$) with 1% (v/v) TMS.

Experimental Coating Formulation

The SMA additive was incorporated into a coating formulation containing only polyurethane. There were six experimental formulations, with a seventh formulation with no SMAA incorporated, as shown in Table 4.1. The formulation F1 is used as an example for the procedure used to make these coatings based off ~25 g total solids weight. Acrylic polyol (29.7501 g), Desmodur Z 4470 BA (10.2474 g), acetylacetone (2.2225 g), and a solution of DBTDAc 1% in MAK (1.1113 g) were added to a FlakTek Inc

MAX 40 translucent mixing cup, sealed, and stirred for 1 hr using Teflon coated stir bars on a stir plate at room temperature. Then, the SMAA (0.9178 g) was added to the container, placed in a FlakTek SpeedMixer (model: DAC 150FVZ-K), and mixed for five minutes at 3500 rpm to ensure smooth mixing of additive and bulk coating components. Formulations were immediately cast on several 3” x 6” steel and aluminum panels, as well as 4” x 8” aluminum panels primed with Intergard 264 *via* air-assisted spray application, using an R.D. Specialties formed draw down rod with an 8-mil wet-film thickness. In addition, approx. 250 µL of formulation mixture were deposited into plastic 24-well plates with primed aluminum disks glued to the bottom of the wells. After application using both methods, substrates and well plates were cured ambiently for 24 h, and then placed into a curing oven for 45 min at 80 ℃.

Commercial Standard and Control Coatings

In addition to a base polyurethane coating, which did not contain any SMAA, several commercial AF/FR standard and control coatings were analyzed in parallel with experimental coatings. All coatings were prepared according to manufacturer’s specifications on primed 4” x 8” aluminum panels or deposited into plastic 24-well plates as described previously. Descriptions and composition of these coatings can be found in appendix C (Table C1).

Surface Characterization

Attenuated Total Reflectance Fourier Transform-Infrared Spectroscopy (ATR-FT-IR)

ATR-FT-IR spectra were gathered for experimental coatings using a Thermo Scientific Nicolet 8700 FT-IR spectrometer, with a Smart iTR diamond plate ATR sampling accessory. A total of 64 scans were taken after a background spectrum was gathered, with corrections for atmospheric water and carbon dioxide peaks.

Water/Methylene Iodide Contact Angle and Subsequent Surface Energy Calculations (WCA/MICA/SE)

A Krüss DSA100 drop shape analyzer (Krüss, Germany), with Advance™ processing software, was used to measure the water contact angle (WCA) and methylene iodide contact angle (MICA) of experimental samples before water ageing. The coated samples were placed on the sample holder and clamped to prevent warping of the substrate. After ensuring the stage was level, ~6 µL of water and methylene iodide was deposited onto samples using a dual-pressure dosing unit. Measurements were recorded after a delay of 5 s to allow the drop to settle. Three separate locations on the coated panels

(top, middle, and bottom) were used to gather contact angle values, with measurements being taken over the course of 10 minutes, in 2-minute intervals. Surface energies were calculated for each time interval utilizing the Owens-Wendt method.[48]

Advancing and Receding Water Contact Angle Measurements

Measurements of advancing and receding water contact angles (Adv./Rec.) were taken utilizing a Krüss DSA100 drop shape analyzer (Krüss, Germany), with Advance™ processing software. To take these measurements, the sample stage was set to tilting mode, and samples coated with experimental formulations were clamped firmly to the holder. A drop of water, ~25 µL, was dispensed from a syringe onto the surface, with the stage set at 0°. Next, the stage was tilted at a rate of 15° min^{-1}, with images being captured every 10 s. Images were analyzed to determine the point at which the droplet began to move. At this point, the advancing and receding contact angles were recorded. This procedure was performed at the top, middle, and bottom of each experimental coating.

Atomic Force Microscopy (AFM)

An Oxford Asylum Jupiter XR atomic force microscope and controller (CA, USA) was used to take images of the surfaces of experimental coatings formulations. In general, a silicon cantilever (AC240TS-R3) with a resonant frequency of 50-90 kHz and a spring constant of 0.6-3.5 N/m from Oxford Instruments (MA, USA) was affixed to the cantilever holder and calibrated following the instruments instructions. A 100 x 100 µm area of the coatings surface was scanned in air, and height and phase imaged were gathered.

X-Ray Photoelectron Spectroscopy (XPS)

A Thermo Scientific K-alpha X-ray photoelectron spectrometer was utilized to determine the elemental composition of the experimental coatings. This instrument uses a monochromatic Al Kα (1486.68 eV) X-ray source with an Ar^+ ion source capable of a beam energy of up to 4000 eV. Before performing depth profiling on the experimental formulations, an etch rate calibration step was performed. A relatively thin film of polyurethane was prepared on a silicon wafer *via* spin coating at 6000 rpm for 35 s, using a Laurell WS-400A-6NPP spin coater. The sample was cured following the same procedure mentioned above, and then a section of the coating was etched using a Trion Technology Phantom II Inductively Coupled Plasma etch system (ICP). After etching, step-height between the bare silicon

surface and the PU coating was measured utilizing a KLA-Tencor profilometer to determine coating thickness. The coating thickness was determined to be 3.902 ± 0.111 µm. To determine the etch rate through the PU, depth profiling was performed using a 1000 eV Ar^+ source sputtering on an area of 400 x 400 µm in 1-minute intervals for 30 minutes at a time, until the silicon substrate was reached. Chamber pressure was maintained below 3.2 x 10^{-7} Torr, with photoemission lines for C1s, N1s, O1s, and Si2p collected after each etch for an interval of 10s at a constant analyzer pass energy of 200 eV. Etch rate through the PU coating determined with this method was 0.1183 nm s^{-1}. After the etching calibration was performed, depth profiling experiments on free films of were performed using the parameters mentioned above. The exception being the depth profiling was only carried out over 30 etch cycles, with an average of three compositional scans represented for each cycle, and atomic concentrations were quantified utilizing Thermo Avantage® processing software.

Transmission Electron Microscopy (TEM)

Specimens for transmission electron microscopy were embedded in EPON-araldite-DDSA epoxy with DMP-30 accelerator and sectioned at 60-90 nm thickness on an RMC MT XL ultramicrotome (Boeckeler Instruments, Tucson, Arizona USA). Sections were collected on copper grids with a formvar-carbon supporting film (Ted Pella, Inc., Redding, California USA). Observation and imaging were performed on a JEOL JEM-1400 electron microscope (JEOL Inc., Peabody, Massachusetts, USA) operating at 120 kV and equipped with an AMT NanoSprint 15L bottom-mount camera (AMT Imaging, Woburn, Massachusetts USA).

Coating Properties Testing

Crosshatch adhesion tests were performed according to ASTM 3359-17, using test method B. A cutting tool was used to make one patterned cut, with six teeth, and then making another cut going across the first pattern at 90°. The patterned area was inspected to ensure the cutting tool had made it to the metal substrate, and then a strip of adhesive tape was flattened over the cut area, made sure air pockets had been removed, and then removed with constant force at as close to 180° as possible. The patterned area was then inspected for any loss of coating material and reported on a scale from 0-5B, with 0B indicating complete removal of coating material, and 5B designating no removal of coating from the substrate.

Flexibility assessed *via* conical mandrel bend tests were performed according to ASTM D522-17. Samples were placed in the apparatus and bent to approx. 135°. Visual inspection of the bent samples was used to determine any visible cracking, and if cracking occurred, the point at which the crack ended was reported in cm. This represents a measure of crack resistance and flexibility, with no cracking attributed to highly flexible coatings, with increasing length of crack denoting reduced flexibility performance.

A modification of ASTM D5402-19 was used to determine the amount of double-rubs a coating could withstand until coating damage was observed. A hammer (~0.5 kg) was wrapped with 100% cotton cheesecloth around its head to form at least 3 layers, and then soaked until dripping with methyl ethyl ketone. An area of 1” x 4” was selected on coated samples and the hammer was placed onto the surface and rubbed up and down (one double-rub) with minimal force, until the substrate was seen. The cheesecloth was re-wet as needed, with new cheesecloth being replaced every 100 double-rubs.

Hardness of experimental coatings was also determined using pencil hardness according to ASTM D3363-20. In this method, samples were placed on a flat surface, and pencils with hardness values ranging from the hardest 8H to the softest 9B were pushed across the sample at a 45° angle for a length of 0.25”. The level of pencil hardness where there was no visible gouging of the coatings surface was recorded as the pencil hardness value. Lastly, coating thickness was determined using a BYK byko-test 8500 dry film thickness gauge. Three different locations (top, middle, bottom) of the coated samples were measured after calibration and reported as an average thickness.

Water Ageing

Experimental coatings were placed in circulating tap water tanks for 28 days at ambient temperature for ‘preleaching’ treatment, with the tanks being automatically refilled every 4 h. Once coated samples had been preleached, panels and well plates with deposited coating were removed, rinsed with deionized water, and left to dry overnight.

Biological Laboratory Assays

An important part of evaluating the anti-fouling and fouling-release properties of coatings systems is the selection of marine organisms known to be aggressive marine foulants when performing these biological assays. Much work has gone into developing standardized testing methods utilized here at NDSU. These assays involve several microfoulants such as the marine bacterium *Cellulophaga lytica* and marine diatom *Navicula incerta*, with macrofoulants including marine algae *Ulva linza* and marine barnacle *Amphibalanus amphitrite*. Recently, Stafslien et al. showed that there was a strong, positive correlation between these laboratory assays, and real-world field testing environments.[49] Therefore, the procedures developed for *C. lytica*[50, 51], *N. incerta*[52, 53], *U. linza*[50, 52], and *A. amphitrite*[54, 55] are used throughout this work and the details of which can be found in appendix C.

Statistical Analysis

Minitab statistical software was used to perform one-way ANOVA on the attachment/settlement and release data for laboratory biological assays involving *U. linza*, *N. incerta*, *C. lytica*, and *A. amphitrite*. The results of these assays were treated as a completely randomized design, setting amount of SMAA (wt. %) as the singular factor. The highest water pressures (138 kPa for *C. lytica* and N. incerta, or 110 kPa for *U. linza*) were used for the statistical analysis, with the biomass growth and biomass remaining as measurable quantities. The significance level (α) was set at $\alpha = 0.05$, with statistically significant results having *P*-values < 0.05. Tukey method was used to make comparisons between difference of means with each treatment group. Means that do not share a letter in Tables C2-C8.

Results and Discussion

Recently, much of the research on the development of coatings for the protection of marine biofouling has been focused around amphiphilic (heterogenous) surfaces.[34, 40, 42, 43] The use of a hydrophilic component, along with a largely hydrophobic component, has been shown to combine the strong AF properties of hydrophilic surfaces, with the excellent FR properties of more hydrophobic surfaces. The aim of using these heterogenous surfaces is to provide broad-spectrum protection against marine biofouling that, in some cases, may surpass the performance of commercially available FR paints. A popular method of introducing amphiphilic character into a coating network, is to utilize polymers, or small molecules, that contain hydrophilic and hydrophobic components, and react them within the coating

matrix. While effective in producing a heterogenous surface, a balance between the hydrophilic and hydrophobic components is paramount, as an unbalance of these moieties can affect the fouling protection performance.[34] Another method to produce these heterogenous surfaces is to incorporate a non-reactive, amphiphilic, surface modifying additive. Often, these additives are blended into traditional FR coatings that contain hydrophobic components such as PDMS or fluoroalkyl containing polymers. This is thought to facilitate the diffusion of the additive to the surface, populating the highly hydrophobic surface with hydrophilic domains.[44] However, little work has been performed investigating the performance of these additives in traditionally non-FR coatings. The aim of this study was to investigate how the incorporation of a surface modifying amphiphilic additive (SMAA), composed of PDMS and PEG, affects the AF/FR properties, as well as the surface and bulk physical properties, of a pure polyurethane coating.

Synthesis of the SMAA was performed *via* Karstedt's catalyst assisted hydrosilylation of a previously synthesized allyl terminated PEG of 750 $\bar{M}_n$ (APEG-750), and a polymethylhydrosiloxane (PMHS) with a molecular weight of 1900-2000 g mol^{-1}, and 15-18 mol% Si-H repeating units. FT-IR and ^{1}H-NMR were performed to confirm successful synthesis of these materials and detailed spectra are shown in Figures C4-C7 in appendix C. The disappearance of allyl and hydride functional groups in the spectra taken using these spectroscopic methods, as well as the appearance of characteristic peaks for ethylene oxide (EO) and siloxane groups point towards a successful synthesis.

After SMAA synthesis, experimental coatings formulations were prepared, with the compositions shown in Table 4.1. Once these coatings had fully cured, ATR-FT-IR, WCA/MICA measurements, advancing and receding WCA measurements, AFM, XPS, and TEM were performed to characterize the surfaces. The coatings surfaces were compared to a pure polyurethane with no incorporated SMAA.

ATR-FT-IR was one method used to detect the compositional changes of these surfaces due to incorporation of SMAA into the PU. As the amount of additive is increased, significant increases in the intensity of several peaks' characteristic to PDMS and PEG were expected on the surface of the coatings. Figure 4.1 details the fingerprint region of the ATR-FT-IR spectra for formulations F1-F7 shown in Table 4.1. There are three main peaks of interest in these spectra to determine the effect of SMAA on surface composition for these coatings. The first being the C-O-C (ether) stretching signal, indicative of the EO

groups from PEG. If PEG is present, a relatively sharp peak is seen around 1100 cm^{-1}. In F1-F3, there is a gradual increase in SMAA amount, with the amount of PEG being controlled in the coating formulation at 2.5, 5, and 7.5 wt.%. This can be seen in the intensity of the ether signal as beginning to form with only 2.5 wt.% PEG, with a slight increase once the amount reached 5 wt.%. Lastly, F3 had the most intense signal from PEG out of these three formulations, corresponding to the largest PEG content of 7.5 wt.%. A similar, gradual increase of signal intensity is seen concerning both the Si-O-Si stretching (1000-1100 cm^{-1}) and Si-C vibrations (800 cm^{-1}) from the PDMS backbone of the SMAA. In F4-F6, there again is an increase in signal intensity for peaks corresponding to PEG and PDMS. The total amount of PDMS was controlled in these formulations at 2.5, 5, and 7.5 wt.%. Due to the structure of the additive containing more PEG than PDMS on a wt.% basis, at each level of PDMS in the formulation, there is almost double the amount of PEG. This can be seen in the ATR-FT-IR spectra of F5 and F6, which have significantly more PEG in the formulation than the highest amount seen in formulations F1-F3. Lastly, these formulations were compared to a pure polyurethane with no incorporated SMAA (F7). Peaks from PEG and PDMS are not seen in this formulation, which provides confidence that any surface compositional change is due solely to the incorporation of SMAA. Overall, ATR-FT-IR was able to provide insight into how the surface composition of a PU coating changes when increasing amounts of PEG and PDMS are incorporated into the formulation by way of surface modifying amphiphilic additive.

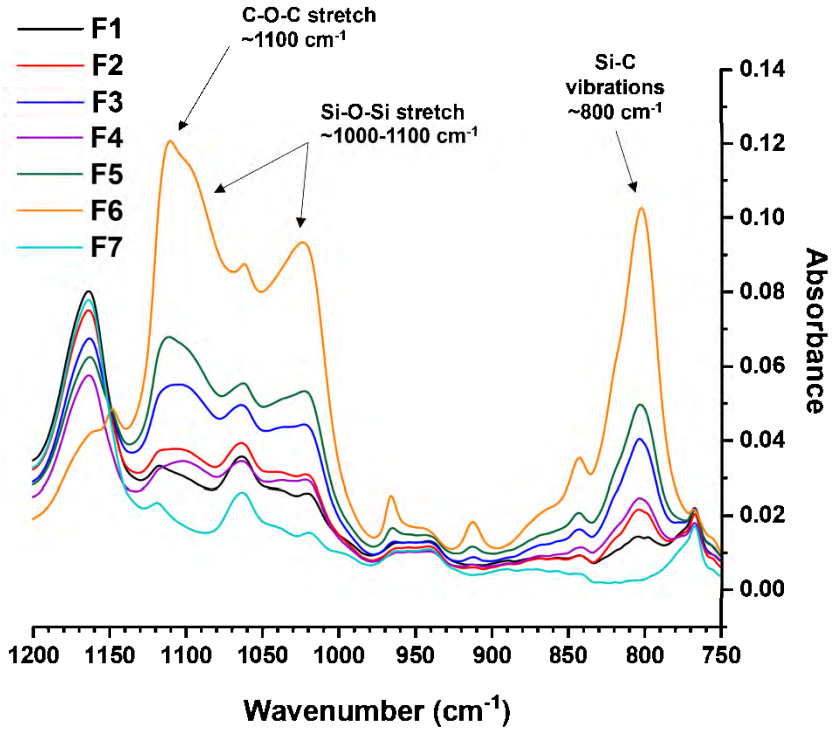

Figure 4.1. ATR-FT-IR spectra of formulations F1-F7 shown in Table 4.1. Characteristic peaks belonging to PEG and PDMS are labeled with their respective wavenumber values.

Another method of surface characterization utilized in this study was the determination of water and methylene iodide contact angles (WCA/MICA) for the calculation of surface free energy (SE) of the experimental coatings. These measurements can provide insight into how the SMAA arranges at the surface once it has diffused through the PU matrix. In addition, advancing and receding contact angles were measured using the tilting drop method, and were used to determine WCA hysteresis. This can provide valuable information about the heterogeneity of these surfaces. Figure 4.2A and 4.2B show the WCA/MICA and subsequent SE calculations, while Figure 4.2C and 4.2D show the advancing and receding contact angles, along with calculated WCA hysteresis. First, the contact angle measurements and surface free energy for the purely PU surface are around 85° and 45 mN/m respectively, and do not show a significant change after 10 min. For formulations F1 and F2, there is a significant increase in contact angle seen at 0 minutes, when compared to PU. This also translates to a lower surface free energy, which is likely due to the presence of PDMS in the SMAA backbone populating the surface. There is also a slightly larger decrease in WCA after 10 min than the PU surface. This could be due to the

PEG chains rearranging at the surface, lowering the WCA values, while increasing surface free energy. Formulation F4 also shows similar values to F1 and F2, likely due to their similar amounts of SMAA blended into the PU matrix.

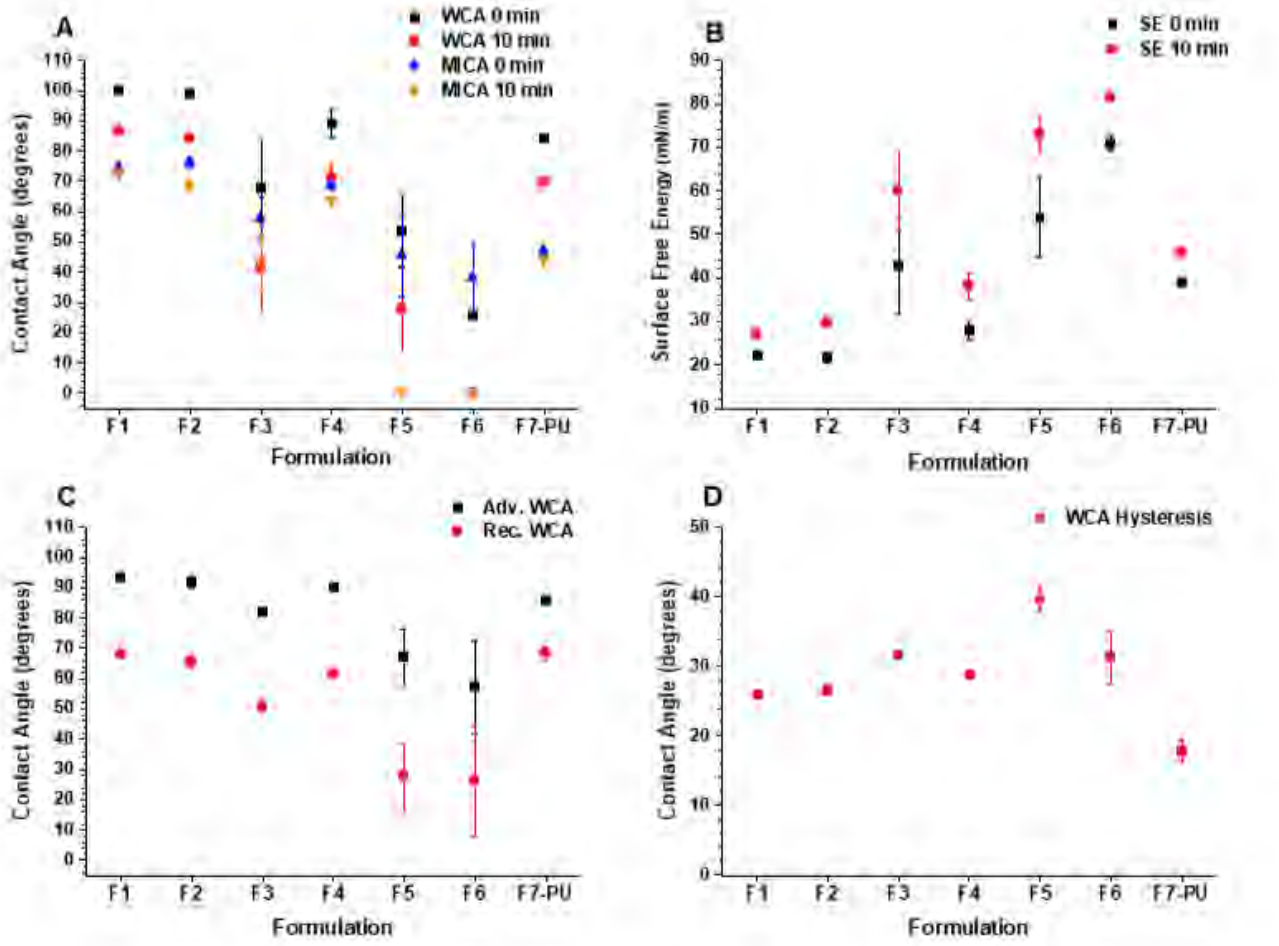

Figure 4.2. Water contact angle (WCA) and methylene iodide contact angle (MICA) are shown in plot A. Surface free energies for experimental formulations are shown in plot B. Advancing and receding WCA, as well as WCA hysteresis calculations are shown in plots C and D respectively. Each plot refers to the experimental formulations shown in Table 4.1.

However, formulations F3, F5, and F6 display significantly lower contact angles at 0 min, with a very significant decrease after 10 min. In fact, the WCA after 10 min for F6 is 0°, typically seen in a completely wetted surface. As expected, the surface free energies of these formulations are also significantly higher than the other experimental formulations, despite having a higher overall PDMS content in the coating. A possible explanation for this behavior is that there could be a threshold of PEG content needed to be reached before more significant changes are seen at the surface of this specific coating system. As the amount of PEG increased from 2.5% in F1, to 5% in F2, there was not as

significant a change in values. But once the amount of PEG reached 7.5%, as in F3, these changes are now seen. The level of PEG in formulations F4-F6, is significantly higher than in F1-F3, with F6 having theoretically over 14% of PEG, which helps explain the completely wetted surface, and extremely high surface energy. Lastly, the advancing and receding contact angles display similar trends. Formulations that have higher PEG content show lower advancing and receding contact angles, with the largest difference shown in F5. The contact angle hysteresis values differ slightly between F1-F3, with F5 and F6 showing the highest values. In any case, these surfaces had significantly higher hysteresis values than the pure PU coating. These changes are likely caused by the migration of SMAA through the PU, producing a more heterogenous surface. In summary, the incorporation of SMAA into these coatings was shown to produce significant changes in their surfaces, with greater effects seen with increasing PEG content.

Atomic force microscopy (AFM), a technique used to investigate the surface morphology and structure of a variety of materials, was also utilized in this work to study the changes in the PU's surface upon incorporation of varying levels of SMAA. Figure 4.3 shows the 100 x 100 µm phase and height images of formulations F1-F7 from Table 4.1. The pure PU control formulation, F7, shows a largely homogenous surface in phase images. Usually, differences in intensity of color (lighter or darker) on the surfaces of these materials signifies the presence of chemically different materials, such as PDMS or PEG. The amount, size, and shape of these phase-different domains is thought to be a function of the individual concentrations of PDMS and PEG, as well as the overall concentration of SMAA in the PU formulation. This, along with the changes in intensity of a phase image, provide insight into how heterogenous a surface is. In Figure 4.3, F1, containing the lowest amount of SMAA, shows the smallest domain sizes and frequency. While the surface indeed indicates the presence of the SMAA, containing both PEG and PDMS, it is not yet saturated with additive. When the SMAA amount is increased in F2 and F3, both the number of domains, and the size of these domains increased significantly. Also, the phase image for F3 begins to show smaller, circular domains interspersed between the larger domains present. This points to the surface beginning to become saturated with additive, almost forming a layer of free-floating oil on the surface. The phase image for F4 shows a frequency and size of domains on the surface closer to F2, which is likely due to both having almost the same amount of SMAA blended into the PU.

Again, as the overall amount of SMAA is increased in F5 and F6, significant changes in surface morphology are seen. In F5, domains begin to take on an irregular shape, with many more smaller domains in-between. And finally, in F6, the surface is completely saturated with SMAA, forming a well-defined layer of 'amphiphilic oil' at the surface.

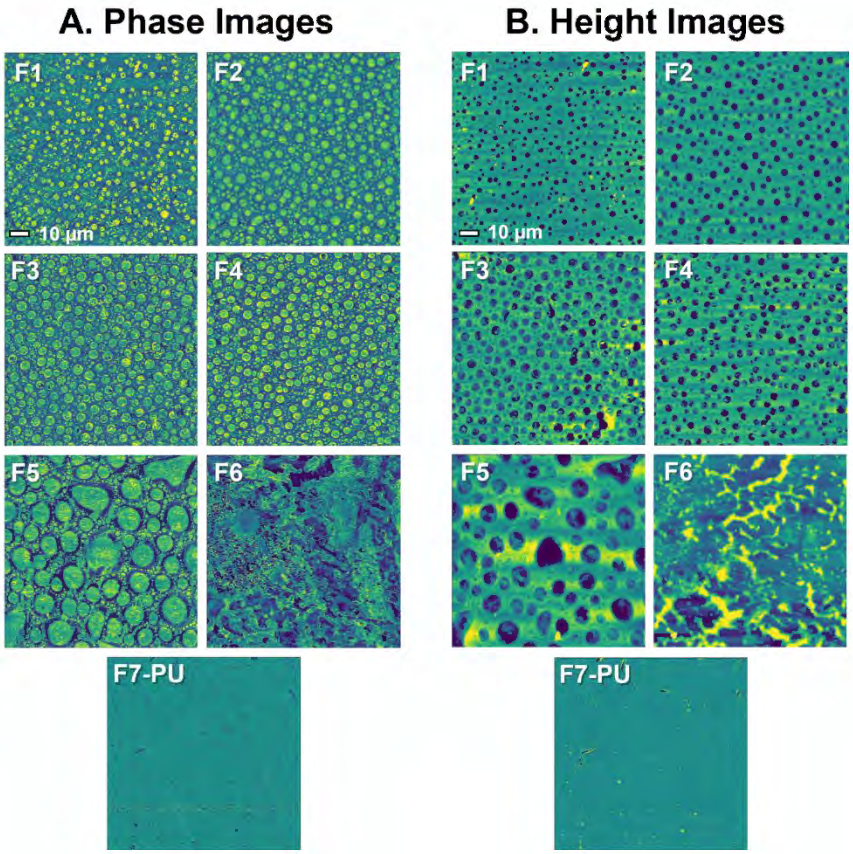

Figure 4.3. A. Phase images of experimental formulations F1-F7 shown in Table 4.1. B. Height images for these experimental formulations. Each image is for an area of 100 x 100 µm.

As with the phase images taken of these formulations, the height images in Figure 4.3 show similar trends. In these images, the darker an area, the more recessed it is, with lighter regions being raised from the surface. This provides further evidence that the domains identified in the phase images are indeed made up of SMAA, consisting of PEG and PDMS. The recessed height of these PDMS containing domains may be due to surface saturation of additive, with the domains getting larger and deeper as SMAA concentration is increased. Lastly, surface roughness values (R_q and R_a) were determined and can be seen in Table C9 in appendix C. It was shown that as concentration SMAA was increased in formulations F1-F3, and F4-F6, there was a significant increase in roughness compared to

the smooth PU control, F7. The increase in surface heterogeneity of these additive formulations can explain this significant change, which is supported through ATR-FT-IR and contact angle measurements. Overall, AFM was a useful technique used to investigate how the incorporation of SMAA affected the surface morphology of a pure PU coating system.

X-ray Photoelectron Spectroscopy (XPS) was used to quantify the elemental compositions of the experimental formulations when performing depth profiling experiments. A depth profiling calibration experiment was performed to determine the average etch rate of the Ar^+ beam source through a thin coating of pure PU. The atomic concentrations (%) of C1s, O1s, and Si2p atoms, plotted against the etching depth (nm), is shown in Figure 4.4A-C for the tops of free films for formulations F1-F7. It is clear to see significant trends in all three elemental species (C, O, Si) for these formulations, due to the incorporation of varying amounts of SMAA into PU. As the SMAA is incorporated at low levels, such as in F1 and F2, there is a decrease in C % in the first 5-10 nm of the coating surface, with a significant increase in both O % and Si % when compared to F7-PU. These changes in surface composition start to diminish as the etch depth is increased, levelling out before 30 nm, with atomic concentrations around 85% for C, 8% for O, and between 3-5% for Si. In F3, which has an increased amount of SMAA blended into the coating, these same changes in elemental composition are seen, albeit at a much more significant intensity. Most notably, higher concentrations of Si and O atoms are seen at deeper depths into the coating before levelling out. Similar trends are observed in formulations F4-F6, where Si and O % are shown to compose almost half of the surface composition. The formulation with the highest amount of SMAA, F6, shows concentrations of these elements starting to level past 70 nm, much farther than formulations with less SMAA, with around 55% C, 25% O, and 18% Si. As increases in SMAA incorporation are made, the surface elemental composition changes drastically. This supports the other surface characterization methods observation that increasing concentrations of SMAA produce significant changes in the surfaces of these coatings.

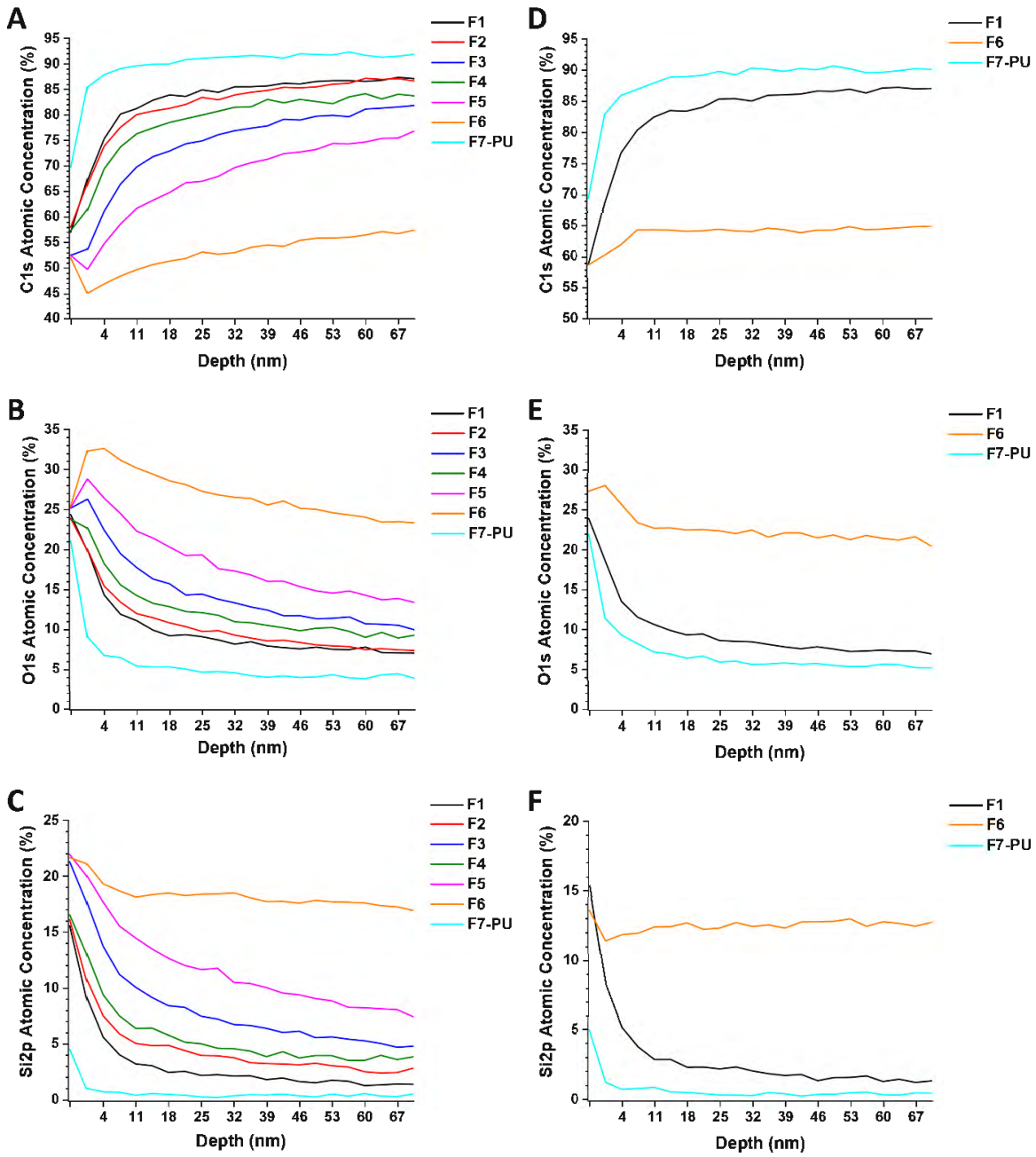

Figure 4.4. XPS depth profiling data for formulations F1-F7 shown in Table 4.1. A, B, and C correspond to the depth profile for the C1s, O1s, and Si2p atoms respectively for the tops of the films. D, E, and F contain depth profile data for these atoms for the bottoms of the films.

In addition to performing XPS measurements on the top of free films for these formulations, the bottom of films for formulations F1, F6, and F7 were subjected to depth profiling experiments. The C1s, O1s, and Si2p atomic concentrations are shown in Figure 4.4D-F. Each formulation shows almost identical atomic concentrations as on the top surface of these free films. It was not totally unexpected for

this to occur, seeing as how the SMAA is relatively low molecular weight, lending itself to diffusion through the PU network. However, the most notable observation is that even at low SMAA levels, it seems there is complete dispersion throughout the PU coating, with higher atomic concentrations from the additive observed around the first 10 nm into the surface but levelling out to a constant amount in the bulk of the coating. This can have significant effects regarding the physical properties of these coatings such as adhesion, hardness, and flexibility, which is important when placing these coatings in a harsh marine environment.

Transmission Electron Microscopy (TEM) was also performed to gather cross sectioned images of films for formulations F1-F7. Figure 4.5 contains the images from F1, F6, and pure PU F7, showing the tops of these films next to air. The formulations containing SMAA both show lighter domains, likely to be concentrations of PEG chains from additive domains, evenly distributed throughout the films thickness. These domains are much larger in F6, which contains the highest concentration SMAA, and therefore the highest concentration of PEG in the overall coating formulation. The pure PU coating of F7 does not show these domains, and mostly resembles the environment surrounding the sample.

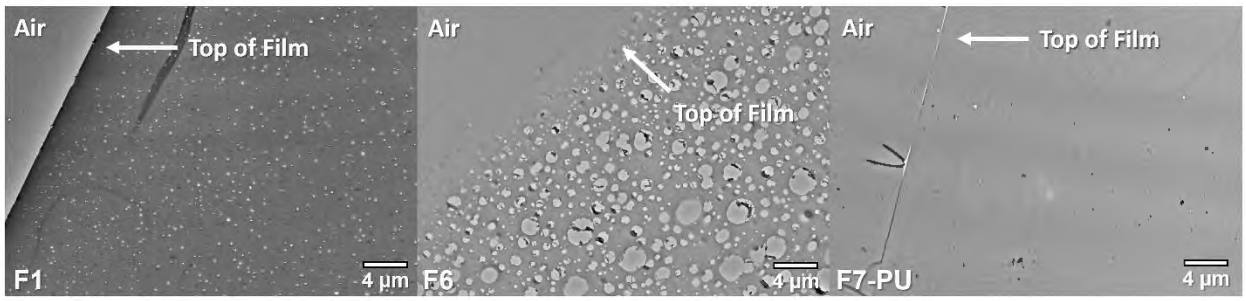

Figure 4.5. TEM images for F1 (left), F6 (middle), and F7(right). The top of the films is facing the left side of the images, next to the air interface.

In addition, the topmost section of these additive films (0-100 nm) does not seem to contain these lighter domains from large concentrations of PEG. Instead, it is likely that these surfaces are dominated by the PDMS component in these additives, as they would appear darker in contrast due to the increased density of the silicon atoms. This is supported by the data from XPS depth profiling in Figure 4.4, as the silicon concentration is highest, within the first 100 nm of the coating, with the oxygen concentration seen at higher levels than silicon once the etching depth is increased, likely from PEG chains on the SMAA.

Physical property characterization of these coatings was also performed according to several ASTM standardized methods. Results from these testing methods are shown in Table C10 in the appendix C. In general, it was shown that as the amount of SMAA was increased in experimental formulations, coating physical properties significantly decreased. Most notably are the solvent resistance and adhesion properties of these additive formulations. The formulations with the highest concentration of SMAA, F5 and F6, have significantly less solvent resistance, displayed poor flexibility, were softer, and completely delaminated from the substrate during cross-hatch adhesion testing compared to the pure PU coating in F7. This loss of performance can be severely detrimental in harsh marine environments. The reasons behind this are likely the large domains of unreacted SMAA that are dispersed throughout the coating, as seen in TEM images in Figure 4.5. The large concentrations of additive (shown to be dispersed throughout the bulk) could be a source of failure during physical property testing, contributing to loss of adhesion to the substrate. Additionally, these additives were shown to contain large concentrations of PEG, which swell in aqueous environments, also leading to severe delamination from the substrate. Adhesion to the substrate is perhaps the most important physical property of coatings used for fouling protection, as any loss in adhesion can lead to a surface no longer protecting against the build-up of fouling organisms. It is therefore important to reach a critical balance of hydrophobic and hydrophilic group contributions from these surface modifying amphiphilic additives if they are to be used as the AF/FR component in traditionally non-FR coatings systems.

After experimental, standard, and control formulations shown in Table 4.1 and Table C1 had been pre-leached in circulating water tanks for 28 days, leachate toxicity assessments were performed before biological assay testing to assess AF/FR of marine organisms *U. linza*, *N. incerta*, and *C. lytica*. General procedures and results (Figure C8-C10) for these toxicity assays can be found in appendix C and follow previously described methods.[50-53] Toxicity was determined based on the amount of growth of these organisms in solutions containing overnight extracts of the coatings in artificial seawater (ASW) and nutrients. There was found to be no apparent toxicity to any of the organisms tested compared to a positive growth control, indicating that these experimental formulations are indeed non-toxic and should not compromise the results for AF and FR biological assays.

One major marine foulant of concern is the green macroalgae *Ulva linza*. This alga is present throughout the world's oceans and significantly contributes to the negative effects of biofouling of ships hulls.[56] Typically, motile spores of *U. linza* (ca 5µm in length) travel through seawater, searching for a suitable surface to settle onto. Once attached to these surfaces, they undergo germination and develop into sporelings (young plants), producing protein-based adhesives to strengthen their adhesion.[57] The settlement and adhesion of *U. linza* is greatly affected by the surface wettability of the substrate. In general, spores tend to settle more strongly on hydrophilic surfaces, but the resultant sporelings tend to adhere more strongly. The opposite is true for hydrophobic surfaces, where they adhere weakly to the surface, despite having a higher density of spore settlement.[58-60] Therefore, a heterogenous surface, composed of hydrophilic and hydrophobic moieties are thought to provide a good balance of resistance to settlement, while also providing good FR properties towards these organisms.

Settlement and growth of *U. linza* sporelings over 7 days is shown in Figure C11. Overall, there was no significant differences between experimental formulations containing SMAA. However, these surfaces did show slightly lower biomass growth than the control PU and commercial FR standard IS1100SR coatings. The inclusion of SMAA with hydrophilic PEG did not seem to greatly reduce the settlement of these sporelings, while the formulations with the highest PDMS content at the surface did not show increased settlement either. However, significant changes in removal performance for experimental formulations containing SMAA are seen (Table C3). The biomass remaining after water-jetting at 18, 67, and 110 kPa of these formulations is shown in Figure 4.6. First, formulations F1-F3 contain the lowest amount of SMAA in the coating and showed the highest amount of biomass remaining among the experimental formulations, as well as the control pure PU formulation F7. This could be due to these formulations having large amounts of PEG, with little PDMS content from the SMAA at the surface. These surfaces also generally had the lowest amount of heterogeneity throughout these formulations. This results in domains that are further spaced out, which could allow the sporelings of *U. linza* to spread their adhesive more effectively. In contrast, formulations F4-F6 showed significantly lower biomass remaining than the other experimental formulations, including PU F7, despite having the highest amount of PEG in the coating. But the concentration of PDMS at the surface is also the highest, with F6 having the highest amount determined via XPS depth profiling. Since these surfaces are not homogenous,

composed of primarily PEG or PDMS alone, the heterogeneity is likely a driving factor in lowering the adhesion strength of these sporelings. Producing surfaces with larger, more irregular domains of PEG and PDMS may help disrupt the adhesive action of this macroalga. Smaller domains as seen in F1-F3 may not cover enough area to disrupt the glycoprotein-based adhesive on a macroscale. Overall, the formulations with the highest amounts of SMAA, and thus higher heterogeneity, produced surfaces that had the lowest amounts of biomass remaining, being comparable to commercial FR standard IS100SR.

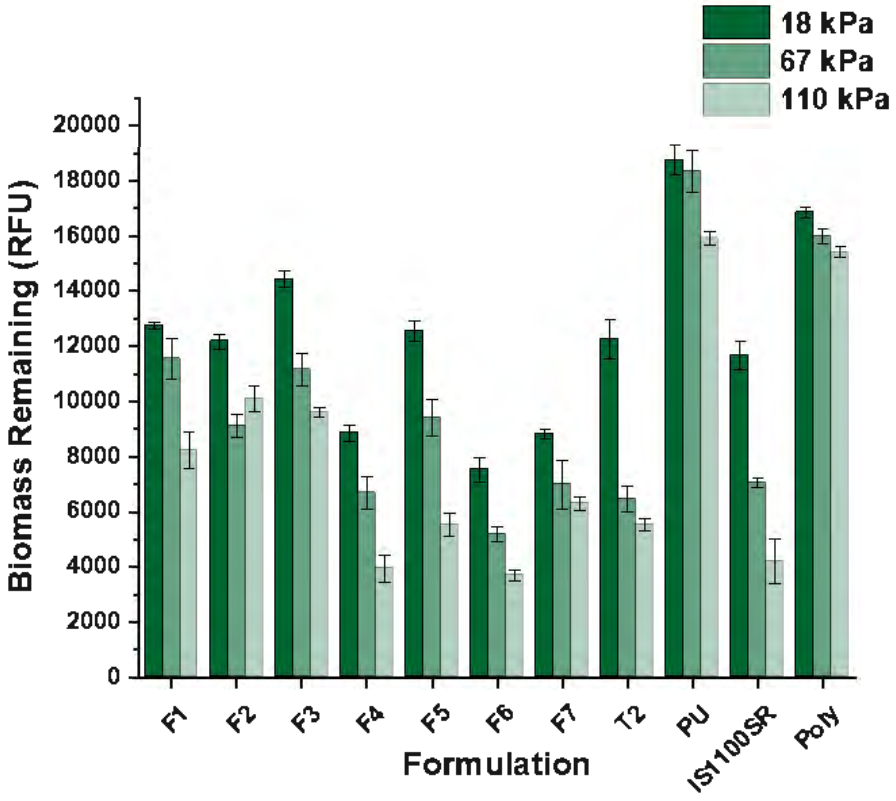

Figure 4.6. Removal of *U. linza* sporelings at water-jet treatments of 18 (green), 67 (light green), and 110 kPa (lightest green) measured using biomass remaining *via* relative fluorescence units (RFU). Bars represent the average removal from six replicates with standard deviation. The X-axis is labeled to indicate formulation number as described in Table 4.1, along with commercial standards and controls in Table C1.

Another marine biofoulant of interest is the microalga slime-forming diatom *Navicula incerta*. These diatoms have been shown to prefer attachment on hydrophobic surfaces, with very strong adhesion to hydrophobic substrates consisting of silicon containing moieties like PDMS.[17, 61] Again, cell attachment results, shown in Figure 4.7, do not show any significant change within experimental coatings. In fact, there was no significant difference between any of the evaluated formulations including controls and commercial FR standards (Table C4). The biomass remaining after water-jetting pressures of 138

kPa are also shown in Figure 4.7. Here, each SMAA containing experimental formulation (F1-F6) had lower biomass remaining than the pure PU F7, with those containing the highest amounts of SMAA and heterogeneity (F5 and F6), performing better than commercial FR standard IS1100SR (Table C5). This result was observed despite most of these experimental formulations containing a significant amount of PDMS at the surface, which these organisms adhere strongly to. There was no significant difference between the SMAA containing formulations, despite the range of heterogeneities and surface compositions of PEG and PDMS seen. In the removal data shown for *U. linza*, only once the domains of SMAA, contributing to the surface heterogeneity, became larger and more irregular, the removal properties increased. This could be due to the reduced spacing between domains, which has been shown to reduce sporeling adhesion to surfaces.[62] But, even at low loadings of SMAA, as shown in F1, there were enough heterogenous domains at the surface to disrupt adhesion of the diatoms to the coatings. In addition to the size of these surface domains, it is likely that the large concentration of PEG in these domains (seen as the lighter colored phases in TEM images) significantly contributes to reducing the adhesion strength of the diatoms. In summary, *N. incerta* diatoms adhered very weakly to SMAA containing formulations, with most of these coatings performing better than commercial FR standards.

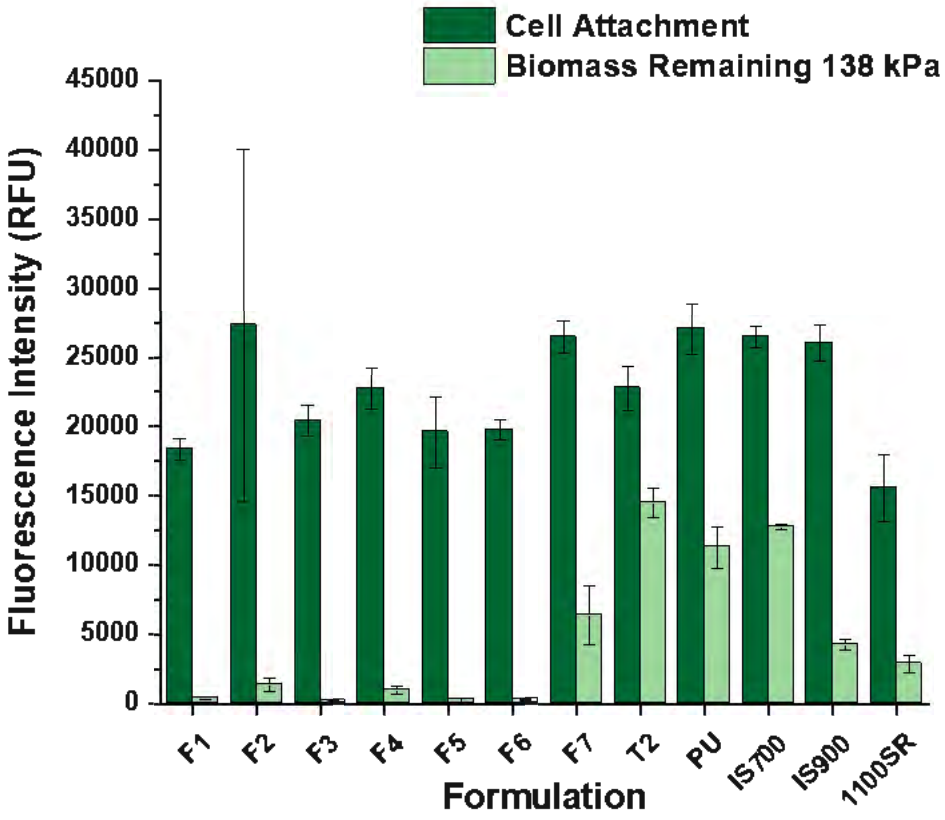

Figure 4.7. Cell attachment and biomass of *N. incerta* remaining after water-jet treatment at 138 kPa water column pressure. The dark green bars represent diatom cell attachment, while light green bars represent biomass remaining after water-jet treatment at 138 kPa for four replicate measurements and standard deviations. The X-axis is labeled to indicate formulation number in Table 4.1, along with commercial standards and controls shown in Table C1.

Other common marine biofoulants include several species of marine bacterium. *Cellulophaga lytica* is a major contributor to this phenomenon and is found globally in marine environments.[6] Marine bacteria, including *C. lytica*, primarily 'float' through seawater, depositing themselves on submerged structures including ships hulls. Once in contact with these surfaces, there is a rapid secretion of proteins, polysaccharides, nucleic acids, and other extracellular polymeric substances (EPS). These secretions act to 'condition' the surface to make it more favorable for prolonged adhesion, and also aid in the process of colony and biofilm formation, making it even more difficult to remove these organisms.[63] These molecular components often contain several hydrophilic and hydrophobic motifs, allowing these bacterium to settle on either hydrophilic or hydrophobic, homogenous surfaces.[5] It is thus favorable to utilize amphiphilic, heterogenous surfaces to reduce the growth and adhesion of these organisms.

The biofilm growth and removal towards *C. lytica* for the experimental formulations is shown in Figure 4.8. There was no significant difference in the biofilm growth between formulations containing SMAA (Table C6). However, these formulations had significantly less growth on the surface when compared to the pure PU F7, along with controls and commercial FR standards. Even at small concentrations of SMAA, there is a heterogenous surface with sufficient PEG content to reduce the growth of this bacterium. When subjected to water-jetting at 138 kPa, a similar trend is seen. Additive containing formulations again show very little difference between biomass remaining results when increases in SMAA content are considered, while outperforming most of the control and standard formulations, except for IS900 and IS1100SR (Table C7). As in results seen for the removal assays involving *N. incerta*, the ratio of PDMS and PEG in domains from the SMAA are effective in producing FR surfaces even at the lowest concentrations. This provides more evidence of the effectiveness of these types of heterogenous surfaces for the protection against several marine fouling organisms.

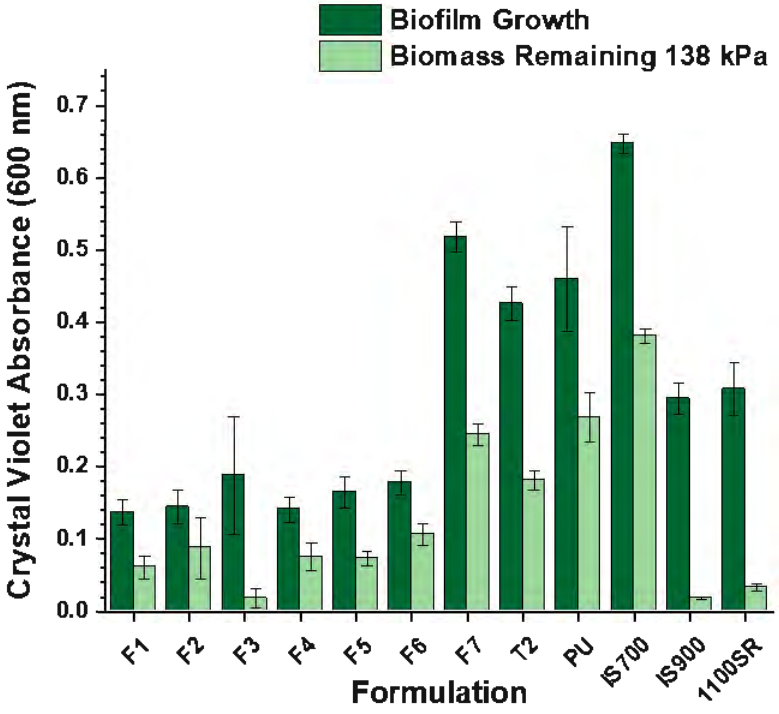

Figure 4.8. Bacterial biofilm growth and retention of *C. lytica* after water-jet treatment at 138 kPa water column pressure. The dark green bars represent biofilm growth, whilst the light green bars represent biomass remaining after water-jet treatment at 138 kPa for 4 replicate measurements with standard deviations. The X-axis is labeled to indicate formulation number in Table 4.1, along with commercial standards and controls in Table C1.

When evaluating surfaces for AF/FR performance, in addition to utilizing soft macrofoulers and microfoulants such as *U. linza*, *N. incerta*, and *C. lytica*, it is also desirable to include hard fouling microorganisms such as the marine barnacle *Amphibalanus amphitrite*. Barnacles are aggressive foulants, causing significant increases in drag for ocean going vessels, reducing overall performance.[1, 64] A major reason for such heavy fouling caused by these barnacles is largely due to the makeup of their specialized adhesive, or 'barnacle cement', that is used to anchor themselves to submerged structures. This cement consists primarily of proteins containing hydrophilic and hydrophobic regions, as well as smaller molecules such as enzymes and phenolic compounds acting as crosslinkers to strengthen this protein-based adhesive.[65, 66] As well as being a very robust and strong adhesive, the cement from this species of barnacle was shown to spread more rapidly on hydrophilic surfaces, but also obtaining relatively high adhesion strengths on surfaces with a dominant hydrophobic character.[54, 67] Thus, while heterogenous surfaces may likely perform well, balancing the hydrophilic and hydrophobic components is important to obtain coatings with optimal AF/FR performance.

Reattached barnacle adhesion strength was determined *via* measurement of the force needed to dislodge barnacles from the surface of the coatings and is shown in Figure 4.9. It was observed that there were virtually no significant differences in the force needed to remove between experimental formulations with incorporated SMAA (Table C8). The only experimental formulation which showed a significantly lower removal force than pure PU F7, was formulation F4, performing close to commercial FR standard IS1100SR. Although, removal strength is the primary measurable unit, other factors can influence how well a surface performs. If there are signs of barnacle basal plate breakage, this could mean an overall higher adhesion strength to the substrate. And, in some surfaces, if there are fewer barnacles reattached to the surface, the surface could be more resistant to the primary adhesive action. This is seen in F4, with only three of six barnacles reattaching to the surface. Overall, performance of these SMAA containing formulations generally decreases as the amount of additive is increased. This is likely due to the significantly larger surface concentrations of PEG, causing the adhesive to be spread more easily. While PDMS concentration also increases with these formulations, it is likely not at sufficient levels to disrupt this process, and therefore contribute to lowering overall adhesion strength of the barnacles.

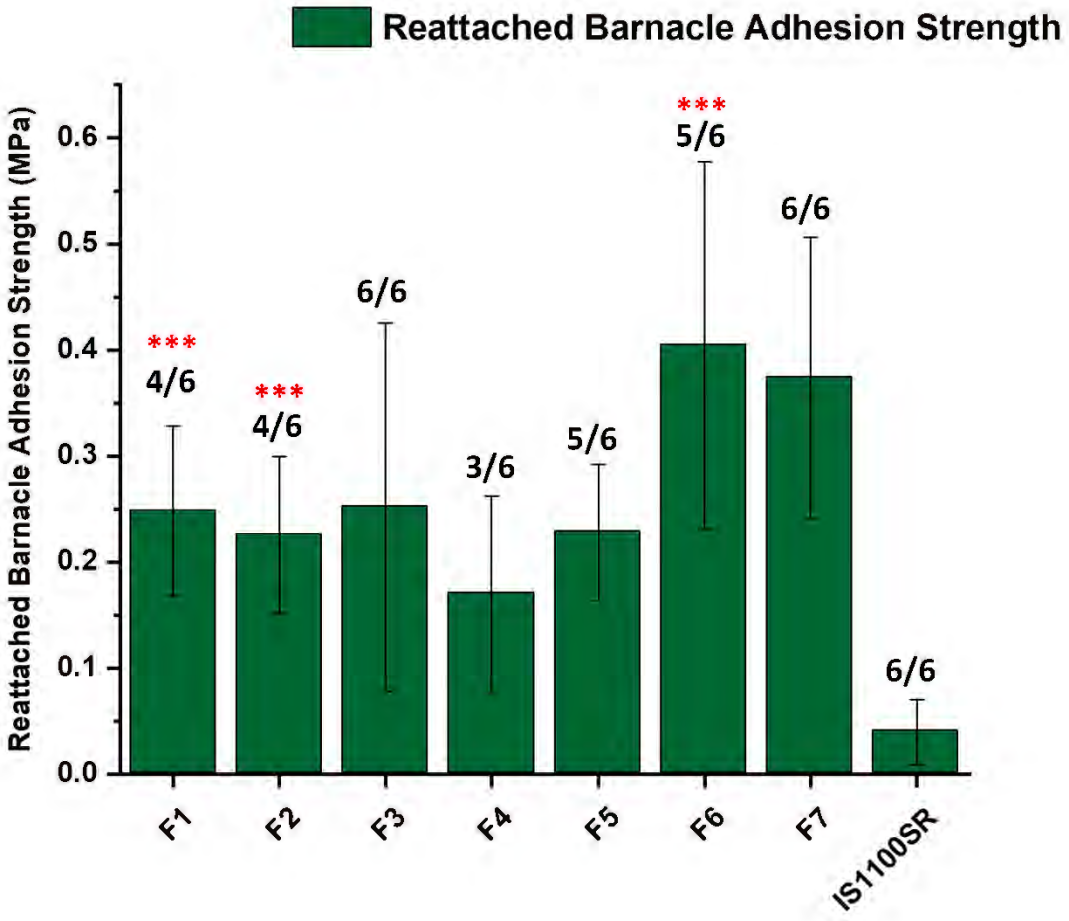

Figure 4.9. Reattached barnacle adhesion strength of *A. amphitrite*. Each bar represents the average adhesion strength of successfully pushed off barnacles. The ratio corresponds to the number of attached barnacles over the number of total available barnacles. *** denotes the breakage of an attached barnacle upon removal. The X-axis is labeled to indicate formulation number in Table 4.1, along with commercial standards and controls in Table C1.

Conclusions

A surface modifying amphiphilic additive (SMAA) composed of PDMS and PEG was incorporated into a purely PU coating that is traditionally non-fouling-release. This grafted co-polymer has a partial comb-like structure with an almost two-fold mol % of PEG compared to PDMS. Thus, as concentration of PDMS is increased in the coating, there was inherently a higher concentration of PEG, which self-stratifies to the surface along with PDMS. Coatings that were prepared displayed amphiphilic, heterogenous surfaces as shown through ATR-FT-IR, contact angle measurements, AFM, XPS, and TEM surface characterizations. ATR-FT-IR showed that as the concentration of SMAA increased, signals from PDMS and PEG also increased, concluding that they had segregated to the surface. The surface

energies of the surfaces of these coatings increased with higher concentrations of additive, largely due to the high amount of PEG at the surface. Contact angle hysteresis values and AFM images showed the heterogenous nature of these surfaces, with higher additive incorporation inducing larger changes in surface morphology. Depth profiling during XPS measurements was used to determine elemental composition of these coatings up to a depth of ~100 nm from the surface. It was observed that increases in additive concentration was responsible for a direct increase in Si and O atomic percentage in this range, leading to a surface enriched with additive in formulations with the highest SMAA concentrations. TEM was useful in determining the extent of additive dispersion throughout the PU bulk. As the concentration of additive increased, larger areas of concentrated additive were seen, with these domains being dispersed throughout the entire coating. Additionally, physical property determination for these formulations showed that as additive amount was increased, adhesion performance, solvent resistance, and flexibility were significantly poorer than the PU formulation with no incorporated additive.

Biological assays were also performed for these coatings, and overall, it was observed that incorporation of SMAA was able to impart AF/FR properties in a non-FR PU coating system. During evaluations with the macroalgae *U.* linza, formulations that contained the highest amounts of incorporated SMAA had significantly lower biomass remaining than control PU formulation, with some even performing comparable to commercial FR standard IS1100SR. When microalgae diatom *N. incerta* performance was evaluated, all experimental coatings displayed excellent FR properties, with virtually no biomass remaining after water-jetting, performing significantly better than commercial FR standard IS1100SR. These experimental coatings also showed desirable AF/FR properties towards the marine bacteria *C. lytica*. Biofilm growth and adhesion were significantly less than that of the control PU, with performing comparable to commercial standards. Lastly, marine barnacle reattachment and adhesion measurements showed that these formulations had performance equal to the control PU, with some formulations having high barnacle reattachment strength. In addition, barnacle basal plates broke upon push off on several of the experimental coating surfaces, which is typically an indication of strong adhesion to the coating. Only one formulation (F4) showed an improvement of barnacle adhesion strength, as well as only having three out of six barnacles able to reattach. Overall, these SMAA containing polyurethane coatings displayed desirable properties for use as a fouling protection system. However, future work should be concerned

with improving the performance towards marine barnacles, as well as addressing issues surrounding loss of mechanical coating properties when additive concentration is increased in the coating bulk. This study highlights the need for an increased fundamental understanding between the structure and chemical composition of the amphiphilic additive, and how this translates to both the AF/FR and mechanical properties of several coatings systems such as polyurethanes.

References

1. Yebra, D. M.; Kiil, S. K.; Dam-Johansen, K., Antifouling Technology—Past, Present and Future Steps Towards Efficient and Environmentally Friendly Antifouling Coatings. *Prog. Org. Coat.* **2004,** *50* (2), 75.

2. Hellio, C.; Yebra, D. M., *Advances in Marine Antifouling Coatings and Technologies*. 2009.

3. Callow, M. E.; Callow, J. A., Marine Biofouling: A Sticky Problem. *Biologist* **2002,** *49* (1), 10.

4. Steinberg, P. D.; De Nys, R.; Kjelleberg, S., Chemical cues for surface colonization. *Journal of chemical ecology* **2002,** *28* (10), 1935-1951.

5. Lejars, M.; Margaillan, A.; Bressy, C., Fouling release coatings: a nontoxic alternative to biocidal antifouling coatings. *Chemical reviews* **2012,** *112* (8), 4347-4390.

6. Callow, J. A.; Callow, M. E., Trends in the development of environmentally friendly fouling-resistant marine coatings. *Nature Communications* **2011,** *2*, 244.

7. Schultz, M. P.; Bendick, J. A.; Holm, E. R.; Hertel, W. M., Economic Impact of Biofouling on a Naval Surface Ship. *Biofouling* **2011,** *27* (1), 87.

8. Magin, C. M.; Cooper, S. P.; Brennan, A. B., Non-Toxic Antifouling Strategies. *Mater. Today* **2010,** *13* (4), 36.

9. Drake, J. M.; Lodge, D. M., Hull fouling is a risk factor for intercontinental species exchange in aquatic ecosystems. *Aquatic Invasions* **2007,** *2* (2), 121-131.

10. Jones, G., The battle against marine biofouling: a historical review. *Advances in marine antifouling coatings and technologies* **2009**, 19-45.

11. Abioye, O. P.; Loto, C.; Fayomi, O., Evaluation of anti-biofouling progresses in marine application. *Journal of Bio-and Tribo-Corrosion* **2019,** *5* (1), 1-8.

12. Konstantinou, I. K.; Albanis, T. A., Worldwide Occurrence and Effects of Antifouling Paint Booster Biocides in the Aquatic Environment: A Review. *Environ. Int.* **2004,** *30* (2), 235.

13. Ytreberg, E.; Karlsson, J.; Eklund, B., Comparison of toxicity and release rates of Cu and Zn from anti-fouling paints leached in natural and artificial brackish seawater. *Science of the Total Environment* **2010,** *408* (12), 2459-2466.

14. Matthiessen, P.; Reed, J.; Johnson, M., Sources and potential effects of copper and zinc concentrations in the estuarine waters of Essex and Suffolk, United Kingdom. *Marine Pollution Bulletin* **1999,** *38* (10), 908-920.

15. Baker, T. J.; Tyler, C. R.; Galloway, T. S., Impacts of metal and metal oxide nanoparticles on marine organisms. *Environmental pollution* **2014,** *186*, 257-271.

16. Soon, Z. Y.; Jung, J.-H.; Jang, M.; Kang, J.-H.; Jang, M.-C.; Lee, J.-S.; Kim, M., Zinc pyrithione (ZnPT) as an antifouling biocide in the marine environment—a literature review of its toxicity, environmental fates, and analytical methods. *Water, Air, & Soil Pollution* **2019,** *230* (12), 1-18.

17. Holland, R.; Dugdale, T. M.; Wetherbee, R.; Brennan, A. B.; Finlay, J. A.; Callow, J. A.; Callow, M. E., Adhesion and Motility of Fouling Diatoms on a Silicone Elastomer. *Biofouling* **2004,** *20* (6), 323.

18. Watermann, B.; Berger, H. D.; Sönnichsen, H.; Willemsen, P., Performance and effectiveness of non-stick coatings in seawater. *Biofouling* **1997,** *11* (2), 101-118.

19. Selim, M. S.; Shenashen, M.; El-Safty, S. A.; Higazy, S.; Selim, M. M.; Isago, H.; Elmarakbi, A., Recent progress in marine foul-release polymeric nanocomposite coatings. *Progress in Materials Science* **2017,** *87*, 1-32.

20. Kostina, N. Y.; Sharifi, S.; de los Santos Pereira, A.; Michálek, J.; Grijpma, D. W.; Rodriguez-Emmenegger, C., Novel antifouling self-healing poly (carboxybetaine methacrylamide-co-HEMA) nanocomposite hydrogels with superior mechanical properties. *Journal of Materials Chemistry B* **2013,** *1* (41), 5644-5650.

21. Liu, C.; Xie, Q.; Ma, C.; Zhang, G., Fouling release property of polydimethylsiloxane-based polyurea with improved adhesion to substrate. *Industrial & Engineering Chemistry Research* **2016,** *55* (23), 6671-6676.

22. Rath, S.; Chavan, J.; Sasane, S.; Patri, M.; Samui, A.; Chakraborty, B., Two component silicone modified epoxy foul release coatings: Effect of modulus, surface energy and surface restructuring on pseudobarnacle and macrofouling behavior. *Applied Surface Science* **2010,** *256* (8), 2440-2446.

23. Sommer, S.; Ekin, A.; Webster, D. C.; Stafslien, S. J.; Daniels, J.; VanderWal, L. J.; Thompson, S. E. M.; Callow, M. E.; Callow, J. A., A Preliminary Study on the Properties and Fouling-Release Performance of Siloxane-Polyurethane Coatings Prepared from Pdms Macromers. *Biofouling* **2010,** *26* (8), 961.

24. Bodkhe, R. B.; Thompson, S. E. M.; Yehle, C.; Cilz, N.; Daniels, J.; Stafslien, S. J.; Callow, M. E.; Callow, J. A.; Webster, D. C., The Effect of Formulation Variables on Fouling-Release Performance of Stratified Siloxane-Polyurethane Coatings. *Journal of Coatings Technology Research* **2012,** *9* (3), 235.

25. Ekin, A.; Webster, D. C., Combinatorial and High-Throughput Screening of the Effect of Siloxane Composition on the Surface Properties of Crosslinked Siloxane–Polyurethane Coatings. *J. Comb. Chem.* **2007,** *9* (1), 178.

26. Hu, P.; Xie, Q.; Ma, C.; Zhang, G., Silicone-based fouling-release coatings for marine antifouling. *Langmuir* **2020,** *36* (9), 2170-2183.

27. Truby, K.; Wood, C.; Stein, J.; Cella, J.; Carpenter, J.; Kavanagh, C.; Swain, G.; Wiebe, D.; Lapota, D.; Meyer, A., Evaluation of the performance enhancement of silicone biofouling-release coatings by oil incorporation. *Biofouling* **2000,** *15* (1-3), 141-150.

28. Galhenage, T. P.; Hoffman, D.; Silbert, S. D.; Stafslien, S. J.; Daniels, J.; Miljkovic, T.; Finlay, J. A.; Franco, S. C.; Clare, A. S.; Nedved, B. T.; Hadfield, M. G.; Wendt, D. E.; Waltz, G.; Brewer, L.; Teo, S. L. M.; Lim, C.-S.; Webster, D. C., Fouling-Release Performance of Silicone Oil-Modified Siloxane-Polyurethane Coatings. *ACS Applied Materials & Interfaces* **2016,** *8* (42), 29025-29036.

29. Milne, A., Anti-fouling marine compositions. Google Patents: 1977.

30. Brady, R. F., Fouling-release coatings for warships. *Defence Science Journal* **2005,** *55* (1), 75.

31. Edwards, D. P.; Nevell, T. G.; Plunkett, B. A.; Ochiltree, B. C., Resistance to Marine Fouling of Elastomeric Coatings of Some Poly (Dimethylsiloxanes) and Poly (Dimethyldiphenyl-Siloxanes). *Int. Biodeterior. Biodegrad.* **1994,** *34*, 349.

32. Nurioglu, A. G.; Esteves, A. C. C., Non-toxic, non-biocide-release antifouling coatings based on molecular structure design for marine applications. *Journal of Materials Chemistry B* **2015,** *3* (32), 6547-6570.

33. Wyszogrodzka, M.; Haag, R., Synthesis and characterization of glycerol dendrons, self-assembled monolayers on gold: a detailed study of their protein resistance. *Biomacromolecules* **2009,** *10* (5), 1043-1054.

34. Galli, G.; Martinelli, E., Amphiphilic polymer platforms: surface engineering of films for marine antibiofouling. *Macromolecular rapid communications* **2017,** *38* (8), 1600704.

35. Martinelli, E.; Sarvothaman, M. K.; Galli, G.; Pettitt, M. E.; Callow, M. E.; Callow, J. A.; Conlan, S. L.; Clare, A. S.; Sugiharto, A. B.; Davies, C., Poly (dimethyl siloxane)(PDMS) network blends of amphiphilic acrylic copolymers with poly (ethylene glycol)-fluoroalkyl side chains for fouling-release coatings. II. Laboratory assays and field immersion trials. *Biofouling* **2012,** *28* (6), 571-582.

36. Benda, J.; Stafslien, S.; Vanderwal, L.; Finlay, J. A.; Clare, A. S.; Webster, D. C., Surface modifying amphiphilic additives and their effect on the fouling-release performance of siloxane-polyurethane coatings. *Biofouling* **2021**, 1-18.

37. Rufin, M. A.; Ngo, B. K. D.; Barry, M. E.; Page, V. M.; Hawkins, M. L.; Stafslien, S. J.; Grunlan, M. A., Antifouling silicones based on surface-modifying additive amphiphiles. *Green Materials* **2017,** *5* (1), 4-13.

38. Seetho, K.; Zhang, S.; Pollack, K. A.; Zou, J.; Raymond, J. E.; Martinez, E.; Wooley, K. L., Facile synthesis of a phosphorylcholine-based zwitterionic amphiphilic copolymer for anti-biofouling coatings. *ACS Macro Letters* **2015,** *4* (5), 505-510.

39. Wang, S.-Y.; Fang, L.-F.; Cheng, L.; Jeon, S.; Kato, N.; Matsuyama, H., Improved antifouling properties of membranes by simple introduction of zwitterionic copolymers via electrostatic adsorption. *Journal of Membrane Science* **2018,** *564*, 672-681.

40. Koschitzki, F.; Wanka, R.; Sobota, L.; Gardner, H.; Hunsucker, K. Z.; Swain, G. W.; Rosenhahn, A., Amphiphilic Zwitterionic Acrylate/Methacrylate Copolymers for Marine Fouling-Release Coatings. *Langmuir* **2021,** *37* (18), 5591-5600.

41. Guazzelli, E.; Perondi, F.; Criscitiello, F.; Pretti, C.; Oliva, M.; Casu, V.; Maniero, F.; Gazzera, L.; Galli, G.; Martinelli, E., New amphiphilic copolymers for PDMS-based nanocomposite films with long-term marine antifouling performance. *Journal of Materials Chemistry B* **2020,** *8* (42), 9764-9776.

42. Guo, H.; Chen, P.; Tian, S.; Ma, Y.; Li, Q.; Wen, C.; Yang, J.; Zhang, L., Amphiphilic Marine Antifouling Coatings Based on a Hydrophilic Polyvinylpyrrolidone and Hydrophobic Fluorine–Silicon-Containing Block Copolymer. *Langmuir* **2020,** *36* (48), 14573-14581.

43. Rahimi, A.; Stafslien, S. J.; Vanderwal, L.; Finlay, J. A.; Clare, A. S.; Webster, D. C., Amphiphilic zwitterionic-PDMS-based surface-modifying additives to tune fouling-release of siloxane-polyurethane marine coatings. *Progress in Organic Coatings* **2020,** *149*, 105931.

44. Noguer, A. C.; Olsen, S.; Hvilsted, S.; Kiil, S., Diffusion of surface-active amphiphiles in silicone-based fouling-release coatings. *Progress in Organic Coatings* **2017,** *106*, 77-86.

45. Wenning, B. M.; Martinelli, E.; Mieszkin, S.; Finlay, J. A.; Fischer, D.; Callow, J. A.; Callow, M. E.; Leonardi, A. K.; Ober, C. K.; Galli, G., Model amphiphilic block copolymers with tailored molecular weight and composition in PDMS-based films to limit soft biofouling. *ACS Applied Materials & Interfaces* **2017,** *9* (19), 16505-16516.

46. Majumdar, P.; Ekin, A.; Webster, D. C., Thermoset Siloxane—Urethane Fouling Release Coatings. ACS Publications: 2007.

47. Olsen, S.; Yebra, D. Polysiloxane-based fouling release coats including enzymes. EP2726559B1, April, 5th, 2017.

48. Owens, D. K.; Wendt, R. C., Estimation of the Surface Free Energy of Polymers. *J. Appl. Polym. Sci.* **1969,** *13* (8), 1741.

49. Stafslien, S. J.; Sommer, S.; Webster, D. C.; Bodkhe, R.; Pieper, R.; Daniels, J.; Vander Wal, L.; Callow, M. C.; Callow, J. A.; Ralston, E.; Swain, G.; Brewer, L.; Wendt, D.; Dickinson, G. H.; Lim, C. S.; Teo, S. L. M., Comparison of Laboratory and Field Testing Performance Evaluations of Siloxane-Polyurethane Fouling-Release Marine Coatings. *Biofouling* **2016,** *32* (8), 949.

50. Stafslien, S. J.; Bahr, J. A.; Daniels, J. W.; Wal, L. V.; Nevins, J.; Smith, J.; Schiele, K.; Chisholm, B., Combinatorial Materials Research Applied to the Development of New Surface Coatings Vi: An Automated Spinning Water Jet Apparatus for the High-Throughput Characterization of Fouling-Release Marine Coatings. *Rev. Sci. Instrum.* **2007,** *78* (7), 072204.

51. Stafslien, S.; Daniels, J.; Mayo, B.; Christianson, D.; Chisholm, B.; Ekin, A.; Webster, D.; Swain, G., Combinatorial Materials Research Applied to the Development of New Surface Coatings. Iv: A High-Throughput Bacterial Retention and Retraction Assay for Screening Fouling-Release Performance of Coatings. *Biofouling* **2007,** *23* (1), 45.

52. Cassé, F.; Stafslien, S. J.; Bahr, J. A.; Daniels, J.; Finlay, J. A.; Callow, J. A.; Callow, M. E., Combinatorial Materials Research Applied to the Development of New Surface Coatings V. Application of a Spinning Water-Jet for the Semi-High Throughput Assessment of the Attachment Strength of Marine Fouling Algae. *Biofouling* **2007,** *23* (2), 121.

53. Callow, M. E.; Callow, J. A.; Conlan, S.; Clare, A. S.; Stafslien, S., Efficacy testing of nonbiocidal and fouling-release coatings. *Biofouling methods* **2014**, 291-316.

54. Rittschof, D.; Orihuela, B.; Stafslien, S.; Daniels, J.; Christianson, D.; Chisholm, B.; Holm, E., Barnacle Reattachment: A Tool for Studying Barnacle Adhesion. *Biofouling* **2008,** *24* (1), 1.

55. Stafslien, S.; Daniels, J.; Bahr, J.; Chisholm, B.; Ekin, A.; Webster, D.; Orihuela, B.; Rittschof, D., An Improved Laboratory Reattachment Method for the Rapid Assessment of Adult Barnacle

Adhesion Strength to Fouling-Release Marine Coatings. *Journal of Coatings Technology and Research* **2012,** *9* (6), 651.

56. Hoipkemeier-Wilson, L.; Schumacher, J. F.; Carman, M. L.; Gibson, A. L.; Feinberg, A. W.; Callow, M. E.; Finlay, J. A.; Callow, J. A.; Brennan, A. B., Antifouling Potential of Lubricious, Micro-Engineered, Pdms Elastomers against Zoospores of the Green Fouling Alga Ulva (Enteromorpha). *Biofouling* **2004,** *20* (1), 53.

57. Stanley, M. S.; Callow, M. E.; Callow, J. A., Monoclonal antibodies to adhesive cell coat glycoproteins secreted by zoospores of the green alga Enteromorpha. *Planta* **1999,** *210* (1), 61-71.

58. Callow, M. E.; Callow, J.; Ista, L. K.; Coleman, S. E.; Nolasco, A. C.; López, G. P., Use of self-assembled monolayers of different wettabilities to study surface selection and primary adhesion processes of green algal (Enteromorpha) zoospores. *Applied and Environmental Microbiology* **2000,** *66* (8), 3249-3254.

59. Callow, J. A.; Callow, M. E.; Ista, L. K.; Lopez, G.; Chaudhury, M. K., The influence of surface energy on the wetting behaviour of the spore adhesive of the marine alga Ulva linza (synonym Enteromorpha linza). *Journal of the Royal Society Interface* **2005,** *2* (4), 319-325.

60. Statz, A.; Finlay, J.; Dalsin, J.; Callow, M.; Callow, J. A.; Messersmith, P. B., Algal antifouling and fouling-release properties of metal surfaces coated with a polymer inspired by marine mussels. *Biofouling* **2006,** *22* (6), 391-399.

61. Finlay, J. A.; Callow, M. E.; Ista, L. K.; Lopez, G. P.; Callow, J. A., The influence of surface wettability on the adhesion strength of settled spores of the green alga Enteromorpha and the diatom Amphora. *Integrative and comparative biology* **2002,** *42* (6), 1116-1122.

62. Schumacher, J. F.; Carman, M. L.; Estes, T. G.; Feinberg, A. W.; Wilson, L. H.; Callow, M. E.; Callow, J. A.; Finlay, J. A.; Brennan, A. B., Engineered antifouling microtopographies–effect of feature size, geometry, and roughness on settlement of zoospores of the green alga Ulva. *Biofouling* **2007,** *23* (1), 55-62.

63. Bazaka, K.; Jacob, M. V.; Crawford, R. J.; Ivanova, E. P., Plasma-assisted surface modification of organic biopolymers to prevent bacterial attachment. *Acta biomaterialia* **2011,** *7* (5), 2015-2028.

64. Demirel, Y. K.; Uzun, D.; Zhang, Y.; Fang, H.-C.; Day, A. H.; Turan, O., Effect of barnacle fouling on ship resistance and powering. *Biofouling* **2017,** *33* (10), 819-834.

65. Khandeparker, L.; Anil, A. C., Underwater adhesion: the barnacle way. *International Journal of Adhesion and Adhesives* **2007,** *27* (2), 165-172.

66. Burden, D. K.; Spillmann, C. M.; Everett, R. K.; Barlow, D. E.; Orihuela, B.; Deschamps, J. R.; Fears, K. P.; Rittschof, D.; Wahl, K. J., Growth and development of the barnacle Amphibalanus amphitrite: time and spatially resolved structure and chemistry of the base plate. *Biofouling* **2014,** *30* (7), 799-812.

67. Di Fino, A.; Petrone, L.; Aldred, N.; Ederth, T.; Liedberg, B.; Clare, A. S., Correlation between surface chemistry and settlement behaviour in barnacle cyprids (Balanus improvisus). *Biofouling* **2014,** *30* (2), 143-152.

CHAPTER 5. EVALUATION OF ADHESION AND FOULING-RELEASE PROPERTIES OF NON-TOXIC FOULING-RELEASE COATINGS APPLIED TO OIL BOOM MATERIALS

Introduction

The usage of petroleum-based hydrocarbons carries significant negative environmental, ecological, and health concerns. One major concern is the increase in greenhouse gas emissions, and the pollution of local environments and atmosphere through the processing or burning of this fossil fuel.[1-3] This also heavily impacts the health of local ecosystems and human life, potentially killing off both flora and fauna, with several diseases and illnesses in humans linked to these petroleum-based hydrocarbons.[4-9] Another concern with using petroleum-based hydrocarbons is that many consumer products derived from this fossil fuel, such as many types of plastics, also negatively impact the environment and can be toxic to human health.[10-14] Lastly, the transportation and storage of oil, especially in marine environments, brings about new environmental challenges as large spills and containment leaks can devastate local ecosystems.

Examples of such spills include the oil supertanker *Exxon Valdez* spill in 1989 near Prince William Sound, Alaska, the widely destructive *Deepwater Horizon* offshore oil well spill in the Gulf of Mexico in 2010, and the *Sanchi* oil tanker collision off the coast of Shanghai, China in 2018. When such a spill occurs, a spreading process begins within the first few hours, creating a thin layer of oil that floats above the water commonly referred to as an ‘oil slick’.[15] These oil slicks can be many square kilometers in size and spread rapidly across bodies of water. And where these patches of oil go, many detrimental environmental effects follow.[16-21] To combat the spread of these oil spills, as well as remove them from marine environments, several oil spill response methods are often employed. These can include the use of chemical dispersing agents to break up the slick, where oil droplets get dispersed in the nearby water column, nutrient, and surfactant formulations to enhance biodegradation, chemical barriers or collectants that facilitate the recovery of oil, and sometimes the burning of surface oils.[15, 19] But perhaps one of the most important aspects of an oil spill response is the use of special oil boom containment systems.

Aside from facilitating the cleanup and remediation of oil spills, these oil boom systems are also commonly deployed around ships in harbor as either permanent installations or being deployed from a storage reel to contain passive oil leaks.[22, 23] The oil that leaks out of ships in harbor may not always produce the massive quantity of oil that is produced through large offshore oil spills, but it still causes significant detrimental effects on local marine environments.[24-26] These containment systems are mainly composed of a fabric skirt connected with floats, and a ballast to help keep the oil boom in place. As these oil booms are deployed, several factors such as weight of the system, flexibility or rigidity of the fabric skirt, size and frequency of waves caused by higher nautical wind speeds, and composition of oil can affect containment performance.[15, 27] Such a loss in performance typically results in the exodus of oil, either above or below, the oil boom, causing environmental damage. In addition, the accumulation of biofouling onto the components of these oil boom systems can also significantly affect performance. These attached marine foulants cause an increase in mass, as well as impede the barrier properties of the skirt fabric, both leading to a breakdown in protection. Marine biofouling is a very complex and dynamic phenomenon that involves over 4000 fouling species.[28] Several different factors such as the wide number of species, different sizes of organisms, their local populations in different marine environments, and the numerous substrates submerged in marine environments make it difficult to combat this phenomenon.[29-31]

One solution is to regularly clean these oil boom systems of this biofouling. But permanent deployments can prove a challenge to continuously remove built up biofouling, and repeated cleanings and redeployments of mobile boom systems greatly increase operating costs. Another solution is to use anti-fouling (AF)/fouling-release (FR) paints typically used on the hulls of ships to help prevent this unwanted biofouling. These coatings could be applied on the skirt fabric (where most of the fouling occurs) and has the potential to provide better cleanability, and subsequently, an oil boom system better protected against marine biofouling. However, another issue arises where these paints do not adhere well to these materials, quickly leading to damage, and loss of performance. Many of the oil boom fabrics consist of types of synthetic fiber that has been embedded in thick layers of different polymeric materials such as polyurethanes, or polyvinyl chloride. Adhesion of coatings to a variety of polymeric substrates

has long been an issue in several different fields of study and should be addressed to develop a coating system capable of providing lasting coverage for oil boom fabrics.[32-34]

This study was concerned with developing a method for testing the adhesion of several coatings used in FR systems when applied to commonly used oil boom fabric substrates. These substrates were treated with several different combinations of surface treatments including sandblasting or corona treatment, as well as five different chlorinated polyolefin adhesion promoters. Small-scale samples were prepared and treatment groups which included combinations of surface treatment, adhesion promoter, and coating type were evaluated using our developed water-jet adhesion testing procedure. Data from this testing was compiled, and promising treatment groups were selected for large-scale field testing to evaluate cleanability and FR performance at a test site located in Port Canaveral, Florida Institute of Technology, FL, US.

Experimental

Materials

Solvents used during this work include acetone, hexanes, toluene, methyl amyl ketone (MAK), and xylenes, and were purchased from Sigma Aldrich (MO, USA). Methylene iodide used during surface characterization was also purchased from Sigma Aldrich (MO, USA). Chlorinated polyolefin adhesion promoters, with trade names CP 164-1, CP 343-1, CP 730-1, and CP 515-2, were provided by Eastman Chemical Company (TN, USA). Oil boom fabric belting materials, labeled as Globeboom® Desmi black, orange, and orange-textured, were purchased from Desmi (VA, USA). Remaining belting materials, labeled as Permafence® Elastec black and orange were purchased from Elastec Inc. (IL, USA). Materials used for the preparation of a siloxane-polyurethane (SiPU) coating system (A4-20) were prepared according to previous work.[35] Polyisocyanate Desmodur Z 4470 BA was provided by Covestro LLC (PA, USA). Acetylacetone and dibutyltin diacetate (DBTDAc) were purchased from Sigma Aldrich (MO, USA). Lastly, Intersleek® 731 tie-coat was provided by AkzoNobel, International Paint LLC (TN, USA), and Hempasil Nexus® 23702 tie coat and Hempasil® X3+ fouling-release topcoat were provided by Hempel (TX, USA).

Experimental Approach

Oil boom systems, more specifically, long-term containment systems, are a vital component in limiting the environmental impact of oil leaks and spills coming from ships moored in harbor for extended periods of time. Some of the major performance criteria for oil-containment boom systems include hydrodynamic performance, material weight, flexibility, ease of deployment, and overall barrier properties to various mixtures of oil commonly seen during oil spill events. In addition to these properties, more attention is being directed towards the performance of oil boom materials against marine biofouling. As these long-term oil booms sit in marine environments, the accumulation of bio-foulants causes a large increase in weight across the structure, resulting in a loss of oil containment. Therefore, the application and performance of several anti-fouling (AF) and fouling-release (FR) coatings have been investigated on these oil boom materials. However, proper adhesion of these coatings to the various belting materials has proven difficult to achieve, which again results in a significant loss of performance.

The main objective of this work was to identify a series of surface treatments, adhesion promoters, or a combination of both, that could achieve increased adhesion of common FR coatings to several oil boom fabrics, providing good FR properties, while retaining oil containment performance. Three different coatings were utilized during this study, a siloxane-polyurethane FR coating labeled A4-20. Intersleek® 731, a silicone elastomer tie-coat for Intersleek® 1100SR, a commercially available FR coating, and Hempasil Nexus® 23702, a tie-coat for commercially available FR coating Hempasil® X3+. These coatings were applied to five different, several millimeters thick, oil boom belting fabrics. Two of these substrates are made of mats of woven polyester fibers, embedded in a millimeter's thick layer of polyvinyl chloride (PVC) and are designated as DB and EB during experiments. The other three are again mats of polyester fibers, but these are embedded within a thick layer of polyurethane (PU), designated as DO, EO, and DO-T. Surface treatments were also performed on these fabrics before application of coatings and include sandblasting the surface of the fabric, as well as performing corona surface treatment. Lastly, fabrics were also treated with a series of chlorinated polyolefin adhesion promoters labeled 164-1, 343-1, 730-1, and 515-2. Treatment groups were also established which did not receive any surface treatment, or adhesion promoters, before application of coatings. All treatment groups were subjected to water immersion in circulating tap water tanks, in one-month intervals, prior to adhesion

testing. There was a total of 6 replicates prepared for each surface treatment, adhesion promoter, and coating used. Time period one was established as 30 days immersion, with one replicate from each treatment group being selected for adhesion testing using a water-jet adhesion testing apparatus. Time period six was established at 180 days immersion, where afterwards, adhesion evaluation was completed. A test matrix for all relevant treatment groups (1,350 treatments) can be seen in Table 5.1.

Table 5.1. All possible treatment groups that include the five different belting fabrics, three different surface treatment groups, five different adhesion promoter groups, three different coatings, using one replicate per time period at thirty-day intervals

Substrate Type	Surface Treatment	Adhesion Promoter	Coating Formulations	Replicates (one per time period)
1 - Desmi Orange (DO)	No Treatment Sandblasting Corona	No AP AP - 164 AP - 343 AP - 515 AP - 730	A4-20 Nexus tie-coat Intersleek® tie-coat	Time 1 - 30 days Time 2 - 60 days Time 3 - 90 days Time 4 - 120 days Time 5 - 150 days Time 6 - 180 days
2 - Desmi Orange – Textured (DO-T)	No Treatment Sandblasting Corona	No AP AP - 164 AP - 343 AP - 515 AP - 730	A4-20 Nexus tie-coat Intersleek® tie-coat	Time 1 - 30 days Time 2 - 60 days Time 3 - 90 days Time 4 - 120 days Time 5 - 150 days Time 6 - 180 days
3 - Desmi Black (DB)	No Treatment Sandblasting Corona	No AP AP - 164 AP - 343 AP - 515 AP - 730	A4-20 Nexus tie-coat Intersleek® tie-coat	Time 1 - 30 days Time 2 - 60 days Time 3 - 90 days Time 4 - 120 days Time 5 - 150 days Time 6 - 180 days
4 - Elastec Orange (EO)	No Treatment Sandblasting Corona	No AP AP - 164 AP - 343 AP - 515 AP - 730	A4-20 Nexus tie-coat Intersleek® tie-coat	Time 1 - 30 days Time 2 - 60 days Time 3 - 90 days Time 4 - 120 days Time 5 - 150 days Time 6 - 180 days
5 - Elastec Black (EB)	No Treatment Sandblasting Corona	No AP AP - 164 AP - 343 AP - 515 AP - 730	A4-20 Nexus tie-coat Intersleek® tie-coat	Time 1 - 30 days Time 2 - 60 days Time 3 - 90 days Time 4 - 120 days Time 5 - 150 days Time 6 - 180 days

Small-Scale Surface Preparation

Fabric substrates that were used throughout this study were supplied in large sheets. To prepare the substrates for eventual surface treatment and application of coatings, a JET Tools® woodworking bandsaw (model# JWBS-14CS) was used to cut samples with dimensions approximately 2” x 3”.

Surface Characterization

Water and Methylene Iodide Contact Angles

A First Ten Angstroms FTA100 series dynamic contact angle analyzer was used to measure water, and methylene iodide, contact angles of the five different substrates before surface treatment and coating application. Cut samples of substrate were placed on the sample platform and held down by clips. A drop of Milli-Q water, approximately 1 µL in volume, was placed on the surface of the substrate and left for ~10 s to let the drop settle, and an image was captured. This was performed a total of six times, and FTA image processing software was then used to calculate contact angle values. Lastly, surface energies (mN/m) from these contact angles were determined utilizing the Owens-Wendt method.[36]

Attenuated Total Reflectance Fourier-Transform Infrared Spectroscopy (ATR-FTIR)

A Thermo Scientific Nicolet 8700 FT-IR spectrometer, equipped with a smart iTR diamond plate ATR sampling accessory, was used to gather ATR-FTIR spectra for all five substrates before surface treatment and coating application.

Surface Treatment and Application of Adhesion Promoters and Coatings

Substrate samples that were assigned to the sandblasting surface treatment group were treated via an abrasive blasting cabinet (McMaster Carr, product #3283K1). Aluminum oxide grit (ComCo, product #PD1003-25), with an average particle size of 50 µm was delivered to surfaces at ~60 psi air pressure, ~2 in. from the surface of the substrates. Both sides of the samples surface were treated this way, with excess blasting media being blown off with pressurized air.

To prepare samples in the corona surface treatment groups, a portable corona treatment instrument was provided by Tantec A/S (IL, USA). This LabTEC® unit was capable of 200 W output from a metallic spherical head. Untreated samples were placed in a 2 x 3 grid on the sample area and the generator output was calibrated at 100 W. Next, the metallic head was passed over these samples ~1 in.

from the surface. One complete pass, back and forth across the samples, took approximately 5 seconds to perform.

After surface treatments, sample substrates in the adhesion promoter treatment groups were coated with promoter solutions that act as a primer layer before application of FR coatings and tie-coats. Chlorinated polyolefin (CPO) adhesion promoters were first dissolved in toluene at 10 wt.% solids. Then, using a 3 in. foam brush, solutions were applied to substrates, making sure complete coverage was achieved, and then let dry overnight.

Lastly, FR and tie-coats were applied to all substrates. The formulation for FR coating A4-20 was applied as previously described.[35]Formulations for Intersleek® 731 and Hempasil Nexus® 23702 tie-coats were prepared according to the manufacturer's instructions by adding each respective crosslinker component and binder resin to 100 mL mixing containers, sealed, and then mixed using a FlakTek SpeedMixer™ DAC 150FVZ-K for 5 min at 3500 rpm. Total weights for all coatings formulations were below 100 g at a time. Each formulation was applied to sample substrates using disposable 3" foam brushes until complete coverage was achieved. Coated samples were left to cure under ambient conditions for 1 week before water immersion.

Development of a Water-Jet Adhesion Testing Apparatus

To get a more accurate representation on how the adhesion performance of these coatings would change depending on surface treatment and/or adhesion promoter incorporation, a water-jet testing apparatus was designed and fabricated at NDSU. The unit consisted of a pressure washer unit (North Star, Northern Tool and Equipment item#1571102), with the handle mounted onto a moving track. This track was powered by a small DC motor, coupled with a DC speed control unit. The pressure pump from the unit was mounted below the control box, can deliver variable water pressures from 100-1600 psi, and was fitted with a pressure gauge. Lastly, the apparatus was fitted with a rigid plastic collection tank, which also has fittings where a sample holder can be bolted into place during testing. Several different spray nozzles can be used with this system, with the distance between the sample surface and nozzle being ~7 in. Figure 5.1 details the fully assembled apparatus used for water-jet adhesion testing of small-scale samples.

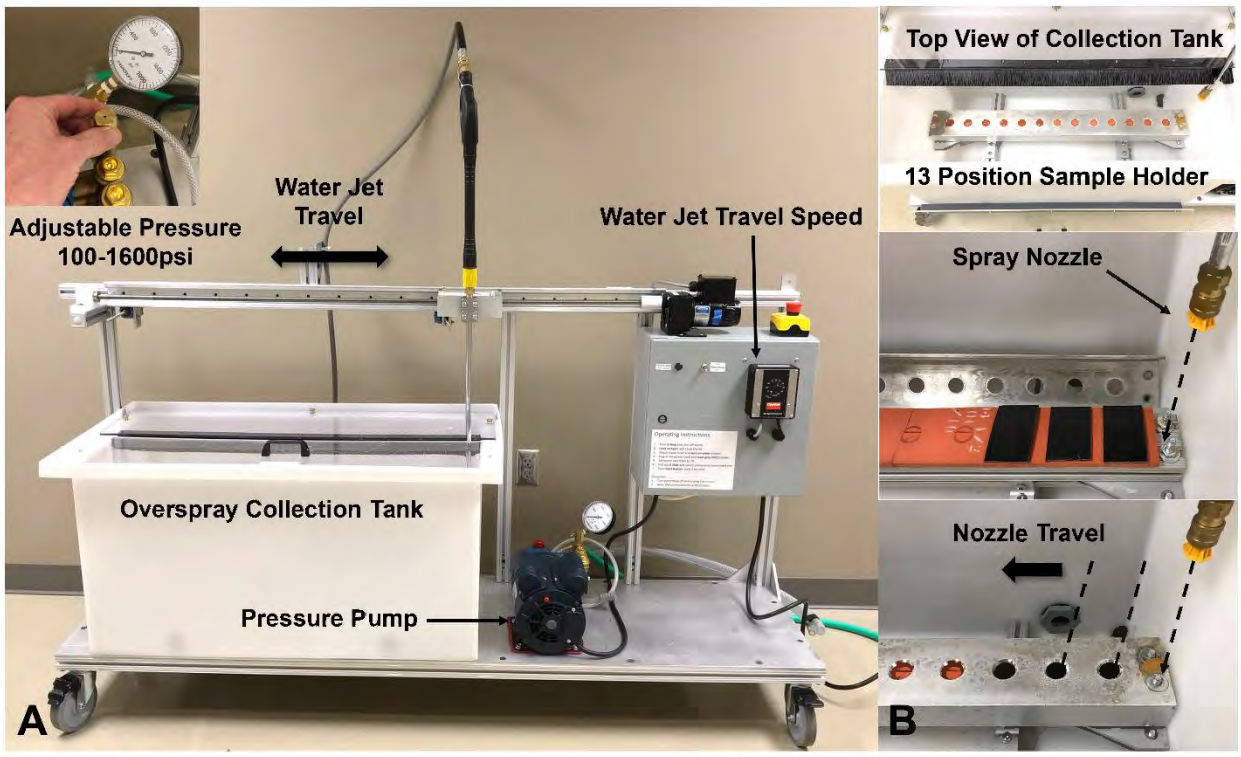

Figure 5.1. A) Diagram of the water-jet adhesion testing apparatus B) Close-up images of the sample holder in the collection tank, spray nozzle distance to sample, and the fully assembled sample holder showing which way the nozzle moves.

Water Ageing and Development of a Water-Adhesion Test Method

Coated samples with the various treatment groups were split up into six time periods (30, 60, 90, 120, 150, and 180 days) that would undergo water immersion before adhesion testing. Samples were placed into water tanks filled with circulating tap water until each respective time interval was reached. When samples were ready for testing, they were removed from the tanks, wiped clean with paper towels, and left to dry overnight before testing using the water-jet adhesion testing apparatus.

To gather meaningful adhesion performance data from a very large number of samples, a test method was developed based on a qualitative approach to interpreting results. It was determined that using a spray nozzle with 0° of angle (straight waterjet) would provide the best results in causing enough damage to the coatings to classify adhesion performance between treatment groups. This stream of water was directed at samples held in place by the sample holder, with a sample area 1 in. in diameter. Pressures used during this testing started including 100, 200, 300, 400, 600, 800, 1000, and 1200 psi. Failure categories were set as 0F, 1F, 2F, and 3F. If there was no visible damage to the coating at a set

water pressure, that sample would receive a 0F rating. Once the first sign of slight damage was seen, the coating received a 1F failure rating. If there was minor delamination, the coating received a 2F failure rating, and if there was complete delamination or damage to the coating, the coating received a 3F failure rating. A procedure for performing this testing is as follows. Samples were placed in the sample holder and bolted into the collection tank. The unit was turned on via a control box and water pressure initially set to 100 psi, and the moving track set to speed ‘6’ (approximately 8.5 mm/s). Next, a run was performed consisting of two full passes over the surface of the samples. After this run, coating appearance and damage was assessed. Failure ratings were assigned if any coating showed damage, and a picture was taken. Then, the pressure was increased to 200 psi, and another run was performed, again taking pictures of any new damage to coatings. If a coating was damaged previously, but worsened to one of the higher failure categories, this was recorded at the psi the run was performed at. These steps were repeated for all the water pressures used, or until each coating received a 3F failure rating.

Large Scale Field Testing

Once small-scale water-jet adhesion testing had been performed, candidates for large-scale field testing were selected. To prepare these samples, chosen substrates were cut to 6” x 24” dimensions using a woodworking bandsaw. Mounting holes (~3/8” diameter) were punched into the tops of samples, and then surface treatments were performed, if needed, and application of coatings was carried out utilizing a 9” polyester paint roller. Prepared samples were labeled with metal tags, and then sent to the Florida Institute of Technology for immersion at their Port Canaveral field test site. Samples were submerged 0.5 m below the water and visual inspections were carried out every month, for seven months. After visual inspection, cleanings were performed every two months using a commercial pressure washer. To clean these samples, the tip (40° spray angle) of the nozzle is placed ~4 in. normal to the surface of the substrate. Cleaning was carried out at 1000 psi and 2000 psi, and if there was still leftover biofouling, a more aggressive rotary tip was used at 1000 psi. Samples were then placed back into the test site after pictures were taken.

Results and Discussion

As with many other structures submerged in a marine environment, oil boom systems used to contain oil leakage/spillage from ships in harbor rapidly begin to accumulate marine biofouling upon

deployment. This biofouling leads to an increase in mass, causing the boom to sag, compromising containment performance, and leading to an uncontrolled oil leak that is detrimental to the environment. Anti-fouling (AF), or fouling-release (FR) paints have been used to deter attachment of these marine foulants, prolonging oil boom lifetimes, improving performance. In addition, these oil boom systems are often deployed from stationary 'spools' to surround ships in harbor for oil containment. Maintenance of these materials includes removing them from water to remove any accumulated debris, oil, or marine foulants. Therefore, as well as providing fouling protection, FR coatings have been identified as candidates for increasing the 'cleanability' of these systems to prolong service life.

However, many of these paints do not adhere well to the type of oil boom fabrics used, and quickly experience damage to the coating, resulting again in a loss of containment and cleanability performance. This study aims to investigate whether a combination of surface treatments and adhesion promoters can be utilized to improve the adhesion of several different FR coatings to oil boom fabrics, for the improvement of fouling protection and cleanability. A total of 5 different oil boom fabrics were used, mainly consisting of fibers coated with either polyvinyl chloride (PVC) or polyurethane (PU). Two different surface treatments were performed on substrates, sandblasting and corona treatment, with 4 different chlorinated polyolefin adhesion promoters being applied as a 'primer layer' before application of commercial FR tie-coats Intersleek® 731 and Hempasil Nexus® 23702, as well as a siloxane-polyurethane FR coating A4-20. Small-scale samples of the various treatment groups were prepared and adhesion to the substrates was evaluated using a water-jet adhesion apparatus. Promising candidates were then selected for large-scale field testing to assess 'real-world' performance.

Small-scale samples were prepared by cutting the substrates shown in Table 5.1 into 2" x 3" rectangles with a woodworking bandsaw. An example of these uncoated and untreated substrates is shown in Figure 5.2. Elastec black and Elastec orange look almost identical to Desmi black and Desmi orange respectively.

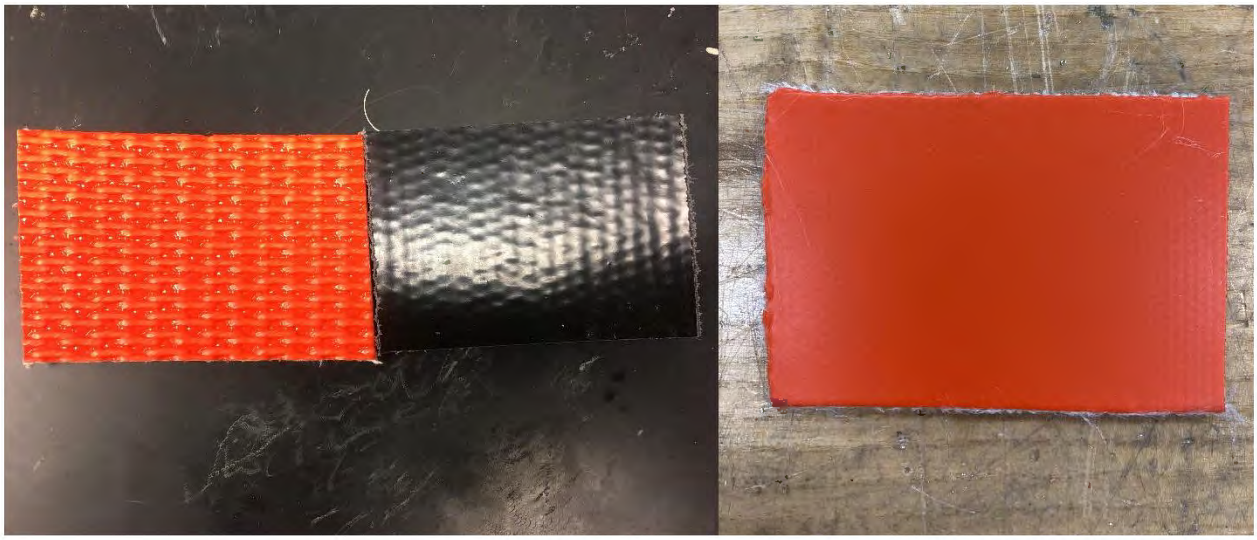

Figure 5.2. From left to right; Uncoated and untreated substrate samples of Desmi Orange – Textured, Desmi Black, and Desmi Orange.

Before these samples were subjected to surface treatments, surface characterizations such as water contact angle (WCA), methylene iodide contact angle (MICA), and attenuated total reflectance Fourier-transform infrared spectroscopy (ATR-FTIR) were performed to determine the composition and general surface properties of the various substrates. Water contact angle, methylene iodide contact angle values, and surface energies of the substrates are shown in Table 5.2. The adhesion of a coating to a substrate is largely affected by the surface properties, both chemical and physical, between them.[37, 38] Generally, as the surface energy increases for a given substrate, surface wetting becomes more favorable, potentially increasing adhesion strength through stronger molecular forces.[37, 39] However, paint formulations often have many different polymeric binders, crosslinkers, and other small molecules that can affect how well a paint spreads across a substrate, making the process of adhesion a dynamic and complex event. A common practice is to pair surfaces with compatible surface energies and surface tension (‘like prefers like’) or modify the surface with various surface treatment techniques to make adhesion more favorable. The surface energies of these substrates were determined and provide some valuable insight into how well various FR coatings can adhere to the chosen oil boom fabrics.

Table 5.2. Water contact angles (WCA), methylene iodide contact angles (MICA), and calculated surface energies of the five different untreated, and uncoated oil boom fabric substrates

Substrate	WCA (°)	MICA (°)	Surface Energy (mN/m)	Dispersive Component (mN/m)	Polar Component (mN/m)
Desmi Orange	64 ± 3	13 ± 4	53.1	44.1	8.9
Desmi Orange - Textured	110 ± 5	75 ± 4	20.2	20.0	0.2
Desmi Black	80 ± 4	52 ± 4	35.4	29.7	5.7
Elastec Orange (Textured)	92 ± 6	68 ± 7	25.2	21.7	3.5
Elastec Black	71 ± 5	36 ± 5	44.7	37.0	7.7

The orange substrates consisted of mats of polyester fibers embedded in a thick layer of polyurethane, while the black substrates were fibers embedded in polyvinyl chloride (PVC). When looking at surface energies of these substrates, two main differences were determined. First, the surface energy of the smooth Desmi orange sample compared to the textured Desmi orange and Elastec orange samples was significantly higher. It is possible that the much greater surface energy seen in Desmi orange samples is largely because of the properties of the polyurethane material. Whereas the significantly lower surface energies of the textured orange samples are likely due to surface structure (roughness) as these samples share similar polyurethane compositions as seen in the smooth orange sample. Secondly, there is a difference between the black samples coated with PVC and the orange samples regardless of textured surfaces. These samples generally showed surface energies than the smooth polyurethane Desmi orange, but higher surface energies than the textured polyurethane coated orange samples. From these results these surfaces each have differing surface energies that can make it problematic when choosing a FR coating system that works well with these types of materials.

Another surface characterization method, ATR-FTIR, was used to gain more information about the composition of these oil boom substrates. Figure 5.3 shows the ATR-FTIR spectra for the two orange textured substrates, as well as the smooth orange substrate, with Figure 5.4 showing spectra of the two black substrates.

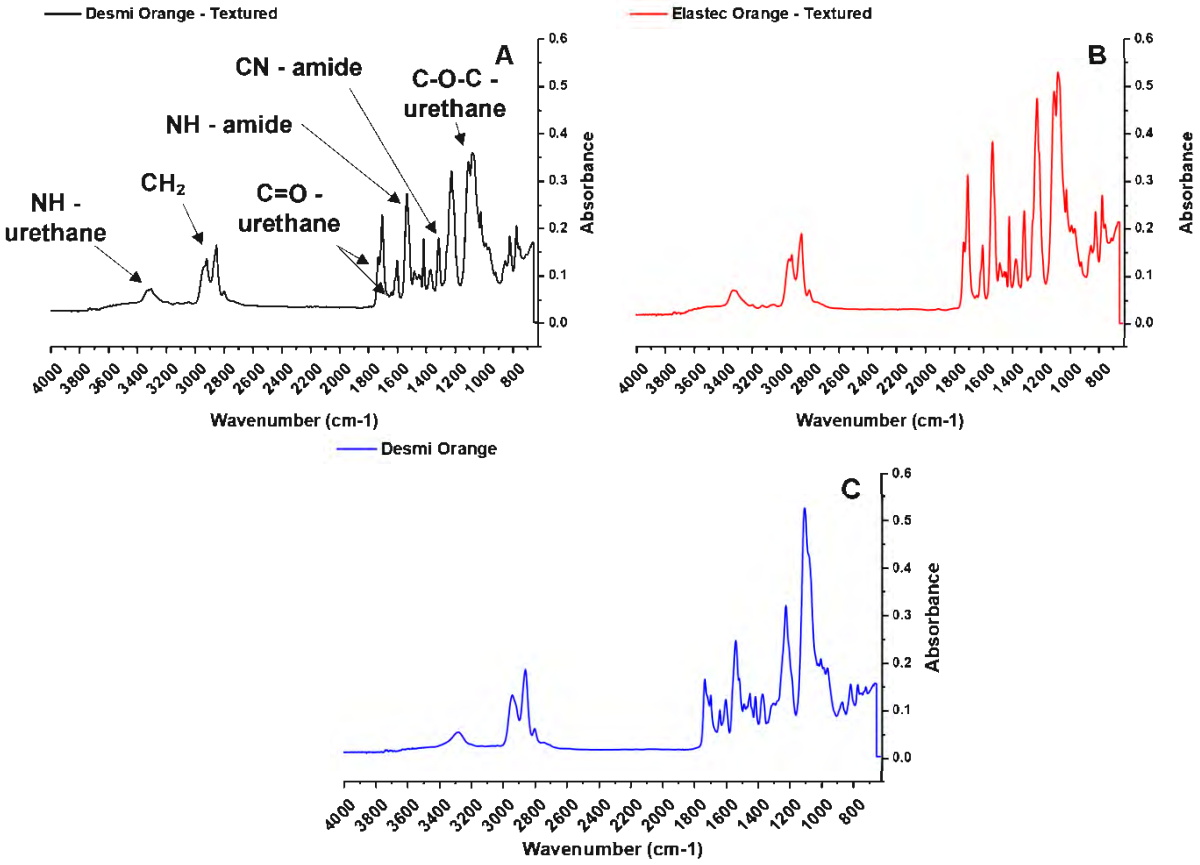

Figure 5.3. ATR-FTIR spectra for A) Desmi orange-textured, B) Elastec orange – textured, and C) smooth Desmi orange substrates.

Spectra A – C in Figure 5.3 all had very similar significant peaks, with only changes in absorbance being seen. Each substrate displayed peaks that signal a composition largely made up of polyurethane. The N-H stretching peak from urethane linkages is seen around 3300 cm^{-1}, with characteristic CH_2 stretching, common in many polymers, found between 2950 and 2850 cm^{-1}. Two significant C=O peaks were also detected at 1730 and 1650 cm^{-1}. The N-H and C-N peaks, resulting from amide linkages, are seen at 1530 and 1310 cm^{-1} respectively. Lastly, a characteristic C-O-C ether stretching, common in several polyurethane compositions, is seen around 1100 cm^{-1}.

Spectra A and B in Figure 5.4 again both had two very similar sets of significant peaks. But, instead of a polyurethane composition, these substrates had peaks that were characteristic of polyvinyl chloride polymers. The CH_2 stretching along the backbone of PVC is seen between 2960 and 2870 cm^{-1}, with aliphatic C-H stretching seen at 1426 and 1250 cm^{-1}. Stretching of between aliphatic C-C is seen at 1018 cm^{-1}, with the characteristic C-Cl peak appearing at 692 cm^{-1}.

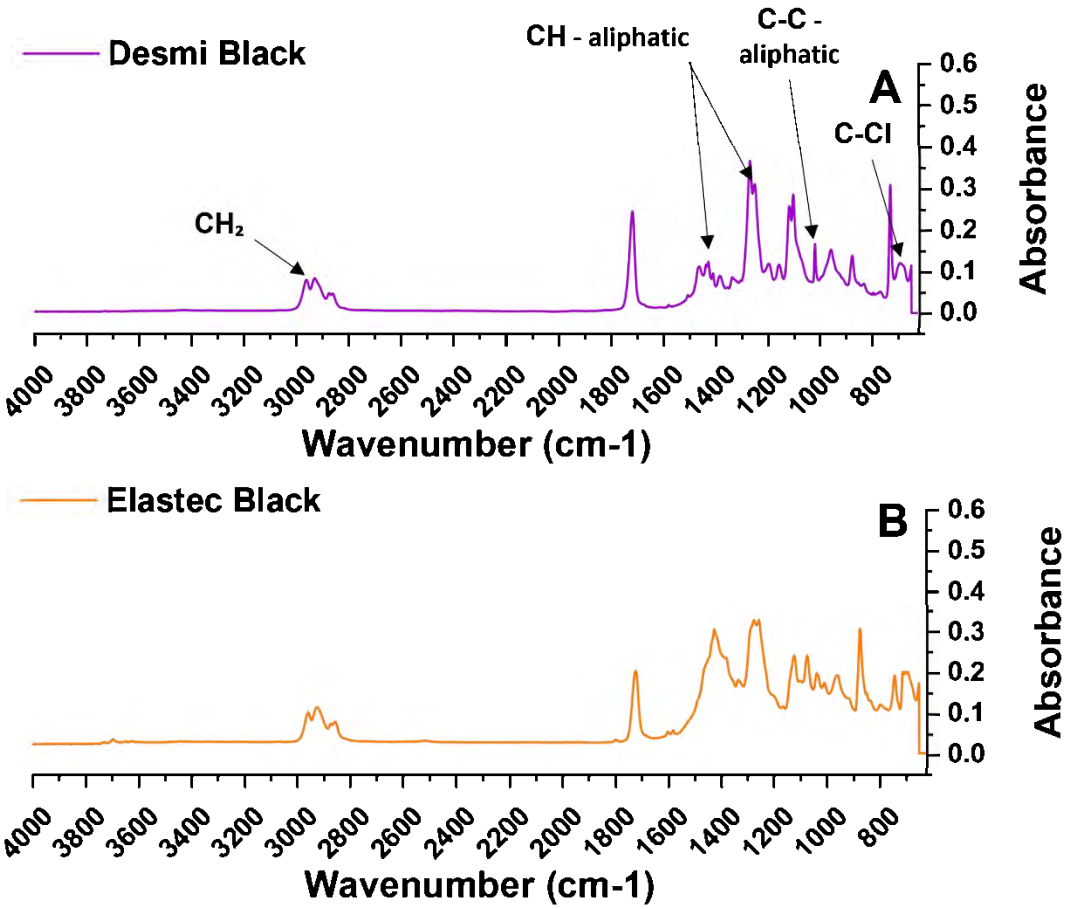

Figure 5.4. ATR-FTIR spectra for A) Desmi black, and B) Elastec black substrates.

The ATR-FTIR spectra that were gathered, along with the determined surface energies, help to confirm our hypothesis that these substrates each have varying surface properties brought about by material composition and preparation. This makes choosing the ideal coating system for all substrates difficult, meaning, the siloxane-polyurethane may work well for the orange polyurethane-based substrates, but may exhibit poorer performance on black polyvinyl chloride-based substrates.

After characterizing the surface of these substrates, surface treatments were carried out and adhesion promoters applied to the appropriate treatment groups. Substrates appeared visibly roughened after sandblasting treatment, whereas there was no change in physical appearance of samples subjected to corona surface treatment. However, surface energy values for these corona-treated samples were significantly higher than untreated substrates. The four different adhesion promoters applied to substrates each spread uniformly across the surface, resulting in a slightly glossy thin coating after drying.

Once all samples were treated with either surface treatments or adhesion promoters, the three different coatings were applied to the necessary treatment groups. Figure 5.5 shows substrates with no surface treatment or adhesion promoter layer coated with A4-20, Intersleek® tie-coat, and Hempasil Nexus® tie-coat.

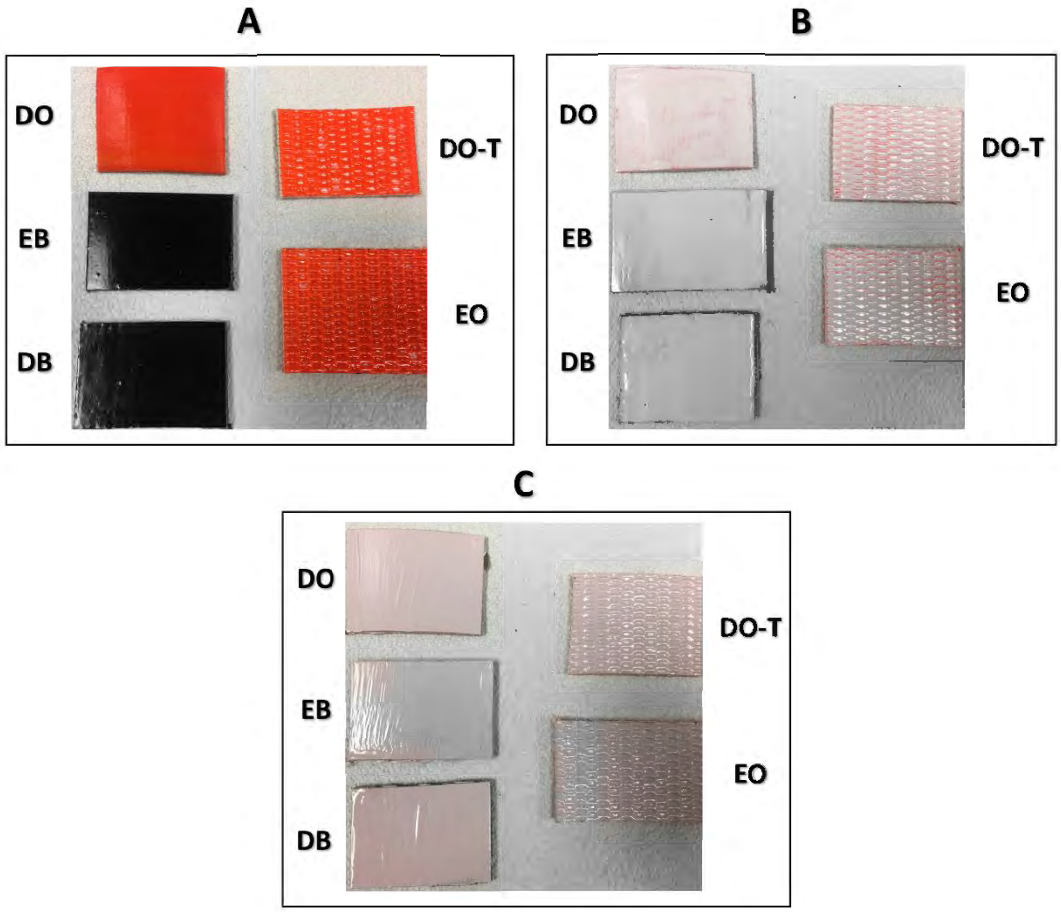

Figure 5.5. A) Samples coated with FR coating A4-20 B) Samples coated with Intersleek® tie-coat C) Samples coated with Hempasil Nexus® tie-coat.

Both A4-20 and Hempasil Nexus® tie-coat wet the substrates well and spread across to form a uniform film. But Intersleek® tie-coat did not wet the surface effectively, requiring more material to coat the substrates. As seen in Figure 5.5B, thin areas of coating appeared due to pooling of coating formulation, showing signs of the substrates in some treatment groups. It was unclear if the addition of adhesion promoters significantly affected this surface spread. However, this tie-coat would eventually be covered with a fouling-release topcoat, and as such, coated substrates were determined to still have sufficient coverage to analyze water-jet adhesion properties. One other issue arose after coating samples

with A4-20 and Hempasil Nexus® tie-coat on each of the substrates. As the cured substrates were flexed, or bent outward, cracking/delamination began to occur in the coating, which can be seen in Figure 5.6.

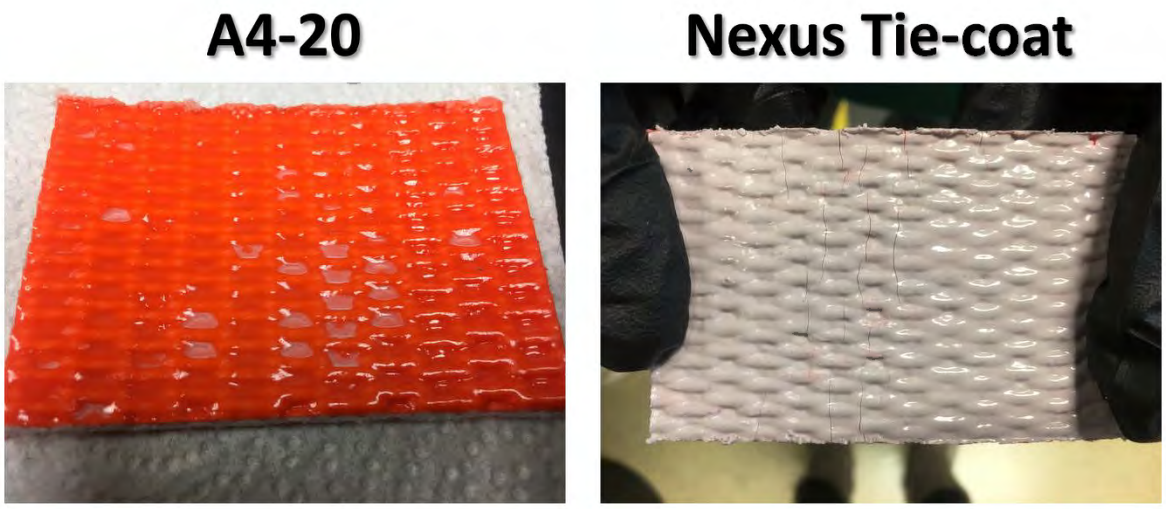

Figure 5.6. From left to right; DO-T substrate coated with A4-20; DO-T substrate coated with Hempasil Nexus® tie-coat.

These coated samples did not experience these defects with regular handling of the substrates, and it did take some force to induce cracking, therefore, samples were used as is for water-jet adhesion testing. But this does highlight the issue that these coatings were not specifically designed for application on rigid, or flexible, oil boom fabric materials, signaling a need for a dedicated coating system for these materials.

Once sample substrates were fully coated with coatings A4-20 SiPU, Intersleek® Tie-coat, or Hempasil Nexus® tie-coat, water-jet adhesion was performed. The water-jetting procedure was designed to induce damage to the coatings to differentiate between adhesion performance of the different treatment groups, with a jet of water being delivered at several different pressures. Qualitative failure ratings were developed to better understand the results from this procedure. Failure rating 0F is giving to samples that show no damage, 1F is for samples that show slight damage to the coatings surface, 2F is given to samples that experience more significant damage including minor delamination, and 3F is for samples that experience severe damage, usually leading to complete delamination of the coating from the sample substrate. Examples of failure ratings are shown in Figure 5.7.

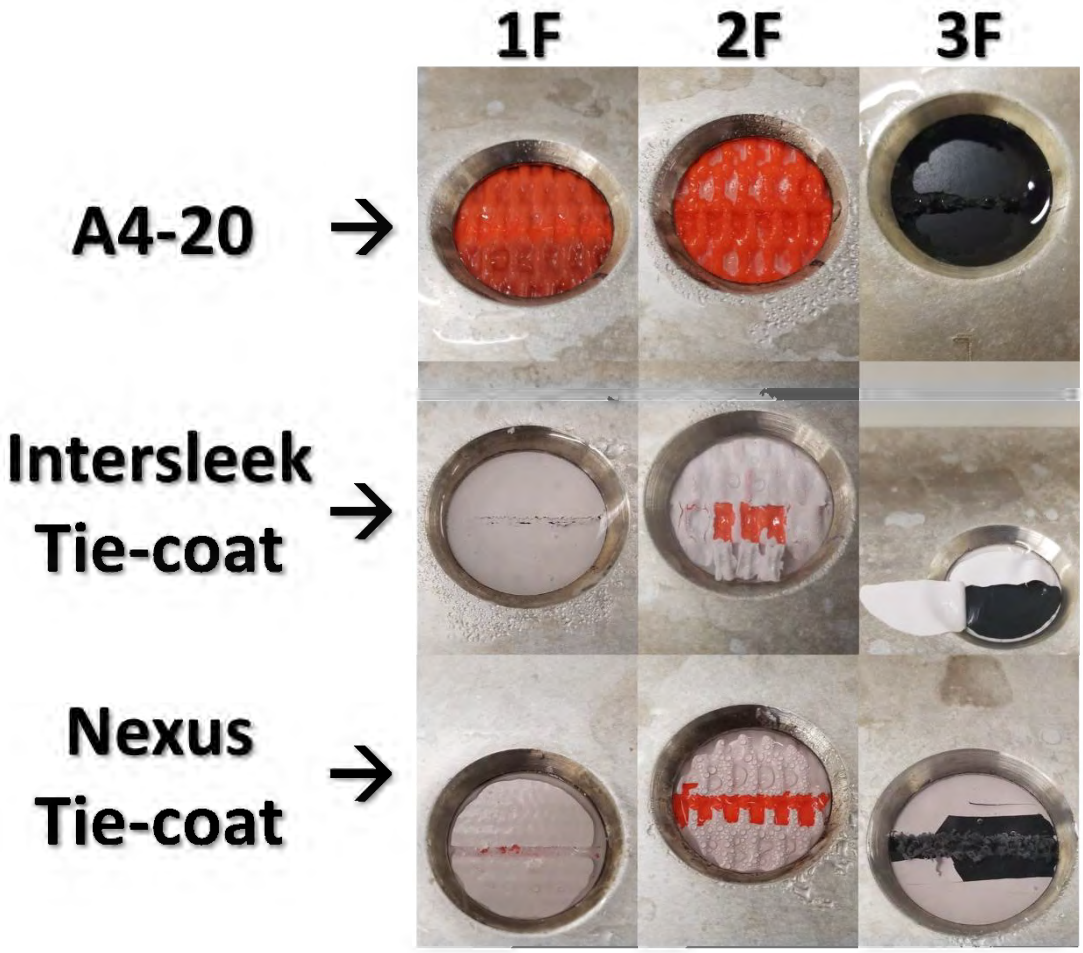

Figure 5.7. Failure ratings 1F, 2F, and 3F, for A4-20 (top row), Intersleek® tie-coat (middle row), and Nexus tie-coat (bottom row).

At each water pressure, any damage to the coatings was assessed after one full pass of the water jet. After each subsequent pass of increasing water pressures, if more damage occurred to the coating, this was recorded, and the increased failure ratings were assigned at that specific water pressure. This data collection procedure was repeated for each period of water ageing (Periods 1-6) and results were interpreted.

One general observation seen during the adhesion testing was that differences in adhesion performance between treatment groups did not significantly change as each time period was evaluated. However, overall performance for all treatment groups worsened after subsequent periods, with the highest levels of failure seen in time period 6, where samples had been immersed for 180 days in circulating water tanks. Another observation is that the coating type used showed more significant differences in terms of failure ratings than any combination of surface treatment and adhesion promoter

application on each substrate type. Throughout this testing method, treatment groups involving the Intersleek® tie-coat, regardless of substrate type, surface treatment, or adhesion promoter application, performed significantly worse than other coatings. This coating type failed at very low water pressures (in some cases as low as 100 psi), and when failure did occur, complete delamination from the substrate was often seen. This is likely due to the soft, rubbery nature of this tie-coat. When used traditionally as a tie-coat for other FR topcoats developed by International Paint on the rigid, metal hulls of marine vessels, these coatings also tend to be damaged easily when encountering hard, sharp objects. But one positive observation to note is that these coatings responded very well to flexing of oil boom substrates, resisting cracking seen in other coating types used.

The other two coating types used, A4-20 siloxane-polyurethane, and Hempasil Nexus® tie-coat performed better overall compared to the Intersleek® tie-coat. Hempasil tie-coat is a much more rigid coating, making it more likely to resist higher water pressures, with the highest failure rating (3F) seen mostly on rigid substrates such as Desmi orange. A4-20 is also a harder, more rigid coating than the soft elastomeric Intersleek® tie-coat, and it was seen that lower failure ratings occurred across all substrate types, showing better adhesion performance than Hempasil tie-coat. Some of the factors that contribute to this superior performance could be that A4-20 is a good blend of hardness, and elasticity somewhere between Intersleek® tie-coat and Hempasil tie-coat. In addition, since A4-20 is largely made up of a polyurethane, and three out of the five different substrates were composed of polyurethane, the substrate to coating compatibility is higher, resulting in better adhesion overall.

When adhesion promoters were applied to substrates as a ‘primer’ before coating, there did not seem to be a major advantage over treatment groups that used no adhesion promoter. However, in the textured substrates (Desmi orange textured and Elastec orange), adhesion promoters AP-343 and AP-515 did show slightly lower failure ratings for each coating type. This could be due to the increased wettability offered by these adhesion promoters, allowing the coating to spread more evenly within the textured ‘pockets’ of these substrates. Additionally, it was seen that there was no significant difference in adhesion performance on substrates that underwent either sandblasting or corona treatment before coating application, except for the textured substrates. In these treatment groups, the sandblasting

treatment performed the best overall, which could be due to the increased roughness imparted to the surface of these substrates, allowing a more favorable surface for adhesion of the coatings.

Overall, several combinations of treatments and coatings were identified that provided superior adhesion performance relative to the other treatment groups for each individual substrate type. A summary of these samples is shown in Table 5.3.

Table 5.3. Combinations of surface treatment, adhesion promoter, and coating type recommended for use on each substrate type to achieve the highest adhesion performance

Substrate Type	Recommended Surface Treatment	Recommended Adhesion Promoter Treatment	Recommended Coating
1 - Desmi Orange	No Treatment	No Adhesion Promoter or AP-515	A4-20
2 - Desmi Orange (Textured)	Sandblasting	AP-343 or AP-515	A4-20
3 - Desmi Black	No Treatment	No Adhesion Promoter or AP-515	A4-20
4 - Elastec Orange	Sandblasting	AP-515	A4-20
5 - Elastec Black	No Treatment	No Adhesion Promoter or AP-515	A4-20

After water-jet adhesion testing was completed on small sample treatment groups, promising candidates for large-scale field testing were selected. Six different treatment groups were selected, each with six replicates, and large samples (6 in. x 24 in.) were prepared and sent to the Florida Institute of Technology's field-testing site in Port Canaveral. Substrates selected included the smooth, rigid, polyurethane-based Desmi orange, and the other substrate used was the textured, flexible, polyurethane-based Desmi orange – textured. The textured substrates were treated by sandblasting before application of coatings. The coatings used were A4-20 and Hempasil tie-coat along with Hempasil® X3+ fouling release topcoat. Table 5.4 describes each treatment group with an assigned sample ID used in field testing pictures.

Table 5.4. Sample ID's and descriptions for each treatment group evaluated during large-scale field testing

Sample ID	Substrate Type	Surface Treatment	Coating Type
#1	Desmi Orange	No Treatment	A4-20
#2	Desmi Orange – Textured	Sandblasted	A4-20
#3	Desmi Orange	No Treatment	Hempasil® X3+
#4	Desmi Orange – Textured	Sandblasted	Hempasil® X3+
#5	Desmi Orange	No Treatment	None
#6	Desmi Orange – Textured	Sandblasted	None

Coated samples were immersed for seven months, with visual inspections to assess fouling coverage in one-month intervals, with cleanings every two months. The purpose of this field testing was to determine if small-scale adhesion performance results can translate to a more 'real-world' application using these larger substrates, while also testing fouling and cleanability performance. The fouling community these samples are exposed to largely include diverse biofilms, barnacles, encrusting bryozoans, tunicates, and tubeworms. Two different tips were utilized during cleaning procedures. A standard fan-type nozzle was used at 1000 and 2000 psi, 4 in. away from the substrates, and if any fouling remained, a rotary-type nozzle was used mainly at 1000 psi. The rotary-type nozzle is a more aggressive form of cleaning typically seen on these types of substrates.

Samples were immersed at the test site in April of 2020 and removed in December of 2020. Throughout this time, the water temperature and salinity levels fluctuate, which are factors that have been shown to influence the local fouling environment in terms of species diversity and overall amount of fouling that typically occurs.[31] However, some general observations can still be made on the different treatment groups that were immersed during field testing. After one-month of immersion, macrofouling coverage on treatment groups with coated substrates was generally lower than those with no fouling-release coating applied. Out of the experimental treatment groups, samples coated with Hempasil® X3+, on either smooth or textured substrates, performed the best. This was also seen at subsequent visual inspections, with very high levels (>80% macrofouling surface coverage) starting around three months of immersion, despite cleaning surfaces at after the two-month visual inspection. However, sample #3 from Table 5.4, which was the smooth, rigid, Desmi orange substrate coated with Hempasil® X3+, experienced

severe coating delamination after being cleaned and was removed from water immersion. This damage can be seen in Figure 5.8.

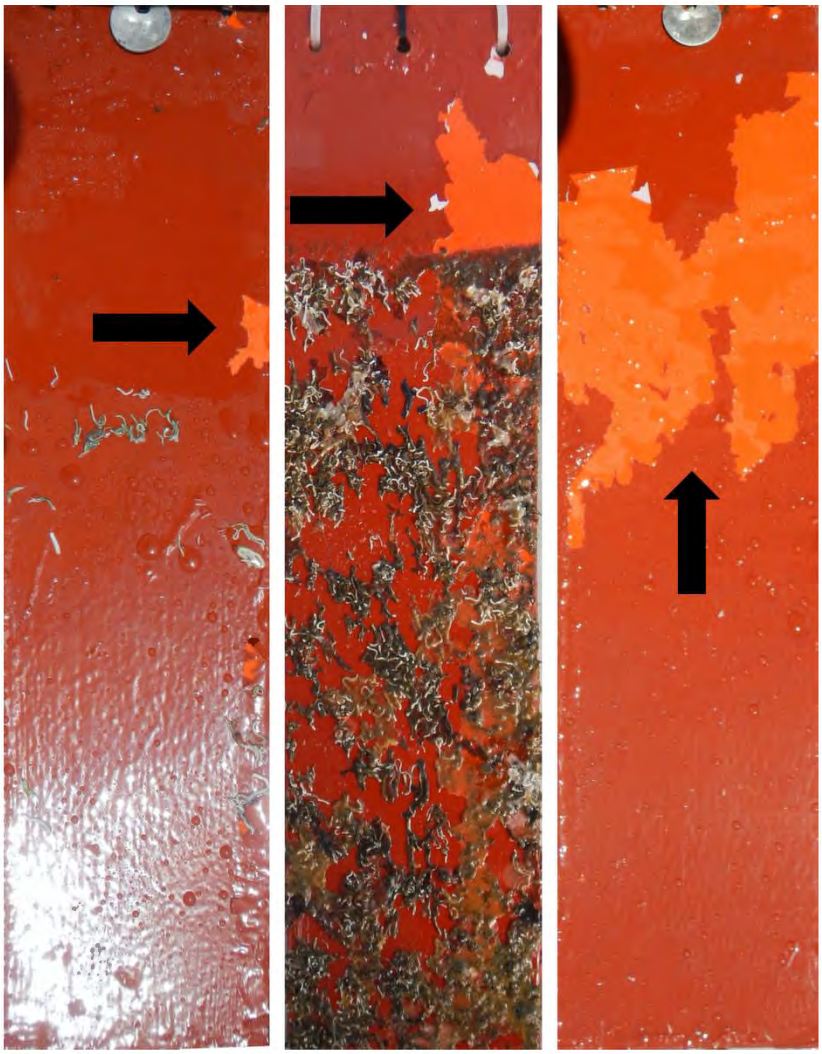

Figure 5.8. Panels from sample ID #3 from Table 5.4. Black arrows point to areas of severe coating delamination after aggressive hydro blasting at higher water pressures.

Due to the rigid nature of both the substrate and the coating, if large stressors such as bending or flexing occur, damage almost immediately becomes apparent, leading to such delamination when cleaning at high water pressures. This observation was not as prevalent in small scale adhesion testing for this type of substrate as the samples were harder to flex.

It was not unexpected that during the period of highest fouling (July-October), the fouling coverage was higher, and although a drop in fouling coverage is seen in the five and six-month inspections, fouling coverage again increases to near 100% macrofouling coverage for all coated and

non-coated substrates after seven months of immersion and the third round of cleaning. As the amount of fouling generally decreases during the winter months, coupled with the high macrofouling coverage seen, samples were removed from immersion at this time. Again, these results were not unexpected as the fouling-release coated samples are not exactly 'anti-fouling', where organisms are prevented from adhering. Instead, these coatings allow for a weak adhesion of organisms, which can be cleaned more easily than other uncoated substrates. Examples of samples covered with macrofouling during visual inspections are shown in Figure 5.9.

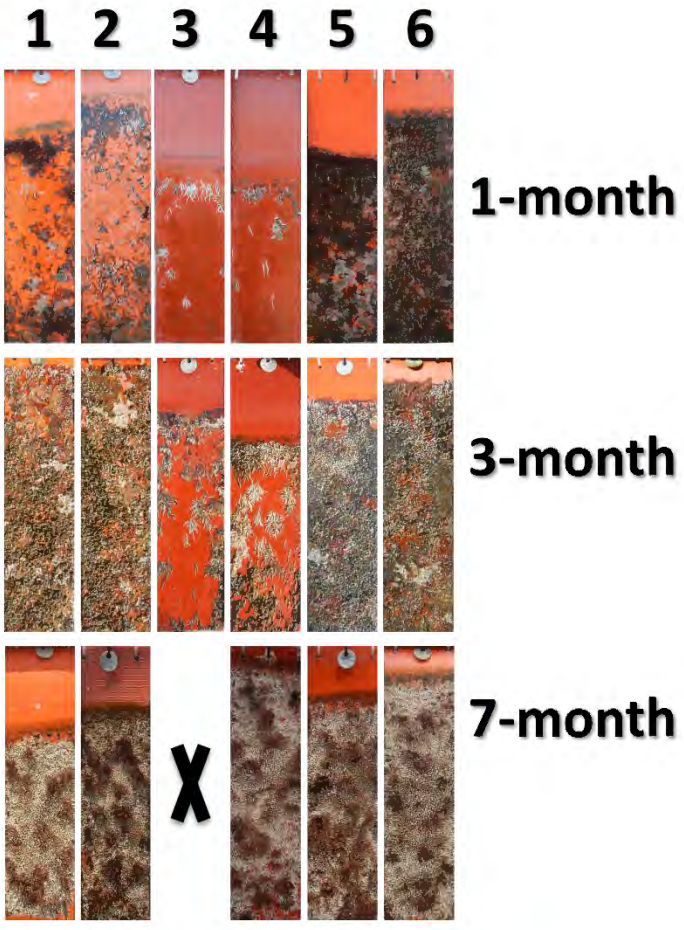

Figure 5.9. Visual inspection of panels from sample ID's 1-6 from Table 4 after one (top), three (middle), and seven-month (bottom) intervals. The small black 'X' denotes the removal of panels with sample ID #3 due to severe coating delamination.

During the first interval of cleaning (two-months), the standard tip used at 1000 psi was able to clear some of the accrued biofouling, with much of the larger organisms such as tubeworms, barnacles, and encrusting bryozoan remaining. More of these foulants were removed once pressures were

increased to 2000 psi, but barnacles and tubeworms remained on panels. However, as the tip used was switched to a rotary tip at 1000 psi, a much more aggressive form of cleaning, panels were cleared of virtually all biofouling. But, as shown in Figure 5.8, this mode of cleaning produced severe delamination in smooth Desmi orange panels, untreated, and coated with Hempasil® X3+. Figure 5.10 shows the results of using the different spray nozzle tips to remove fouling from panels in the first round of cleaning.

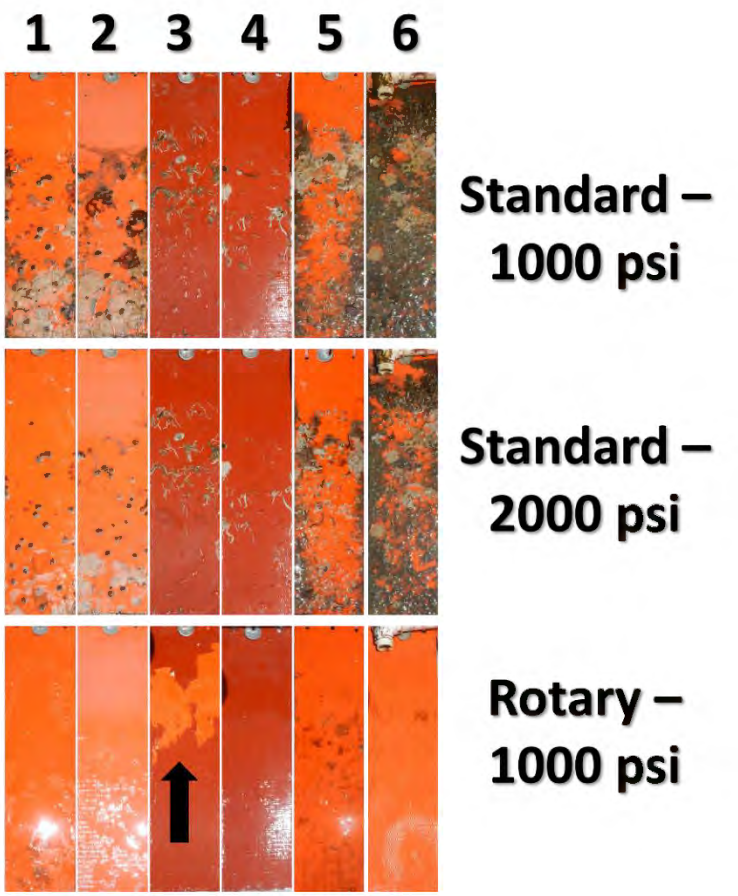

Figure 5.10. First cleaning of panels with sample ID's 1-6 from Table 5.4 after being subjected to a standard spray tip at 1000 (top) and 2000 psi (middle), and a rotary tip at 1000 psi (bottom) after two-months immersion. The black arrow designates severe coating delamination in sample #3 after rotary tip cleaning.

Cleanability of all samples from the second round of cleaning (four-months) was poorer than the previous round, with much of the fouling remaining after using the standard tip at both 1000 and 2000 psi. When the rotary tip was used at 1000 psi, panels coated with A4-20 or Hempasil® X3+ had much of the biofouling removed, while control panels still had a fair number of barnacles and tubeworms remaining. Only after using the rotary tip at 2000 psi were all panels, including uncoated controls, cleaned of

remaining biofouling. However, as mentioned previously, this period of cleaning fell within the period of heaviest fouling, so it is not unexpected for basal fouling levels to be higher than normal. Lastly, after the third round of cleaning (six-months), a similar trend was seen as in the second round of cleaning, but while fouling coverage was greater, and cleanability poorer on control panels, coated panels seemed to have better cleanability even after immersion for six months. Figure 5.11 details the differences in cleanability between coated and uncoated panels after six months of immersion.

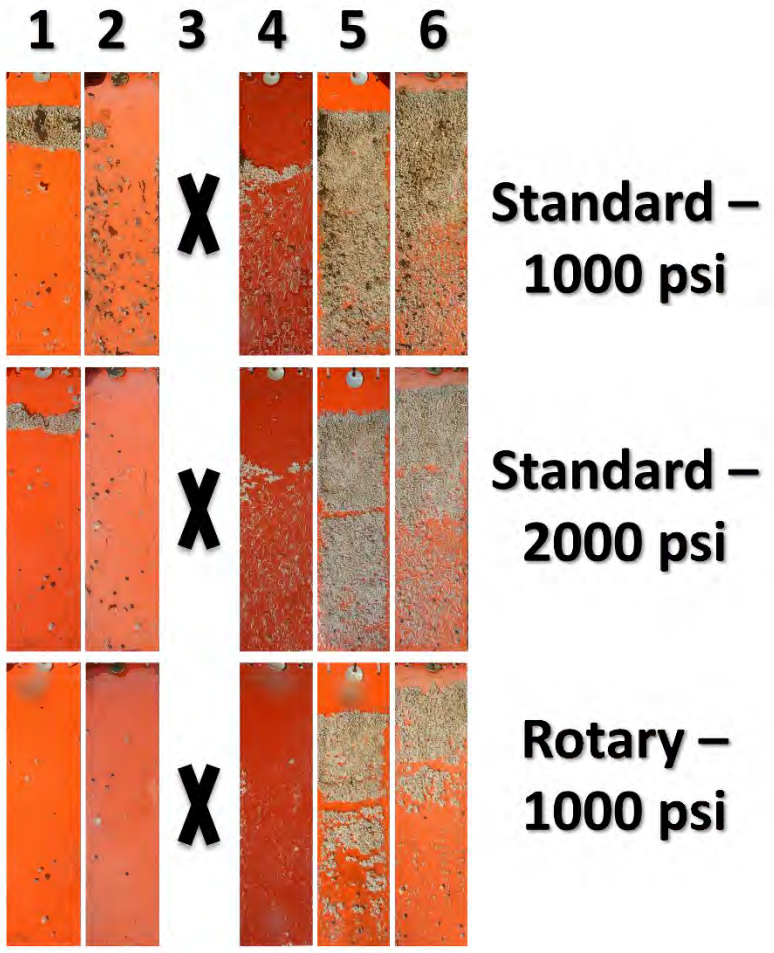

Figure 5.11. Third cleaning of panels with sample ID's 1-6 from Table 5.4 after being subjected to a standard spray tip at 1000 (top) and 2000 psi (middle), and a rotary tip at 1000 psi (bottom) after six months immersion. The red 'X's' in the column of sample ID #3 denote the removal of these coatings after sever delamination in cleaning period one.

Throughout each of these cleanings one overall observation was that coated samples were able to be cleaned at lower pressures using the standard tip, as opposed to using the more aggressive cleaning method involving the rotary tip. Effectiveness did begin to drop off after four-months of

immersion, with coatings delamination issues being seen in rigid, smooth, Desmi orange substrates coated with Hempasil® X3+. In addition, substrates coated with A4-20 did not show as severe delamination, but after six-months immersion, the edges of the coatings begin to lift off from the substrate. Overall, it was shown that the usage of these two FR coatings improves the cleanability of these oil boom substrates compared to uncoated panels, but the effective lifetime is limited. During lower-fouling periods, early spring or late autumn, coated samples may be able to provide better cleanability results, with this effect being diminished as heavier fouling periods occur.

Conclusion

This study was concerned with the adhesion performance of several coatings systems on oil boom substrates after surface treatment or application of adhesion promoters. Five different oil boom materials were selected, with three of these being composed of mainly polyester fibers embedded in polyurethane, and two being composed of polyester fibers being embedded in polyvinyl chloride. These substrates were cut to a size of ~2” x 3” to prepare samples for surface analysis and small-scall waterjet adhesion testing. Substrates were subjected to either sandblasting or corona surface treatment methods before application of four different chlorinated polyolefins (CPO) as a ‘primer’ layer. After this combined surface treatment, three separate coatings were applied to these treated substrates. In addition, treatment groups which included coated substrate that did not involve any type of surface treatment, were prepared, and analyzed alongside treated substrates. Each treatment group included a sample that was immersed in circulating tap water for 30, 60, 90, 120, 150, and 180 days before waterjet adhesion was performed.

During surface analysis of uncoated substrates, the surface energies varied greatly between substrates that consisted mostly of polyurethane and those that were composed of polyvinyl chloride impregnated polyester fibers. The same was true between textured substrates and non-textured, or smooth substrates. These differences in surface energies can greatly affect the wetting of coatings onto these substrates, which in turn, can affect the adhesion properties. ATR-FTIR was useful in confirming the presence of chemical groups belonging to polyurethane and polyvinyl chloride. The presence of these groups at the surface can also affect the adhesion properties of the various coatings analyzed. Once surface analysis had been carried out, samples for each treatment group were prepared for small-scale

waterjet adhesion testing. Visual inspection of these samples showed that both A4-20 and Hempasil® Nexus tie-coat spread evenly across surfaces, while the Intersleek® tie-coat displayed poor spreading, with some treatment groups exhibiting areas of more coating material as opposed to some areas where the substrate could be seen. This was likely due to the very low surface energy of this tie-coat, making it difficult to spread across such varied materials as the oil boom substrates. Additionally, longer periods of water ageing of these samples provided similar trends as seen in shorter periods of immersion, with a general increase in failure seen in all treatment groups.

After performing waterjet adhesion on experimental treatment groups, several conclusions can be made. Regarding coating type, the Intersleek® tie-coat performed the worst, having a greater number of the highest failure ratings even at lower pressures. The Hempasil® tie-coat performed much better, only achieving the highest failure ratings typically at the highest water pressures. A4-20 performed the best overall, with lower incidence of high failure ratings. The best performing substrate types were the textured Desmi orange and Elastec orange substrates. This is thought to be because the peaks of valleys of the surface could better disperse localized water pressures acting upon the coating/substrate interface. Surface treatments and adhesion promoters did not seem to have a large effect on the adhesion properties of these coatings regarding damage caused by a focused stream of water. But sandblasting did seem to improve adhesion performance on textured substrates. Overall, A4-20 on textured substrates performed the best overall and is a promising candidate for large-scale field testing.

Lastly, four different treatment groups were selected for field testing. These treatment groups, along with two control substrates, Desmi orange and Desmi orange textured, were subjected to visual inspections monthly, with three cleaning periods at the two, four, and sixth-month time intervals. Observations showed that each treatment group, that contained A4-20 and the Hempasil® X3+ FR coating system, produced better cleanability results when compared to oil boom fabric alone. This performance was more pronounced during periods of lower fouling such as early spring or late autumn. However, after seven months of immersion, coating damage was seen in each of the coated systems, with the treatment group with Hempasil® X3+ coated on smooth Desmi orange substrate experiencing severe delamination, needing to be removed from testing. Still, the work performed in this study was able to identify several coatings, surface treatment, and substrate combinations that could improve the

adhesion performance and cleanability of oil boom fabrics used in static containment. Future work should be concerned with developing a coating system specific to the most widely used oil boom fabrics as compatibility between coating and substrate surface chemistry is of utmost importance.

References

1. Kumar, A.; Choudhary, S., Energy Requirement, Resources and Future Management: A Review. *Indian Journal of Pure & Applied Physics (IJPAP)* **2021,** *59* (11), 779-784.

2. Nazir, M. S.; Mahdi, A. J.; Bilal, M.; Sohail, H. M.; Ali, N.; Iqbal, H. M. N., Environmental impact and pollution-related challenges of renewable wind energy paradigm–a review. *Science of the Total Environment* **2019,** *683*, 436-444.

3. Lior, N., Energy resources and use: The present situation and possible paths to the future. *Energy* **2008,** *33* (6), 842-857.

4. Ramadass, K.; Megharaj, M.; Venkateswarlu, K.; Naidu, R., Ecotoxicity of measured concentrations of soil-applied diesel: Effects on earthworm survival, dehydrogenase, urease and nitrification activities. *Applied Soil Ecology* **2017,** *119*, 1-7.

5. Labud, V.; Garcia, C.; Hernandez, T., Effect of hydrocarbon pollution on the microbial properties of a sandy and a clay soil. *Chemosphere* **2007,** *66* (10), 1863-1871.

6. Alkio, M.; Tabuchi, T. M.; Wang, X.; Colon-Carmona, A., Stress responses to polycyclic aromatic hydrocarbons in Arabidopsis include growth inhibition and hypersensitive response-like symptoms. *Journal of Experimental Botany* **2005,** *56* (421), 2983-2994.

7. Xu, X.; Hu, H.; Kearney, G. D.; Kan, H.; Sheps, D. S., Studying the effects of polycyclic aromatic hydrocarbons on peripheral arterial disease in the United States. *Science of the total Environment* **2013,** *461*, 341-347.

8. Lin, C.-K.; Hung, H.-Y.; Christiani, D. C.; Forastiere, F.; Lin, R.-T., Lung cancer mortality of residents living near petrochemical industrial complexes: a meta-analysis. *Environmental Health* **2017,** *16* (1), 1-11.

9. Kuppusamy, S.; Maddela, N. R.; Megharaj, M.; Venkateswarlu, K., Impact of total petroleum hydrocarbons on human health. In *Total Petroleum Hydrocarbons*, Springer: 2020; pp 139-165.

10. Hahladakis, J. N.; Velis, C. A.; Weber, R.; Iacovidou, E.; Purnell, P., An overview of chemical additives present in plastics: Migration, release, fate and environmental impact during their use, disposal and recycling. *Journal of hazardous materials* **2018,** *344*, 179-199.

11. Depledge, M. H.; Galgani, F.; Panti, C.; Caliani, I.; Casini, S.; Fossi, M. C., Plastic litter in the sea. *Marine Environmental Research* **2013,** *92*, 279-281.

12. Brouwer, R.; Hadzhiyska, D.; Ioakeimidis, C.; Ouderdorp, H., The social costs of marine litter along European coasts. *Ocean & coastal management* **2017,** *138*, 38-49.

13. Koelmans, A. A.; Besseling, E.; Shim, W. J., Nanoplastics in the Aquatic Environment. Critical Review. In *Marine Anthropogenic Litter*, Bergmann, M.; Gutow, L.; Klages, M., Eds. Springer International Publishing: Cham, 2015; pp 325-340.

14. Prata, J. C.; da Costa, J. P.; Lopes, I.; Duarte, A. C.; Rocha-Santos, T., Environmental exposure to microplastics: An overview on possible human health effects. *Science of the Total Environment* **2020,** *702*, 134455.

15. Doerffer, J. W., *Oil spill response in the marine environment*. Elsevier: 2013.

16. Lin, Q.; Mendelssohn, I. A., Impacts and recovery of the Deepwater Horizon oil spill on vegetation structure and function of coastal salt marshes in the northern Gulf of Mexico. *Environmental science & technology* **2012,** *46* (7), 3737-3743.

17. Corn, M. L., *Deepwater Horizon oil spill: coastal wetland and wildlife impacts and response*. DIANE Publishing: 2010.

18. Zhang, B.; Matchinski, E. J.; Chen, B.; Ye, X.; Jing, L.; Lee, K., Marine oil spills—oil pollution, sources and effects. In *World seas: an environmental evaluation*, Elsevier: 2019; pp 391-406.

19. Chen, B.; Ye, X.; Zhang, B.; Jing, L.; Lee, K., Chapter 22 - Marine Oil Spills—Preparedness and Countermeasures. In *World Seas: an Environmental Evaluation (Second Edition)*, Sheppard, C., Ed. Academic Press: 2019; pp 407-426.

20. Chen, J.; Zhang, W.; Wan, Z.; Li, S.; Huang, T.; Fei, Y., Oil spills from global tankers: Status review and future governance. *Journal of cleaner production* **2019,** *227*, 20-32.

21. Peterson, C. H.; Rice, S. D.; Short, J. W.; Esler, D.; Bodkin, J. L.; Ballachey, B. E.; Irons, D. B., Long-term ecosystem response to the Exxon Valdez oil spill. *Science* **2003,** *302* (5653), 2082-2086.

22. Dorrler, J. S. In *Limited Oil Spills In Harbor Areas*, 1969; American Petroleum Institute: pp 151-156.

23. Jimenez, J. F.; Giron-Sierra, J. M., USV based automatic deployment of booms along quayside mooring ships: Scaled experiments and simulations. *Ocean engineering* **2020,** *207*, 107438.

24. Hassler, B., Accidental Versus Operational Oil Spills from Shipping in the Baltic Sea: Risk Governance and Management Strategies. *AMBIO* **2011,** *40* (2), 170-178.

25. Trozzi, C.; Vaccaro, R., Environmental impact of port activities. *WIT Transactions on The Built Environment* **2000,** *51*.

26. Wilson, C. K. *An assessment of the environmental impacts from the discharge of bilge water in the Norfolk Naval Station Harbor*; PENNSYLVANIA STATE UNIV UNIVERSITY PARK: 1991.

27. Fingas, M., *Handbook of oil spill science and technology*. John Wiley & Sons: 2014.

28. Yebra, D. M.; Kiil, S. K.; Dam-Johansen, K., Antifouling Technology—Past, Present and Future Steps Towards Efficient and Environmentally Friendly Antifouling Coatings. *Prog. Org. Coat.* **2004,** *50* (2), 75.

29. Callow, M. E.; Callow, J. A., Marine Biofouling: A Sticky Problem. *Biologist* **2002,** *49* (1), 10.

30. Callow, J. A.; Callow, M. E., Trends in the Development of Environmentally Friendly Fouling-Resistant Marine Coatings. *Nat. Commun.* **2011,** *2*, 244.

31. Hellio, C.; Yebra, D. M., *Advances in Marine Antifouling Coatings and Technologies*. 2009.

32. Kaplan, S., Plasma processes for wide fabric, film and non-wovens. *Surface and Coatings Technology* **2004,** *186* (1-2), 214-217.

33. Holme, I., Adhesion to textile fibres and fabrics. *International journal of adhesion and adhesives* **1999,** *19* (6), 455-463.

34. Liu, X.-D.; Sheng, D.-K.; Gao, X.-M.; Li, T.-B.; Yang, Y.-M., UV-assisted surface modification of PET fiber for adhesion improvement. *Applied Surface Science* **2013,** *264*, 61-69.

35. Bodkhe, R. B.; Thompson, S. E. M.; Yehle, C.; Cilz, N.; Daniels, J.; Stafslien, S. J.; Callow, M. E.; Callow, J. A.; Webster, D. C., The Effect of Formulation Variables on Fouling-Release Performance of Stratified Siloxane-Polyurethane Coatings. *Journal of Coatings Technology Research* **2012,** *9* (3), 235.

36. Owens, D. K.; Wendt, R. C., Estimation of the Surface Free Energy of Polymers. *J. Appl. Polym. Sci.* **1969,** *13* (8), 1741.

37. Packham, D. E., Surface energy, surface topography and adhesion. *International journal of adhesion and adhesives* **2003,** *23* (6), 437-448.

38. Croll, S. G., Surface roughness profile and its effect on coating adhesion and corrosion protection: A review. *Progress in Organic Coatings* **2020,** *148*, 105847.

39. Asmatulu, R.; Erukala, K. S.; Shinde, M.; Alarifi, I. M.; Gorji, M. R., Investigating the effects of surface treatments on adhesion properties of protective coatings on carbon fiber-reinforced composite laminates. *Surface and Coatings Technology* **2019,** *380*, 125006.

CHAPTER 6. ACETOACETYLATION OF A HYPERBRANCHED POLYGLYCEROL FOR USE IN SILOXANE-POLYURETHANE FOULING-RELEASE COATINGS

Introduction

Marine biofouling is commonly referred to as the undesirable growth and accumulation of marine organisms on structures submerged in seawater.[1] Due to the significant usage of marine vessels as a means of transporting people and goods across the world's oceans, this is a globally prevalent problem with numerous negative economic and environmental effects. As biofouling accumulates on the hulls of ships, a significant increase in drag and fuel consumption is seen, leading to an overall increase of highly detrimental greenhouse gas emissions and economic cost of operation. For example, the United States Navy spends almost 56 million dollars per year to operate their mid-sized destroyers, with this amount increasing to almost 1 billion dollars after a period of 15 years, due to increased maintenance, cleaning, paint refinishing, and additional fuel consumptions costs caused by marine biofouling.[2] Additionally, the potential for the introduction of aggressive, invasive species in non-native environments is high due to the large number of various species that act as fouling-organisms.[2-4] This phenomenon, in addition to being highly detrimental to a ship's performance, is also an extremely complex, dynamic process that can make it difficult to protect against. There are thought to be over 4000 different micro- and macrofouling species, which have a wide variety of adhesion mechanisms and composition of adhesive.[5, 6] This process also occurs on a dynamic timescale, with the first 'conditioning' layer (largely made up of proteins, nutrients, and other small molecules) being formed within seconds of immersion in a marine environment.[5] Subsequent stages occur over minutes, hours, and even days, as the settlement and adhesion of marine bacterium, algae, barnacles, mussels, and tunicates continues.[7]

To prevent this accumulation of fouling layers, numerous methods of protection have been used over the centuries of navigating the world's oceans. Some of the traditional anti-fouling (AF) methods involved the usage of lead, or copper alloy sheaths that would kill organisms trying to settle on the hulls of ships. Mixtures of tar and hot pitch were also used to great effect on wooden ships, producing a highly toxic surface for these marine organisms.[1, 7] With significant advances of polymer technologies occurring

in the mid-20th century, biocide containing self-polishing polymer resin based coatings quickly became the gold standard in AF protection.[1] A very potent biocide, tributyltin (TBT), saw widespread use in many AF paint formulations, but concerns over the poisoning of local marine ecosystems caused a ban on using these tin-containing biocides by the International Maritime Organization (IMO) in 2008.[6, 8] Therefore, current AF paints utilize other biocides such as zinc or copper oxides, as well as the use of organic 'co-biocides'. While these biocides are effective, they are still observed to accumulate in marine environments, which can be detrimental to marine and human life.[9-12] To address this issue, research has been focused on developing non-toxic fouling-release (FR) coating systems. These types of coatings function by providing a surface that organisms weakly adhere to, where hydrodynamic forces attained at cruising speeds is often enough to remove the marine foulants.[5, 7] Traditional FR technologies involve the usage of low surface energy materials like polydimethylsiloxane (PDMS) and polyfluoroalkyl (PFA) polymers in the coating matrix. While generating surfaces which have excellent FR properties, these systems often lack the mechanical durability and adhesion needed to last in a harsh marine environment, typically requiring several additional 'tie-coats' for long-term performance.[1, 13, 14] To this end, self-stratifying siloxane-polyurethane (SiPU) FR coatings were developed. These coatings showed good adhesion to the substrate, superior mechanical durability compared to traditional FR systems, all while maintaining good FR properties at the surface.[15, 16] Although this newer generation of FR coatings showed good FR performance, their hydrophobic nature left them vulnerable to the settlement of organisms that prefer to settle on these surfaces such as the marine diatom *Navicula incerta*.[17, 18] In an attempt to provide a more heterogenous surface, able to prevent the attachment of a broad range of fouling organisms while also maintaining good removal properties, much research is now focused on the generation of amphiphilic surfaces, containing both hydrophilic and hydrophobic moieties.[19-21]

As mentioned previously, the process of attachment and adhesion to submerged substrates is dynamic, involving very complex interactions between the organisms and the substrate that they are looking to adhere to.[6, 22] One of the more significant interactions is that of the association of settling marine organisms with a conditioning layer consisting of nutrients, proteins, and other adhesion promoting macromolecules on submerged surfaces.[23] Hence, methods utilized to enhance the protein resistance, and disrupt the formation of this conditioning layer may provide a significant increase in

fouling resistant properties of surfaces. This can be accomplished *via* incorporating hydrophilic moieties such as polyethylene glycol (PEG), zwitterionic species, polyelectrolyte layers, and peptide mimicking 'peptoids' into traditional FR coating systems.[19, 24-30] These surfaces typically provide protein resistance by generating a 'hydration' layer, which minimizes the interfacial surface energy through hydrophilic group/water molecule complexes.[31, 32] The disruption of this hydration layer is highly thermodynamically unfavorable, providing an unsuitable surface for many marine foulants to settle.[33, 34] PEG, while not having the strongest interactions with water out of these hydrophilic moieties, is perhaps the most widely used and adaptable material for providing protein, and subsequent marine foulant, resistance. Several systems have been developed to incorporate these moieties in a coating matrix, as well as their use in surface modifying additives.[29, 35-39] However, despite these desirable properties of protein resistance afforded by incorporating PEG into these coatings, there are concerns about its thermal and oxidative stability, which could lead to degradation in a marine environment and subsequent loss of performance.[40, 41]

To address the potential issues of degradation of PEG in marine environments, the use of hyperbranched polyglycerols (HBPGs) have been explored. These materials are complex, globular macromolecules with a high density of glycerol units.[42] Due to the presence of these glycerol units, and free hydroxyl groups, surfaces composed of HBPGs are highly hydrophilic, forming strong interactions with water, and are attractive candidates for developing surfaces to resist protein attachment.[43-45] In addition to favorable properties of protein resistance, HBPGs also show greater resistance to various modes of abiotic and biotic degradation, making them an potential alternative to traditional PEG based FR coatings systems.[46-48] Surfaces are typically modified with HBPGs *via* 'grafting-to' processes, or by incorporating them into a coating matrix with a variety of reactive methods.[49-51] Although these types of coatings incorporating HBPGs have excellent protein resistance, there are still concerns regarding the mechanical durability, and commercial feasibility of these systems.

In this initial investigation of using HBPGs as hydrophilic non-reactive additives for FR coatings systems, the synthesis of HBPGs, and subsequent functionalization with acetoacetate groups, was performed. Hyperbranched polyglycerol was synthesized *via* ring-opening multi-branching polymerization (ROMBP) with partially deprotonated trimethylolpropane (TMP) and glycidol as the addition monomer at a

15:1 monomer to initiator ratio. Hydroxyl content was then measured via hydroxyl titrations, with FT-IR, ^{1}H-NMR, and ^{13}C-NMR utilized to determine successful synthesis. Then, HBPG was acetoacetylated with TBAA, and characterized *via* previous spectroscopic methods. Acetoacetylation was performed to protect free hydroxyl groups from reacting with various curing mechanisms during coating incorporation such as polyurethane formation *via* isocyanate/hydroxyl reactions.

Experimental

Materials

Solvents used during experiments included methanol, acetone, and dimethylformamide (DMF). These were purchased from Sigma Aldrich (MO, USA). Trimethylolpropane (TMP), potassium methylate (30-35% solution in methanol), glycidol, and cation exchange resin DOWEX 50WX8 were also purchased from Sigma Aldrich (MO, USA). Acetoacetylation reagent tert-butyl acetoacetate (TBAA) was provided by Eastman Chemical Company (TN, USA). Deuterated dimethyl sulfoxide (DMSO-d6) was also purchased from Sigma Aldrich (MO, USA). Acetic anhydride, pyridine, as well as potassium bromide optical discs used during FT-IR experiments, were purchased from Alfa Aesar (MA, USA). Phenolphthalein indicator and 0.5 N sodium hydroxide (NaOH) were purchased from VWR International (PA, USA).

Experimental Approach

Several different approaches to combating the phenomenon of marine biofouling involve the usage of fouling-release (FR) coatings systems that contain hydrophobic and hydrophilic domains such as polydimethylsiloxane (PDMS) and polyethylene glycol (PEG). These amphiphilic surfaces have been shown to have increased FR performance due to the low-surface energy component of the coating, while also increasing the anti-fouling (AF) performance by incorporating hydrophilic moieties that form a ‘hydration layer’, resisting the initial attachment of organisms to the surface. While surfaces that have sufficient concentrations of a hydrophilic component, such as PEG, display improved fouling resistance properties, there are concerns of significant biotic and abiotic degradation in marine environments, resulting in a loss of protection.[40, 41, 52, 53]

The objective for this work was to synthesize a hydrophilic, hyperbranched polyglycerol (HBPG) unreactive additive for future incorporation in a siloxane containing polyurethane (SiPU) FR coating. Hyperbranched variants of linear polymers such as PEG show an increase in resistance to thermal and

oxidative degradation, important attributes for polymers placed in marine environments.[43, 47, 50] In addition, surfaces that include these HBPGs display a significant increase in antifouling performance when compared to linear analogues such as PEG. Much of the recent literature has been concerned with depositing HBPGs as layered systems on surfaces, or by incorporating them into a coating system. However, to the best of the author's knowledge, there is little work investigating their AF efficacy as unreactive surface modifying additives.

The hyperbranched polyglycerols, synthesized *via* anionic ring-opening multi-branching polymerization (ROMBP), were also modified with acetoacetate groups. This was done to prevent reaction of hydroxyl groups on unmodified HBPG, and the isocyanate used to form the polyurethane bulk during eventual incorporation of these additives into SiPU FR coatings. Once these coatings were immersed in a marine environment, hydrolysis of acetoacetate groups readily occurs, providing increased hydrophilicity from exposed hydroxyl end groups, potentially leading to surfaces with desirable AF properties. Several characterization methods such as FT-IR, ^{1}H-NMR, ^{13}C-NMR, and hydroxyl equivalent weight titrations were utilized to determine successful synthesis of both HBPG and acetoacetylated HBPG (AA-HBPG).

Synthesis of Hyperbranched Polyglycerol (HBPG)

The synthesis of hyperbranched polyglycerol was performed utilizing anionic ring-opening multi-branching polymerization (ROMBP) detailed in previous literature.[54] Below, in Figure 6.1, is shown a general scheme for this polymerization, with a general procedure for the synthesis of HBPG having a monomer to initiator equivalence ratio of 15:1. Reagent amounts were based upon OH equivalents. First, trimethylolpropane (TMP, 2.52 g; 0.056 eq) was added to a 250 mL, 2-neck round bottom flask, and was partially deprotonated (~10% based off equivalents) with potassium methylate in methanol (33% w/v) (1.20 g solution; 0.0056 eq solid $KOCH_3$). This mixture was stirred for 30 minutes under inert atmosphere, and then excess methanol was removed *via* vacuum distillation. A 2-neck adaptor was then affixed to one neck of the flask to allow for a nitrogen inlet and a mechanical stirrer placed in the other neck. The mixture was placed in an oil bath and temperature was set at 95℃. Once the mixture had reached this temperature, glycidol (78.59 g; 0.839 eq), cooled in an ice water bath, was added at a rate of 0.070 mL/min. After the addition, product was dissolved in methanol and neutralized by filtering over cation

exchange resin DOWEX 50WX8. The polymer was then precipitated twice from methanol to acetone and dried for at least 15 h at 80℃. The synthesized HBPG was a transparent, slightly yellow, highly viscous liquid, with a yield of ~65%.

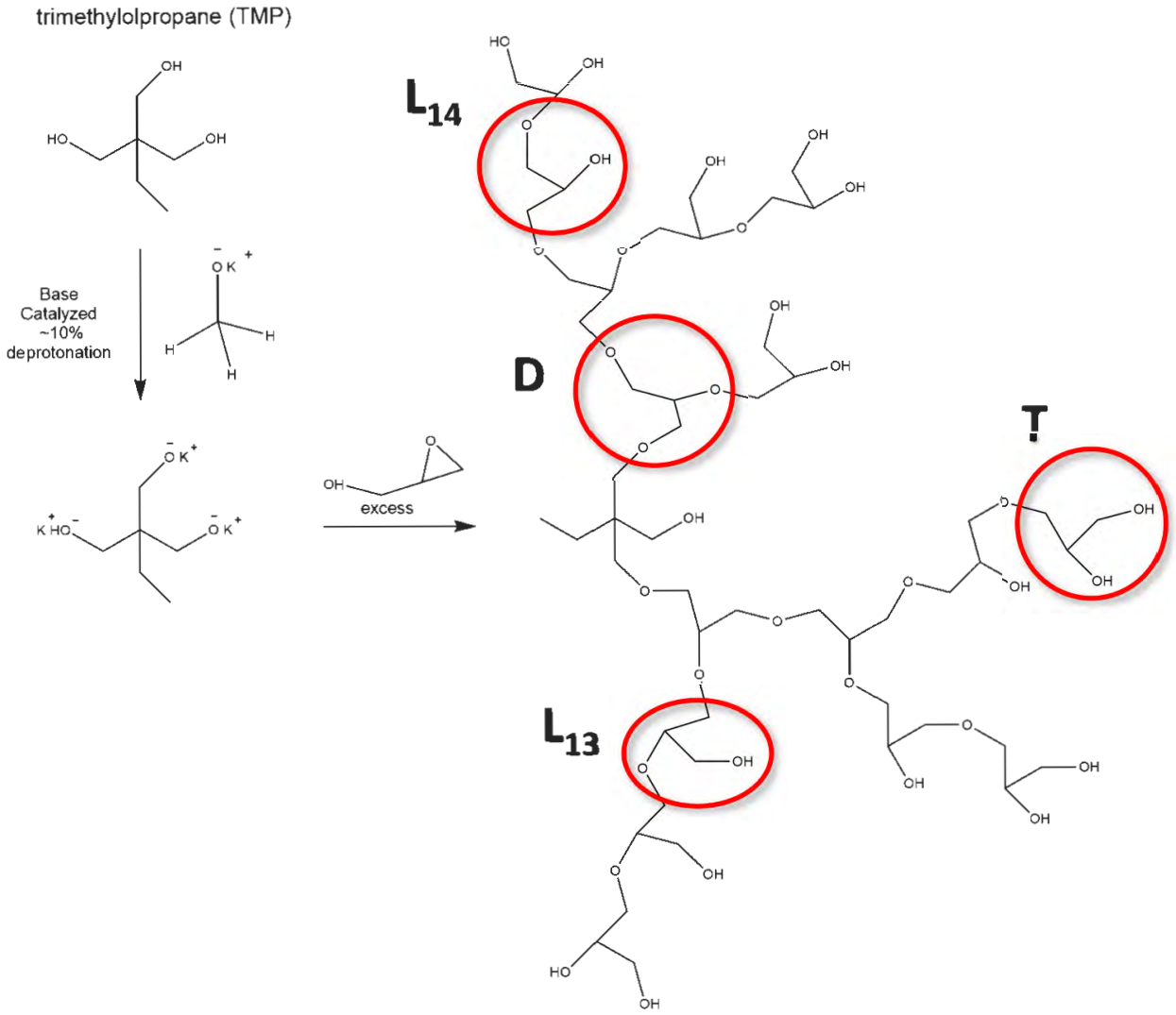

Figure 6.1. Synthetic scheme for the ROMBP of TMP with glycidol to form HBPGs. The red circled areas indicate the four different architectures of subsequent additions of glycidol. These include terminal (T), dendritic (D), linear 1,3 (L13) and linear 1,4 (L14).

Hydroxyl Equivalent Weight Titrations

To determine the hydroxyl group content of synthesized HBPG, necessary for the functionalization using acetoacetate, hydroxyl equivalent weight titrations were performed. A general procedure, modified from ASTM E222-17, is as follows. First, acetylation reagent was made by mixing 10.5 mL of acetic anhydride with 100 mL of pyridine and placed in a dark bottle. Next, indicator solution

was prepared by adding 1 g of phenolphthalein to 100 mL of pyridine. Sample (~0.5 g) was then added to a 250 mL Erlenmeyer flask, along with 25.0 mL of acetylation reagent. The flask was affixed with a cold-water condenser, placed in an oil bath, and heated at reflux temperature for 1.5 h. After leaving the flask to cool, the condenser was rinsed with ~25 mL of deionized water, and then the flask was left to return to room temperature. Next, 1.0 mL of phenolphthalein indicator was added to the flask, and subsequently titrated with 0.5 N NaOH until a faint pink endpoint persists for at least 15 s. This procedure was repeated to gather three replicates, and blank titrations were performed with each sample titration, with the omission of the sample. Hydroxyl number was then calculated utilizing the equation presented in ASTM E222-17, with the hydroxyl equivalent weight being determined by dividing the molecular weight of potassium hydroxide multiplied by 1000, by the average hydroxyl number.

Acetoacetylation of HBPGs

Once HBPGs had been successfully synthesized, the acetoacetylation of the free hydroxyl groups was performed according to previous literature.[55] A general procedure for this reaction is as follows, with a detailed scheme shown in Figure 6.2. HBPG (21.3723 g) was added to a 250 mL and dissolved with DMF (64.25 g) to obtain a ~25 wt.% solution. The flask was equipped with a nitrogen inlet, thermocouple probe, and a dean-stark apparatus with coil condenser attached. The mixture was placed in an oil bath and heated at 140℃ while stirring with a Teflon coated magnetic stir bar. Once this temperature had been reached, tert-butyl acetoacetate (TBAA) (4.2649 g) was added to ensure a conversion of hydroxyl to acetoacetate of 100%. The reaction was maintained at 140℃ while monitoring the amount of t-butanol collected in the dean-stark. The reaction was completed when ~2.5 mL of t-butanol was collected. DMF was then removed under reduced pressure. The synthesized AA-HBPG was a transparent, amber colored, viscous liquid.

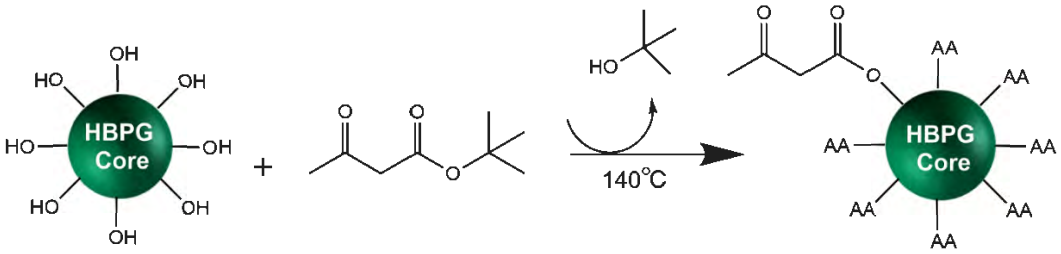

Figure 6.2. Reaction scheme showing the capping of hydroxyl groups from synthesized HBPG with acetoacetate functional groups.

Fourier Transform - Infrared Spectroscopy

A Thermo Scientific Nicolet 8700 FT-IR spectrometer was used to determine the successful synthesis of HBPG and AA-HBPG. Liquid samples of polymer were spread over a potassium bromide optical disk and placed in the instrument after obtaining a background spectrum.

^{1}H-NMR and ^{13}C-NMR

A JOEL-ECA 400 MHz FT-NMR instrument was used to collect and record the proton and carbon NMR spectra for HBPG, AA-HBPG, and associated reagents. Bruker TopSpin® NMR processing software was utilized to analyze peaks. All samples were dissolved in deuterated DMSO (DMSO-d6) with 1% (v/v) TMS.

Results and Discussion

Non-toxic, fouling-release (FR) coatings have been used extensively to protect ocean going vessels from the problem of marine biofouling. While these coatings are more environmentally friendly than commonly used, biocide-containing anti-fouling (AF) paints, their effectiveness against the prevention of biofouling settlement is typically lower than AF paints and is an area of intense research focus. Several different approaches have been utilized involving the introduction of both hydrophobic and hydrophilic groups into coatings systems, providing a heterogeneous surface which has shown improved fouling-resistance towards a variety of marine foulants. However, concerns over the stability and prolonged effectiveness of hydrophilic moieties such as PEG have led to the investigation of other hydrophilic polymers. To this end, hyperbranched polyglycerols (HBPGs) were identified as having higher resistance to several forms of degradation that PEG typically experiences in marine environments, as well as potentially increasing the fouling-resistant properties of these amphiphilic, heterogenous surfaces. This work involved the initial investigation of the synthesis of these HBPGs, as well as acetoacetylation functionalization to produce a highly hydrophilic additive that does not react with the isocyanate in a siloxane-polyurethane (SiPU) FR coating.

After synthesis of HBPGs *via* ring-opening multi-branching polymerization with TMP as initiator and with slow addition of glycidol, hydroxyl equivalent weight titrations were performed to assess the hydroxyl content of the polymer. The average hydroxyl content was determined to be ~800 g/eq. This

helps confirm the ring-opening of glycidol upon each successive branch and is needed for determining the amounts of TBAA necessary for complete conversion to acetoacetate functionality.

In addition to determining hydroxyl content of HBPGs, FT-IR was performed on synthesized polymer, as well as glycidol for comparison. FT-IR spectra are shown below in Figure 6.3.

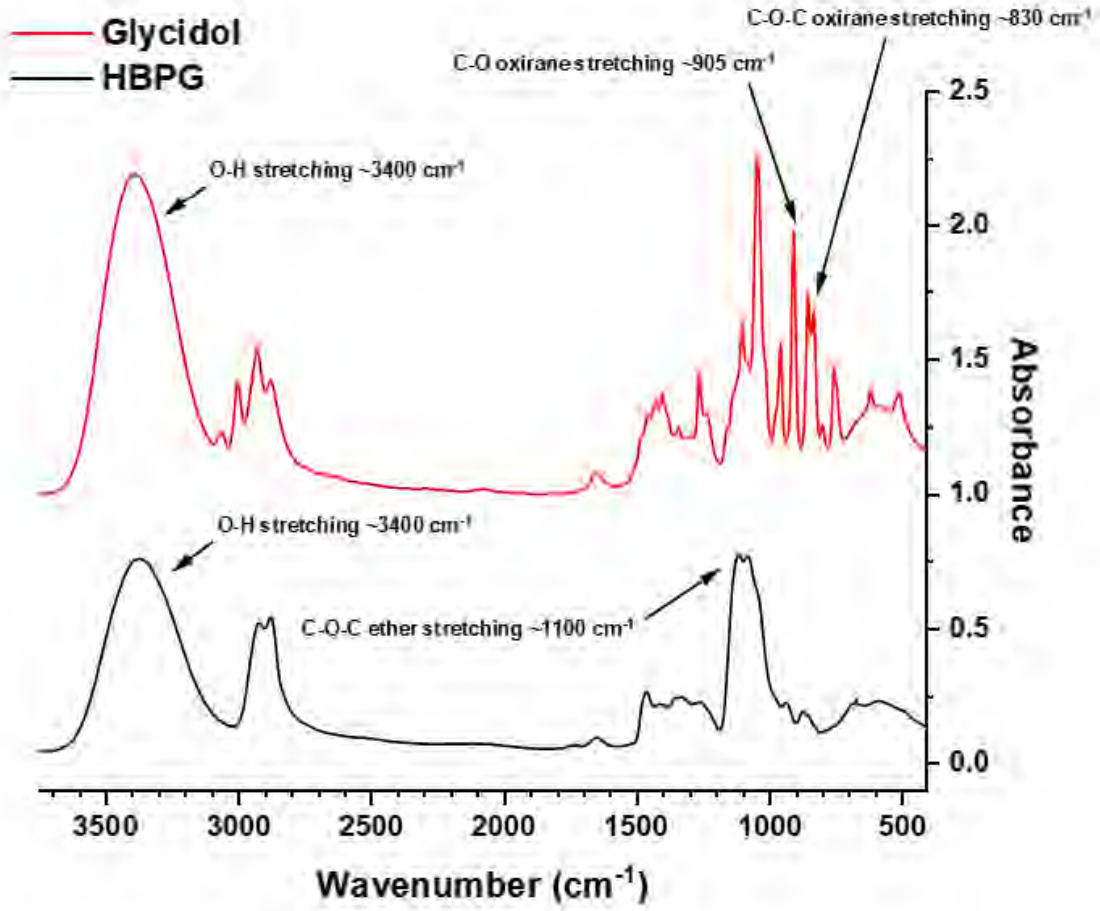

Figure 6.3. FT-IR spectra detailing the characteristic peaks for glycidol, in red, and synthesized HBPG in black.

A very prominent hydroxyl peak can be seen ~3400 cm^{-1} for both glycidol and synthesized HBPG, albeit a reduced intensity from HBPG. Another peak of interest is seen ~1100 cm^{-1} for HBPG and is due to the generation of C-O-C (ether) linkages from the ring-opening of glycidol. Lastly, two peaks at ~905 cm^{-1} and ~830 cm^{-1} are seen in the spectrum for glycidol. These are indicative of C-O and C-O-C oxirane stretching respectively and are not seen in the spectrum for synthesized HBPG. While this spectroscopic method does not reveal insight into the branching character, or if initiator was incorporated into the

polymer, it does provide evidence that oxirane rings had been opened, leading to ether linkages seen within this HBPG.

To further investigate the successful synthesis of HBPG, ^{1}H-NMR and ^{13}C-NMR spectra were gathered. Shown below in Figure 6.4 are ^{1}H-NMR spectra for this HBPG synthesis.

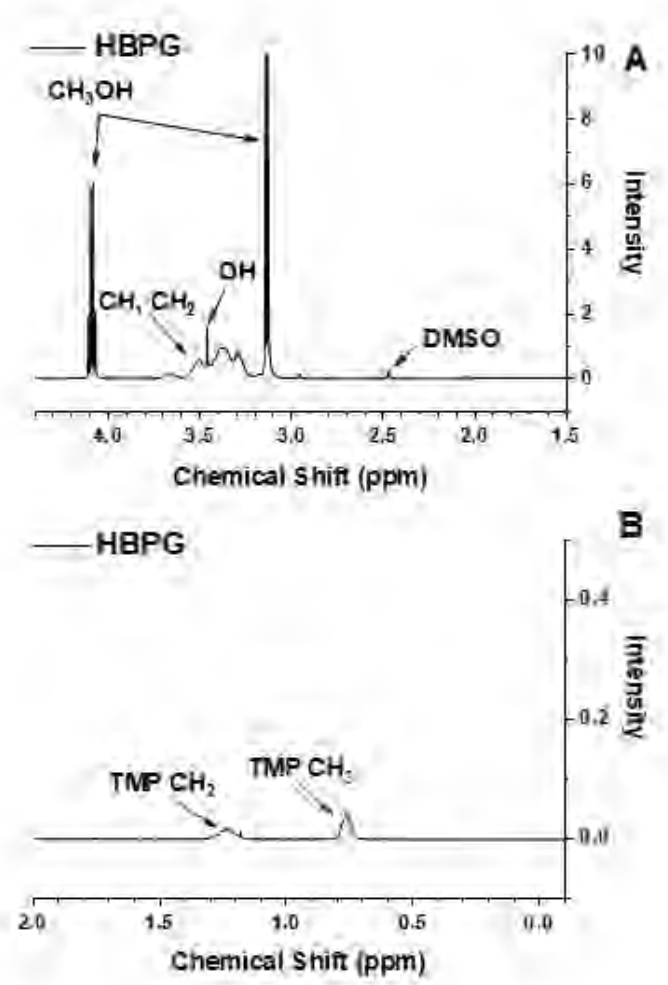

Figure 6.4. ^{1}H-NMR spectra for the synthesized HBPG. A) Peaks associated with the methylene and methine protons on branching sites. B) Peaks associated with TMP initiator.

While carbon NMR provides a clearer picture of the different branching groups such as dendritic (D), terminal (T), linear 1,3 (L_{13}) and linear 1,4 (L_{14}), proton NMR still provides insight on the presence or absence of peaks specific to these HBPGs. First, in 6.4A, there are two prominent peaks that belong to residual methanol in the polymer at ~4.1 ppm and 3.1 ppm. Also, a small amount of DMSO-d5 is seen at ~2.5 ppm. More importantly, there are characteristic peaks associated with the methylene and methine protons attached to carbons belonging to the different branching groups. These occur in a broad range

from ~3.2-3.7 ppm. The last peak of note in 6.4A belongs to proton from free hydroxyl groups at ~3.5 ppm. Secondly, in 6.4B, there appears peaks from the methylene and methyl protons from TMP initiator around 1.3 ppm and 0.8 ppm respectively. These spectra provide evidence that TMP initiator was successfully incorporated into the synthesized HBPG.

The ^{13}C-NMR spectrum for the synthesized HBPG can be seen in Figure 6.5.

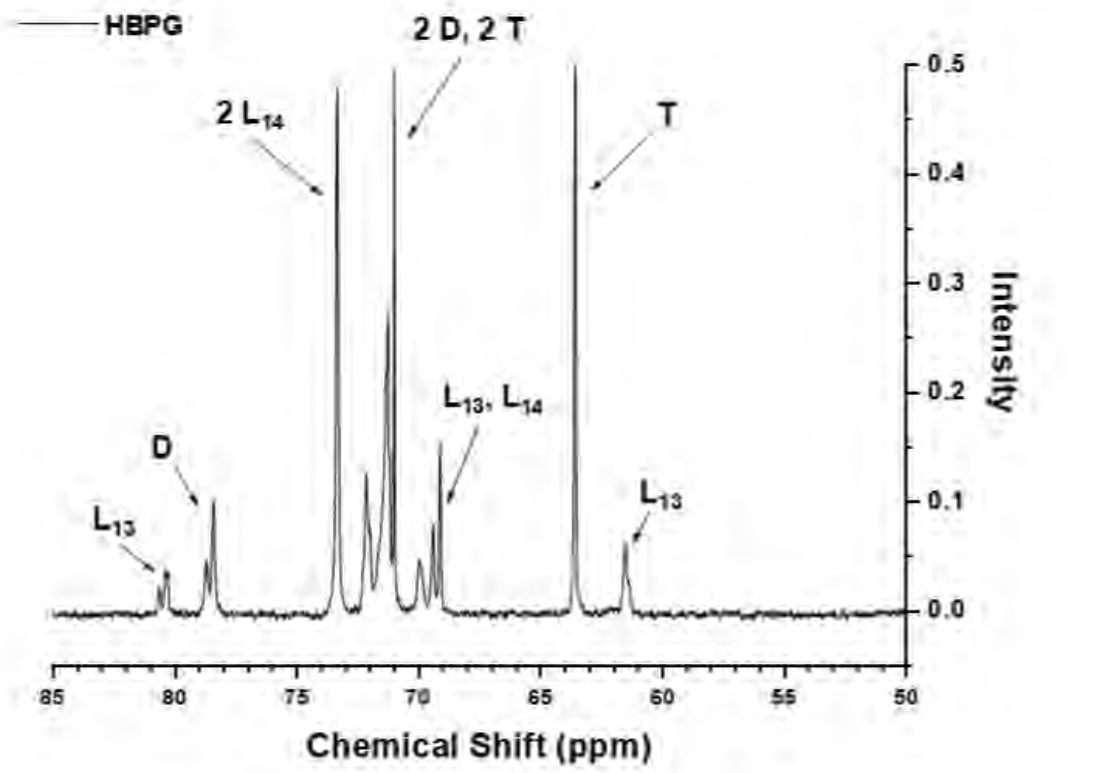

Figure 6.5. ^{13}C-NMR spectrum for the synthesized HBPG.

There are several characteristics peaks belonging to the carbons on branching units of synthesized HBPG in Figure 6.5. Carbons from L_{13} units are seen around 81, 69-70, and 61.5 ppm, while carbons from L_{14} units (a similar branching unit to L_{13}) are seen around 73.5, and 69-70 ppm. Dendritic branching unit carbons appear around 79 and 72 ppm, while terminal branching unit carbons appear around 72 ppm (like dendritic units) and 64 ppm. This, along with the proton peaks shown in Figure 6.4, point to a successful synthesis of HBPG.

Using the determined hydroxyl equivalent weight of the synthesized HBPG, the functionalization of free hydroxyl groups to acetoacetate groups was carried out using TBAA, high heat, and no catalyst.

The product was dried to remove as much solvent as possible and characterized using FT-IR, with the spectra being shown in Figure 6.6.

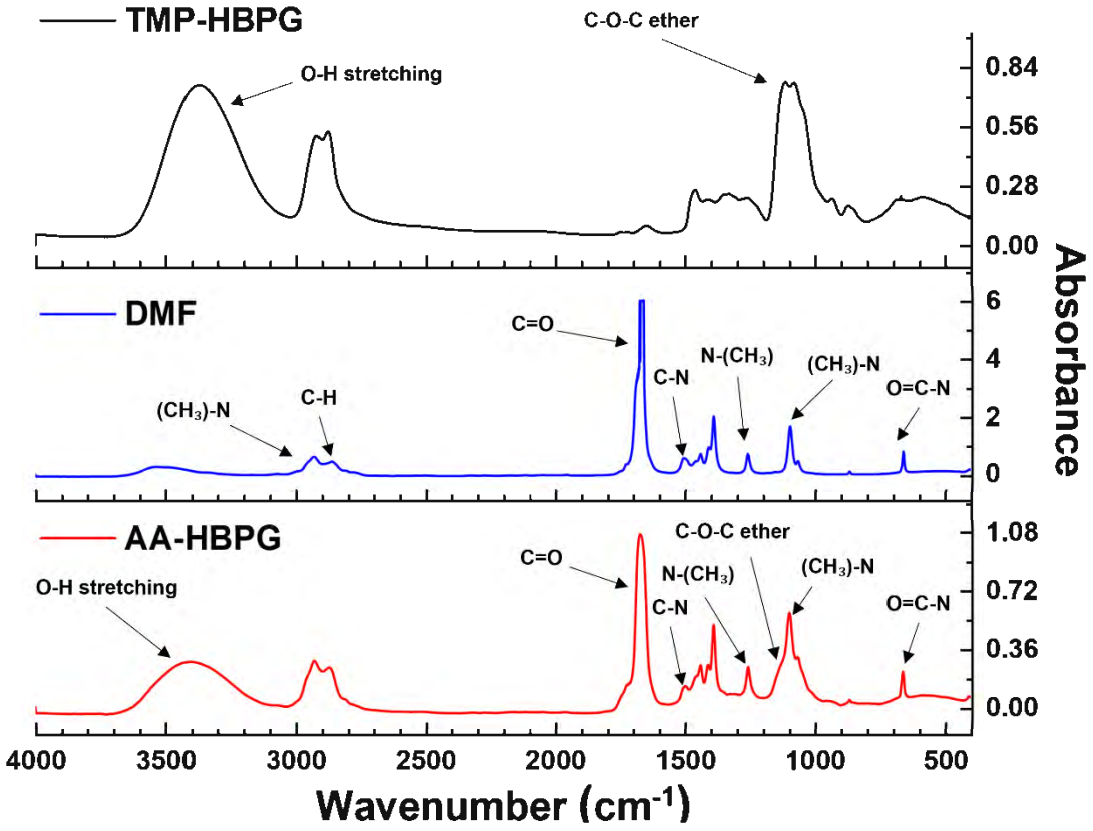

Figure 6.6. FT-IR spectra involving synthesized HBPG in black, with DMF (solvent used during synthesis) shown in blue, and the acetoacetylated HBPH shown in red.

FT-IR is helpful in identifying the presence of several functional groups after the acetoacetylation reaction of HBPG. In Figure 6.6, the C-O-C ether stretching seen around 1100 cm^{-1} points to the presence of branching units of HBPG in the acetoacetylated product. But this peak is not as prominent as in the plot for AA-HBPG. Additionally, there is a reduction in the hydroxyl peak seen around 3400 cm^{-1}, which gives insight into a potentially incomplete conversion as a near 100% conversion would entail the disappearance of this peak. The spectrum for DMF was included to determine the appearance of new peaks seen in the AA-HBPG spectrum versus the HBPG peaks. As is shown in Figure 6.6, peaks corresponding to vibrations of groups (CH_3)-N, C-H, C=O, C-N, and O=C-N around 2929, 1256, 1091, 865, 2875, 1685, 1502, and 659 cm^{-1} respectively. These same characteristic peaks for DMF can be seen in the AA-HBPG spectrum. This observation, along with the still significant OH signal, could mean that

there was incomplete acetoacetylation of the free hydroxyl groups. Overall, FT-IR spectra detailed the presence of these functional groups, but more detailed characterization such as ^{1}H-NMR and ^{13}C-NMR are needed to confirm this observation.

Spectra gathered from ^{1}H-NMR experiments were useful in determining if acetoacetate groups had been incorporated into HBPG and can be shown in Figure 6.7.

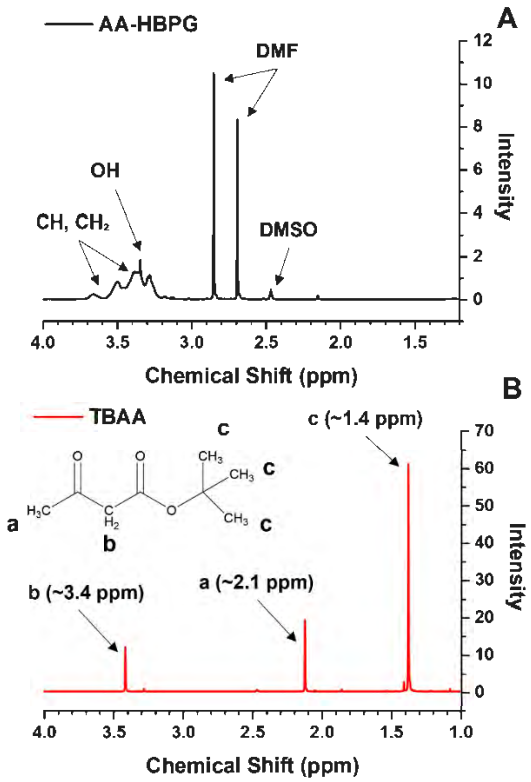

Figure 6.7. ^{1}H-NMR spectra analyzing the functionalization of HBPG with acetoacetate. A) Peaks associated with the methylene, methine, and potential acetoacetate protons of AA-HBPG in black. B) Peaks associated with the protons from the two chemical environments for methyl, and the methylene proton peaks for TBAA in red.

In 6.7A, we can see the proton peaks associated with the AA-HBPG, which still contains the methylene and methine protons from branching units of HBPG around 3.2-3.7 ppm. In addition, there is still a significant proton peak from the hydroxyl group of HBPG shown around 3.5 ppm. This helps confirm what was shown in the FT-IR spectra in Figure 6.6, where there was a significant hydroxyl signal, which could be due to incomplete conversion for the acetoacetylation of HBPG. While acetoacetate species undergo keto-enol tautomerism, where the enol form contains a hydroxyl proton, the proton for the hydroxyl group in AA-HBPG is almost identical to the peak seen for HBPG in Figure 6.4. In 6.7B, the

protons associated with TBAA are shown. There are three sharp sets of peaks that appear at 3.4 (b), 2.1 (a), and 1.4 (c) ppm. Looking at the spectra in 6.7A for comparison, there doesn't appear to be any peak associated with protons from the methyl groups (c, 1.4 ppm) on the butyl group of TBAA. This is promising as any remnant of this signal would likely mean an incomplete transesterification of acetoacetate. In addition, there doesn't appear to be a significant sign of the (a) and (b) protons from the acetoacetate group around 2.1 and 3.4 ppm respectively. However, there were two very prominent peaks associated with the solvent DMF around 2.7 and 2.9 ppm. This helps to confirm that there is a significant presence of DMF in the AA-HBPG mixture. Carbon NMR was also used in conjunction with these measurements to provide a more detailed picture on the incorporation of acetoacetate into HBPG.

Carbon NMR spectra gathered for TBAA and AA-HBPG are shown below in Figure 6.8. The six peaks from the carbons in TBAA are shown in 6.8A. Here, the methyl carbon furthest from the tert-Butyl group (a) shows up around 30 ppm. The next carbons of interest are the keto-ester carbons from the carbonyl groups (b and d), which appear around 201 ppm and 167 ppm respectively. The carbon of the methylene group between carbonyls is seen around 52 ppm, with the quaternary carbon of the tert-Butyl group being located around 82 ppm. Lastly, the methyl groups of the tert-Butyl group appear around 28 ppm. In 6.8B, the spectrum for AA-HBPG is shown. Here, peaks corresponding to the branching unit carbons can be clearly seen between 61.5-81 ppm. The quaternary carbon is also shown around 40 ppm, providing evidence that the hyperbranched structure, with incorporated initiator is still intact. However, peaks that correspond to the acetoacetate group are now shown. Instead, the characteristic peaks for the solvent DMF are clearly seen around 162, 36, and 31 ppm. Perhaps the most significant carbon peak that was expected is the methylene carbon (c) between the carbonyl carbons. If this peak was present around 52 ppm, it would provide evidence to the incorporation of the acetoacetate group into the HBPG. In summary, spectra obtained *via* FT-IR, ^{1}H-NMR, and ^{13}C-NMR point to an unsuccessful acetoacetylation of the HBPG. It is possible that during the reaction, the mixture was heated too aggressively, for too long, which lead to boiling off TBAA, which explains its absence in these spectra. Also, if there was an incomplete, or inability for the TBAA to react with hindered hydroxyls, the process of removing excess solvent could also remove TBAA from the mixture as its boiling point is significantly lower than that of DMF.

Conclusion

In this work, a hyperbranched polyglycerol (HBPG) was synthesized *via* ring-opening multi-branching polymerization (ROMBP) using trimethylolpropane (TMP) as initiator, and glycidol as the monomer. After characterization utilizing hydroxyl equivalent weight titrations, FT-IR, ^{1}H-NMR, and ^{13}C-NMR, acetoacetylation of the free hydroxyl groups of HBPG was attempted using tert-Butyl acetoacetate. The spectroscopic methods were again utilized, and it was determined that there was an incomplete acetoacetylation of free hydroxyl groups. As this is work is in the beginning stages, there are several paths forward in generating these highly hydrophilic additives for use in FR marine coatings. The characterization of the HBPG could be expanded to include molecular weight determinations using MALDI-ToF techniques, as well as Gel Permeation Chromatography (GPC) or Vapor Pressure Osmometry (VPO). In addition to determining the molecular weight, MALDI-ToF can be utilized to confirm the successful incorporation of initiator, presence of macrocyclic impurities during ROMBP, as well as determine if oligomerization of the glycidol monomer had occurred. These techniques would provide the researcher with a better overall understanding of these HBPGs, facilitating the next step in the process, acetoacetylation of these polymers. To obtain these functionalized polymers, careful control of temperature during the acetoacetylation reactions, as well as different solvent combinations that do not undergo transesterification could be utilized to improve this process. Lastly, other characterization methods such as phosphorous NMR, concerned with quantification of the number of free hydroxyl groups, as well as determining acetoacetate functionality of these polymers could be employed to better understand the acetoacetylation reaction for these HBPGs.

References

1. Yebra, D. M.; Kiil, S. K.; Dam-Johansen, K., Antifouling Technology—Past, Present and Future Steps Towards Efficient and Environmentally Friendly Antifouling Coatings. *Prog. Org. Coat.* **2004,** *50* (2), 75.

2. Schultz, M. P.; Bendick, J. A.; Holm, E. R.; Hertel, W. M., Economic Impact of Biofouling on a Naval Surface Ship. *Biofouling* **2011,** *27* (1), 87.

3. Callow, M. E.; Callow, J. A., Marine Biofouling: A Sticky Problem. *Biologist* **2002,** *49* (1), 10.

4. Drake, J. M.; Lodge, D. M., Hull fouling is a risk factor for intercontinental species exchange in aquatic ecosystems. *Aquatic Invasions* **2007,** *2* (2), 121-131.

5. Lejars, M.; Margaillan, A.; Bressy, C., Fouling release coatings: a nontoxic alternative to biocidal antifouling coatings. *Chemical reviews* **2012,** *112* (8), 4347-4390.

6. Callow, J. A.; Callow, M. E., Trends in the development of environmentally friendly fouling-resistant marine coatings. *Nature Communications* **2011,** *2*, 244.

7. Hellio, C.; Yebra, D. M., *Advances in Marine Antifouling Coatings and Technologies*. 2009.

8. Konstantinou, I. K.; Albanis, T. A., Worldwide Occurrence and Effects of Antifouling Paint Booster Biocides in the Aquatic Environment: A Review. *Environ. Int.* **2004,** *30* (2), 235.

9. Ytreberg, E.; Karlsson, J.; Eklund, B., Comparison of toxicity and release rates of Cu and Zn from anti-fouling paints leached in natural and artificial brackish seawater. *Science of the Total Environment* **2010,** *408* (12), 2459-2466.

10. Matthiessen, P.; Reed, J.; Johnson, M., Sources and potential effects of copper and zinc concentrations in the estuarine waters of Essex and Suffolk, United Kingdom. *Marine Pollution Bulletin* **1999,** *38* (10), 908-920.

11. Amara, I.; Miled, W.; Slama, R. B.; Ladhari, N., Antifouling processes and toxicity effects of antifouling paints on marine environment. A review. *Environmental toxicology and pharmacology* **2018,** *57*, 115-130.

12. Lim, C. Y.; Yoo, Y. H.; Sidharthan, M.; Ma, C. W.; Bang, I. C.; Kim, J. M.; Lee, K. S.; Park, N. S.; Shin, H., Effects of copper(I) oxide on growth and biochemical compositions of two marine microalgae. *Journal of Environmental Biology* **2006,** *27* (3), 461-466.

13. Magin, C. M.; Cooper, S. P.; Brennan, A. B., Non-Toxic Antifouling Strategies. *Mater. Today* **2010,** *13* (4), 36.

14. Watermann, B.; Berger, H. D.; Sönnichsen, H.; Willemsen, P., Performance and effectiveness of non-stick coatings in seawater. *Biofouling* **1997,** *11* (2), 101-118.

15. Sommer, S.; Ekin, A.; Webster, D. C.; Stafslien, S. J.; Daniels, J.; VanderWal, L. J.; Thompson, S. E. M.; Callow, M. E.; Callow, J. A., A Preliminary Study on the Properties and Fouling-Release Performance of Siloxane-Polyurethane Coatings Prepared from Pdms Macromers. *Biofouling* **2010,** *26* (8), 961.

16. Bodkhe, R. B.; Thompson, S. E. M.; Yehle, C.; Cilz, N.; Daniels, J.; Stafslien, S. J.; Callow, M. E.; Callow, J. A.; Webster, D. C., The Effect of Formulation Variables on Fouling-Release Performance of Stratified Siloxane-Polyurethane Coatings. *Journal of Coatings Technology Research* **2012,** *9* (3), 235.

17. Finlay, J. A.; Callow, M. E.; Ista, L. K.; Lopez, G. P.; Callow, J. A., The Influence of Surface Wettability on the Adhesion Strength of Settled Spores of the Green Alga Enteromorpha and the Diatom Amphora. *Integr. Comp. Biol.* **2002,** *42* (6), 1116.

18. Holland, R.; Dugdale, T. M.; Wetherbee, R.; Brennan, A. B.; Finlay, J. A.; Callow, J. A.; Callow, M. E., Adhesion and Motility of Fouling Diatoms on a Silicone Elastomer. *Biofouling* **2004,** *20* (6), 323.

19. Galli, G.; Martinelli, E., Amphiphilic polymer platforms: surface engineering of films for marine antibiofouling. *Macromolecular rapid communications* **2017,** *38* (8), 1600704.

20. Leonardi, A. K.; Ober, C. K., Polymer-based marine antifouling and fouling release surfaces: strategies for synthesis and modification. *Annual review of chemical and biomolecular engineering* **2019,** *10*, 241-264.

21. Pade, M.; Webster, D. C., Self-stratified siloxane-polyurethane fouling-release marine coating strategies: A review. Central West Publishing: Australia: 2019; pp 1-36.

22. Rosenhahn, A.; Schilp, S.; Kreuzer, H. J.; Grunze, M., The role of “inert” surface chemistry in marine biofouling prevention. *Physical Chemistry Chemical Physics* **2010,** *12* (17), 4275-4286.

23. Iguerb, O.; Poleunis, C.; Mazéas, F.; Compère, C.; Bertrand, P., Antifouling Properties of Poly(methyl methacrylate) Films Grafted with Poly(ethylene glycol) Monoacrylate Immersed in Seawater. *Langmuir* **2008,** *24* (21), 12272-12281.

24. Lin, X.; Xie, Q.; Ma, C.; Zhang, G., Self-healing, highly elastic and amphiphilic silicone-based polyurethane for antifouling coatings. *Journal of Materials Chemistry B* **2021,** *9* (5), 1384-1394.

25. Yi, L.; Xu, K.; Xia, G.; Li, J.; Li, W.; Cai, Y., New protein-resistant surfaces of amphiphilic graft copolymers containing hydrophilic poly (ethylene glycol) and low surface energy fluorosiloxane side-chains. *Applied Surface Science* **2019,** *480*, 923-933.

26. Yu, W.; Wanka, R.; Finlay, J. A.; Clarke, J. L.; Clare, A. S.; Rosenhahn, A., Degradable hyaluronic acid/chitosan polyelectrolyte multilayers with marine fouling-release properties. *Biofouling* **2020,** *36* (9), 1049-1064.

27. Koschitzki, F.; Wanka, R.; Sobota, L.; Gardner, H.; Hunsucker, K. Z.; Swain, G. W.; Rosenhahn, A., Amphiphilic Zwitterionic Acrylate/Methacrylate Copolymers for Marine Fouling-Release Coatings. *Langmuir* **2021,** *37* (18), 5591-5600.

28. Barry, M. E.; Davidson, E. C.; Zhang, C.; Patterson, A. L.; Yu, B.; Leonardi, A. K.; Duzen, N.; Malaviya, K.; Clarke, J. L.; Finlay, J. A., The role of hydrogen bonding in peptoid-based marine antifouling coatings. *Macromolecules* **2019,** *52* (3), 1287-1295.

29. Benda, J.; Stafslien, S.; Vanderwal, L.; Finlay, J. A.; Clare, A. S.; Webster, D. C., Surface modifying amphiphilic additives and their effect on the fouling-release performance of siloxane-polyurethane coatings. *Biofouling* **2021**, 1-18.

30. Rahimi, A.; Stafslien, S. J.; Vanderwal, L.; Finlay, J. A.; Clare, A. S.; Webster, D. C., Amphiphilic zwitterionic-PDMS-based surface-modifying additives to tune fouling-release of siloxane-polyurethane marine coatings. *Progress in Organic Coatings* **2020,** *149*, 105931.

31. Nurioglu, A. G.; Esteves, A. C. C., Non-toxic, non-biocide-release antifouling coatings based on molecular structure design for marine applications. *Journal of Materials Chemistry B* **2015,** *3* (32), 6547-6570.

32. Andrade, J. D.; King, R. N.; Gregonis, D. E.; Coleman, D. L. In *Surface characterization of poly (hydroxyethyl methacrylate) and related polymers. I. Contact angle methods in water*, 1979; Wiley Online Library: pp 313-336.

33. Heuberger, M.; Drobek, T.; Spencer, N. D., Interaction forces and morphology of a protein-resistant poly (ethylene glycol) layer. *Biophysical journal* **2005,** *88* (1), 495-504.

34. Jeon, S.; Lee, J.; Andrade, J.; De Gennes, P., Protein—surface interactions in the presence of polyethylene oxide: I. Simplified theory. *Journal of colloid and interface science* **1991,** *142* (1), 149-158.

35. Rufin, M. A.; Ngo, B. K. D.; Barry, M. E.; Page, V. M.; Hawkins, M. L.; Stafslien, S. J.; Grunlan, M. A., Antifouling silicones based on surface-modifying additive amphiphiles. *Green Materials* **2017,** *5* (1), 4-13.

36. Gudipati, C. S.; Greenlief, C. M.; Johnson, J. A.; Prayongpan, P.; Wooley, K. L., Hyperbranched fluoropolymer and linear poly (ethylene glycol) based amphiphilic crosslinked networks as efficient antifouling coatings: an insight into the surface compositions, topographies, and morphologies. *Journal of Polymer Science Part A: Polymer Chemistry* **2004,** *42* (24), 6193-6208.

37. Galhenage, T. P.; Webster, D. C.; Moreira, A. M. S.; Burgett, R. J.; Stafslien, S. J.; Vanderwal, L.; Finlay, J. A.; Franco, S. C.; Clare, A. S., Poly (ethylene) glycol-modified, amphiphilic, siloxane–polyurethane coatings and their performance as fouling-release surfaces. *Journal of Coatings Technology and Research* **2017,** *14* (2), 307-322.

38. Su, X.; Yang, M.; Hao, D.; Guo, X.; Jiang, L., Marine antifouling coatings with surface topographies triggered by phase segregation. *Journal of Colloid and Interface Science* **2021,** *598*, 104-112.

39. Shang, D.; Sun, X.; Shen, X.; Hang, J.; Jin, L.; Shi, L., Effects of PEG-TMS on the stability and antifouling performances of hydrocarbon-modified amphiphilic xerogel coatings. *Progress in Organic Coatings* **2018,** *121*, 142-150.

40. Camós Noguer, A.; Olsen, S. M.; Hvilsted, S.; Kiil, S., Long-term stability of PEG-based antifouling surfaces in seawater. *Journal of Coatings Technology and Research* **2016,** *13* (4), 567-575.

41. Han, S.; Kim, C.; Kwon, D., Thermal/oxidative degradation and stabilization of polyethylene glycol. *Polymer* **1997,** *38* (2), 317-323.

42. Abbina, S.; Vappala, S.; Kumar, P.; Siren, E. M.; La, C. C.; Abbasi, U.; Brooks, D. E.; Kizhakkedathu, J. N., Hyperbranched polyglycerols: recent advances in synthesis, biocompatibility and biomedical applications. *Journal of Materials Chemistry B* **2017,** *5* (47), 9249-9277.

43. Jafari, M.; Abolmaali, S. S.; Najafi, H.; Tamaddon, A. M., Hyperbranched polyglycerol nanostructures for anti-biofouling, multifunctional drug delivery, bioimaging and theranostic applications. *International Journal of Pharmaceutics* **2020,** *576*, 118959.

44. An, X.; Zhang, K.; Wang, Z.; Ly, Q. V.; Hu, Y.; Liu, C., Improving the water permeability and antifouling property of the nanofiltration membrane grafted with hyperbranched polyglycerol. *Journal of Membrane Science* **2020,** *612*, 118417.

45. Andrade, B.; Knewstub, S. N.; Harris, K.; Tucker, C. J.; Katz, J. S.; Zimmerman, S. C., Nonionic surfactant properties of amphiphilic hyperbranched polyglycerols. *Langmuir* **2020,** *36* (34), 10103-10109.

46. Chen, P.-R.; Wang, T.-C.; Chen, S.-T.; Chen, H.-Y.; Tsai, W.-B., Development of antifouling hyperbranched polyglycerol layers on hydroxyl poly-p-xylylene coatings. *Langmuir* **2017,** *33* (51), 14657-14662.

47. Siegers, C.; Biesalski, M.; Haag, R., Self-assembled monolayers of dendritic polyglycerol derivatives on gold that resist the adsorption of proteins. *Chemistry–A European Journal* **2004,** *10* (11), 2831-2838.

48. Sunder, A.; Mülhaupt, R.; Haag, R.; Frey, H., Hyperbranched polyether polyols: a modular approach to complex polymer architectures. *Advanced Materials* **2000,** *12* (3), 235-239.

49. Pranantyo, D.; Xu, L. Q.; Neoh, K. G.; Kang, E.-T.; Teo, S. L.-M., Antifouling coatings via tethering of hyperbranched polyglycerols on biomimetic anchors. *Industrial & Engineering Chemistry Research* **2016,** *55* (7), 1890-1901.

50. Kulka, M. l. W.; Donskyi, I. S.; Wurzler, N.; Salz, D.; Özcan, O. z.; Unger, W. E.; Haag, R., Mussel-inspired multivalent linear polyglycerol coatings outperform monovalent polyethylene glycol coatings in antifouling surface properties. *ACS Applied Bio Materials* **2019,** *2* (12), 5749-5759.

51. Wanka, R.; Aldred, N.; Finlay, J. A.; Amuthalingam, A.; Clarke, J. L.; Clare, A. S.; Rosenhahn, A., Antifouling properties of dendritic polyglycerols against marine macrofouling organisms. *Langmuir* **2019,** *35* (50), 16568-16575.

52. Kawai, F., Microbial degradation of polyethers. *Applied Microbiology and Biotechnology* **2002,** *58* (1), 30-38.

53. Bernhard, M.; Eubeler, J. P.; Zok, S.; Knepper, T. P., Aerobic biodegradation of polyethylene glycols of different molecular weights in wastewater and seawater. *Water Research* **2008,** *42* (19), 4791-4801.

54. Sunder, A.; Hanselmann, R.; Frey, H.; Mülhaupt, R., Controlled synthesis of hyperbranched polyglycerols by ring-opening multibranching polymerization. *Macromolecules* **1999,** *32* (13), 4240-4246.

55. Krall, E. M.; Serum, E. M.; Sibi, M. P.; Webster, D. C., Catalyst-free lignin valorization by acetoacetylation. Structural elucidation by comparison with model compounds. *Green Chemistry* **2018,** *20* (13), 2959-2966.

CHAPTER 7. OVERALL CONCLUSIONS AND FUTURE WORK

In this dissertation, much of the work was concerned with the use of surface modifying amphiphilic additives (SMAAs) to generate amphiphilic surfaces to improve broad spectrum fouling-release (FR) performance in coatings intended for use in a marine environment. Several established coating systems, making use of a self-stratifying siloxane-polyurethane (SiPU), were considered as 'vehicles' for these additives. In addition, more fundamental aspects of how these SMAAs interacted with base coatings systems such as a pure polyurethane (PU) were explored, providing a framework of study that could be applied to a wide variety of other SMAAs and next generation FR coating systems. Lastly, work was performed to address the issue of marine biofouling of oil boom fabrics, used to contain oil spills surrounding ships in harbor. Several coating systems were investigated, including the well-established SiPU formulation A4-20, to assess their adhesion and performance on several different kinds of fabrics. This work is one of the first examples of expanding the techniques and coatings systems used throughout this dissertation to surfaces other than the hulls of ocean-going vessels.

As detailed in Chapter 2, non-reactive surface modifying amphiphilic additives (SMAA) were incorporated into a previously developed SiPU formulation (A4-20) to improve broad spectrum FR properties. These additives were synthesized *via* hydrosilylation between various polymethylhydrosiloxanes (PMHS), and allyl terminated polyethylene glycol monomethyl ethers (APEG). A total of twenty-four different SMAAs were synthesized which included variations in PEG chain grafting density through changes in co-polymer architecture (fully grafted comb-like, partially grafted, star copolymer), as well as variations in PDMS backbone molecular weight and grafted PEG chain molecular weight. Coatings were prepared by incorporating these additives at 1, 5, and 10 wt.% concentrations in A4-20 SiPU. These formulations were then evaluated in a set of AF/FR biological screening assays using marine bacterium *Cellulophaga lytica* and marine diatom *Navicula incerta*. Several formulations with varying amount, and type, of SMAA were selected for further surface characterization, as well as AF/FR biological assays involving macroalgae *Ulva linza*, marine barnacle *Amphibalanus amphitrite*, and marine mussel *Geukensia demissa*. Surface analysis utilizing water and methylene iodide contact angle (WCA/MICA) analysis showed that incorporation of SMAAs was able to modify the surface energy characteristics, with formulations containing SMAAs with the lowest molecular weights of PEG chains

introduces the most significant changes. AFM was also performed in the dry and hydrated state (imaged under a drop of deionized water) for these selected formulations to determine the presence of PDMS and PEG domains on the surface. It was shown that the incorporation of these SMAAs induced significant surface morphological changes in the dry state when compared to the control A4-20 formulation. In the hydrated state, these surfaces experienced even greater differences in phase and height images, largely due to the rearrangement and 'swelling' of PEG chains from the additives. Consequently, the formulations which contained SMAAs having the highest molecular weights of grafted PEG chains, as well as having the lowest grafting density, brought about the largest change in surface morphology. Lastly, biological assays involving micro- and macrofoulants *C. lytica*, *N. incerta*, *U. linza*, *A. amphitrite*, and *G. demissa* were performed on selected formulations. Overall, several formulations displayed improved AF/FR properties compared to control A4-20, performing comparable to commercial FR standard Intersleek® 1100SR, with broad-spectrum performance seen in formulations that had the highest molecular weight of PEG chains at 750 g/mol, with varying grafted chain density. As shown through both surface characterization and AF/FR biological assays, the ability of SMAA to diffuse through the coating to the surface, coupled with higher molecular weight PEG chains, were two of the most influential factors in generating an amphiphilic coating surface with good AF/FR performance.

As this was a rather large set of formulations to screen (~72), there are several paths that can be taken to further refine this investigation of using SMAAs in a traditionally hydrophobic SiPU. There could be further investigation into the architecture of the additive, and how it affects several of the properties discussed. Interestingly, the SMAA which contained 750 g/mol PEG chains, grafted to the hydride functional cyclosiloxane, D4H, showed excellent AF/FR properties, despite having very little relative siloxane content overall. It is thought that due to the star co-polymer structure, this would affect how these additives associate with themselves, and the different phases within the siloxane-polyurethanes. Work can be focused on how the variations in additive structure affect its diffusion through the coating bulk, as well as determining the amount of additive that is extracted from various coating systems. Also, there could be further investigation into synthesizing these types of additives with both PEG and PDMS chains grafted to siloxane backbones. Introducing these PDMS chains into the additive could significantly affect how they are dispersed within the coating matrix, affecting several surface and AF/FR properties. Lastly,

a study could be designed to explore how blends of SMAA types, even including different co-polymer structures such as di-block, or tri-block additives, could affect the properties of these traditional FR coating systems.

The observations of improved AF/FR performance in systems involving incorporation of SMAAs into a hydrophobic SiPU prompted an investigation into how these additives interacted with an inherently amphiphilic coating matrix. In Chapter 3, a selected SMAA with a siloxane backbone partially grafted with PEG chains of 350 g/mol was incorporated into a previously developed amphiphilic SiPU. This coating matrix was made by reacting an isocyanate pre-polymer with carbinol-terminated PDMS and hydroxy-terminated PEG, and then reacting this further with additional isocyanate and acrylic polyol to form a self-stratifying amphiphilic SiPU. The concentrations of PDMS and PEG in the pre-polymer were varied, along with formulations containing 5 and 10 wt.% of SMAA relative to total formulation solids weight. Several surface characterization methods such as dynamic WCA/MICA/SE measurements, ATR-FTIR, and AFM showed that significant changes in surface activity (increase and decreases in surface energy over time) and surface morphology occurred when the ratio of PDMS and PEG was changed in the pre-polymer. In addition, the incorporation of increasing amounts of SMAA significantly affected these properties as well, producing surfaces with a highly heterogenous character. Biological assays utilizing the model organisms *C. lytica*, *N. incerta*, *U. linza*, *A. amphitrite*, and *G. demissa* were performed and several coatings formulations were identified that had significantly better FR performance than the control amphiphilic SiPU, as well as performing comparable or better than commercial FR standards such as Intersleek® 900 and Intersleek® 1100SR. In addition, nearly each coating formulation that had either 5 or 10 wt.% of SMAA showed a spontaneous release of *U. linza* sporelings before removal assays. Overall, it was shown that the incorporation of SMAA, even at a concentration of 5 wt.%, has the largest effect on decreases adhesion strength across all fouling organisms studied, providing broad-spectrum FR performance with these formulations. In addition, it was observed that as the pre-polymer composition consisted solely of PEG, FR performance decreased significantly, with organisms such as *A. amphitrite*, and *G. demissa*, adhering strongly to these surfaces.

Some future directions for the work performed in Chapter 3 includes the continued investigation of using SMAAs in this coating system. There are several different additives that were synthesized in a

previous study that could be applied to this system. The one chosen for the current study however, only contained partially grafted backbones of siloxane with PEG chains of 350 g/mol. An interesting set of additives would be those with star co-polymer architecture, or those with siloxane backbones and PEG chains with higher molecular weights. In addition, other hydrophobic and hydrophilic polymers could be used during pre-polymer synthesis and compared to that of PDMS and PEG. Methods to synthesize phenylmethyl siloxane co-polymers with functional groups suitable for reaction between isocyanates, as well as utilizing polysulfobetaine/carboxybetaine or polyvinylpyrrolidone in pre-polymers could be explored. In general, future work should be concerned with more in-depth studies of additive and coating matrix interactions, and how these produce heterogenous domains of varying size and complexity.

The work performed in Chapter 4 was done to study the fundamental aspects of how SMAAs interact with a purely polyurethane coating matrix, as well of their FR performance towards several model organisms. The additive used consisted of a siloxane backbone around 2000 g/mol, with ~15-18 mol% consisting of methylhydrosiloxane (MHS) repeat units used for grafting of PEG chains of 750 g/mol. Formulations were made with varying concentrations of SMAA, with the highest being >20 wt.% relative to total formulation weight solids. A variety of surface characterization techniques were utilized to study these coatings systems. Dynamic WCA/MICA/SE measurements were performed and showed that as the amount of additive increased, more significant increases in surface energy were seen, likely due to the higher amount of PEG containing additive at the surface. In addition, advancing and receding contact angle measurements showed that the contact angle hysteresis, commonly used to indicate surface heterogeneity, increased as the amount of SMAA increased. AFM images in the dry state also helped to confirm this heterogeneity as the domains of PDMS and PEG from the additive became larger and more irregular as the amount of additive increased in the coating's formulations. ATR-FTIR measurements showed that as the amount of additive was increased in the coatings, characteristic peaks pertaining to PDMS, and PEG increased in intensity as well. This observation was further supported *via* XPS measurements. TEM images were also obtained for these formulations, and it was shown that even at the lowest concentrations of additive, there were clear domains throughout the bulk of the coating. As the additive amount increased, these domains got significantly larger, potentially affecting coating physical properties. In fact, the adhesion, flexibility, chemical resistance, and other mechanical properties

decreased dramatically as the amount of additive was increased. This is an unfortunate side effect of using these additives in a purely polyurethane coating as severe coating damage could occur while in marine environments. In terms of FR performance, nearly all the coatings showed significantly lower biomass remaining than the control PU after water jetting was performed for adhesion assays involving *C. lytica*, *N. incerta*, and *U. linza*. These coatings performed especially well against the marine diatom *N. incerta*, showing almost complete removal, which is surprising considering the amount of PDMS at the surfaces of these coatings, which these organisms prefer.

A potential continuation study for this work could be to incorporate several different classes of additives such as PDMS/PEG, zwitterionic, or hydrophobic phenylmethyl containing silicone oils into a polyurethane coating to compare the surface properties and physical coatings properties. This could also be applied to comparing several different coating chemistries like silicone elastomers, epoxy-urethane coatings, or other traditionally non-FR coating systems, focusing on one type of additive. Investigating the diffusion of these additives through the coating system, as well as the formation of lubrication layers and leachability into a marine environment is a much-needed next step for developing SMAAs. These types of studies could provide a robust set of data that can help with identifying which surface modifying additive works best with several different coatings systems to optimize both coating and FR performance over long time periods.

The study in Chapter 5 involved the investigation of adhesion, as well as long-term cleanability performance for several FR coating compositions on various oil boom fabrics. These oil boom containment systems are primarily used to prevent the oil leakage from ships in harbor from escaping into the local marine environment, facilitating clean-up. This work is a departure from the typical application of these coatings to metal substrates, and as such, methods to improve adhesion to these fabrics were explored. Initially, ATR-FTIR and WCA/MICA/SE determinations were performed on five different uncoated oil boom fabrics. It was found that three of the substrates consisted of polyurethane impregnated polyester fibers, with two of them being composed of polyvinyl chloride impregnated fibers. Surface energy values varied greatly between these types of fabrics. In addition, two of the polyurethane type fabrics were textured, which also displayed large differences in SE between smooth and textured substrates. These variations have the potential to greatly affect the spreading and adhesion of the

investigated coatings in this work. The coatings chosen for this work included the siloxane-polyurethane A4-20, Intersleek® commercial FR tie-coat, and Hempasil® commercial FR tie-coat. There were five different chlorinated polyolefin adhesion promoters used as a primer layer for small sample adhesion testing, as well as sandblasting and corona surface treatments. After preparing small 2” x 3” fabric samples for each treatment group, coated samples were subjected to water ageing for six months, with treatment groups removed in one-month intervals, with waterjet adhesion testing performed on these samples. It was observed that A4-20 displayed the best overall adhesion performance, likely due to its similar composition as the surfaces of the fabrics. The use of adhesion promoters did not seem to significantly affect the adhesion, with slight improvements of adhesion seen with samples that were sandblasted beforehand. Lastly, 6” x 24” samples were prepared for field testing at the Florida Institute of Technology testing site to access FR performance, as well as long-term adhesion properties. Textured and smooth polyurethane fabrics were coated with A4-20 and Hempasil® X3+ FR coating and were immersed in seawater for a total of eight months, with cleaning intervals at two, four, and six months. After the initial cleaning period, it was shown that coated samples had superior cleanability performance than control fabrics without either coating. Damage to the coated samples was seen on treatment groups consisting of Hempasil® X3+ on smooth substrates at the most aggressive cleaning protocols. After the third cleaning interval, these panels were removed due to severe coating delamination. A4-20 on the other hand, stood up well to cleaning with the most aggressive water pressures, but did experience some minor delamination after a period of six-months of immersion. Overall, the use of FR coatings on these oil boom fabrics was able to provide superior cleanability than oil boom fabrics alone.

Due to the extremely large sample set (~1440 small scale samples for adhesion testing), future studies would benefit from selecting a smaller set of factors to explore the adhesion and cleanability properties of coatings used for oil boom fabrics. It was determined that A4-20 performed well enough, but there were still issues with delamination as the samples were immersed in seawater. Going forward, a coating system could be developed to cater specifically to the needs of these oil boom fabric materials. A4-20 is still rigid as a FR coating, so incorporating components that would increase flexibility, while still providing a durable surface could be beneficial towards adhesion and cleanability performance. In

addition, these systems are meant for the containment of oil, but measurements of coating stability in the presence of these contaminants was not performed in this work and would be invaluable moving forward.

In the last section of work performed in this dissertation, Chapter 6 involves the continued exploration of novel surface modifying additives utilized to improve the AF/FR properties of several types of coatings systems. This introductory work investigated the synthesis of a highly hydrophilic hyperbranched polyglycerol (HBPG), and subsequent blocking of the free hydroxyl groups using acetoacetylation for use in a siloxane-polyurethane (SiPU) FR coating. Synthesis of HBPG was performed *via* ring-opening multi-branching polymerization (ROMBP) of glycidol, with partially deprotonated trimethylolpropane (TMP) as initiator. Hydroxyl content was determined with hydroxyl number titrations, with spectroscopic methods such as ^{1}H-NMR, ^{13}C-NMR, and FT-IR being used to confirm successful synthesis. It was observed that TMP was incorporated into the HBPG, with the typical branching units being characterized utilizing NMR techniques. Acetoacetylation was performed at 140℃, with no catalyst, and was considered complete when no more t-butanol was collected. The spectroscopic methods were utilized to determine the extent of functionalization with acetoacetate groups. While the structure of HBPG was preserved after this reaction, there was insufficient evidence to support a successful transformation of hydroxyl groups to acetoacetate functionality. It is thought that the highly complex structure could make it more difficult for the tert-butyl acetoacetate (TBAA) to access the hindered hydroxyls. In addition, the solvent used during this reaction was dimethylformamide (DMF), which has a much higher boiling point than TBAA and could potentially interfere with this reaction. There are several characterization techniques and different approaches that can be tried to obtain a higher conversion of HBPG to AA-HBPG. Molecular weight determination could be performed such as MALDI-ToF, GPC, or Vaper Pressure Osmometry (VPO), which would provide a clearer picture of HBPG synthesis by determining presence of macrocyclic impurities, or oligomerization of glycidol monomer. Phosphorous NMR techniques could be utilized to determine content of hydroxyl groups, as well as extent of acetoacetylation. Also, different process conditions could be studied to determine the best combination of solvent, temperature, or potential catalyst to use for a successful acetoacetylation of HBPG. Overall, this work is unfinished and provides ample opportunity for others to continue this unique avenue of developing a novel surface modifying additive for use in FR coatings.

In conclusion, the work performed in this dissertation demonstrated that the design and usage of surface modifying amphiphilic additives (SMAA) based off PDMS and PEG could produce an enhanced amphiphilic and heterogeneous FR coating surface utilizing several different common coatings systems. It was shown that depending on the type of SMAA used, and to what coating it was incorporated in (hydrophobic, amphiphilic, polyurethane), FR performance against several model marine fouling organisms was greatly affected. The abundance of data on the surface and AF/FR properties of these systems utilizing these SMAAs provides a very robust knowledge base for further advancing the fight against marine biofouling. It is the desire for this author to have future research directions firmly establish the more fundamental aspects of how these heterogenous surfaces come about, with less focus on developing a ‘product’, and more on developing processes which make identifying promising approaches to this issue clearer to the scientific community.

APPENDIX A. CHAPTER 2 SUPPLEMENTAL INFORMATION

Experimental Formulations

Table A1. 72 formulated coatings before use in *C. lytica* and *N. incerta* biological assays

Formulation #	Sample ID	Siloxane Backbone	PEG M.W. g/mol	Wt. % Additive
1	991-g-250-1%	HMS-991	250	1
2	991-g-250-5%	HMS-991	250	5
3	991-g-250-10%	HMS-991	250	10
4	992-g-250-1%	HMS-992	250	1
5	992-g-250-5%	HMS-992	250	5
6	992-g-250-10%	HMS-992	250	10
7	993-g-250-1%	HMS-993	250	1
8	993-g-250-5%	HMS-993	250	5
9	993-g-250-10%	HMS-993	250	10
10	301-g-250-1%	HMS-301	250	1
11	301-g-250-5%	HMS-301	250	5
12	301-g-250-10%	HMS-301	250	10
13	501-g-250-1%	HMS-501	250	1
14	501-g-250-5%	HMS-501	250	5
15	501-g-250-10%	HMS-501	250	10
16	D'4-g-250-1%	D'4	250	1
17	D'4-g-250-5%	D'4	250	5
18	D'4-g-250-10%	D'4	250	10
19	991-g-350-1%	HMS-991	350	1
20	991-g-350-5%	HMS-991	350	5
21	991-g-350-10%	HMS-991	350	10
22	992-g-350-1%	HMS-992	350	1
23	992-g-350-5%	HMS-992	350	5
24	992-g-350-10%	HMS-992	350	10
25	993-g-350-1%	HMS-993	350	1
26	993-g-350-5%	HMS-993	350	5
27	993-g-350-10%	HMS-993	350	10
28	301-g-350-1%	HMS-301	350	1
29	301-g-350-5%	HMS-301	350	5
30	301-g-350-10%	HMS-301	350	10
31	501-g-350-1%	HMS-501	350	1
32	501-g-350-5%	HMS-501	350	5
33	501-g-350-10%	HMS-501	350	10
34	D'4-g-350-1%	D'4	350	1
35	D'4-g-350-5%	D'4	350	5
36	D'4-g-350-10%	D'4	350	10
37	991-g-750-1%	HMS-991	750	1
38	991-g-750-5%	HMS-991	750	5
39	991-g-750-10%	HMS-991	750	10
40	992-g-750-1%	HMS-992	750	1
41	992-g-750-5%	HMS-992	750	5
42	992-g-750-10%	HMS-992	750	10
43	993-g-750-1%	HMS-993	750	1
44	993-g-750-5%	HMS-993	750	5
45	993-g-750-10%	HMS-993	750	10
46	301-g-750-1%	HMS-301	750	1

Table A1. 72 formulated coatings before use in *C. lytica* and *N. incerta* biological assays (continued)

Formulation #	Sample ID	Siloxane Backbone	PEG M.W. g/mol	Wt. % Additive
47	301-g-750-5%	HMS-301	750	5
48	301-g-750-10%	HMS-301	750	10
49	501-g-750-1%	HMS-501	750	1
50	501-g-750-5%	HMS-501	750	5
51	501-g-750-10%	HMS-501	750	10
52	D'4-g-750-1%	D'4	750	1
53	D'4-g-750-5%	D'4	750	5
54	D'4-g-750-10%	D'4	750	10
55	991-g-1100-1%	HMS-991	1100	1
56	991-g-1100-5%	HMS-991	1100	5
57	991-g-1100-10%	HMS-991	1100	10
58	992-g-1100-1%	HMS-992	1100	1
59	992-g-1100-5%	HMS-992	1100	5
60	992-g-1100-10%	HMS-992	1100	10
61	993-g-1100-1%	HMS-993	1100	1
62	993-g-1100-5%	HMS-993	1100	5
63	993-g-1100-10%	HMS-993	1100	10
64	301-g-1100-1%	HMS-301	1100	1
65	301-g-1100-5%	HMS-301	1100	5
66	301-g-1100-10%	HMS-301	1100	10
67	501-g-1100-1%	HMS-501	1100	1
68	501-g-1100-5%	HMS-501	1100	5
69	501-g-1100-10%	HMS-501	1100	10
70	D'4-g-1100-1%	D'4	1100	1
71	D'4-g-1100-5%	D'4	1100	5
72	D'4-g-1100-10%	D'4	1100	10

Table A2. Formulations able to be used for *C. lytica* and *N. incerta* biological assays

Formulation #	Sample ID	Siloxane Backbone	PEG M.W. g/mol	Wt. % Additive
1	991-g-250-1%	HMS-991	250	1
2	991-g-250-5%	HMS-991	250	5
3	991-g-250-10%	HMS-991	250	10
4	992-g-250-1%	HMS-992	250	1
5	992-g-250-5%	HMS-992	250	5
6	992-g-250-10%	HMS-992	250	10
7	993-g-250-1%	HMS-993	250	1
8	993-g-250-5%	HMS-993	250	5
9	993-g-250-10%	HMS-993	250	10
10	301-g-250-1%	HMS-301	250	1
11	301-g-250-5%	HMS-301	250	5
12	301-g-250-10%	HMS-301	250	10
13	501-g-250-1%	HMS-501	250	1
14	501-g-250-5%	HMS-501	250	5
15	501-g-250-10%	HMS-501	250	10
16	D'4-g-250-1%	D'4	250	1
17	D'4-g-250-5%	D'4	250	5
18	D'4-g-250-10%	D'4	250	10
19	991-g-350-1%	HMS-991	350	1
20	991-g-350-5%	HMS-991	350	5
21	991-g-350-10%	HMS-991	350	10
22	992-g-350-1%	HMS-992	350	1
23	992-g-350-5%	HMS-992	350	5
24	992-g-350-10%	HMS-992	350	10
25	993-g-350-1%	HMS-993	350	1
26	993-g-350-5%	HMS-993	350	5
27	993-g-350-10%	HMS-993	350	10
28	301-g-350-1%	HMS-301	350	1
29	301-g-350-5%	HMS-301	350	5
30	301-g-350-10%	HMS-301	350	10
31	501-g-350-1%	HMS-501	350	1
32	501-g-350-5%	HMS-501	350	5
33	501-g-350-10%	HMS-501	350	10
34	D'4-g-350-1%	D'4	350	1
35	D'4-g-350-5%	D'4	350	5
36	D'4-g-350-10%	D'4	350	10
37	991-g-750-1%	HMS-991	750	1
38	991-g-750-5%	HMS-991	750	5
39	991-g-750-10%	HMS-991	750	10
40	992-g-750-1%	HMS-992	750	1
41	992-g-750-5%	HMS-992	750	5
42	992-g-750-10%	HMS-992	750	10
43	993-g-750-1%	HMS-993	750	1
44	993-g-750-5%	HMS-993	750	5
45	993-g-750-10%	HMS-993	750	10
46	301-g-750-1%	HMS-301	750	1
47	301-g-750-5%	HMS-301	750	5
48	301-g-750-10%	HMS-301	750	10
49	501-g-750-1%	HMS-501	750	1
50	501-g-750-5%	HMS-501	750	5
51	501-g-750-10%	HMS-501	750	10

Table A2. Formulations able to be used for *C. lytica* and *N. incerta* biological assays (continued)

Formulation #	Sample ID	Siloxane Backbone	PEG M.W. g/mol	Wt. % Additive
52	D'4-g-750-1%	D'4	750	1
53	D'4-g-750-5%	D'4	750	5
54	D'4-g-750-10%	D'4	750	10
55	992-g-1100-1%	HMS-992	1100	1
56	993-g-1100-1%	HMS-993	1100	1
57	993-g-1100-5%	HMS-993	1100	5
58	993-g-1100-10%	HMS-993	1100	10
59	301-g-1100-1%	HMS-301	1100	1
60	301-g-1100-5%	HMS-301	1100	5
61	501-g-1100-1%	HMS-501	1100	1
62	501-g-1100-5%	HMS-501	1100	5
63	501-g-1100-10%	HMS-501	1100	10
64	D'4-g-1100-1%	D'4	1100	1
65	D'4-g-1100-5%	D'4	1100	5

Synthesis of APEG-750

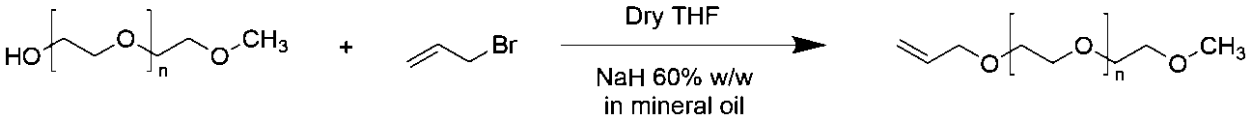

Figure A1. Synthetic scheme for APEG-750.

The synthesis for APEG-750 is shown in Figure A1. First, 750 $\bar{M}_n$ hydroxyl PEG monomethyl ether (45.78 g; 0.061 mol) was added to a 3-neck 500 mL round-bottom flask and dissolved in anhydrous THF (160.0 mL). To a 20 mL glass vial, NaH 60% w/w dispersion in mineral oil (2.9212 g; 0.073 mol) was added, followed by 10.0 mL of anhydrous THF. This NaH/THF mixture was added dropwise to the reaction mixture, which was stirred and cooled in an ice bath to 0°C. After dropwise addition, the reaction mixture was stirred for 2 hours at 0°C. A mixture of allyl bromide (8.7520 g; 0.072 mol) in 80.0 mL of anhydrous THF was then added dropwise to the reaction mixture, warmed to room temperature, and stirred for 24 h. After 24 h, the reaction mixture was filtered to remove any precipitate, with THF being removed under reduced pressure. This yielded a colorless/yellow oil that was dissolved in water (150-200 mL) and extracted with 75 mL of toluene three times to remove unreacted alcohol. The desired product was then extracted into 200 mL of chloroform three times, dried with anhydrous magnesium sulfate, filtered, and then solvent was removed under reduced pressure. FT-IR and ^{1}H-NMR were performed to detect the presence of the allyl group and disappearance of hydroxyl.

Synthesis of SMAA

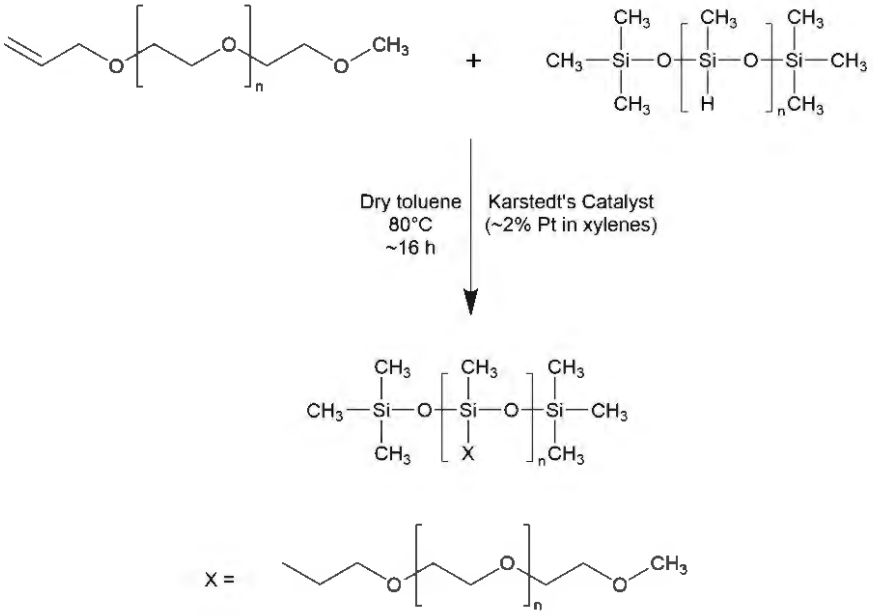

Figure A2. Synthetic scheme for SMAAs.

The synthesis for SMAAs can be seen in Figure A2. The following is a general procedure used to synthesize 991-*g*-350, as well as the other SMAAs. The 350 MW APEG was dried in an oven at >100°C for at least 1 hour before addition. A 100 mL 3-neck round-bottom flask was equipped with a thermocouple, nitrogen inlet, and Teflon coated stir bar. To this flask, HMS-991 (0.9722 g; 0.607 mmol), APEG350 (5.0080 g; 14.3 mmol), and ~30 mL of anhydrous toluene was added. The reaction mixture was stirred for 15 minutes while heating to 80°C. A solution of Karstedt's catalyst in anhydrous toluene was prepared by adding 25 µL (0.0214 g) of the catalyst to 5 mL of anhydrous toluene. Once the temperature of the reaction mixture had reached ~80°C, the catalyst solution was added dropwise, waiting until bubble formation had stopped between additions. This reaction was stirred for at least 16 hours, and then ~3 g of activated carbon (100 mesh) was added, with the temperature increased to 90°C for 2 hours. Next, the reaction mixture was cooled to room temperature, filtered, and any toluene was removed under reduced pressure. FT-IR and ^{1}H-NMR were performed to confirm the disappearance of the allyl group from APEG, the disappearance of the Si-H bond from the PMHS, and the appearance of new proton peaks from the grafted PEG chains. Rotary evaporation was performed on the synthesized additives and afterwards, non-volatile content (ASTM D2369) was determined. All SMAAs had >95% non-volatile content, with the effect of residual toluene being negligible in coatings formulation.

Proton NMR and FTIR Spectra

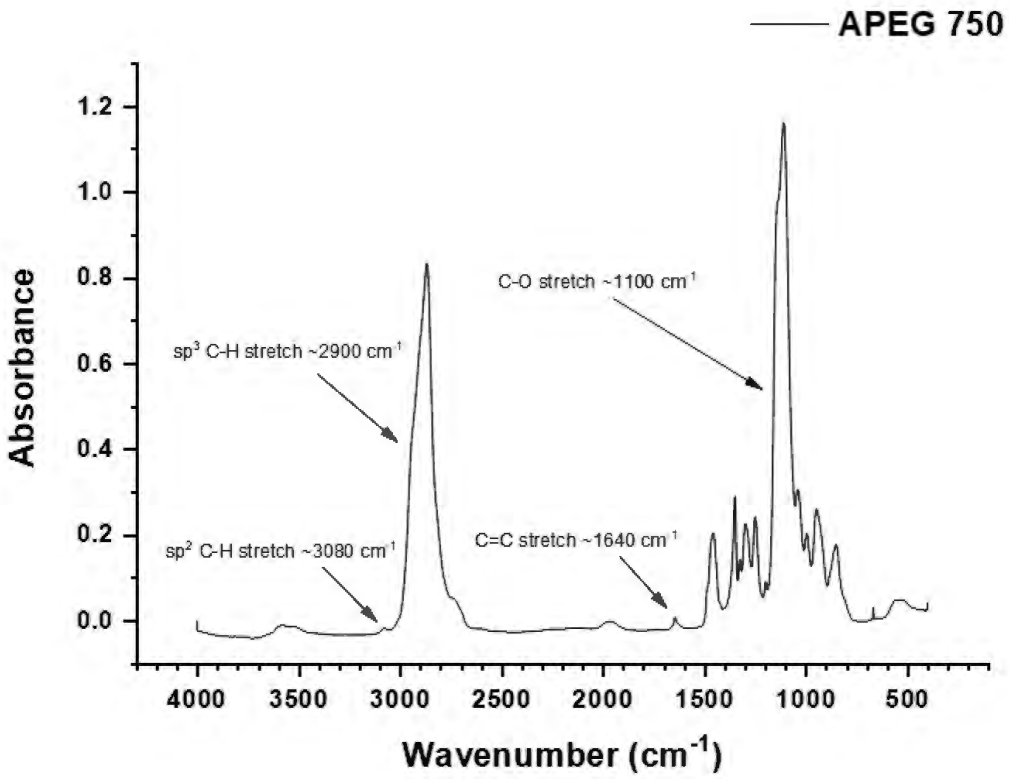

Figure A3. FT-IR spectrum of synthesized APEG 750.

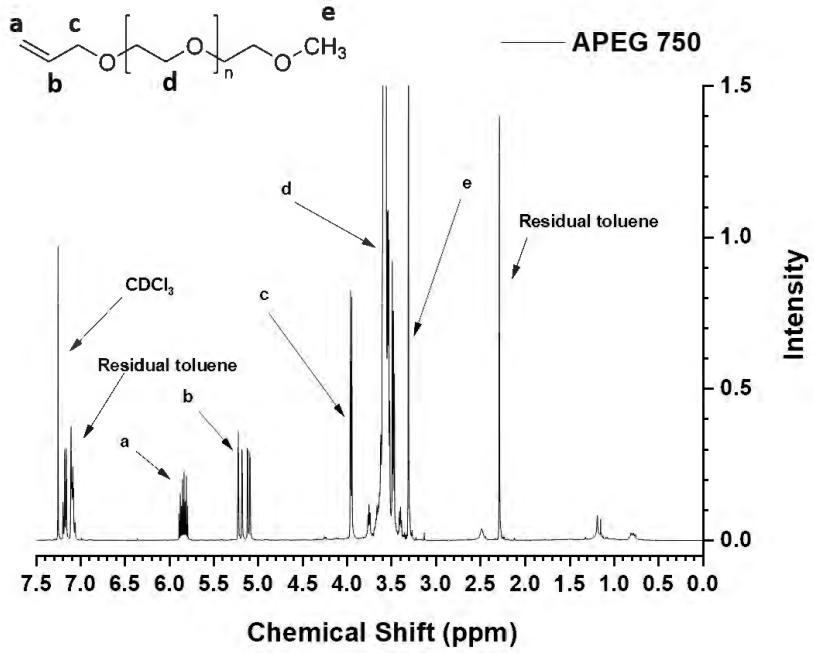

Figure A4. ^{1}H-NMR spectrum of synthesized APEG 750.

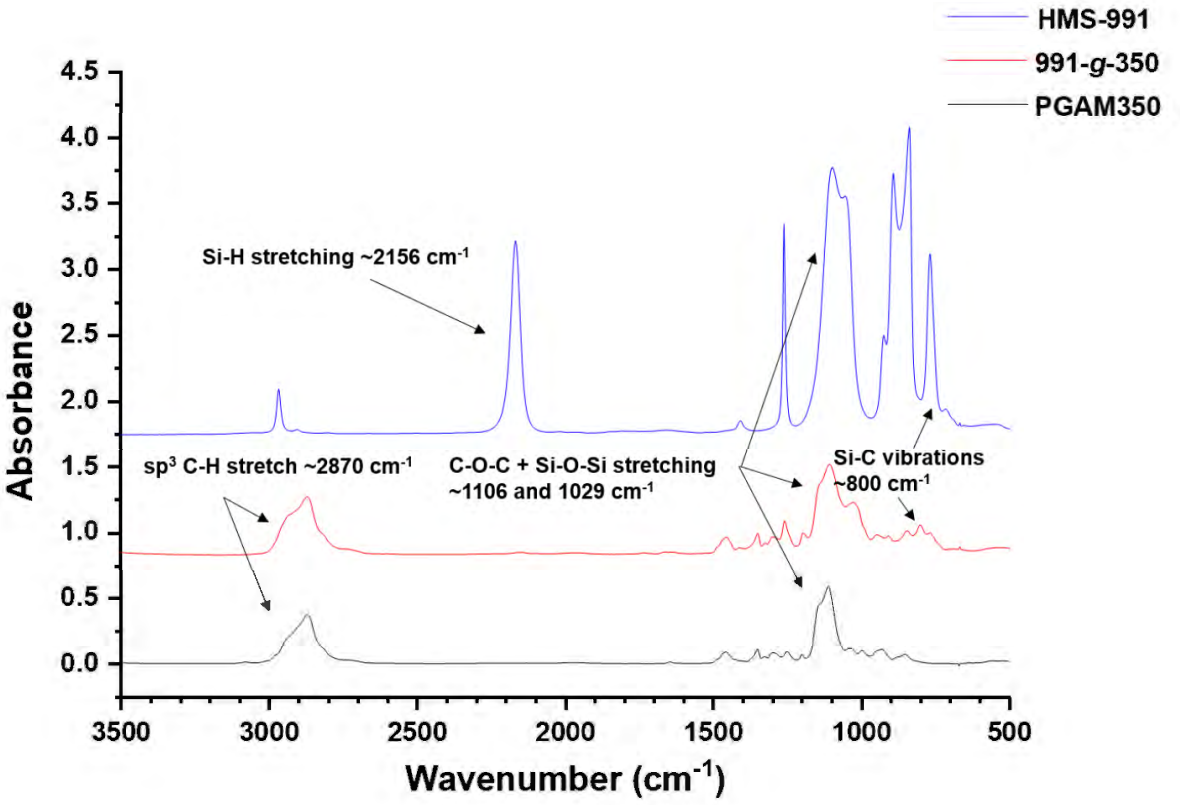

Figure A5. FT-IR spectra for SMAA 991-*g*-350, with Polyglykol AM 350 and HMS-991 for comparison.

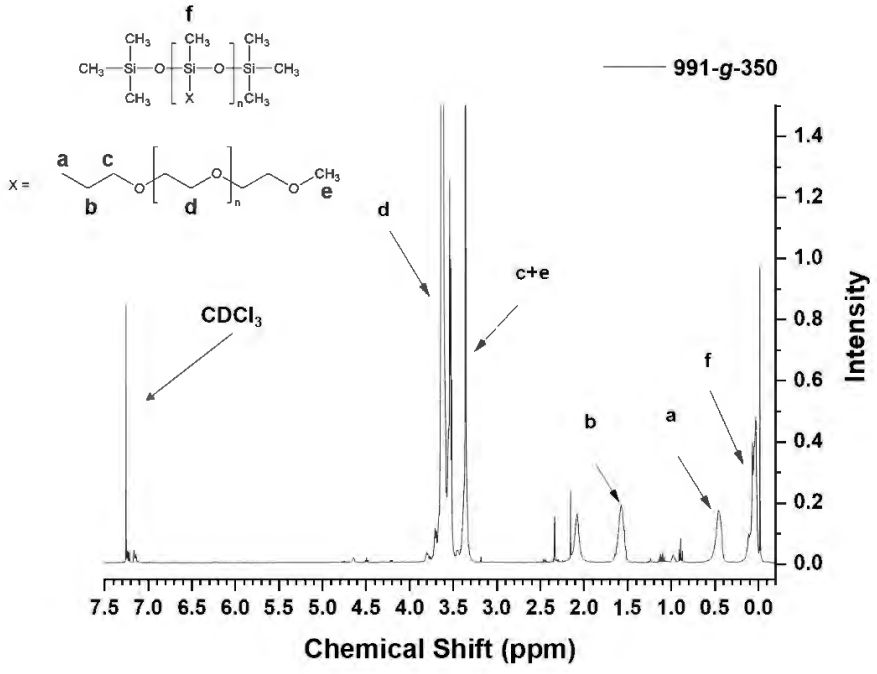

Figure A6. ^{1}H-NMR spectrum for SMAA 991-*g*-350.

Biological Assay Screening Experiments

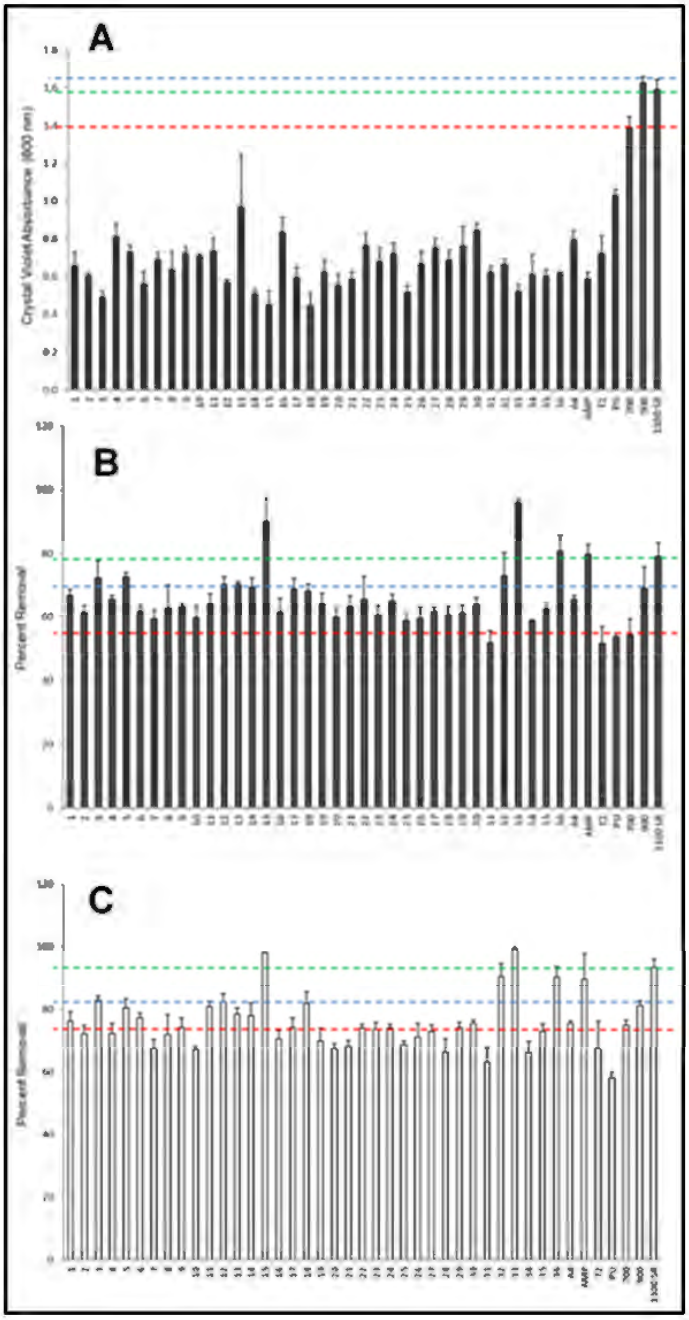

Figure A7. Biofilm growth of *C. lytica* (A) and the percent removal after waterjet at 10 psi (B) and 20 psi (C). Red dashed line is performance of IS700, blue is IS900, and green is IS1100SR. Numbers along the X-axis correspond to sample ID numbers 1-36 from Table A2.

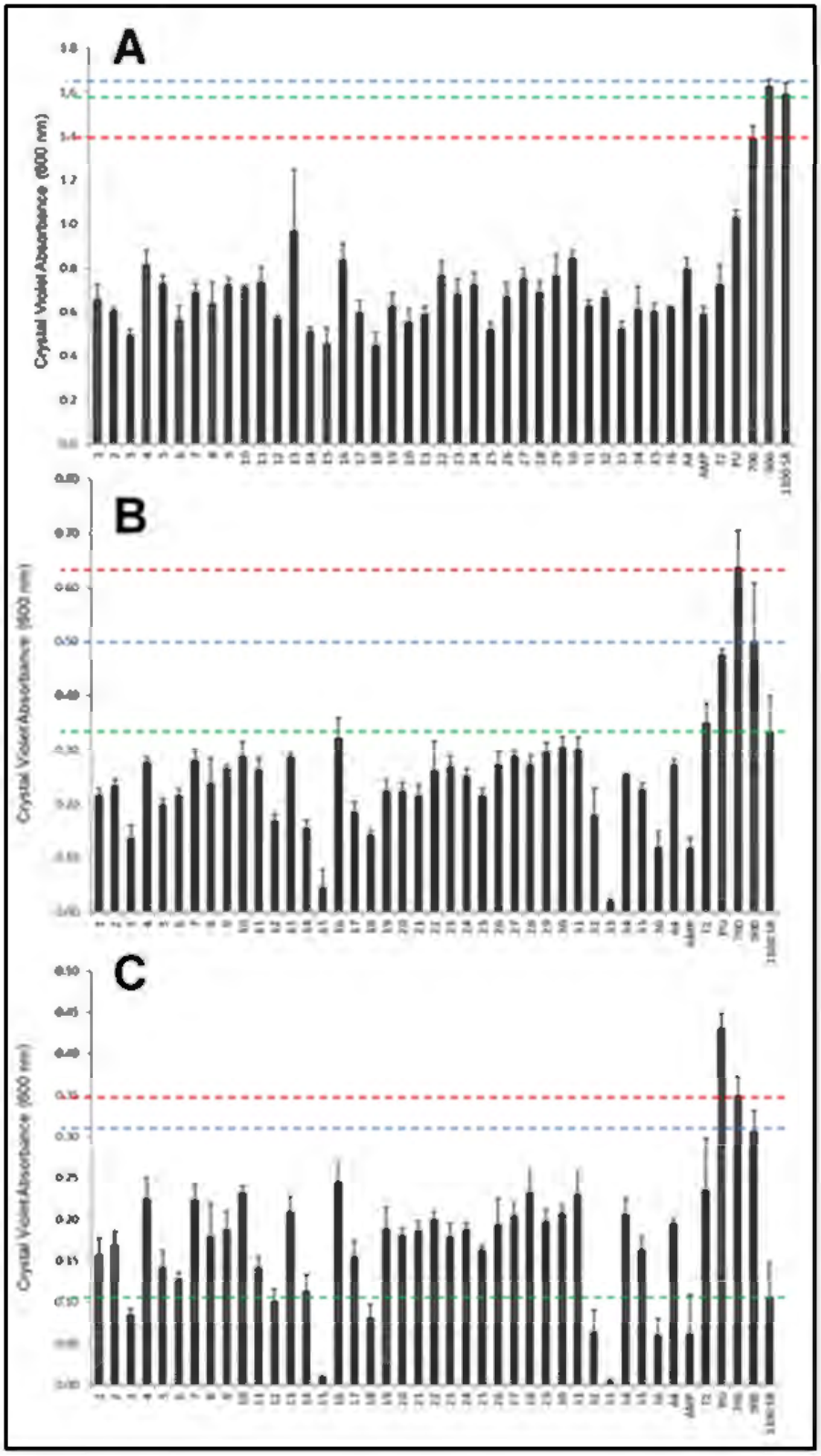

Figure A8. Biofilm growth of *C. lytica* (A) and the biomass remaining after waterjet at 10 psi (B) and 20 psi (C). Red dashed line is performance of IS700, blue is IS900, and green is IS1100SR. Numbers along the X-axis correspond to sample ID numbers 1-36 from Table A2.

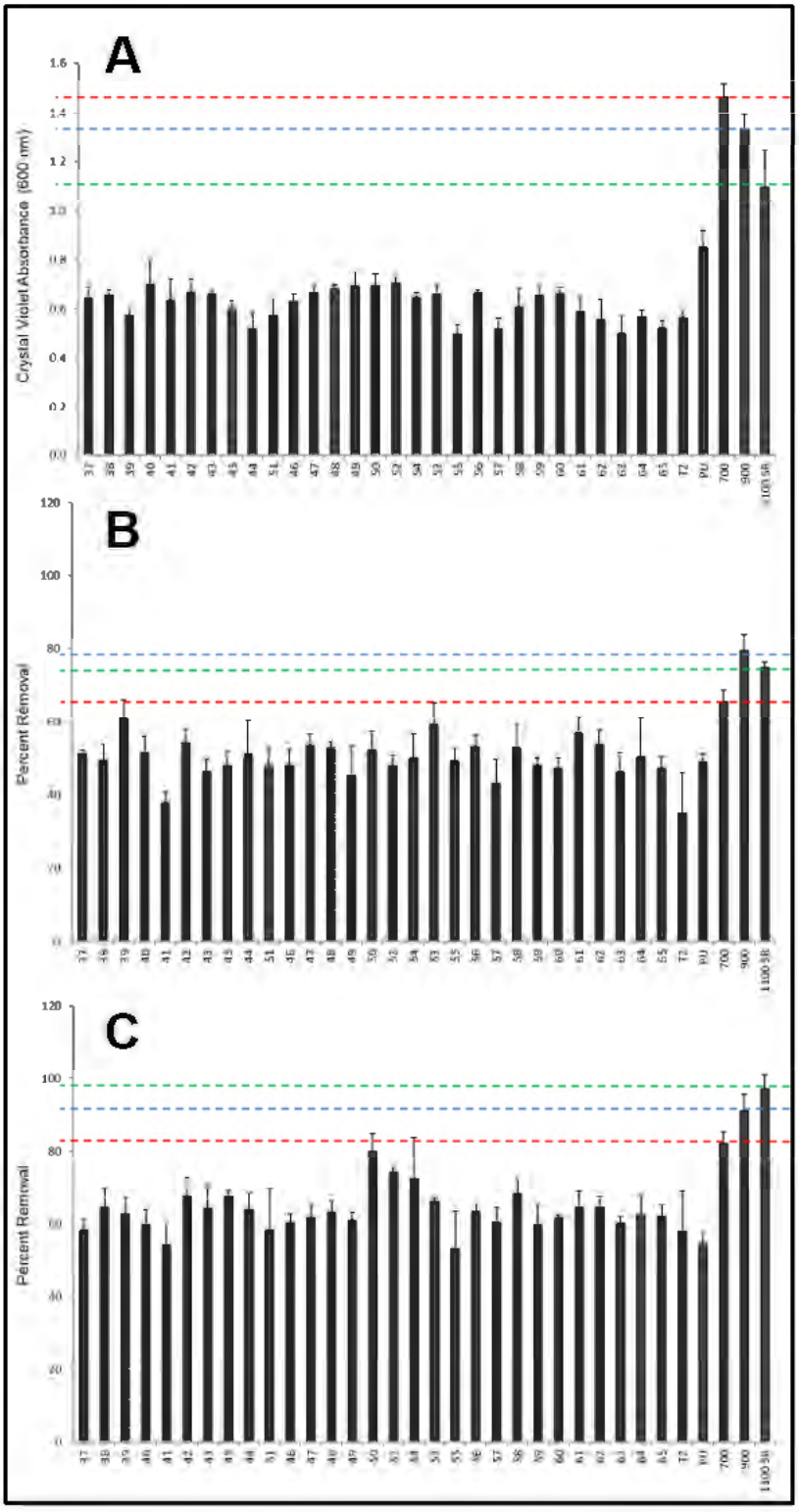

Figure A9. Biofilm growth of *C. lytica* (A) and the percent removal after waterjet at 10 psi (B) and 20 psi (C). Red dashed line is performance of IS700, blue is IS900, and green is IS1100SR. Numbers along the X-axis correspond to sample ID numbers 37-65 from Table A2.

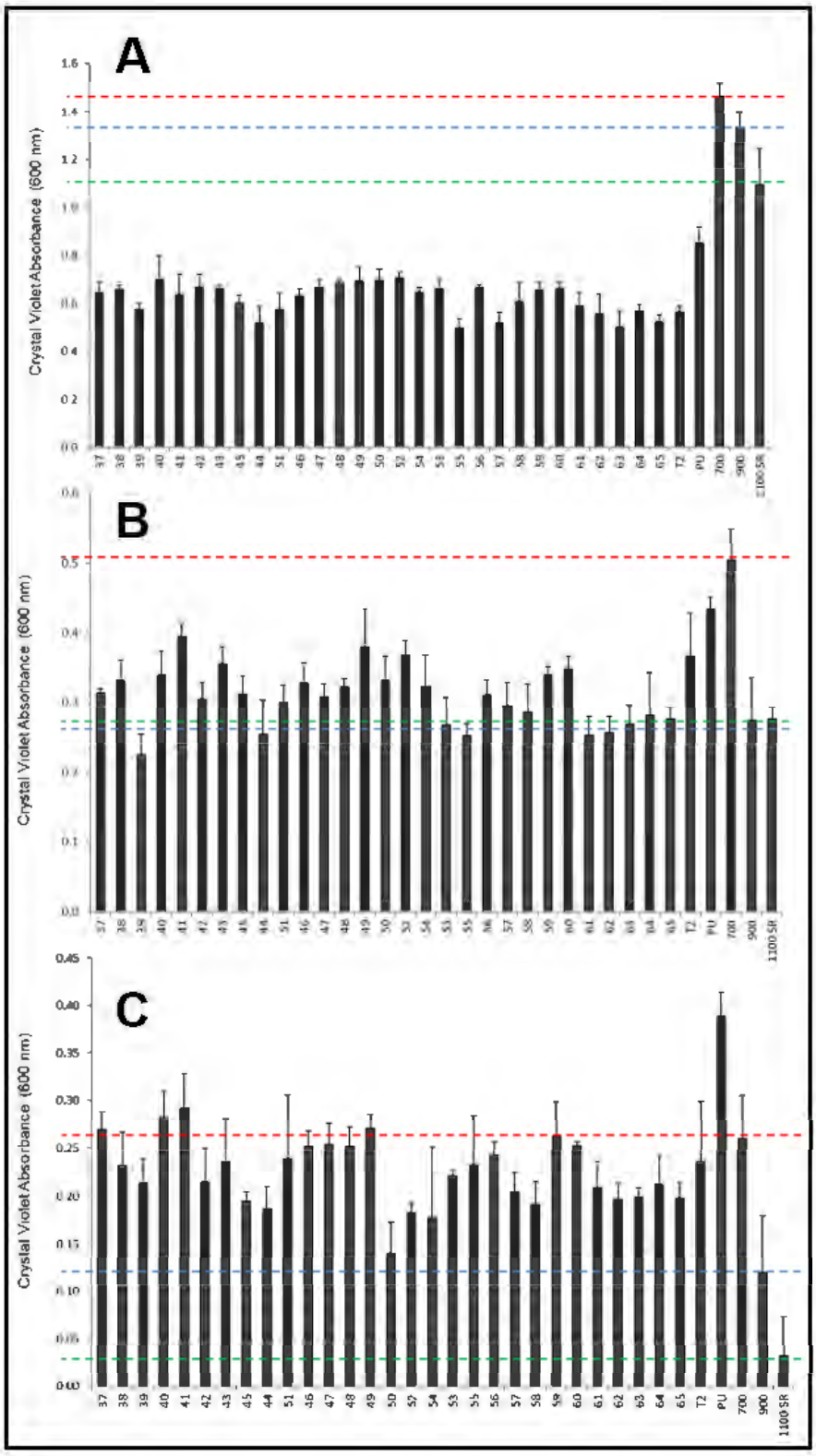

Figure A10. Biofilm growth of *C. lytica* (A) and the biomass remaining after waterjet at 10 psi (B) and 20 psi (C). Red dashed line is performance of IS700, blue is IS900, and green is IS1100SR. Numbers along the X-axis correspond to sample ID numbers 37-65 from Table A2.

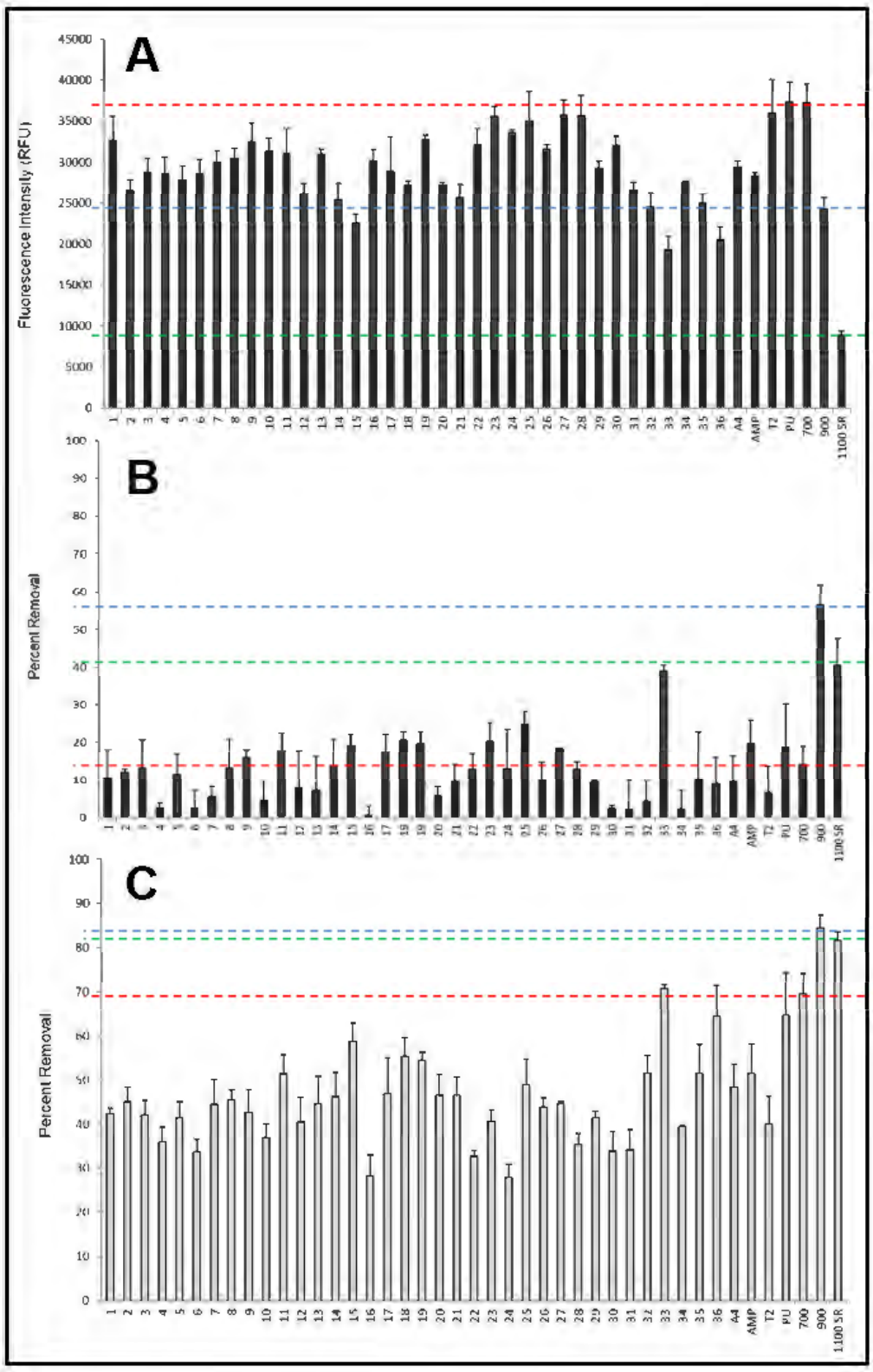

Figure A11. Cell attachment of *N. incerta* (A) and the percent removal after waterjet at 10 psi (B) and 20 psi (C). Red dashed line is performance of IS700, blue is IS900, and green is IS1100SR. Numbers along the X-axis correspond to sample ID numbers 1-36 from Table A2.

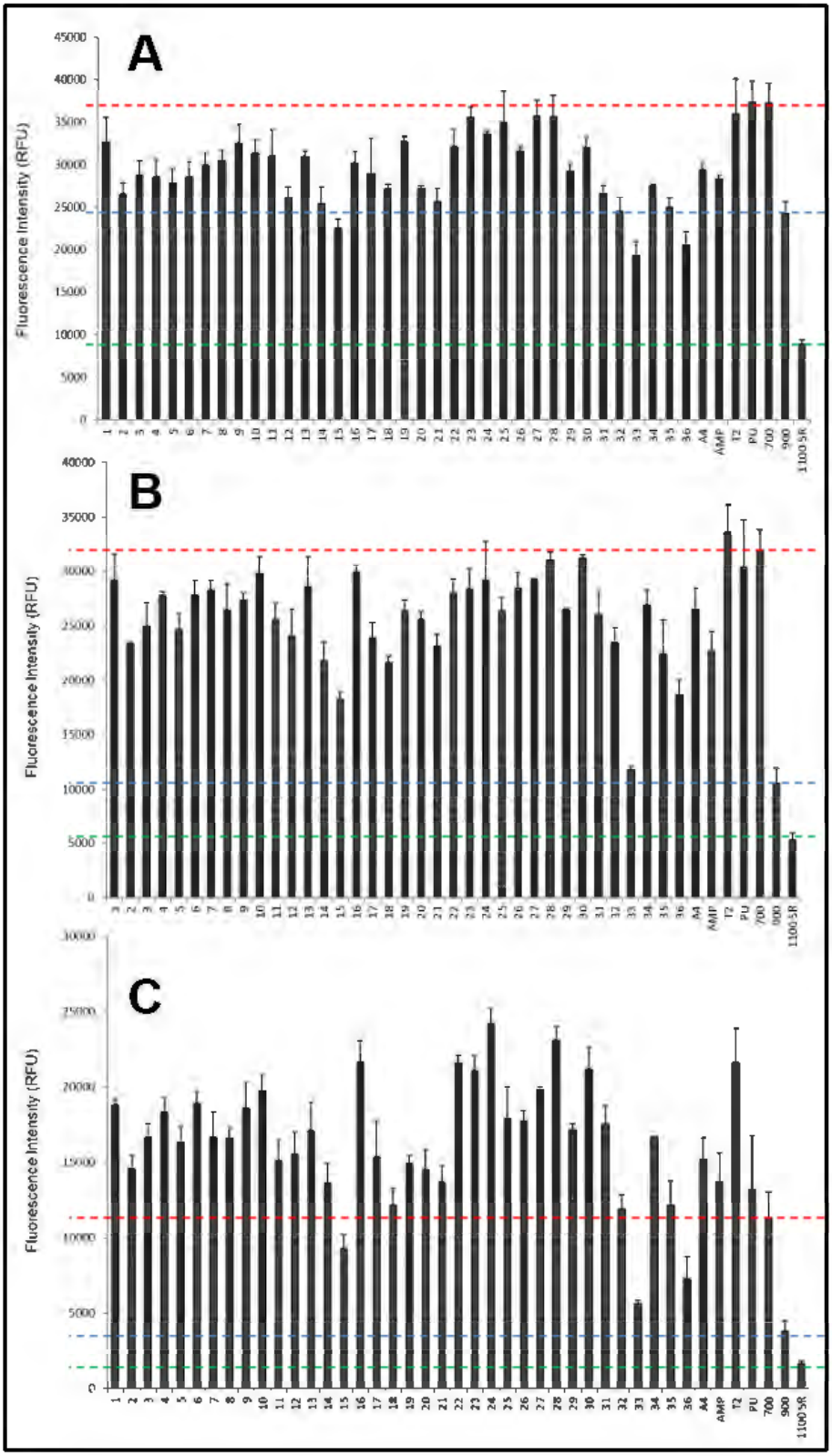

Figure A12. Cell attachment of *N. incerta* (A) and the biomass remaining after waterjet at 10 psi (B) and 20 psi (C). Red dashed line is performance of IS700, blue is IS900, and green is IS1100SR. Numbers along the X-axis correspond to sample ID numbers 1-36 from Table A2.

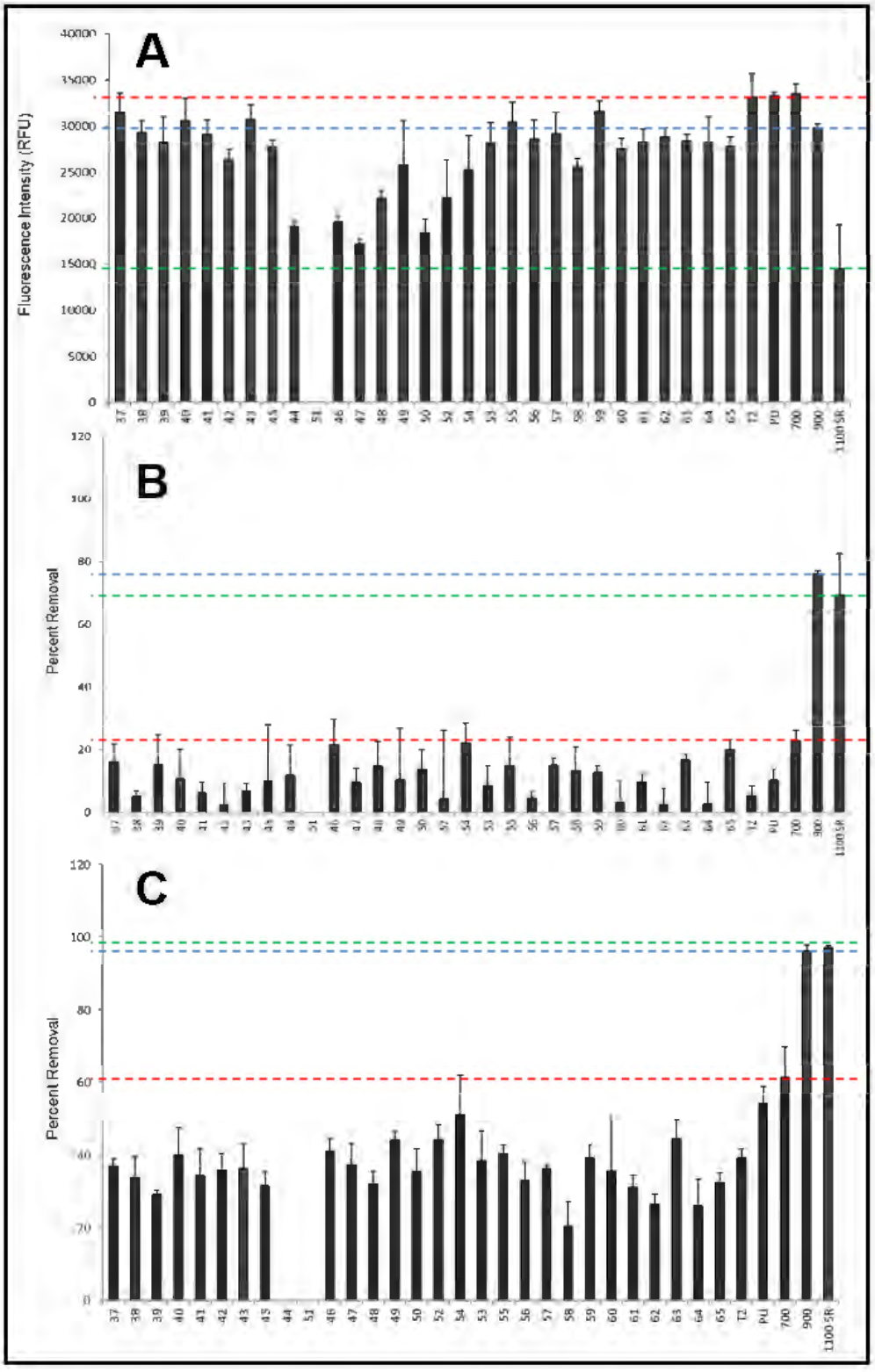

Figure A13. Cell attachment of *N. incerta* (A) and the percent removal after waterjet at 10 psi (B) and 20 psi (C). Red dashed line is performance of IS700, blue is IS900, and green is IS1100SR. Numbers along the X-axis correspond to sample ID numbers 37-65 from Table A2. Samples 44 and 51 could not be assessed completely due to coating damage.

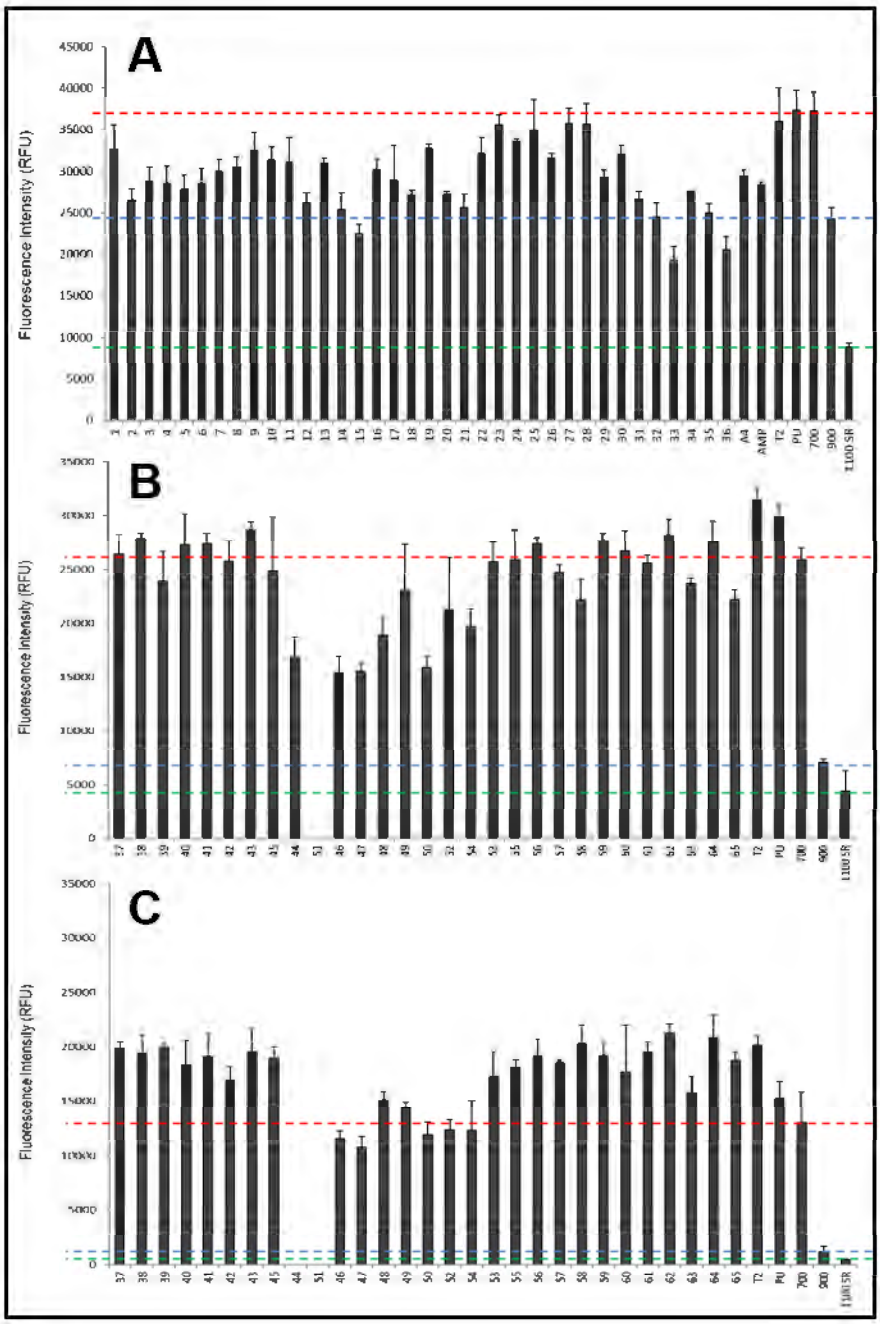

Figure A14. Cell attachment of *N. incerta* (A) and the biomass remaining after waterjet at 10 psi (B) and 20 psi (C). Red dashed line is performance of IS700, blue is IS900, and green is IS1100SR. Numbers along the X-axis correspond to sample ID numbers 37-65 from Table A2. Samples 44 and 51 could not be assessed completely due to coating damage.

Leachate Toxicity Assay (*Navicula incerta*)

Well plates containing coatings formulations were subjected to leachate toxicity assays before analysis of cell attachment and release of *N. incerta*. The details of this experiment have been reported previously. Briefly, well plates with coated discs were incubated in 1 mL of growth medium overnight. Afterwards, a 0.05 mL suspension of *N. incerta* diatom cells (4 $x10^5$ cells mL^{-1}, adjusted to 0.03 OD at absorbance 660 nm) in Guillard's F/2 medium was added to 1 mL of coating leachates. Then, 0.2 mL of combined leachate and *N. incerta* suspension was transferred, in triplicate, to a 96-well array plate. These plates were incubated for 48 h at 18℃ in an illuminated growth cabinet with a 16:8 light to dark ratio and a photon flux density of 33 µmol/m/s. Chlorophyll was then extracted with DMSO and the concentration was quantified using fluorescence spectroscopy with an excitation wavelength of 360 nm and emission wavelength at 670 nm. Growth in coating leachates was reported as fluorescence ratio to a positive growth control (fresh growth medium).

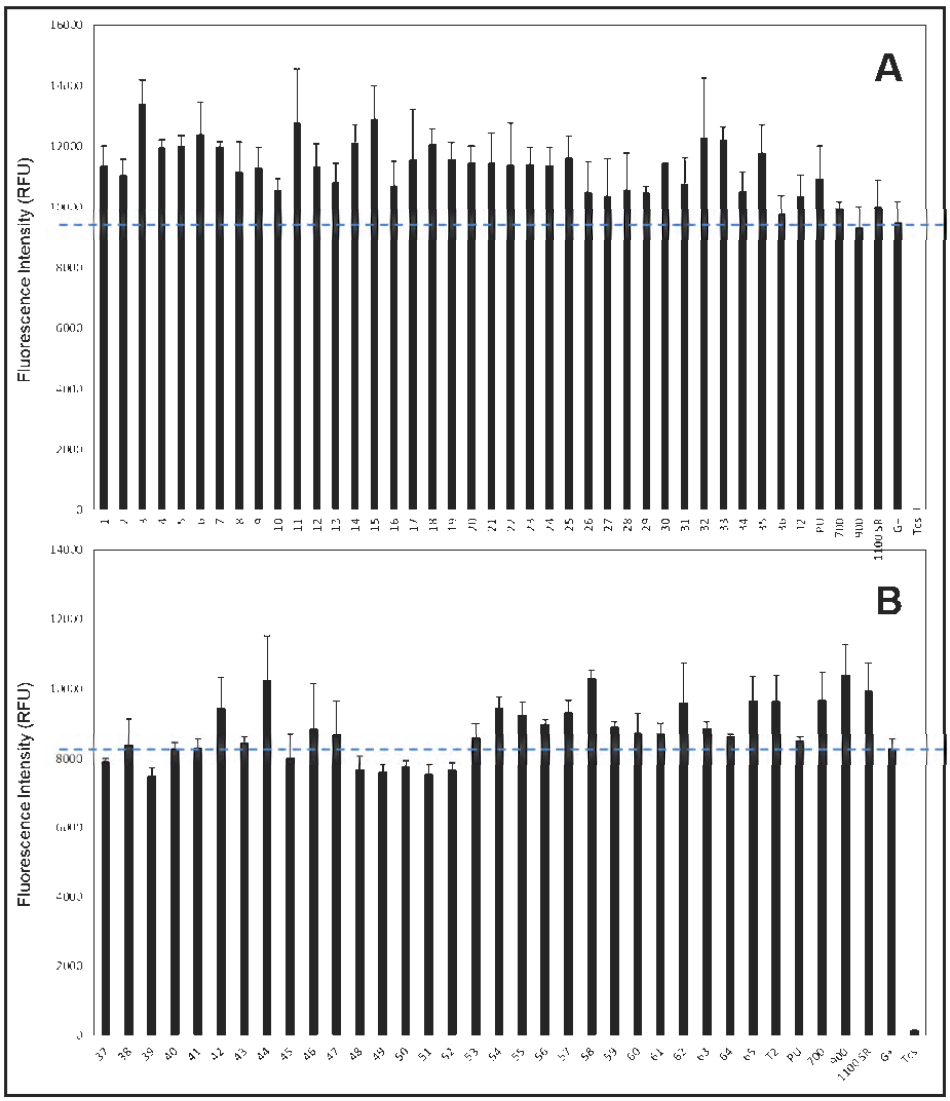

Figure A15. *N. incerta* leachate toxicity of formulations 1-36 (A) and formulations 37-65 (B). Experimental coatings were compared to growth control as shown by blue dashed line. The bars represent biomass (relative fluorescence units) generated in leachates of experimental and control coatings. Numbers along the X-axis in A and B correspond to sample number ID's shown in Table A2.

Leachate Toxicity Assay (*Cellulophaga lytica*)

The toxicity of leachates from experimental coatings was evaluated before analysis of biofilm growth and adhesion of *C. lytica*, and details of this experiment can be found elsewhere.[32] A 1 mL portion of growth medium was added to well plates containing coated discs and incubated overnight. Leachates were collected and 0.05 mL of a suspension of *C. lytica* (10^7 cells/mL in ASW with 0.5 g/L peptone and 0.1 g/L of yeast extract) was added to 1 mL of coating leachate. Then, 0.2 mL of this mixture was transferred to a 96-well plate array, in triplicate, and incubated for 18 h at 28°C. Afterwards, well plates

were rinsed three times with deionized water and then stained with 0.5 mL of crystal violet dye. Crystal violet was then extracted with 0.5 mL of glacial acetic acid and absorbance was measured at 600 nm to determine biomass. Growth in the coating leachates was reported as an absorbance ratio to a positive growth control (fresh growth medium).

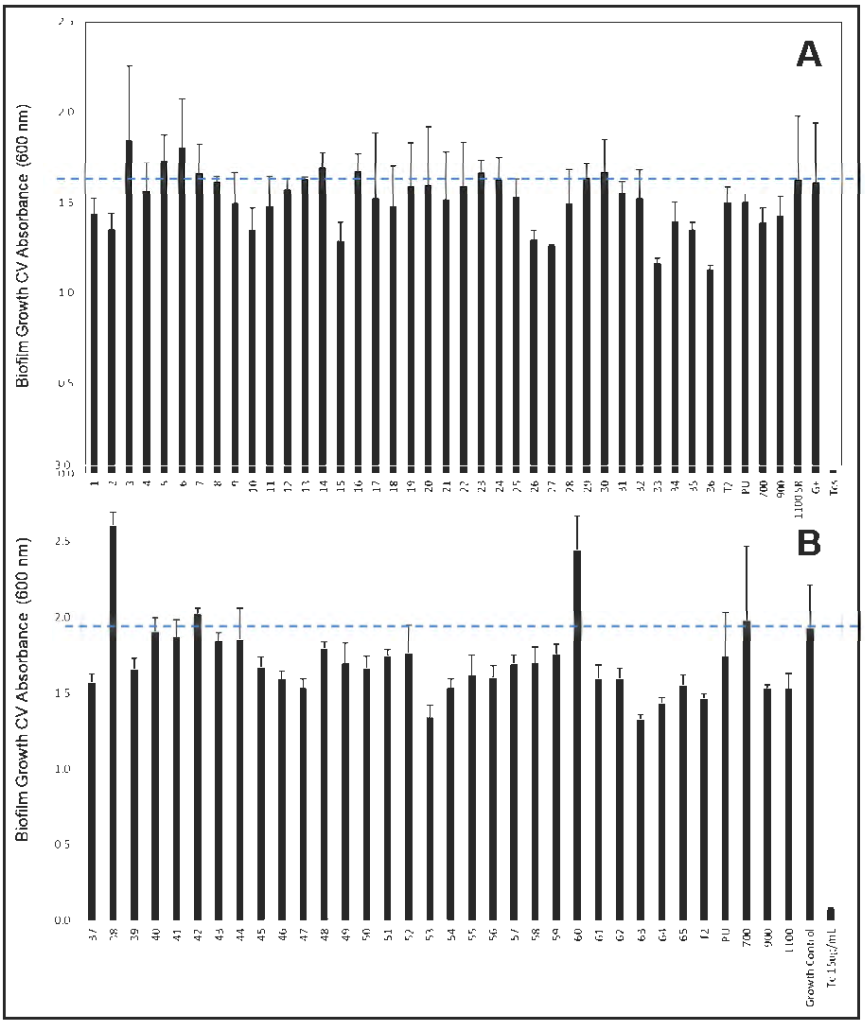

Figure A16. *C. lytica* leachate toxicity of formulations 1-36 (A) and formulations 37-65 (B). Experimental coatings were compared to growth control as shown by blue dashed line. The bars represent biomass (crystal violet absorbance) generated in leachates of experimental and control coatings. Numbers along the X-axis in A and B correspond to sample number ID's shown in Table A2.

Leachate Toxicity Assay (*Ulva linza*)

Before analyzing growth and release of the macroalga *U. linza*, the toxicity of leachates from wells containing coated discs was performed. Briefly, 1 mL of 0.22 µm filtered artificial seawater (FSW) was added to each well and the plates were gently shaken (60 rpm) for 18 h. One mL of leachate from each experimental coating (6 replicates per coating) was then transferred to new 24-well plates. To each

well, a 1 mL suspension of *U. linza* spores, adjusted to 0.05 OD at absorbance 660 nm (3.3 x 10^5 spores mL^{-1}) in double strength enriched seawater medium, was added. The plates were then incubated for 2 h in darkness and room temperature before being transferred to an illuminated incubator at 18℃ with a 16:8 light to dark cycle at a photon flux density of 45 µmol/m/s. After 7 days of growth, the seawater was removed, and chlorophyll was extracted using 1 mL DMSO. Chlorophyll fluorescence was determined at an excitation wavelength of 360 nm and emission at 670 nm. Fluorescence intensity is directly proportional to amount of biomass.

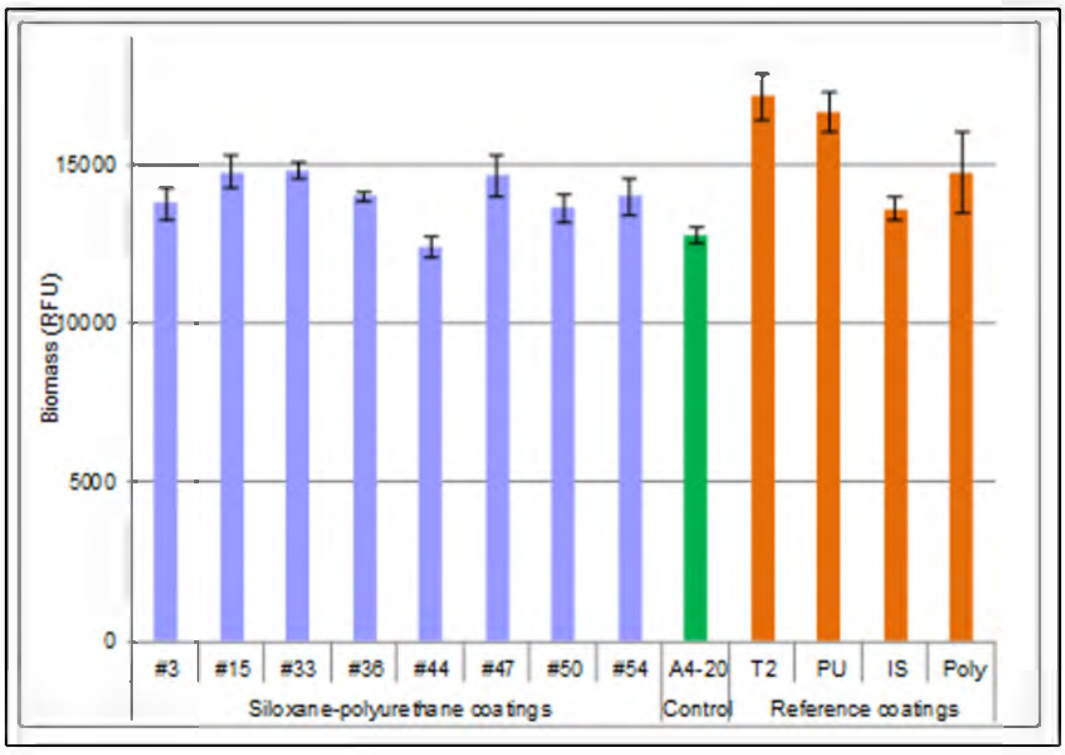

Figure A17. *U. linza* leachate toxicity of selected formulations in Table 2.2. The blue, green, and orange bars represent biomass (relative fluorescence units) generated in leachates of experimental coatings, A4-20 internal control, and standard coatings respectively.

Growth of *U. linza* Sporelings

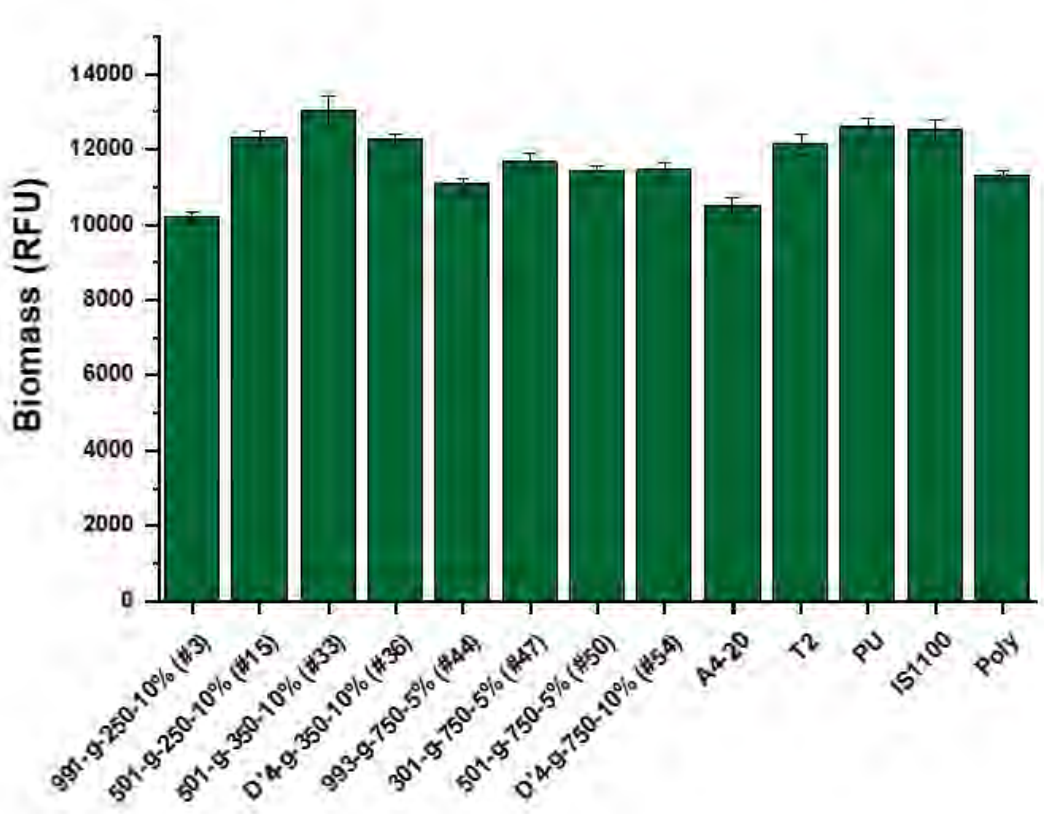

Figure A18. Settlement and growth of sporelings of *U. linza* on experimental formulations. The bars represent the mean biomass from 6 replicates (relative fluorescence units) generated on experimental and control coatings. Error bars show standard error of the means. The X-axis is labeled to indicate formulation number in Table 2.2, along with commercial standards and controls.

Tables of Statistical Analysis

Table A3. Tukey comparison between treatment groups for removal assays of *U. linza* at 110 kPa impact pressure. A4-20 is treated as the internal control, where most comparisons are made

Formulations	N	Mean	Grouping							
T2	6	95.055	A							
IS1100SR	6	93.928	A							
#54	6	71.82		B						
#36	6	71.51		B						
#44	6	69.55		B						
#50	6	65.37		B	C					
A4-20	6	58.03			C	D				
#47	6	51.03				D	E			
#33	6	41.61					E	F		
PU	6	37.88						F		
Poly	6	19.60							G	
#15	6	15.50							G	
#3	6	0.01000								H

Means that do not share a letter are significantly different.

Table A4. Tukey comparison between treatment groups for settlement assays of *N. incerta*. A4-20 is treated as the internal control, where most comparisons are made

Formulations	N	Mean	Grouping				
PU	3	37370	A				
IS700	3	37250	A				
T2	3	36024	A				
A4-20	3	29403		B			
#3	3	28755		B			
#54	3	25281		B	C		
IS900	3	24294		B	C	D	
#15	3	22548			C	D	E
#36	3	20509			C	D	E
#33	3	19272				D	E
#44	3	19131				D	E
#50	3	18442				D	E
#47	3	17225					E
IS1100SR	3	8895					F

Means that do not share a letter are significantly different.

Table A5. Tukey comparison between treatment groups for removal assays of *N. incerta* at a water column pressure of 20 psi. A4-20 is treated as the internal control, where most comparisons are made

Formulations	N	Mean	Grouping						
T2	4	20097	A						
#3	4	16125	A	B					
PU	4	15377	A	B					
A4-20	4	14917		B					
IS700	4	13098		B	C				
#50	4	11720		B	C	D			
#54	4	11506		B	C	D			
#47	4	11046		B	C	D			
#15	4	9146			C	D	E		
#36	4	7375				D	E	F	
#33	4	5325					E	F	
IS900	4	5046					E	F	G
IS1100SR	4	2633.8						F	G
#44	4	0.000000							G

Means that do not share a letter are significantly different.

Table A6. Tukey comparison between treatment groups for growth assays of *C. lytica*. A4-20 is treated as the internal control, where most comparisons are made

Formulations	N	Mean	Grouping			
IS900	3	1.6230	A			
IS1100SR	3	1.5893	A			
IS700	3	1.3903	A			
PU	3	1.0283		B		
A4-20	3	0.7970		B	C	
T2	3	0.7223			C	D
#50	3	0.6960			C	D
#47	3	0.6660			C	D
#36	3	0.61733			C	D
#33	3	0.5207			C	D
#44	3	0.5203			C	D
#3	3	0.4930				D
#54	3	0.479				D
#15	3	0.4530				D

Means that do not share a letter are significantly different.

Table A7. Tukey comparison between treatment groups for removal assays of *C. lytica* at a water column pressure of 20 psi. A4-20 is treated as the internal control, where most comparisons are made

Formulations	N	Mean	Grouping								
PU	4	0.4150	A								
IS700	4	0.34575	A	B							
IS900	4	0.3132		B	C						
#47	4	0.2460			C	D					
T2	4	0.2345			C	D	E				
A4-20	4	0.20125				D	E	F			
#44	4	0.1972				D	E	F	G		
#54	4	0.1578					E	F	G	H	
#50	4	0.1292						F	G	H	I
IS1100SR	4	0.1193							G	H	I
#3	4	0.08575								H	I
#36	4	0.05700									I
#15	4	0.009250									
#33	4	0.00450									

Means that do not share a letter are significantly different.

Table A8. Tukey comparison between treatment groups for reattachment and removal assays of *A. amphitrite.* A4-20 is treated as the internal control, where most comparisons are made

Formulations	N	Mean	Grouping		
#47	6	0.1492	A		
#33	6	0.1100	A	B	
#15	6	0.0961	A	B	C
#36	6	0.07162	A	B	C
IS900	6	0.0699	A	B	C
#3	6	0.0607	A	B	C
IS700	6	0.0438		B	C
A4-20	6	0.0349		B	C
IS1100SR	6	0.0288		B	C
#44	6	0.0197		B	C
#50	6	0.01732			C
#54	6	0.01448			C

Means that do not share a letter are significantly different.

AFM Surface Roughness

Table A9. Root mean square (Rq) and the arithmetic average (Ra) roughness of surfaces of selected formulations measured using Atomic Force Microscopy

Formulation ID	Dry State R_q (nm)	Dry State R_a (nm)	Hydrated State R_q (nm)	Hydrated State R_a (nm)
A4-20	132.0	111.0	116.0	76.0
#33	79.9	57.9	52.8	40.8
#44	94.1	69.4	81.5	64.8
#47	43.0	31.7	84.1	63.3
#50	50.0	39.9	94.2	70.4

APPENDIX B. CHAPTER 3 SUPPLEMENTAL INFORMATION

Isocyanate Titrations

Table B1. Actual and theoretical isocyanate percent of pre-polymer compositions

Formulation (PDMS:PEG)	Theoretical		Actual	
	% Solids	% NCO	% Solids	% NCO
F1 (20:0)	49.70376	0.240781	49.22518	0.086955
F4 (15:5)	51.37623	0.74467	49.74834	0.446702
F7 (10:10)	53.99611	1.175092	50.8961	0.829339
F10 (5:15)	54.804	1.504385	52.10793	0.98286
F13 (0:20)	55.71053	1.741625	52.7626	1.149164

Dryadd Calculations

Table B2. DryAdd calculated percent composition of different molecular species for the reaction between polyisocyanate Desmodur Z 4470 BA (IPDI trimer) and varying amounts of carbinol PDMS and hydroxy terminated PEG. The labeling of '% n (0)' refers to a molecule of IPDI trimer which has three unreacted isocyanate functional groups, with % n (1), % n (2), and % n (3) corresponding to one, two, and three functional groups that have undergone reaction between either the PDMS or PEG molecules, depending on pre-polymer composition

Formulation ID	Desmodur Z 4470 BA Max Functional Groups Reacted				
	PDMS:PEG Composition	% n (0)	% n (1)	% n (2)	% n (3)
F1	(20:0)	9.2	33.3	40.8	16.8
F4	(15:5)	9.1	33.1	41.3	16.5
F7	(10:10)	9.1	33.2	41.1	16.7
F10	(5:15)	9.1	33.3	40.9	16.7
F13	(0:20)	9.4	33.0	40.9	16.8

Gel Permeation Chromatography (GPC)

In Figure B1, plots A and E pertain to F1 and F13 which consist of a pre-polymer PDMS:PEG ratios of 20:0 and 0:20 respectively. Peak 1 in plots A corresponds to the pre-polymer species which has undergone complete reaction with an average of three chains of 10k g/mol PDMS. Peak 2 in plot A corresponds to a pre-polymer species which has undergone a reaction with an average of one chain of PDMS. Peak 3 in plot A corresponds to a pre-polymer polyisocyanate species which has not undergone reaction with any chains of PDMS. Peaks 4 and 5 are low molecular weight species not involved with the pre-polymer composition. In plot E, peak 1 corresponds to pre-polymer species which have reacted with at least one chain of 750 g/mol PEG, with an average of three chains being the most prominent. Peak 2

corresponds to pre-polymer isocyanate species which have not reacted with any chains of PEG. Peaks 3 and 4 in plot E correspond to low molecular weight species which are not involved in pre-polymer compositions.

In plots B-D, peaks 1 and 2 correspond to pre-polymer species that contain a mixture of PDMS and PEG chains reacted with the core polyisocyanate Desmodur Z 4470 BA. Peak 1 in these plots is indicative of the presence of PDMS chains in the pre-polymer composition, and peak 2 is more indicative of the presence of PEG chains in these pre-polymers. As the ratio of PDMS:PEG changes from 15:5 (F4), 10:10 (F7), and 5:15 (F10), the intensity of peak 1 begins to decrease as the intensity of peak 2 increases. This corresponds with an increase in pre-polymer species with more PEG chains than PDMS chains as the ratio is changed.

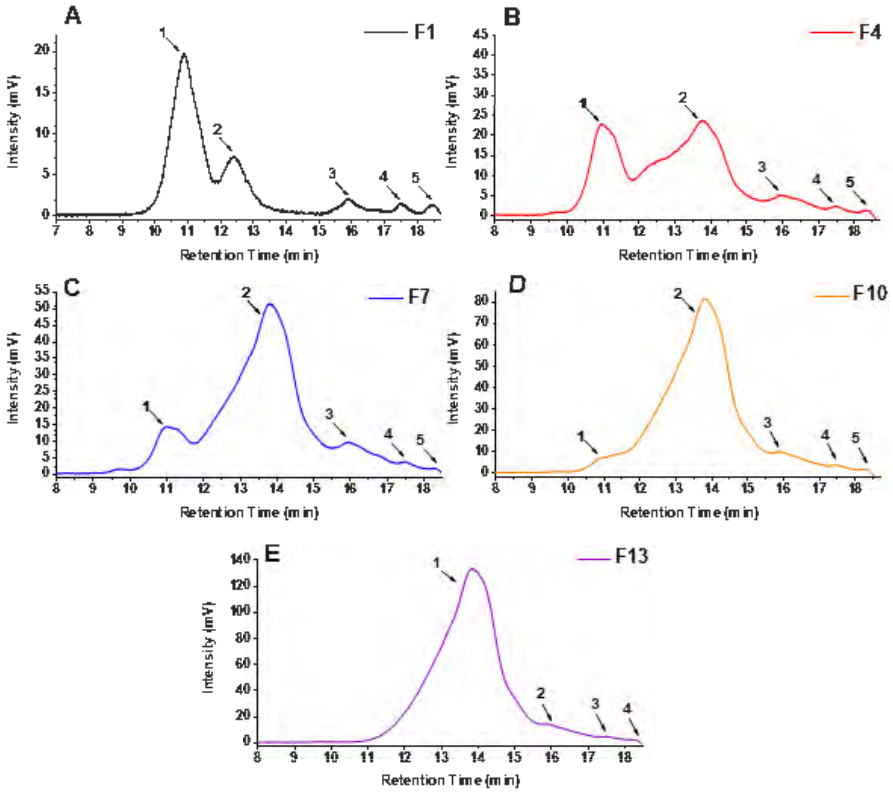

Figure B1. GPC plots for pre-polymer compositions containing no surface modifying amphiphilic additive (SMAA). Plots A-E correspond to formulations F1, F4, F7, F10, and F13, with peaks of interest being labeled 1-5.

Tables of Experimental Formulations

Table B3. Experimental, control, and standard formulations used during leachate toxicity assessments and biological assay testing

Experimental Formulations			
ID	**Prepolymer PDMS % - 10k MW**	**Prepolymer PEG % - 750 MW**	**SMAA wt.%**
F1	20	0	0
F2	20	0	5
F3	20	0	10
F4	15	5	0
F5	15	5	5
F6	15	5	10
F7	10	10	0
F8	10	10	5
F9	10	10	10
F10	5	15	0
F11	5	15	5
F12	5	15	10
F13	0	20	0
F14	0	20	5
F15	0	20	10

Control and Standard Formulations		
ID	**Name**	**Composition**
PU	Polyurethane	NDSU prepared polyurethane standard
T2	Dow Corning® T2	Silicone elastomer commercial FR standard coating
Poly	Polystyrene	Polystyrene negative control
IS700	Intersleek® 700	Intersleek commercial FR standard coating
IS900	Intersleek® 900	Intersleek commercial FR standard coating
IS1100SR	Intersleek® 1100SR	Intersleek commercial FR standard coating with a "slime release" component

Leachate Toxicity Assay (*Ulva linza*)

To investigate whether leachates from coated samples were truly non-toxic, leachate toxicity assays were performed on wells containing coated disks of both experimental and standard/control coatings. Assessments were performed on two batches to minimize error potentially caused by variations in collected *U. linza* spores. A brief description of this assessment is as follows, with a detailed procedure found in previous literature. For each well plate, 1 mL of 0.22 µm filtered artificial seawater (FSW) (Tropic Marin) was added to each well and the plates were gently shaken (60 rpm) for 18 h. One mL of leachate from each experimental coating (6 replicates per coating) was then transferred to new 24-well plates. To

each well, a 1 mL suspension of *U. linza* spores, adjusted to 0.05 OD at absorbance 660 nm (3.3×10^5 spores mL^{-1}) in double strength enriched seawater medium, was added. The plates were then incubated for 2 h in darkness and room temperature before being transferred to an illuminated incubator at 18℃ with a 16:8 light to dark cycle at a photon flux density of 45 µmol/m/s. After 7 days of growth, the seawater was removed, and chlorophyll was extracted using 1 mL DMSO. Chlorophyll fluorescence was determined at an excitation wavelength of 360 nm and emission at 670 nm using a Tecan plate reader. Fluorescence intensity being directly proportional to amount of biomass.

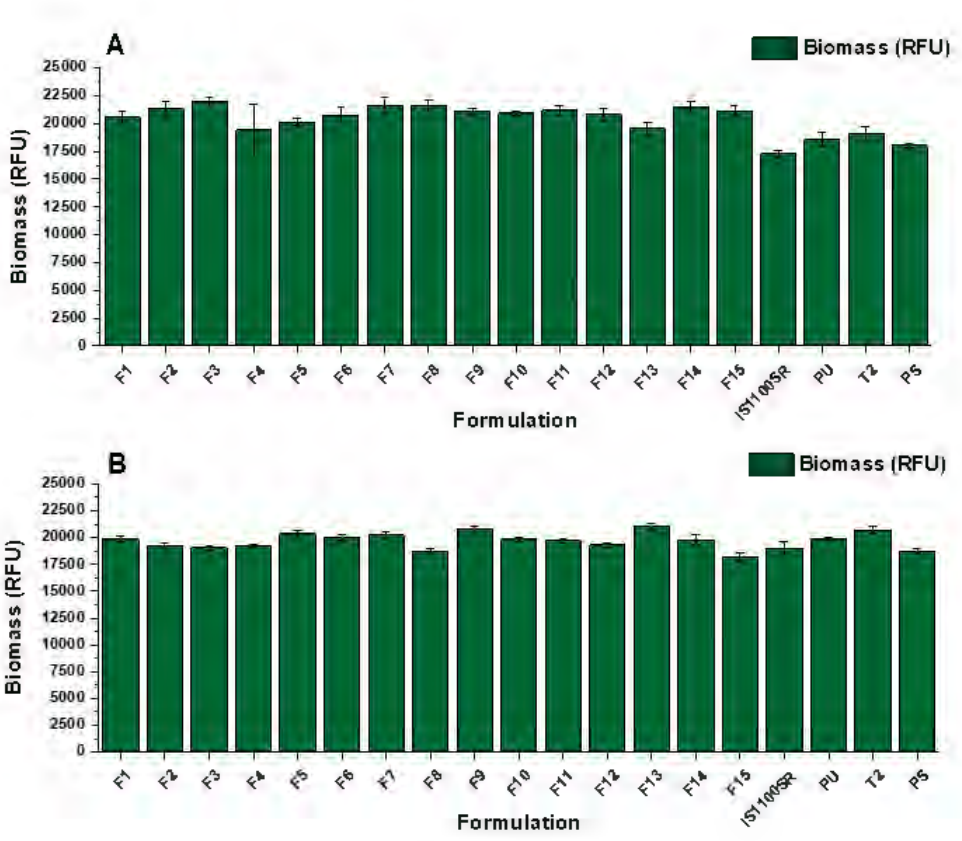

Figure B2. Biomass generation of *U. linza* sporelings grown in leachates from sample sets A and B, collected over an 18-hour period. The X-axis shows the formulation ID as seen in Table B3 with data on the y-axis presented as relative fluorescence units (RFU) measured as extracted chlorophyll. Each column is the mean of 6 replicates. Error bars show standard error of the mean.

Leachate Toxicity Assay (*Navicula incerta*)

As with biological assays involving macroalgae *U. linza*, leachate toxicity assays were performed on coated samples of experimental and control/standard formulations to investigate the toxic nature of leachates towards microalgae *N. incerta* before cell attachment and release assays. The details of this experiment have been reported previously. Briefly, well plates with coated disks were incubated in 1 mL

of growth medium overnight. Afterwards, a 0.05 mL suspension of *N. incerta* diatom cells (4 x10^5 cells mL^{-1}, adjusted to 0.03 OD at absorbance 660 nm) in Guillard's F/2 medium was added to 1 mL of coating leachates. Then, 0.2 mL of combined leachate and *N. incerta* suspension was transferred, in triplicate, to a 96-well array plate. These plates were incubated for 48 h at 18℃ in an illuminated growth cabinet with a 16:8 light to dark ratio and a photon flux density of 33 µmol/m/s. Chlorophyll was then extracted with DMSO and the concentration was quantified using fluorescence spectroscopy with an excitation wavelength of 360 nm and emission wavelength at 670 nm. Growth in coating leachates was reported as fluorescence ratio to a positive growth control (fresh growth medium).

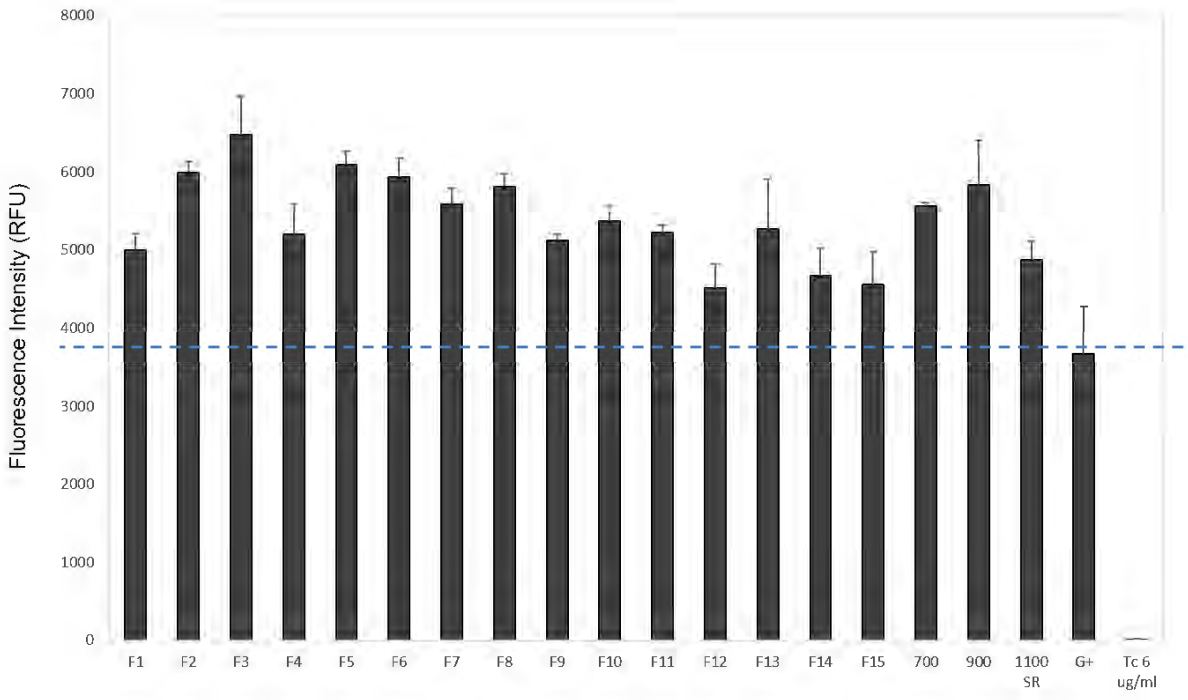

Figure B3. *N*. *incerta* leachate toxicity assessments for experimental, control, and standard formulations. Coatings were compared to a positive growth control as shown by the blue dashed line. The bars represent fluorescence intensity of biomass (RFU) generated in leachates of analyzed coatings. The X-axis shows the formulation IDs seen in Table B3.

Leachate Toxicity Assay (*Cellulophaga lytica*)

The toxicity of leachates from experimental coatings was evaluated before analysis of biofilm growth and adhesion of *C. lytica*, and details of this experiment can be found elsewhere. A 1 mL portion of growth medium was added to well plates containing coated disks and incubated overnight. Leachates were collected and 0.05 mL of a suspension of *C. lytica* (10^7 cells/mL in ASW with 0.5 g/L peptone and 0.1 g/L of yeast extract) was added to 1 mL of coating leachate. Then, 0.2 mL of this mixture was

transferred to a 96-well plate array, in triplicate, and incubated for 18 h at 28℃. Afterwards, well plates were rinsed three times with deionized water and then stained with 0.5 mL of crystal violet dye. Crystal violet was then extracted with 0.5 mL of glacial acetic acid and absorbance was measured at 600 nm to determine biomass. Growth in the coating leachates were reported as an absorbance ratio to a positive growth control (fresh growth medium).

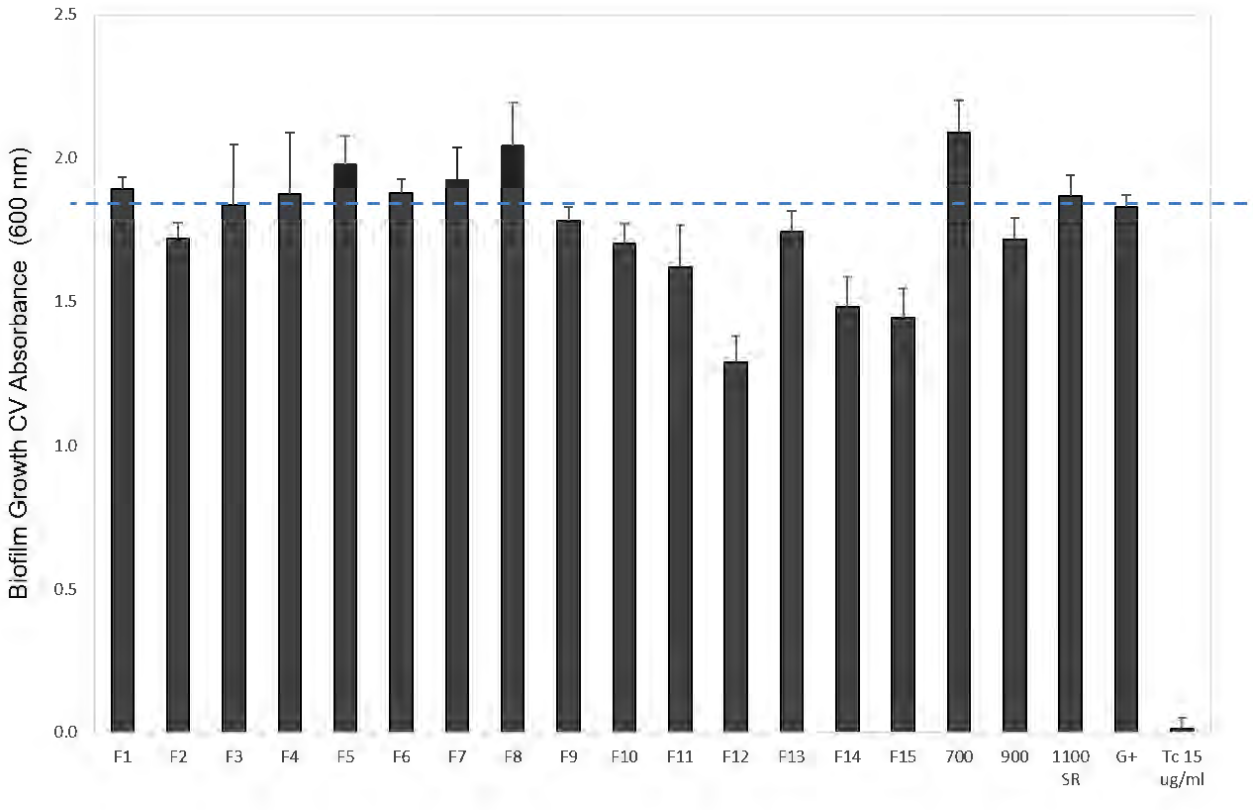

Figure B4. *C. lytica* leachate toxicity assessments for experimental, control, and standard formulations. Coatings were compared to a positive growth control as shown by the blue dashed line. The bars represent crystal violet absorbance of biofilm growth generated in leachates of analyzed coatings. The X-axis shows the formulation IDs seen in Table B3.

Biological Assays Involving *U. linza*, *G. demissa*, and *B. improvisus*

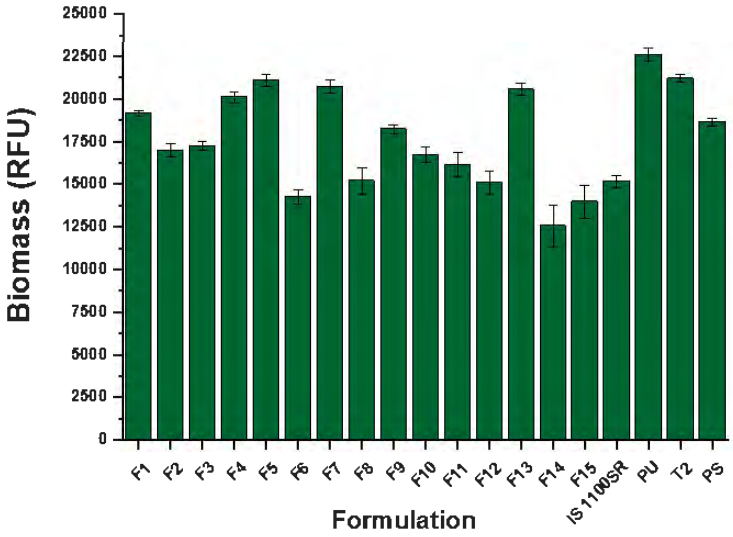

Figure B5. Growth of *U. linza* sporelings on experimental formulations. The bars represent the mean biomass from 6 replicates (relative fluorescence units) generated on experimental and control coatings. Error bars show standard error of the means. The X-axis is labeled to indicate formulation numbers in Table B3, along with commercial standards and controls.

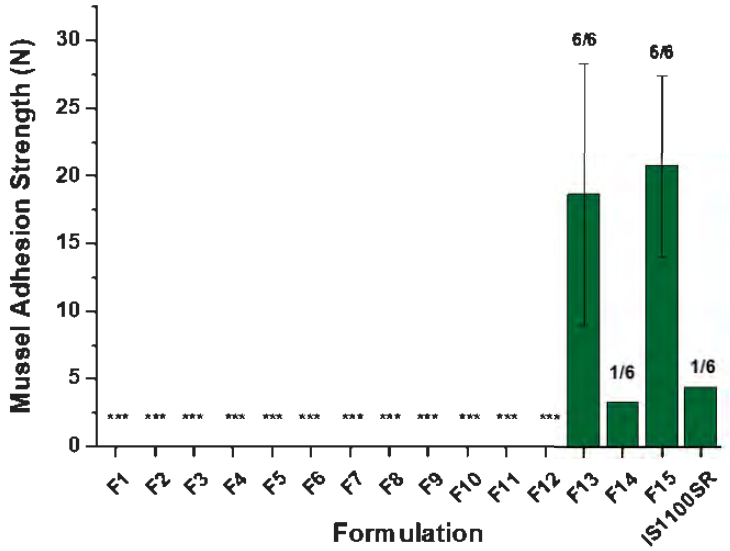

Figure B6 . Mussel removal force of *G. demissa*. Six attempted attachments were performed for each coating. The removal force value represents the average force for removal of successfully attached mussels. The ratio corresponds to the number of attached mussels over the number of total available mussels. *** denotes there were no mussels attached to coatings. The X-axis is labeled to indicate formulation number in Table 3.2, along with commercial standards and controls.

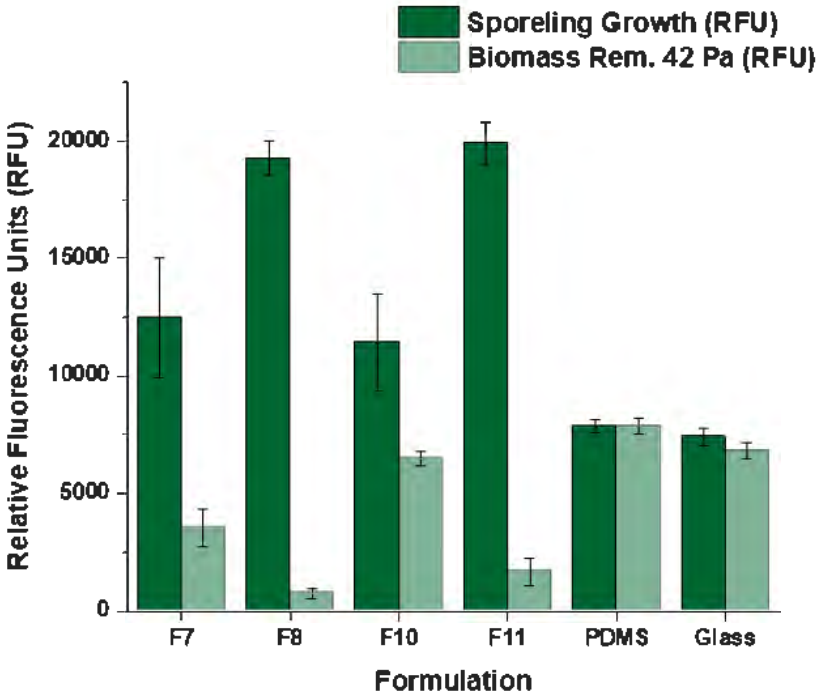

Figure B7. *U. linza* sporeling growth and removal on select formulations in a turbulent flow cell with 42 Pa hydrodynamic shear force. Dark green bars pertain to sporeling growth measured by relative fluorescence units (RFU). Whilst light green bars represent biomass remaining after placing into flow cell. Each point is the mean biomass from 4 replicate slides. The X-axis is labeled to indicate formulation type shown in Table B3. Bars show the standard error of the mean.

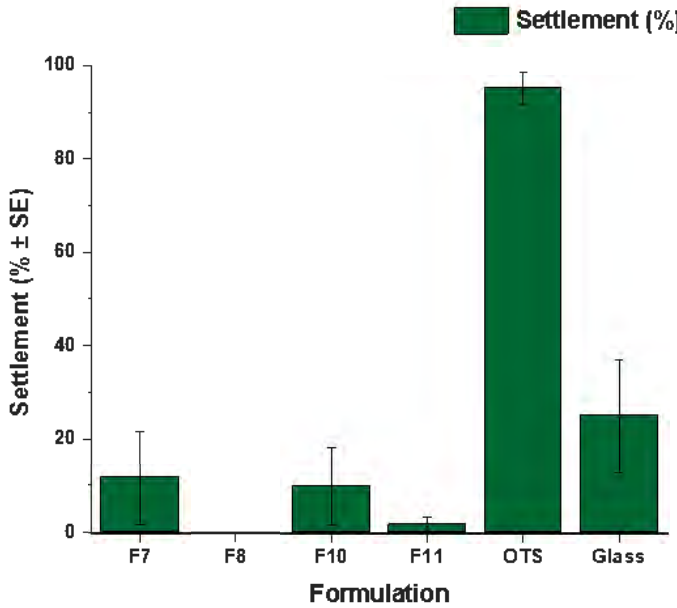

Figure B8. *Balanus improvisus* cyprid larvae settlement on experimental formulations. Settlement % recorded from 6 replicate coated glass slides compared to a glass microscope slide control, and trimethoxy(octadecyl)silane coated glass slide.

Tables of Statistical Analysis

Table B4. Tukey comparisons between formulations with varying pre-polymer composition in growth assays for *U. linza*

Formulations	N	Mean	Grouping		
F7	6	20727	A		
F13	6	20550	A	B	
F4	6	20103	A	B	
F1	6	19147		B	
F10	6	16722			C

Means that do not share a letter are significantly different.

Table B5. Tukey comparisons between all experimental formulations and the commercial standard coatings and internal controls shown in Table B3 for growth assays for *U. linza.*

Formulations	N	Mean	Grouping								
PU	6	22589	A								
T2	6	21208	A	B							
F5	6	21097	A	B							
F7	6	20727	A	B	C						
F13	6	20550	A	B	C						
F4	6	20103	A	B	C						
F1	6	19147		B	C	D					
Poly	6	18638		B	C	D	E				
F9	6	18219			C	D	E				
F3	6	17236				D	E	F			
F2	6	16990				D	E	F	G		
F10	6	16722				D	E	F	G	H	
F11	6	16151					E	F	G	H	
F8	6	15193						F	G	H	I
IS1100SR	6	15160						F	G	H	I
F12	6	15088						F	G	H	I
F6	6	14264							G	H	I
F15	6	13963								H	I
F14	6	12546									I

Means that do not share a letter are significantly different.

Table B6. Tukey comparisons between formulations with varying SMAA wt.% (0, 5, and 10 wt.%) in growth assays for *U. linza*. Highlighted cells have no significant difference as they fail to reject the null hypothesis where means are equal

Grouping Information Using the Tukey Method and 95% Confidence			
Formulations	**N**	**Mean**	**Grouping**
F1	6	19147	A
F2	6	16990	B
F3	6	17236	B

Grouping Information Using the Tukey Method and 95% Confidence			
Formulations	**N**	**Mean**	**Grouping**
F4	6	20103	A
F5	6	21097	A
F6	6	14264	B

Grouping Information Using the Tukey Method and 95% Confidence			
Formulations	**N**	**Mean**	**Grouping**
F7	6	20727	A
F8	6	15193	C
F9	6	18219	B

Grouping Information Using the Tukey Method and 95% Confidence			
Formulations	**N**	**Mean**	**Grouping**
F10	6	16722	A
F11	6	16151	A
F12	6	15088	A

Grouping Information Using the Tukey Method and 95% Confidence			
Formulations	**N**	**Mean**	**Grouping**
F13	6	20550	A
F14	6	12546	B
F15	6	13963	B

*Means that do not share a letter are significantly different

Table B7. Tukey comparisons between formulations with varying pre-polymer composition in growth assays for *C. lytica*

Formulations	N	Mean	Grouping	
F13	3	0.712	A	
F1	3	0.6753	A	B
F4	3	0.6687	A	B
F7	3	0.5107	A	B
F10	3	0.38533		B

Means that do not share a letter are significantly different.

Table B8. Tukey comparisons between all experimental formulations and the commercial standard coatings and internal controls shown in Table B3 for growth assays for *C. lytica*

Formulations	N	Mean	Grouping							
IS900	3	2.0280	A							
IS700	3	1.7687	A	B						
IS1100SR	3	1.5843		B						
PU	3	1.0807			C					
T2	3	0.9840			C	D				
F14	3	0.75600			C	D	E			
F13	3	0.712				D	E	F		
F15	3	0.70733				D	E	F		
F1	3	0.6753				D	E	F	G	
F4	3	0.6687				D	E	F	G	
F7	3	0.5107					E	F	G	H
F6	3	0.5003					E	F	G	H
F2	3	0.4810					E	F	G	H
F5	3	0.4700					E	F	G	H
F12	3	0.4133						F	G	H
F10	3	0.38533						F	G	H
F9	3	0.374							G	H
F3	3	0.3623							G	H
F8	3	0.3583							G	H
F11	3	0.2487								H

Means that do not share a letter are significantly different.

Table B9. Tukey comparisons between formulations with varying SMAA wt.% (0, 5, and 10 wt.%) in growth assays for *C. lytica*. Highlighted cells have no significant difference as they fail to reject the null hypothesis where means are equal

Grouping Information Using the Tukey Method and 95% Confidence			
Formulations	**N**	**Mean**	**Grouping**
F1	3	0.6753	A
F2	3	0.4810	B
F3	3	0.3623	B

Grouping Information Using the Tukey Method and 95% Confidence			
Formulations	**N**	**Mean**	**Grouping**
F4	3	0.6687	A
F5	3	0.5003	A
F6	3	0.4700	A

Grouping Information Using the Tukey Method and 95% Confidence			
Formulations	**N**	**Mean**	**Grouping**
F7	3	0.5107	A
F8	3	0.3740	A
F9	3	0.3583	A

Grouping Information Using the Tukey Method and 95% Confidence			
Formulations	**N**	**Mean**	**Grouping**
F10	3	0.3853	A
F11	3	0.2487	A
F12	3	0.4133	A

Grouping Information Using the Tukey Method and 95% Confidence			
Formulations	**N**	**Mean**	**Grouping**
F13	3	0.7120	A
F14	3	0.7560	A
F15	3	0.7073	A

*Means that do not share a letter are significantly different

Table B10. Tukey comparisons between formulations with varying pre-polymer composition in removal assays for *C. lytica*. Results are insignificant as we fail to reject the null hypothesis where means are equal

Formulations	N	Mean	Grouping
F13	4	0.244	A
F1	4	0.19225	A
F4	4	0.1668	A
F7	4	0.1070	A
F10	4	0.0617	A

Means that do not share a letter are significantly different.

Table B11. Tukey comparisons between all experimental formulations and the commercial standard coatings and internal controls shown in Table B3 for removal assays for *C. lytica*

Formulations	N	Mean	Grouping		
PU	4	0.50150	A		
T2	4	0.2943		B	
F13	4	0.244		B	C
F1	4	0.19225		B	C D
F4	4	0.1668		B	C D
IS900	4	0.1662		B	C D
F15	4	0.1638		B	C D
F14	4	0.1398		B	C D
IS700	4	0.1203		B	C D
F7	4	0.1070		B	C D
F2	4	0.0808			C D
F10	4	0.0617			C D
F8	4	0.03475			D
F5	4	0.03050			D
F6	4	0.0255			D
F12	4	0.00975			D
F9	4	0.009250			D
F11	4	0.00650			D
F3	4	0.00475			D
IS1100SR	4	0.00450			D

Means that do not share a letter are significantly different.

Table B12. Tukey comparisons between formulations with varying SMAA wt.% (0, 5, and 10 wt.%) in growth assays for *C. lytica*. Highlighted cells have no significant difference as they fail to reject the null hypothesis where means are equal

Grouping Information Using the Tukey Method and 95% Confidence			
Formulations	**N**	**Mean**	**Grouping**
F1	4	0.1923	A
F2	4	0.0808	B
F3	4	0.0048	C

Grouping Information Using the Tukey Method and 95% Confidence			
Formulations	**N**	**Mean**	**Grouping**
F4	4	0.1668	A
F5	4	0.0305	B
F6	4	0.0255	B

Grouping Information Using the Tukey Method and 95% Confidence			
Formulations	**N**	**Mean**	**Grouping**
F7	4	0.1070	A
F8	4	0.0348	B
F9	4	0.0093	B

Grouping Information Using the Tukey Method and 95% Confidence			
Formulations	**N**	**Mean**	**Grouping**
F10	4	0.0617	A
F11	4	0.0065	B
F12	4	0.0098	B

Grouping Information Using the Tukey Method and 95% Confidence			
Formulations	**N**	**Mean**	**Grouping**
F13	4	0.2440	A
F14	4	0.1398	A
F15	4	0.1638	A

*Means that do not share a letter are significantly different

Table B13. Tukey comparisons between formulations with varying pre-polymer composition in growth assays for *N. incerta*

Formulations	**N**	**Mean**	**Grouping**	
F1	3	31093	A	
F10	3	27639	A	
F13	3	26871	A	B
F4	3	25903	A	B
F7	3	21535		B

Means that do not share a letter are significantly different.

Table B14. Tukey comparisons between all experimental formulations and the commercial standard coatings and internal controls shown in Table B3 for growth assays for *N. incerta*

Formulations	N	Mean	Grouping						
T2	3	37688	A						
F1	3	31093	A	B					
PU	3	30253	A	B					
F14	3	29750	A	B	C				
F10	3	27639		B	C	D			
F13	3	26871		B	C	D			
F4	3	25903		B	C	D	E		
IS700	3	25249		B	C	D	E		
F5	3	22811		B	C	D	E	F	
F6	3	22749		B	C	D	E	F	
F15	3	21557			C	D	E	F	
F7	3	21535			C	D	E	F	
F8	3	21038				D	E	F	
F11	3	20296				D	E	F	
F12	3	20045				D	E	F	
F2	3	19950				D	E	F	
F9	3	19665				D	E	F	
IS900	3	18223					E	F	G
F3	3	16552						F	G
IS1100SR	3	10781							G

Means that do not share a letter are significantly different.

Table B15. Tukey comparisons between formulations with varying SMAA wt.% (0, 5, and 10 wt.%) in growth assays for *N. incerta*. Highlighted cells have no significant difference as they fail to reject the null hypothesis where means are equal

Grouping Information Using the Tukey Method and 95% Confidence			
Formulations	**N**	**Mean**	**Grouping**
F1	3	31093	A
F2	3	19950	B
F3	3	16552	B

Grouping Information Using the Tukey Method and 95% Confidence			
Formulations	**N**	**Mean**	**Grouping**
F4	3	25903	A
F5	3	22811	A
F6	3	22749	A

Grouping Information Using the Tukey Method and 95% Confidence			
Formulations	**N**	**Mean**	**Grouping**
F7	3	21535	A
F8	3	21038	A
F9	3	19665	A

Grouping Information Using the Tukey Method and 95% Confidence			
Formulations	**N**	**Mean**	**Grouping**
F10	3	27639	A
F11	3	20296	B
F12	3	20045	B

Grouping Information Using the Tukey Method and 95% Confidence			
Formulations	**N**	**Mean**	**Grouping**
F13	3	26871	A
F14	3	29750	A
F15	3	21557	A

*Means that do not share a letter are significantly different

Table B16. Tukey comparisons between formulations with varying pre-polymer composition in removal assays for *N. incerta*. Results are insignificant as we fail to reject the null hypothesis where means are equal

Formulations	N	Mean	Grouping
F4	4	10157	A
F7	4	9985	A
F13	4	9136	A
F1	4	7888	A
F10	4	6714	A

Means that do not share a letter are significantly different.

Table B17. Tukey comparisons between all experimental formulations and the commercial standard coatings and internal controls shown in Table B3 for removal assays for *N. incerta*

Formulations	N	Mean	Grouping								
T2	4	24517	A								
F4	4	10157		B							
F7	4	9985		B	C						
F13	4	9136		B	C	D					
F2	4	8925		B	C	D					
F1	4	7888		B	C	D	E				
F10	4	6714			C	D	E	F			
F8	4	5922				D	E	F	G		
F11	4	4928					E	F	G	H	
F3	4	4597					E	F	G	H	
F5	4	4463						F	G	H	
F6	4	4183						F	G	H	
F14	4	3700						F	G	H	I
PU	4	3646						F	G	H	I
F9	4	3298							G	H	I	J
F12	4	2804							G	H	I	J
IS700	4	2423								H	I	J
F15	4	613.5									I	J
IS900	4	523.0									I	J
IS1100SR	4	326.8										J

Means that do not share a letter are significantly different.

Table B18. Tukey comparisons between formulations with varying SMAA wt.% (0, 5, and 10 wt.%) in removal assays for *N. incerta*

Grouping Information Using the Tukey Method and 95% Confidence			
Formulations	**N**	**Mean**	**Grouping**
F1	4	7888	A
F2	4	8925	A
F3	4	4597	B

Grouping Information Using the Tukey Method and 95% Confidence			
Formulations	**N**	**Mean**	**Grouping**
F4	4	10157	A
F5	4	4463	B
F6	4	4183	B

Grouping Information Using the Tukey Method and 95% Confidence			
Formulations	**N**	**Mean**	**Grouping**
F7	4	9985	A
F8	4	5922	B
F9	4	3298	C

Grouping Information Using the Tukey Method and 95% Confidence			
Formulations	**N**	**Mean**	**Grouping**
F10	4	6714	A
F11	4	4928	A B
F12	4	2804	B

Grouping Information Using the Tukey Method and 95% Confidence			
Formulations	**N**	**Mean**	**Grouping**
F13	4	9136	A
F14	4	3700	B
F15	4	613.5	C

*Means that do not share a letter are significantly different

Table B19. Tukey comparisons between formulations with varying pre-polymer composition in removal assays for *A. amphitrite*

Formulations	N	Mean	Grouping	
F13	6	0.1379	A	
F7	6	0.0653	A	B
F4	6	0.0449	A	B
F10	6	0.0340		B
F1	6	0.01947		B

Means that do not share a letter are significantly different.

Table B20. Tukey comparisons between all experimental formulations and the commercial standard coatings and internal controls shown in Table B3 for removal assays for *A. amphitrite*

Formulations	N	Mean	Grouping	
F13	6	0.1379	A	
F12	6	0.1076	A	B
F14	6	0.0725	A	B
F5	6	0.0667	A	B
F7	6	0.0653	A	B
F15	6	0.0612	A	B
F8	6	0.0537	A	B
F4	6	0.0449	A	B
F11	6	0.0438	A	B
F9	6	0.0369	A	B
F10	6	0.0340	A	B
IS1100SR	6	0.0277		B
F3	6	0.0273		B
F1	6	0.01947		B
F6	6	0.01496		B
F2	6	0.00763		B

Means that do not share a letter are significantly different.

Table B21. Tukey comparisons between formulations with varying SMAA wt.% (0, 5, and 10 wt.%) in removal assays for *A. amphitrite*. Highlighted cells have no significant difference as they fail to reject the null hypothesis where means are equal

Grouping Information Using the Tukey Method and 95% Confidence			
Formulations	**N**	**Mean**	**Grouping**
F1	4	0.0195	A
F2	4	0.0076	A
F3	4	0.0273	A

Grouping Information Using the Tukey Method and 95% Confidence			
Formulations	**N**	**Mean**	**Grouping**
F4	4	0.0449	A
F5	4	0.0667	A
F6	4	0.0150	A

Grouping Information Using the Tukey Method and 95% Confidence			
Formulations	**N**	**Mean**	**Grouping**
F7	4	0.0653	A
F8	4	0.0537	A
F9	4	0.0369	A

Grouping Information Using the Tukey Method and 95% Confidence			
Formulations	**N**	**Mean**	**Grouping**
F10	4	0.0340	A
F11	4	0.0438	A
F12	4	0.1076	A

Grouping Information Using the Tukey Method and 95% Confidence			
Formulations	**N**	**Mean**	**Grouping**
F13	4	0.1379	A
F14	4	0.0725	A
F15	4	0.0612	A

*Means that do not share a letter are significantly different

APPENDIX C: CHAPTER 4 SUPPLEMENTAL INFORMATION

Structure of SMAA

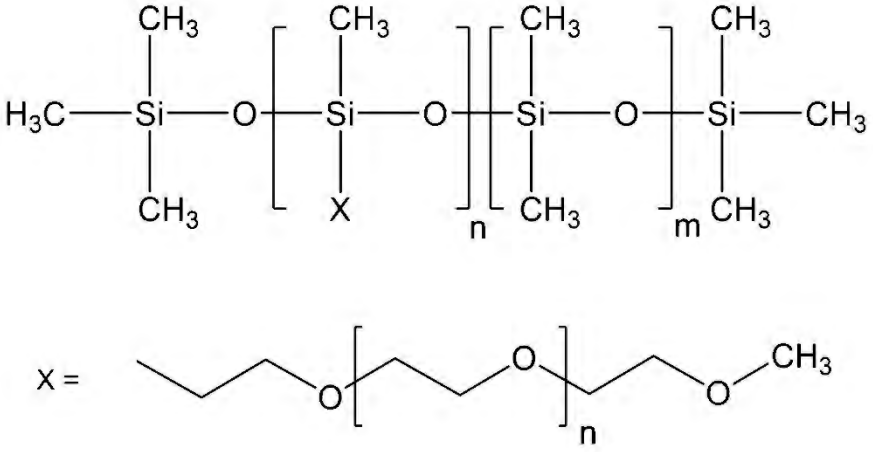

Figure C1. Structure of SMAA. The siloxane backbone consists of a co-polymer between polymethylhydrosiloxane (PMHS) and polydimethylsiloxane (PDMS) with approx. 15-18 mol % consisting of methylhydrosiloxane (MHS) repeat units. 'X' indicates such MHS sites where chains of 750 $\bar{M}_n$ PEG were grafted to.

Synthesis of APEG-750

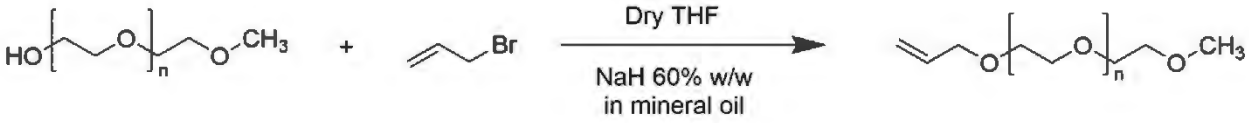

Figure C2. Synthetic scheme for APEG 750.

The synthesis for APEG-750 is shown in Figure C2. First, 750 $\bar{M}_n$ hydroxyl PEG monomethyl ether (45.78 g; 0.061 mol) was added to a 3-neck 500 mL round-bottom flask and dissolved in anhydrous THF (160.0 mL). To a 20 mL glass vial, NaH 60% w/w dispersion in mineral oil (2.9212 g; 0.073 mol) was added, followed by 10.0 mL of anhydrous THF. This NaH/THF mixture was added dropwise to the reaction mixture, which was stirred and cooled in an ice bath to 0°C. After dropwise addition, the reaction mixture was stirred for 2 hours at 0°C. A mixture of allyl bromide (8.7520 g; 0.072 mol) in 80.0 mL of anhydrous THF was then added dropwise to the reaction mixture, warmed to room temperature, and stirred for 24 h. After 24 h, the reaction mixture was filtered to remove any precipitate, with THF being removed under reduced pressure. This yielded a colorless/yellow oil that was dissolved in water (150-200 mL) and extracted with 75 mL of toluene three times to remove unreacted alcohol. The desired product was then extracted into 200 mL of chloroform three times, dried with anhydrous magnesium sulfate,

filtered, and then solvent was removed under reduced pressure. FT-IR and ^{1}H-NMR were performed to detect the presence of the allyl group and disappearance of hydroxyl.

Synthesis of SMAAs

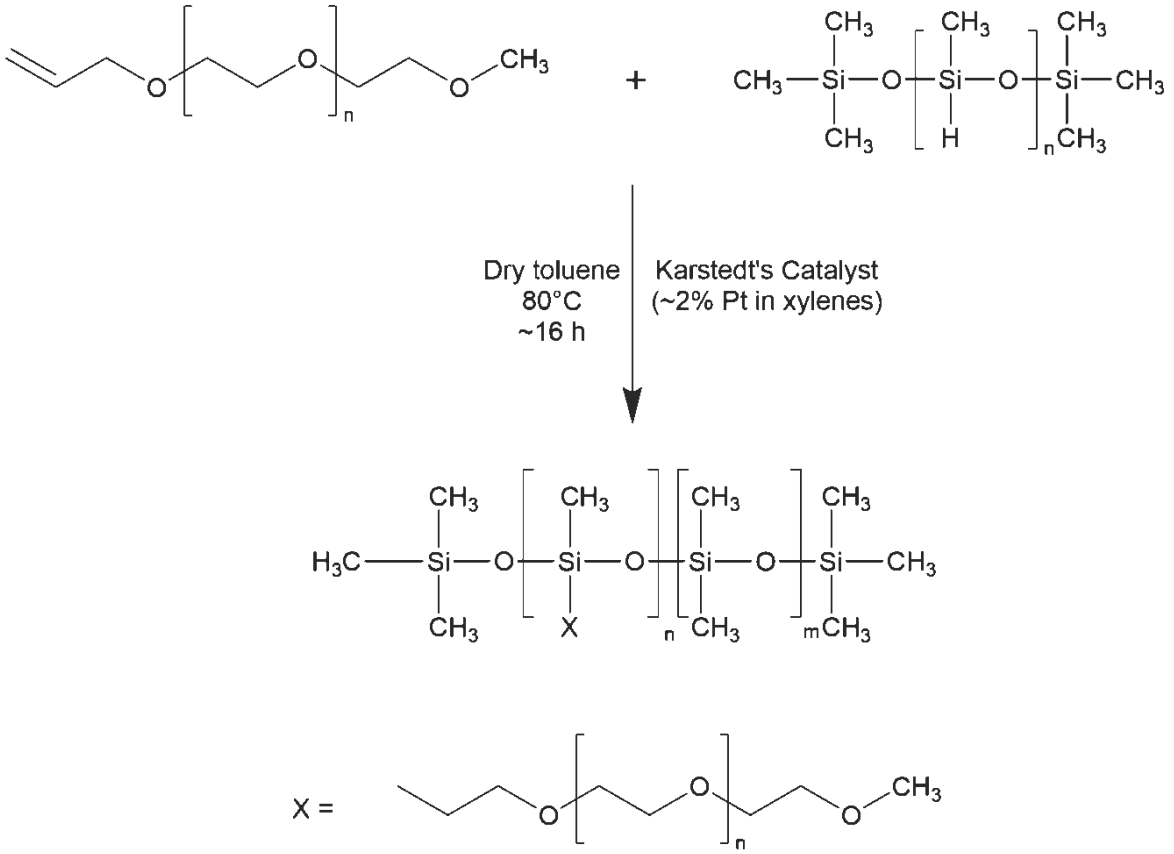

Figure C3. Synthetic scheme for the SMAA used in coating's formulation.

The synthesis for SMAAs can be seen in Figure C3. The following is a general procedure used to synthesize the SMAA described in Figure C1. APEG 750 was dried in an oven at >100°C for at least 1 hour before addition. A 250 mL 4-neck round-bottom flask was equipped with a thermocouple, nitrogen inlet connected to a condenser cooled using cold water, and a Teflon coated stir bar. Silicone rubber septa were affixed to open neck joints, and Teflon sleeves were used between all glass joints. To this flask, APEG750 (10.3627 g; 13.8 mmol) and ~40 mL of anhydrous toluene was added. The reaction mixture was stirred for 15 minutes while heating to 80°C. A solution of Karstedt's catalyst in anhydrous toluene was prepared by adding 75 µL (0.0641 g) of the catalyst to 5 mL of anhydrous toluene. Once the temperature of the reaction mixture had reached ~80°C, the catalyst solution was added. Then, HMS-151 (6.5333 g; 3.35 mmol) was added to an addition funnel along with ~20 mL of anhydrous toluene and

added dropwise over the course of approx. 30 min. This reaction was stirred for at least 16 hours, and then ~3 g of activated carbon (100 mesh) was added, with the temperature increased to 90°C for 2 hours. Next, the reaction mixture was cooled to room temperature, filtered, and any toluene was removed under reduced pressure. FT-IR and ^{1}H-NMR were performed to confirm the disappearance of the allyl group from APEG, the disappearance of the Si-H bond from the PMHS, and the appearance of new proton peaks from the grafted PEG chains. Rotary evaporation was performed on the synthesized additives and afterwards, non-volatile content (ASTM D2369) was determined.

Biological Assays

Table C1. Composition and description of commercial standard and control coatings

Control Name	Control ID	Composition
Polyurethane	PU	NDSU prepared polyurethane standard
Dow Corning® T2	T2	Silicone elastomer commercial FR standard coating
Polystyrene	Poly	Polystyrene negative control
Intersleek® 700	IS700	Intersleek commercial FR standard coating
Intersleek® 900	IS900	Intersleek commercial FR standard coating
Intersleek® 1100SR	IS1100SR	Intersleek commercial FR standard coating with a "slime release" component

Macroalgae 7-Day Growth and Release (Ulva linza)

Samples for this assay included multi-well plates with coated disks glued into the wells and were evaluated after 28 days pre-leaching in circulating tap water. Before the start of the experiment, all multi-well plates were equilibrated in 0.22 µm filtered artificial seawater (FSW) (Tropic Marin) at Newcastle for 2 h. To assess growth and release of *U. linza* sporelings, 1 mL of *U. linza* suspension was adjusted to 3.3 x 10^{5} spores mL^{-1} (0.05 OD at absorbance 660 nm) in single strength enriched seawater medium and added to each well. The spores that settled on the plates were grown for 7 days inside an illuminated incubator at 18℃ with 16:8 light to dark cycle at a photon flux density of 45 µmol/m/s, renewing nutrients every 72 hours. After 7 days of sporeling growth, the biomass that was generated was assessed from a single row of wells (6) from each plate. The remaining rows were subjected to water spraying from a spinjet apparatus at pressures of 18, 67, or 110 kPa. Chlorophyll was extracted by adding 1 mL of DMSO to each well and determination of fluorescence at excitation at 360 nm and emission at 670 nm

wavelengths. The removal of sporelings at each pressure was compared to unsprayed wells with fluorescence being directly proportional to biomass present on each coated surface.

Microalgae 2 h Cell Attachment and Release (Navicula incerta)

A brief description is as follows. A 1 mL suspension of *N. incerta* cells with 4 x 10^5 cells mL^{-1} (adjusted to 0.03 OD at absorbance 660 nm) in Guillard's F/2 medium was deposited into each coated well. To stimulate cell attachment, plates were subjected to static incubation for 2 h under ambient conditions in the dark. The suspension was then removed and wells were subjected to water-jet treatments using a spinjet apparatus. Assessment of cell attachment was performed on the first column of wells (3 wells), which was not subject to water-jet pressures. The second and third columns (3 wells each) were subjected to 69 kPa and 138 kPa psi water pressures respectively for 10 s. To quantify the biomass of the wells, chlorophyll was extracted with 0.5 mL DMSO and fluorescence was measured at an excitation wavelength of 360 nm and emission wavelength of 670 nm. The relative fluorescence units (RFU) was directly proportional to the biomass remaining on coatings surfaces after water-jet treatments. The percent removal of diatom cells was determined by comparing the RFUs of non-jetted and water-jetted wells.

Bacterial Biofilm 24 h Growth and Adhesion (Cellulophaga lytica)

To coated multi-well plates, a 1 mL suspension of marine bacterium *C. lytica*, at 10^7 cells/mL in ASW with 0.5 g/L peptone and 0.1 g/L of yeast extract, was added. These plates were then incubated for 24 h at 28℃ and then gently rinsed 3 times with deionized water to remove any loose bacteria. Again, the first column (3 wells) did not receive water-jet treatments whilst the other two columns (3 wells each) were subjected to 69 kPa and 138 kPa water pressure for 5 s. To determine biomass remaining on the wells that underwent water-jetting, wells were stained with a crystal violet solution (0.3 wt.% in deionized water) for 15 min and then rinsed 3 times with deionized water. Multi-well plates were then dried at ambient conditions for 1 h before extracting the crystal violet dye with 0.5 mL 33% acetic acid solution for 15 min. Resulting eluates (0.15 mL/ well) were measured for absorbance at 600 nm wavelength. The obtained absorbance measurements were directly proportional to the biomass on the coatings surface before and after water-jet treatments.

Adult Barnacle 2-Week Reattachment and Adhesion (Amphibalanus amphitrite)

Primed 102 x 203 mm aluminum panels coated with the experimental formulations were used throughout this experiment. After 28 days pre-leaching in circulating water tanks, adult barnacles (~5 mm in diameter and provided by Duke University Marine Laboratory, Beaufort, North Carolina, USA) attached to silicone substrates (n = 6) were removed and immobilized onto the surface of the experimental coatings. Barnacles could reattach and grow for 2 weeks while immersed in ASW tank systems with daily feeding of brine shrimp. After 2 weeks, barnacles were pushed off the surface with shear force generated by a handheld force gauge mounted on a semi-automated stage. The peak force of removal for each barnacle was recorded along with the base plate area of each dislodged barnacle, which was measured using Sigma Scan Pro 5.0 image analysis software. The adhesion strength (MPa) of each barnacle was calculated by taking the ratio of the force for removal to basal plate area and the average adhesion strength for each coating was reported as the total number of barnacles removed with a measurable force.

Tables of Statistical Analysis

Table C2. Tukey comparisons between formulations with varying amounts of SMAA wt.% in growth assays for *U. linza*. F7 is treated as the internal control PU with no incorporated additive

Factor	N	Mean	Grouping				
PU	6	19652	A				
IS	6	18186	A	B			
F3	6	17365		B	C		
Poly	6	17014		B	C	D	
T2	6	16550		B	C	D	E
F5	6	16335			C	D	E
F6	6	15629				D	E
F4	6	15530				D	E
F7	6	15457				D	E
F1	6	15020					E
F2	6	14934					E

Means that do not share a letter are significantly different.

Table C3. Tukey comparisons between formulations with varying amounts of SMAA wt.% in removal assays for *U*. *linza* at 110 kPa. F7 is treated as the internal control PU with no incorporated additive

Factor	N	Mean	Grouping				
PU	6	15904	A				
Poly	6	15408	A				
F2	6	10089		B			
F3	6	9611		B			
F1	6	8232		B	C		
F7	6	6300			C	D	
F5	6	5533				D	E
T2	6	5530				D	E
IS	6	4209					E
F4	6	3947					E
F6	6	3697					E

Means that do not share a letter are significantly different.

Table C4. Tukey comparisons between formulations with varying amounts of SMAA wt.% in growth assays for *N. incerta*. F7 is treated as the internal control PU with no incorporated additive

Factor	N	Mean	Grouping	
F2	3	27303	A	
PU	3	27066	A	B
IS700	3	26461	A	B
F7	3	26427	A	B
IS900	3	26013	A	B
T2	3	22770	A	B
F4	3	22739	A	B
F3	3	20431	A	B
F6	3	19731	A	B
F5	3	19587	A	B
F1	3	18336	A	B
IS1100SR	3	15587		B

Means that do not share a letter are significantly different.

Table C5. Tukey comparisons between formulations with varying amounts of SMAA wt.% in removal assays for *N. incerta* at 138 kPa. F7 is treated as the internal control PU with no incorporated additive

Factor	N	Mean	Grouping			
T2	4	13431	A			
IS700	4	11990	A			
PU	4	10774	A			
F7	4	7408		B		
IS900	4	3690			C	
IS1100SR	4	2772			C	D
F2	4	1267			C	D
F4	4	927			C	D
F1	4	444.3				D
F5	4	276.5				D
F6	4	273.3				D
F3	4	204.8				D

Means that do not share a letter are significantly different.

Table C6. Tukey comparisons between formulations with varying amounts of SMAA wt.% in growth assays for *C. lytica*. F7 is treated as the internal control PU with no incorporated additive

Factor	N	Mean	Grouping				
IS700	3	0.64687	A				
F7	3	0.5178		B			
PU	3	0.4599		B			
T2	3	0.4256		B			
IS1100SR	3	0.3070			C		
IS900	3	0.2943			C	D	
F3	3	0.1878				D	E
F6	3	0.17793					E
F5	3	0.1645					E
F2	3	0.1440					E
F4	3	0.1408					E
F1	3	0.1368					E

Means that do not share a letter are significantly different.

Table C7. Tukey comparisons between formulations with varying amounts of SMAA wt.% in removal assays for *C. lytica* at 138 kPa. F7 is treated as the internal control PU with no incorporated additive

Factor	N	Mean	Grouping					
IS700	4	0.38905	A					
PU	4	0.2778		B				
F7	4	0.23660		B				
T2	4	0.18430			C			
F6	4	0.11033				D		
F2	4	0.0788				D	E	
F4	4	0.07777				D	E	
F5	4	0.07060				D	E	F
F1	4	0.06445				D	E	F G
IS1100SR	4	0.02935					E	F G
F3	4	0.0275						F G
IS900	4	0.018475						G

Means that do not share a letter are significantly different.

Table C8. Tukey comparisons between formulations with varying amounts of SMAA wt.% in removal assays for *A. amphitrite*. F7 is treated as the internal control PU with no incorporated additive

Factor	N	Mean	Grouping		
F7	6	0.3736	A		
F6	6	0.3370	A	B	
F3	6	0.2517	A	B	C
F5	6	0.1897	A	B	C
F1	6	0.1652	A	B	C
F2	6	0.1503	A	B	C
F4	6	0.0849		B	C
IS1100SR	6	0.0396			C

Means that do not share a letter are significantly different.

Proton NMR and FTIR Spectra

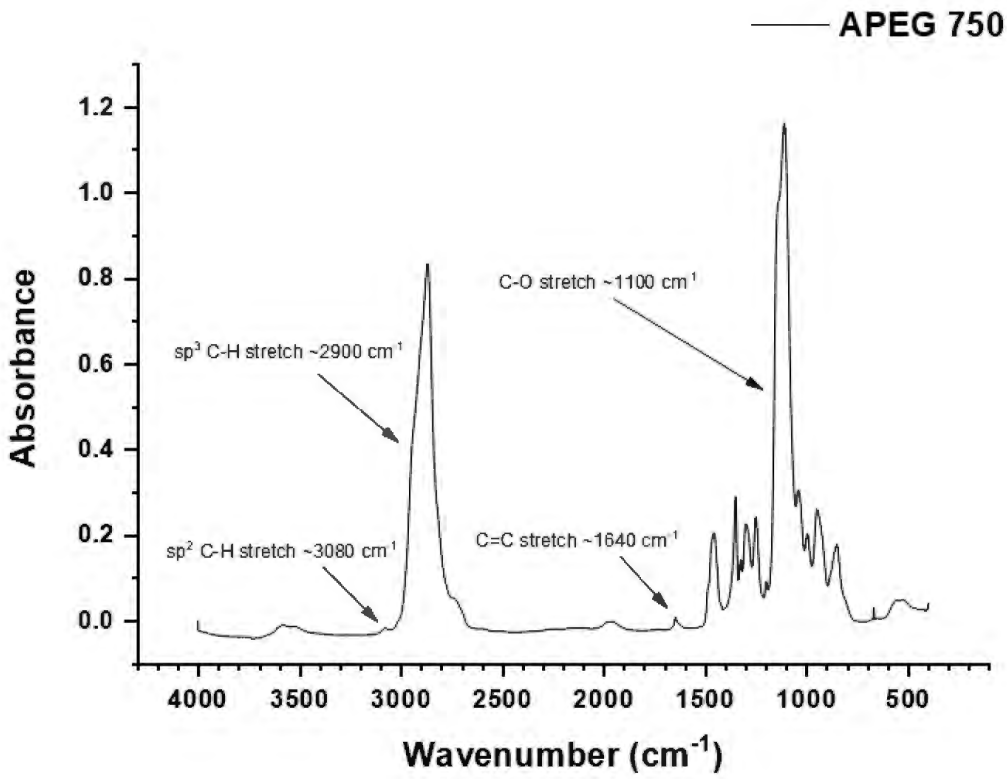

Figure C4. FT-IR spectrum of APEG-750 for use in synthesis of SMAA.

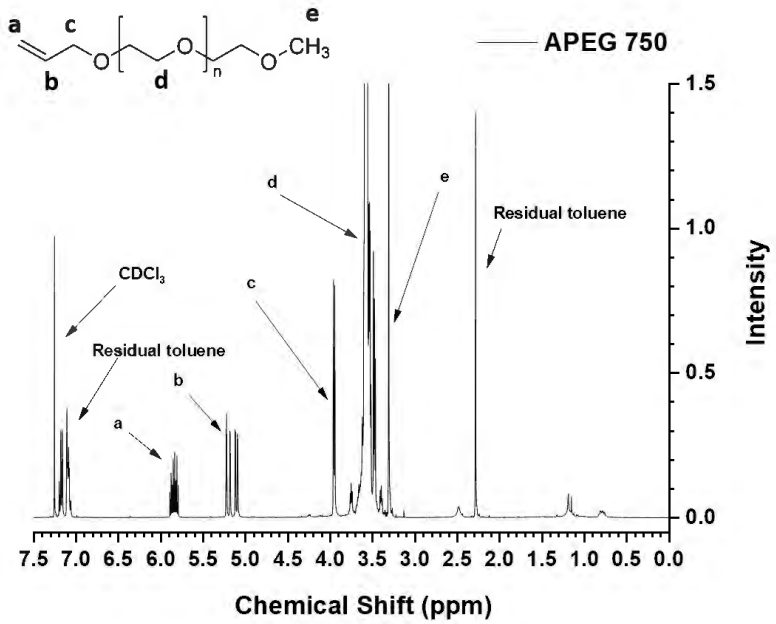

Figure C5. ^{1}H-NMR spectrum of APEG-750 for use in synthesis of SMAA.

The spectra shown above give insight into the success of the synthesis of APEG-750 for use in synthesizing the surface modifying amphiphilic additive used in this study. Figure C4 shows the characteristic peaks that belong to allyl terminated PEG in an FT-IR spectrum. The sp^2 C-H stretching from the allyl group, along with the C=C, can be seen at 3080 cm^{-1} and 1640 cm^{-1}. Characteristic peaks indicative of ethylene oxide (EO) moieties are also seen in sp^3 C-H stretching and C-O stretching at 2900 and 1100 cm^{-1} respectively. Additionally, there is a lack of O-H stretching around 3550-3200 cm^{-1}, indicative of OH functionality from PEG-750, pointing towards successful conversion. The proton NMR spectrum of APEG-750 shown in Figure C5 also indicates a successful synthesis. Protons a (5.83 ppm) and b (5.15 ppm) are seen and belong to the allyl group of APEG-750. Other protons that indicate EO repeating units (c, d, and e) are also shown at 3.94, 3.56, and 3.29 ppm respectively.

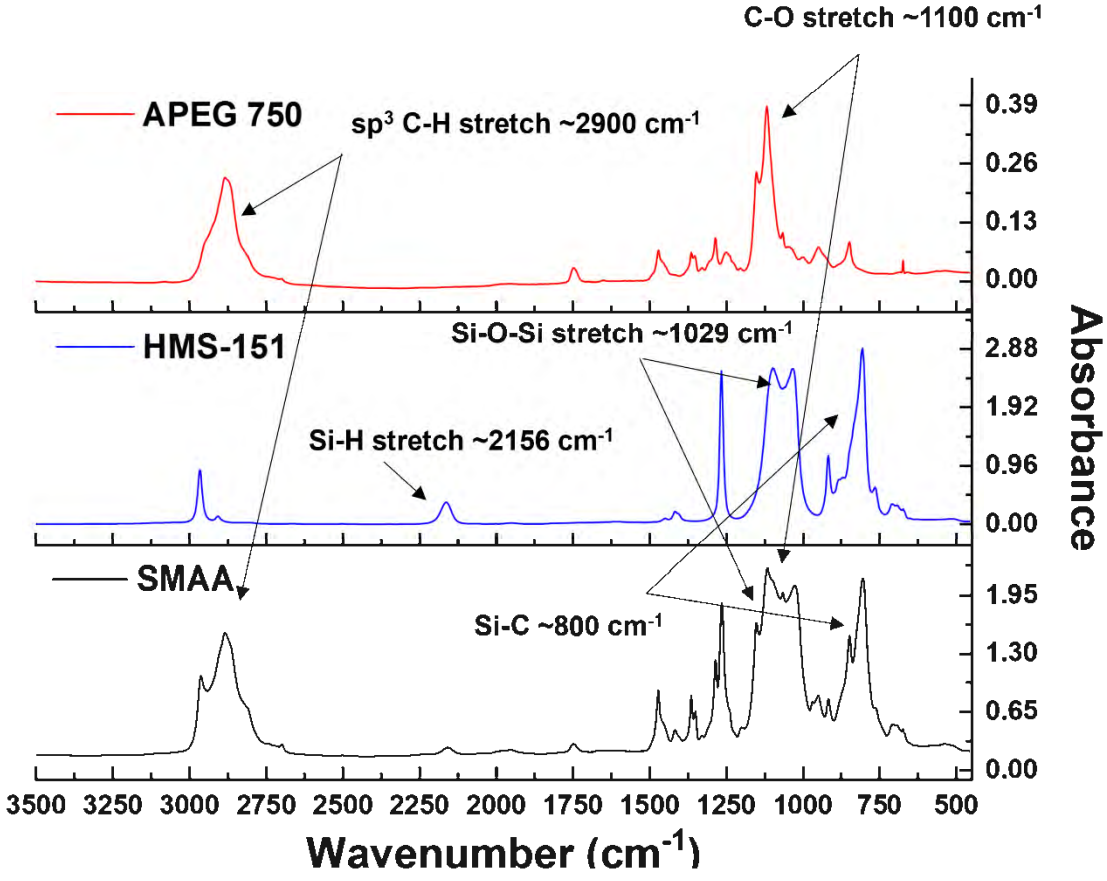

Figure C6. FT-IR spectra of APEG-750, SMAA, and HMS-151 polymethylhydrosiloxane used to confirm successful synthesis of SMAA.

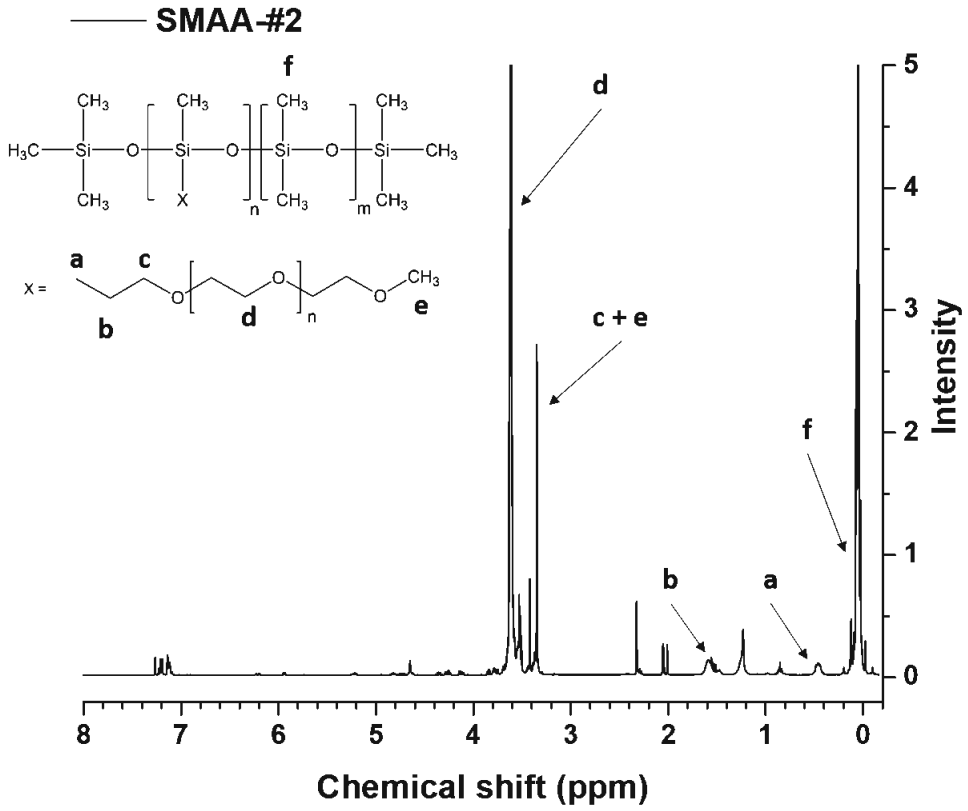

Figure C7. ^{1}H-NMR spectra of the synthesized SMAA.

Spectra shown in Figure C6 and Figure C7 detail the successful synthesis of the surface modifying amphiphilic additive used in this study. In the FT-IR spectrum in Figure C6, peaks belonging to the characteristic C-O stretching (~1100 cm^{-1}) and sp^3 C-H stretching (~2900 cm^{-1}) from PEG repeating units, as well as the Si-O-Si stretching (~1029 cm^{-1}) from siloxane repeating units can be seen in the SMAA spectra. In addition, there is a significant reduction in the Si-H peak around 2156 cm^{-1}, pointing towards a successful synthesis. In Figure C7, proton NMR shows a similar story. The protons from the Si-H functional group (~4.7 ppm) are negligible, and protons characteristic of the allyl group in APEG-750 (5.83 and 5.15 ppm respectively) are not seen. Additionally, proton peaks a (0.45 ppm) and b (1.56 ppm) are seen and represent the 1st and 2nd carbons from the allyl group bonded with silicon in the backbone. Lastly, methyl protons along the silicone backbone (0.04 ppm), along with EO protons at (3.35 and 3.60 ppm) are seen. Both the FT-IR and the ^{1}H-NMR spectra point towards a successful synthesis of the SMAA.

AFM Surface Roughness

Table C9. Surface roughness determinations on experimental formulations F1-F7 shown in Table 4.1

Formulation	R_q (nm)	R_a (nm)
F1	25.336	14.308
F2	38.98	30.027
F3	72.563	53.68
F4	54.157	39.202
F5	142.201	108.727
F6	157.094	115.57
F7-PU	3.257	1.743

Physical Properties of Coatings

Table C10. Coating physical properties for experimental formulations F1-F7

Formulation	MEK Double Rub (No. of Rubs)	Conical Mandrel Bend (mm)	Pencil Hardness (8B-9H; softest to hardest)	Thickness (µm)	Crosshatch Adhesion (0B-5B)
F1	335	Full length of coating (FAIL)	HB	70.8 ± 9.1	4B
F2	250	Full length of coating (FAIL)	2B	64.1 ± 3.7	2B
F3	290	Full length of coating (FAIL)	2B	69.6 ± 6.0	2B
F4	>400	Full length of coating (FAIL)	2B	69.0 ± 3.6	0B
F5	225	Full length of coating (FAIL)	2B	79.5 ± 4.3	0B
F6	100	Full length of coating (FAIL)	4B	67.6 ± 3.5	0B
F7-PU	>400	0 mm (PASS)	3H	80.6 ± 6.0	5B

Leachate Toxicity Assay (*Ulva linza*)

To investigate whether leachates from coated samples were truly non-toxic, leachate toxicity assays were performed on wells containing coated disks of both experimental and standard/control coatings. Assessments were performed on two batches to minimize error potentially caused by variations in collected *U. linza* spores. A brief description of this assessment is as follows, with a detailed procedure found in previous literature. For each well plate, 1 mL of 0.22 µm filtered artificial seawater (FSW) (Tropic

Marin) was added to each well and the plates were gently shaken (60 rpm) for 18 h. One mL of leachate from each experimental coating (6 replicates per coating) was then transferred to new 24-well plates. To each well, a 1 mL suspension of *U. linza* spores, adjusted to 0.05 OD at absorbance 660 nm (3.3 x 10^5 spores mL^{-1}) in double strength enriched seawater medium, was added. The plates were then incubated for 2 h in darkness and room temperature before being transferred to an illuminated incubator at 18℃ with a 16:8 light to dark cycle at a photon flux density of 45 µmol/m/s. After 7 days of growth, the seawater was removed, and chlorophyll was extracted using 1 mL DMSO. Chlorophyll fluorescence was determined at an excitation wavelength of 360 nm and emission at 670 nm using a Tecan plate reader. Fluorescence intensity being directly proportional to amount of biomass.

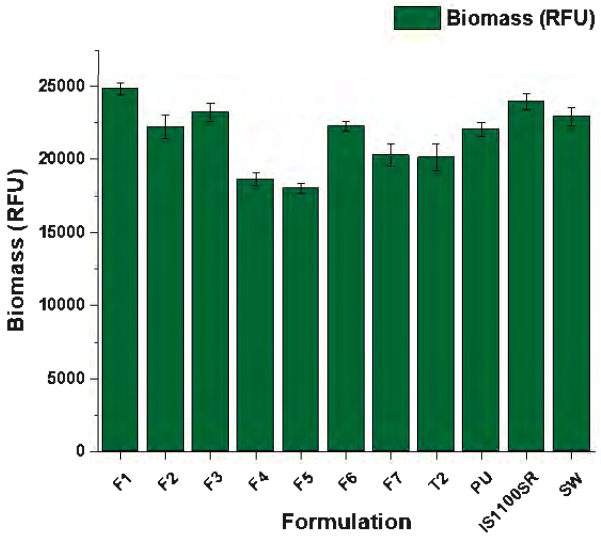

Figure C8. Biomass generation of *U. linza* sporelings grown in leachates from sample set B, collected over an 18-hour period. The X-axis shows the formulation ID as seen in Table 4.1 with data on the y-axis presented as relative fluorescence units (RFU) measured as extracted chlorophyll. Each column is the mean of 6 replicates. Error bars show standard error of the mean. IS1100SR denotes the commercial FR standard coating shown in Table C1, while SW stands for artificial seawater and serves as a positive growth control.

Leachate Toxicity Assay (*Navicula incerta*)

As with biological assays involving macroalgae *U. linza*, leachate toxicity assays were performed on coated samples of experimental and control/standard formulations to investigate the toxic nature of leachates towards microalgae *N. incerta* before cell attachment and release assays. The details of this experiment have been reported previously. Briefly, well plates with coated disks were incubated in 1 mL of growth medium overnight. Afterwards, a 0.05 mL suspension of *N. incerta* diatom cells (4 x10^5 cells

mL^{-1}, adjusted to 0.03 OD at absorbance 660 nm) in Guillard's F/2 medium was added to 1 mL of coating leachates. Then, 0.2 mL of combined leachate and *N. incerta* suspension was transferred, in triplicate, to a 96-well array plate. These plates were incubated for 48 h at 18℃ in an illuminated growth cabinet with a 16:8 light to dark ratio and a photon flux density of 33 µmol/m/s. Chlorophyll was then extracted with DMSO and the concentration was quantified using fluorescence spectroscopy with an excitation wavelength of 360 nm and emission wavelength at 670 nm. Growth in coating leachates was reported as fluorescence ratio to a positive growth control (fresh growth medium).

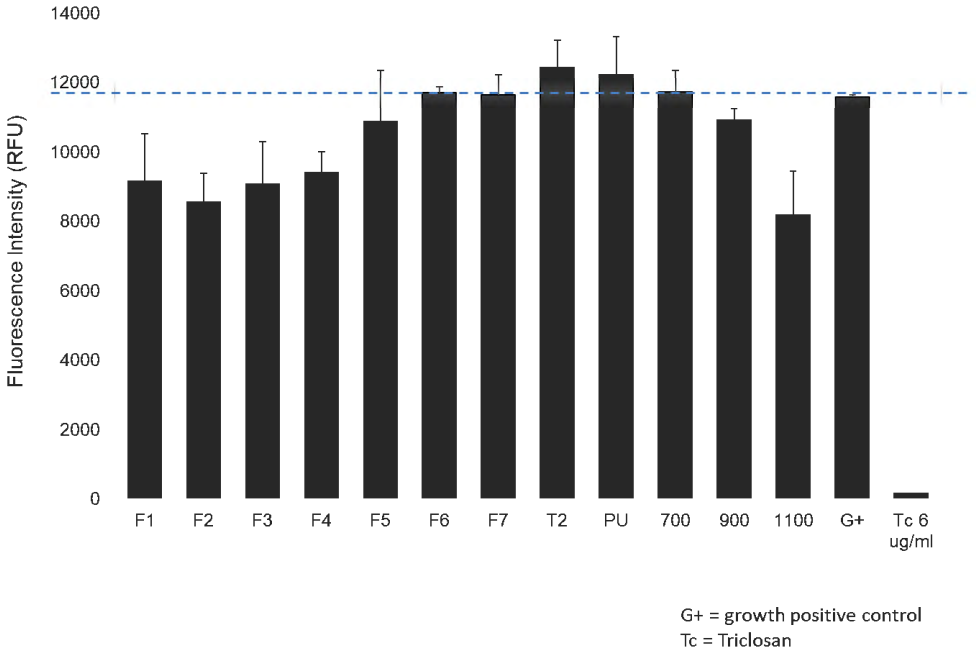

Figure C9. *N*. *incerta* leachate toxicity assessments for experimental, control, and standard formulations. Coatings were compared to a positive growth control (G+) as shown by the blue dashed line. The bars represent fluorescence intensity of biomass (RFU) generated in leachates of analyzed coatings. The X-axis shows the formulation IDs seen in Table 4.1 and Table C1.

Leachate Toxicity Assay (*Cellulophaga lytica*)

The toxicity of leachates from experimental coatings was evaluated before analysis of biofilm growth and adhesion of *C. lytica*, and details of this experiment can be found elsewhere. A 1 mL portion of growth medium was added to well plates containing coated disks and incubated overnight. Leachates were collected and 0.05 mL of a suspension of *C. lytica* (10^7 cells/mL in ASW with 0.5 g/L peptone and 0.1 g/L of yeast extract) was added to 1 mL of coating leachate. Then, 0.2 mL of this mixture was transferred to a 96-well plate array, in triplicate, and incubated for 18 h at 28℃. Afterwards, well plates

were rinsed three times with deionized water and then stained with 0.5 mL of crystal violet dye. Crystal violet was then extracted with 0.5 mL of glacial acetic acid and absorbance was measured at 600 nm to determine biomass. Growth in the coating leachates were reported as an absorbance ratio to a positive growth control (fresh growth medium).

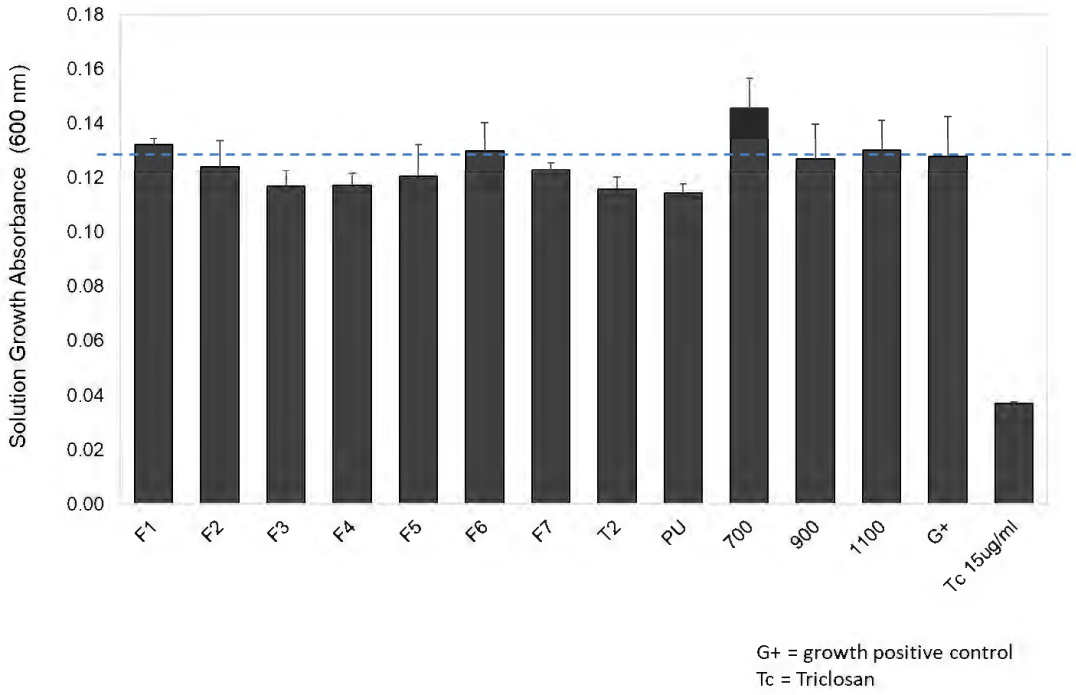

Figure C10. *C. lytica* leachate toxicity assessments for experimental, control, and standard formulations. Coatings were compared to a positive growth control (G+) as shown by the blue dashed line. The bars represent crystal violet absorbance of biofilm growth generated in leachates of analyzed coatings. The X-axis shows the formulation IDs seen in Table 4.1 and Table C1.

Growth of *U. linza* Sporelings

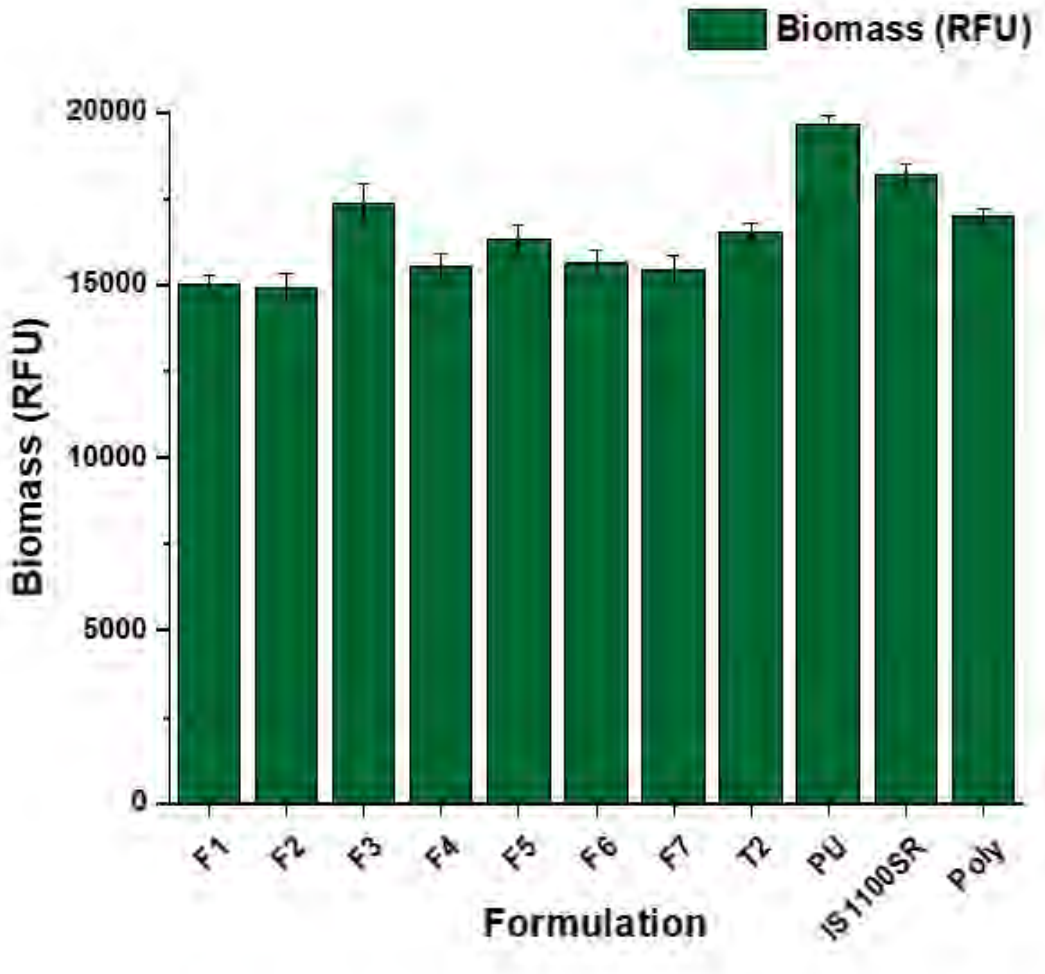

Figure C11. Growth of *U. linza* sporelings on experimental formulations. The bars represent the mean biomass from 6 replicates (relative fluorescence units) generated on experimental and control coatings. Error bars show standard error of the means. The X-axis is labeled to indicate formulation numbers in Table 4.1, along with commercial standards and controls.